Nanocellulose design; characterizing ammonium persulfate oxidation of wood and a non-wood agricultural residual, *Humulus lupulus,* bine from the Yakima valley.

Kurt Joseph Haunreiter

A dissertation

submitted in partial fulfillment of the

requirements for the degree of

Doctor of Philosophy

University of Washington

2022

Reading Committee:

Richard Roy Gustafson, Chair
Renata Bura
Anthony Dichiara

Program Authorized to Offer Degree:

School of Environmental and Forest Sciences

University of Washington

Abstract

Nanocellulose design; characterizing ammonium persulfate oxidation of wood and a non-wood agricultural residual, Humulus lupulus, bine from the Yakima valley.

Kurt Joseph Haunreiter

Chair of the Supervisory Committee:
Dr. Richard Gustafson
Bioresource Science and Engineering

Low density biomass resources such as Humulus lupulus are handicapped by high transportation costs due to widely distributed – low density acreage and the need for densification of the biomass. Life Cycle Assessment aims to assess the impact of segregating the residual woody waste (co-product) of an agricultural crop, hops (Humulus lupulus) on the greenhouse gas (GHG) emissions and on soil carbon sequestration. The growth in the *Humulus lupulus L.* or hops industry, a perennial species, driven by demand from brewers has had annual revenue growth of 11.3% since 2015 making it one of the fastest growing agricultural commodities in the Pacific Northwest(PNW). The high carbohydrate content, 58%, is similar to other lignocellulosic materials suitable for bioenergy feedstocks. The fiber has morphological characteristics similar to hardwood with length and width centered around 0.85 mm and 16.5 μm, respectively.

This fiber presents a sustainable multi-use commodity with excellent application in biobased products and paper making. We demonstrate that the environmentally friendly ammonium persulfate is effective at producing similar surface chemistry in lignin containing wood and non-wood fibers, hop bine, without pretreatment or adjustment of experimental conditions. As-prepared materials exhibited surface charge and crystallinity index ranging from 0.6 mmol/g to 1.4 mmol/g carboxylic acid and 72 to 88%, respectively. The morphological characteristics varied from 48 to 80 for the aspect ratio, from 2.7 to 4.5 nm for the diameter, and from 146 to 247 nm for the length. The response surface model developed in this research allows for designing nanocelluloses with targeted surface charge, crystallinity and aspect ratio.

Nanocellulose fibers (NFCs) were designed using this response surface model to evaluate NFC retention, as well as barrier and strength properties of NFC-reinforced paper. The results demonstrate that low-surface charge nanofiber reinforced paper exhibit reduced air permeability, high fiber retention, and higher tensile strength. We demonstrate that nanofibrillated cellulose, engineered with specific surface charge and aspect ratio, produced via green chemistry, is as effective at improving the physical properties and performance of paper, comparable to nanofibers produced through TEMPO-mediated oxidation.

Preface

This PhD thesis is submitted as the partial fulfillment of the requirements for the PhD degree at the University of Washington. The work included in the thesis was carried out at the School of Environmental and Forest Sciences, Bioresource Science and Engineering Department (Wollenberg Paper & Bioresource Science Center) at the University of Washington from December 2017 to February 2022 under the supervision of Professor Richard Gustafson.

Tulalip, February 2022

Kurt Haunreiter

TABLE OF CONTENTS

List of Figures

List of Tables

ACKNOWLEDGEMENTS

Appreciation is extended to Roy Farms (Moxee, WA) for their generous financial and material support of this research.

I would like to extend my appreciation to my advisor and supervisor, Dr. Rick Gustafson, for allowing me the freedom to define this investigation. A special thank you to Dr. Anthony Dichiara for being available and engaging in our numerous discussions regarding findings and approaches. I would also like to thank Dr. Renata Bura for providing advice on managing the dissertation path.

I am grateful to graduate students Danielle Pascoli, Sheila Goodman, Gabriel Viana Sueth Seufitelli and Heather Wise for discussions that helped expand my own personal knowledge and inspire different approaches in addressing thesis questions. Appreciation is also extended to undergraduate students Daaniya Inez, Jennalise Tripplett, Mazda Hutapea, Cian Scheer, Gloria Agwu, and Chelsea Hanson for their assistance with analytical work and method development.

And lastly appreciation is given to Dr. Elizabeth Van Volkenburgh, my GSR. Had we not had that conversation in fall of 2017 after a buildings committee meeting, I would never have considered going down this path.

DEDICATION

To my wife and best friend of over thirty years, Raquel – whose constant support, strength and perseverance over cancer (three years cancer free!!), I could not have achieved this without you. To my children, Ilyssa and Adrian – for the support and patience that you gave me in pursuing this endeavor. To my mother and in memory of my father, Mary and Steve Haunreiter, for teaching me the value of craftsmanship, art, kindness, imagination, and for instilling in me the desire to leave the world a better place than I found it. And finally, to my grandfather, Chet Bruce, who was the demonstration of a man with character and reminded me to always say thank you.

Chapter 1. INTRODUCTION

1.1 *Cellulose Nanofibers*

Cellulose is the most abundant natural renewable biopolymer on earth that can enhance the environmental sustainability of manufactured products, replace petroleum derived composites and polymers, and is highly functionalizable. The Life-Cycle-Assessment (LCA) process represent it as both a carbon sequestering and atmospheric carbon fixing material[1]. Developing these carbon-neutral resources will shift society away from our dependence on petroleum-based economics, reduce the negative impact on climate change, and develop sustainable industries[2,3]. Cellulosic fibers are derived from lignocellulosic biomass; both woody and non-woody plants. The biomass is composed of cellulose, hemicellulose, lignin and a small percentage of chemical extractives as shown in Figure 1-1. Through various pre-treatment processes, the cellulose fibers are liberated. These in turn can be treated through chemical or mechanical means to extract the nano-fibers important in the development of novel renewable composites.

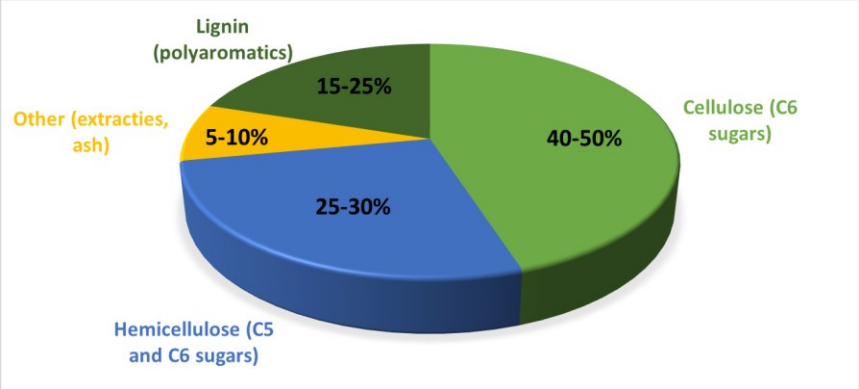

Figure 1-1 Composition of lignocellulosic biomass[4]

The packaging market is moving away from non-recyclable polymers placing increased demand for bio-based materials such as nanofibers[5]. Motivated by global warming and environmental concerns this is driving the reexamination of paper for consumer packaging through the development of environmentally sustainable bio-based nanomaterials. The polymer-based nanofiber market is worth $3,276 million of which cellulose accounts for $483 million. Two of the dominant cellulose-based nano-materials include nanofibrillated cellulose (NFC) and crystalline nanocellulose (CNC), see Figure 1-2.

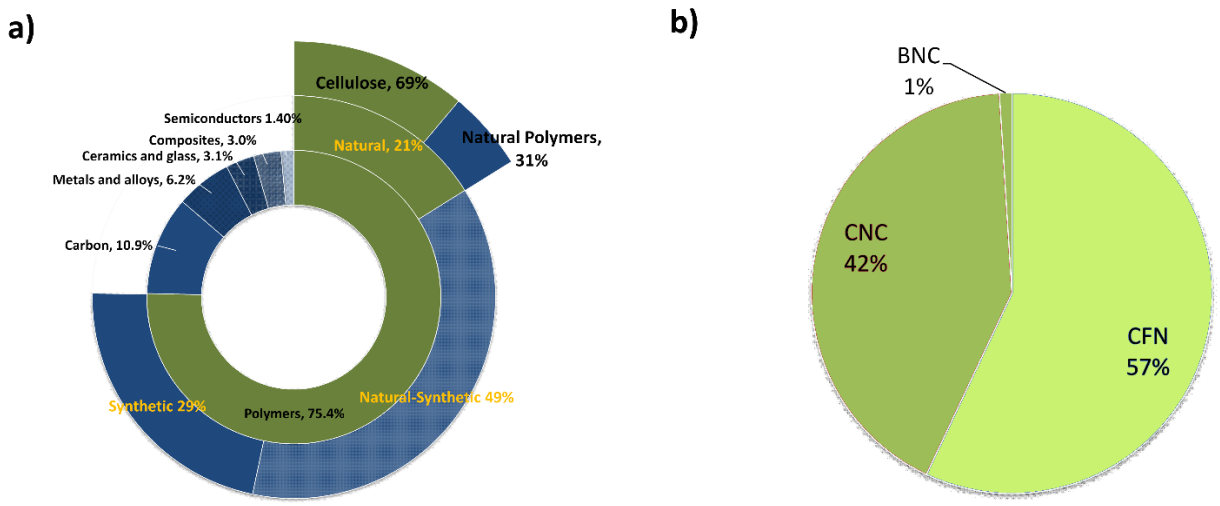

Figure 1-2. a) Global nanofiber market share by type and application, b) Market share by type of cellulose based nano-fiber.

Their high aspect ratio, crystallinity, tunable surface chemistry, biocompatibility and biodegradability have led to a wide range of applications from polymer composites to health care, see Figure 1-3a[6,7]. Paper and packaging represent 32% of global market share for nanocellulose[7]. This has led to numerous research groups investigating nano-fibers as evidenced by the patents issued from 1990 to 2017, see Figure 1-3b. Applications for nanofibers include paper reinforcement, barrier coatings on packaging, paper coatings, and as absorbents in personal care products.

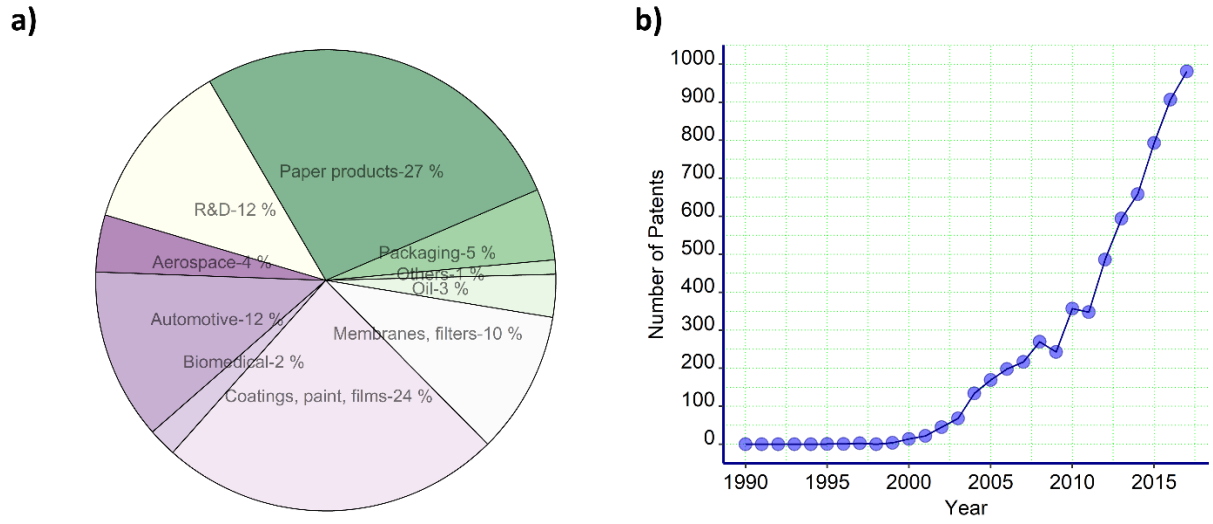

Figure 1-3. a) Global nanocellulose market share by application – 2019, b) Patent applications issued related to Nanofibers globally, 1990-2017.

The growth and demand for nanofibers from lignocellulosic biomass requires expansion and consideration of agricultural residues as alternative to forest residues as the demand for these grow exponentially and in to a likely unsustainable level[8].

1.1.1. Residual biomass Source

Plant residuals provide a lignocellulosic material that are renewable, biodegradable, positive environmental footprint, and can replace petroleum-based polymers. The utilization of lignocellulosic biomass as papermaking fiber is not a new concept. Cotton and hemp were the primary sources of fibers up until the development of the Kraft pulping process in the 1800s. Their composition is very similar to hardwood cellulose, see Figure 1-1. Yet non-wood fibers remain a small percentage today relative to wood fibers sources for the production of paper. These fibers account for only 0.69% of the total fibers used in paper production worldwide[9]. Bagasse, flax, and industrial hemp are the dominant source of herbaceous fibers in the world today. Often these lignocellulosic fiber sources are a residual of the primary product being produced and treated as a

waste stream. A few of the reasons for this are a low bulk density and high moisture content which require storage and handling the dominant wood fiber does not require, meaning that transportation costs are a larger portion of the fixed cost absorption associated with processing. Yields per hectare tend to be lower than forest residuals, for example over a period of 20 years a hectare of industrial hemp may produce 60 MT of biomass[10] where as a hectare of Douglas fir will produce 170 MT of biomass[11]. The fibers produced tend to be shorter and less coarse being more hardwood-like, as a result they cannot be a direct replacement for the longer softwood fibers.

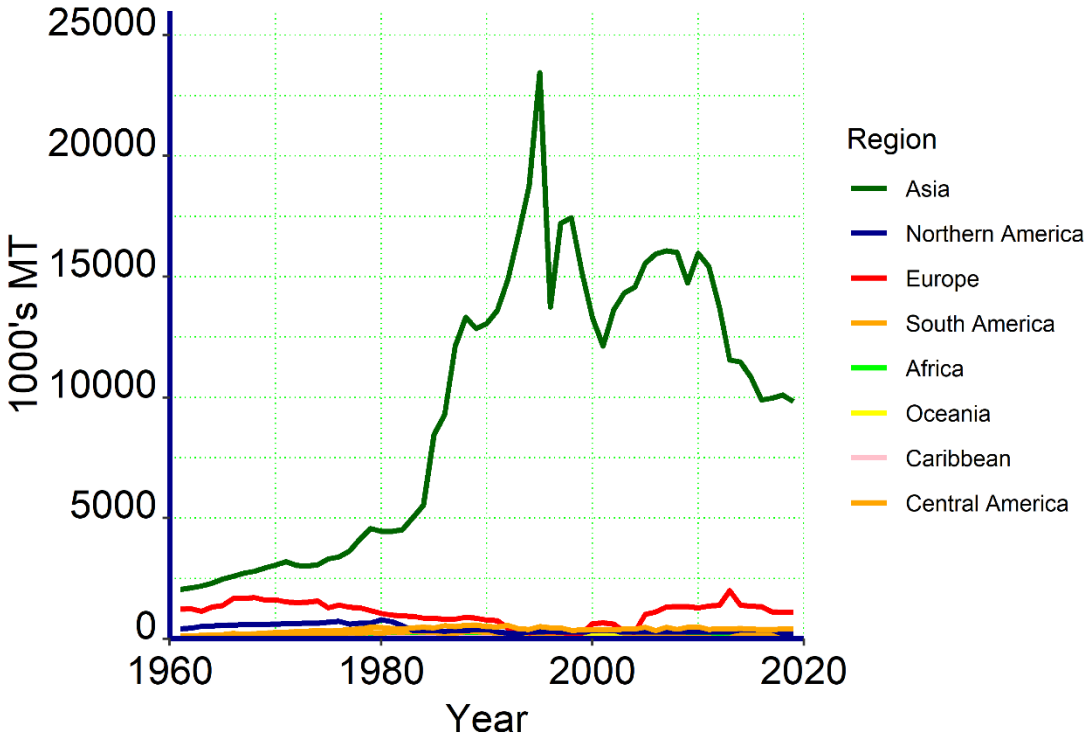

Figure 1-4. Non-wood fiber production by region (FAO statistics)[12]

The ratio of non-wood pulping operations to wood pulping remains dominated by Asian countries, followed by Africa and South America. China drives the Asian consumption of non-wood fibers however since 2000, the proportion of non-wood fiber dropped significantly. This was in part due to a dramatic increase in recycled fiber consumption and an increase in wood pulp imports as per

capita consumption outpaced domestic production[13]. Outside of Asia, non-wood fibers are beginning to gain traction in Europe and North America as the search for renewable biomaterials increase, see Figure 1-4. Not a new idea in the west[14], but one that has gained renewed interest with consideration of what were once waste materials such as hop bine.

1.1.2. Hop Bine

Hop Bine (*Humulus lupulus L.*) hops, is a member of the *Cannabaceae* family of which *Cannabis sativa L.*, industrial hemp, belongs. Hemp has provided fibers for use in papermaking for centuries, therefore, it may be worth considering if hop bine can provide suitable fibers for papermaking or carbohydrates for bioconversion as well. A comparison of the composition of hop bine relative to hemp and softwood fiber and the cellulose fiber characteristics are detailed in Table 1-1 and Table 1-2. The amount of cellulose in hop bine is similar to that of hemp. The fiber length distribution of hop bine is much narrower and consistent with what you would find in a hardwood fiber such as Eucalyptus.

Table 1-1 Comparison of composition of hop stems to other non-wood and wood fibers[15].

FIBER	Cellulose	Hemicellulose	Lignin	Ash	Extractives
HOP	32.9 %	26.0%	25.9%	3.4%	12.0%
Hemp	43.3%	23.7%	24.1%	2.3%	1.1%
Wheat Straw	44.7%	25.2%	20.9%	7.1%	3.9%
Poplar	44.4%	21.2%	21.1%	3.2%	-

Table 1-2. Comparison of morphological properties of hop stems to other non-wood and wood fibers.

FIBER	Length (mm)	Width (µm)
HOP - BINE	0.85-1.3	16.5 +/-5.5
Hemp	5-55	10-51
Eucalyptus	0.87-1.1	15-19
Poplar	0.87-1.1	3.72

It also appears to be more consistent in length than industrial hemp and far less variable in width. When comparing it to Eucalyptus, the length and width are consistent.

A shortage of linen and cloth rags in France during the 18th century led to a French paper maker's inspection of hop bine. The director of the Langlee paper mill near Montargis, Alexandre Léorier Delisle, evaluated various lingo-cellulosic materials such as reed, linden, along with hops as potential replacements for the linen and cloth rag furnish of the time. In the book titled Les Loisirs des bords du Loing, ou Recueil de pièces fugitives, poems by Marie-Joseph-Hippolyte Pelée de Varennes, he published using non-rag paper. At the back of each of the books he published, he included twenty sample leaves, each one identified by the fiber used to produce it; paper de houblon – paper made with hops (bine) as shown in Figure 1-5[16].

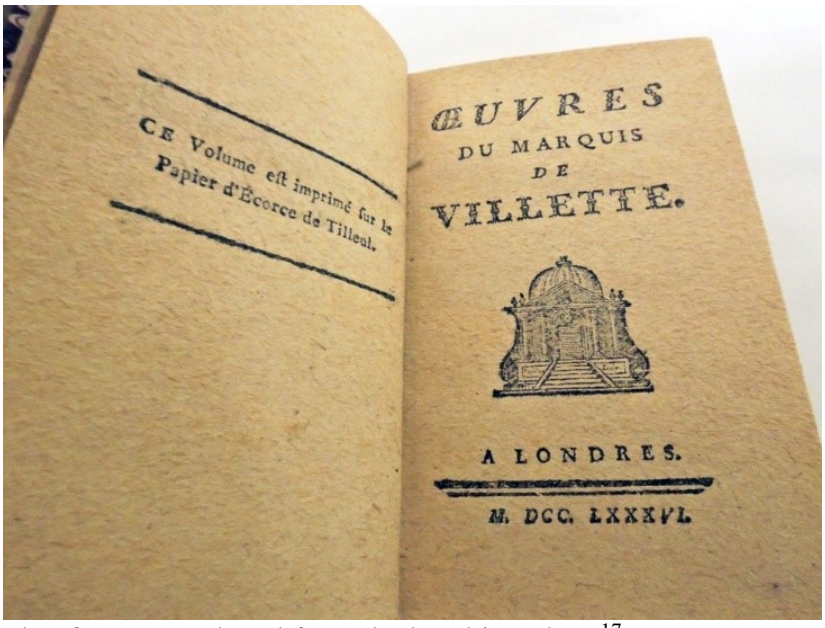

Figure 1-5. Sample of paper produced from the hop bine plant.[17]

Despite this early demonstration of its application to papermaking, there is a scarcity of research since this book was published. Recently, investigations indicate that the material has promise for use as the raw material for bioproduct production[15,18]. Changes in economic conditions and

availability of supply may be responsible for this consideration. The Chinese announced in the third quarter of 2017 that they would be pulling out of the recycled newspaper market. This withdrawal by the Chinese has put pressure on the price and the availability of bleached softwood Kraft pulp in the northwest on regional paper manufacturing and opened non-wood fibers for consideration[19]. Additionally, the rapid expansion in demand for northern bleached softwood Kraft (NBSK) from China, 14% since 2016[20], has placed additional pressures worldwide to consider alternate fiber sources.

As crops allocated to production of renewable resources compete for land previously dedicated to food crops, the residual biomass from hop cultivation offers an inexpensive alternative source of renewable lignocellulosic biomass without cannibalizing a food crop. This fiber presents a sustainable multi-use commodity with excellent application in biobased products and paper making which would otherwise be lost.

1.1.3. Availability of Hop Bine - Eastern Washington

Humulus lupulus varieties are grown in eastern Washington and account for over 79% of the total US production. Although hops cultivation is not the largest agricultural crop in the Yakima Valley; accounting in 2016 for only 1.2% of total cultivated land area or 18,029 hectares. An examination of geographical information system data for the Yakima valley has shown an 80% increase in cultivated acreage from 2014 to 2016, see Figure 1-6. Of the 26 crops that represent 98% of the cultivated land in the Yakima Valley, the cultivation of hops is the fastest growing compared to apples, a 9% increase since 2014, coming in second[21].

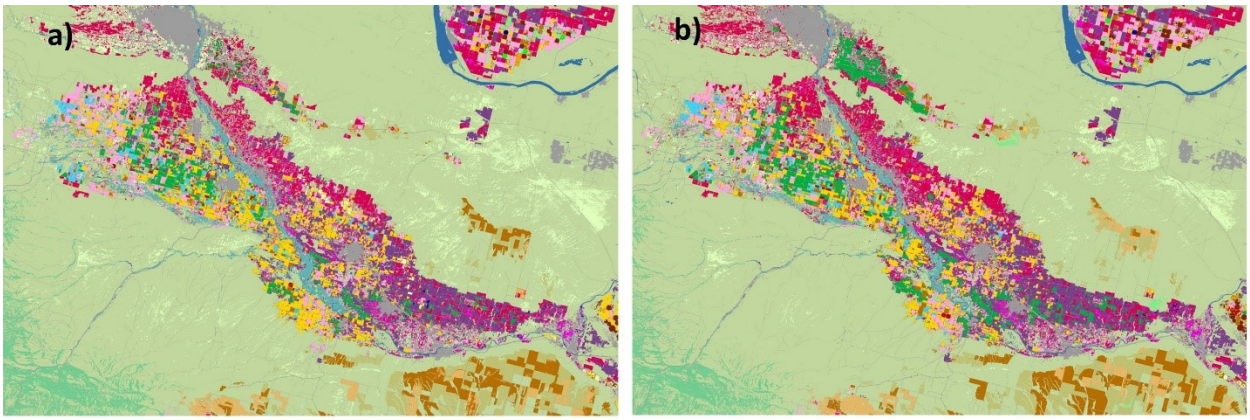

Figure 1-6. a) Yakima Valley 2014 and b) 2016 – Geographical Information Systems data from USDA, green indicates hops acreage

The secondary biomass from hop cultivation is the bine which ends up as silage. This is the primary source of cellulosic fiber in the hop plant and the increase in cultivated acreage may represent a significant source of lignocellulosic biomass. The average volume of hop cone produced per hectare is 1.5 MT. The weight of bine is approximately equal to the weight of the hop cone produced. That would mean 85,000 MT of bine would potentially be available from the state of Washington alone[22]. The low yield per hectare combined with the perennial harvest unfortunately limits the potential that this biomass has for use as a paper making fiber. Conversion to a nanofiber with application in paper making, however, is a potential opportunity.

1.2 *Why Nanofibrillated Cellulose*

1.2.1 Cellulose

Cellulose is the world's most abundant naturally occurring polymer that is insoluble in water. It is difficult to dissolve in water likely due to the intramolecular and intermolecular hydrogen bonds formed[23]. In ionic liquids, cellulose is soluble. Cellulose is conventionally illustrated by the

repeating unit cellobiose, Figure 1-7. It is a polymer of β-(1-4)-linked D-glucopyranosyl units. There is some recent disagreement in the literature that argues that cellobiose is not the repeating unit as it is just one of the resultant products from the acid hydrolysis of cellulose[24]. It is contended that the glucose residue is a more accurate depiction of the repeating unit of cellulose and is sufficient for illustrating and discussing the cellulose molecule, Figure 1-8. These depictions show O-4 as the oxygen attached to the repeating unit not, the O-1. This is due to the OH on the O-1 is the leaving group in formation of glycoside when the C-1 oxygen forms a hydroxyl. As such, both are presented here for review.

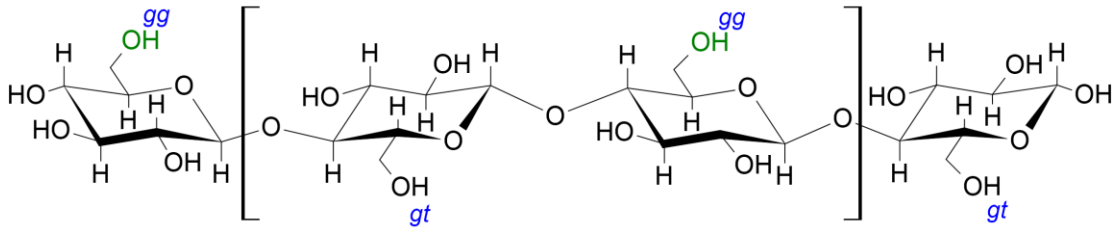

Figure 1-7 Cellobiose repeating unit presented in the chair conformation, gg is gauche-gauche and gt is gauche-trans conformations[25].

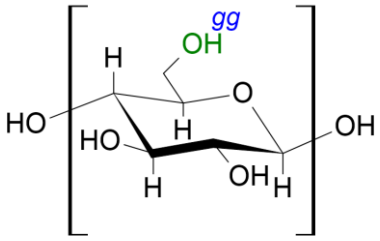

Figure 1-8 Glucopyranose repeating unit presented in the chair conformation.

The conformation is indicated, gauche-gauche and gauche-trans, to show the availability of the C6 hydroxyl for reaction on alternating glucopyranose units. The importance of the C6 hydroxyl and this conformation will become clear in the discussion of nanofiber surface chemistry and the availability of reactive sites on the nanofiber chain.

1.2.2 Lignin

Lignin is an amorphous polymer consisting of substituted phenylpropane units which account for 15-25% of the component constituents in lignocellulosic materials. The primary linkages between phenylpropane units are ether bonds and carbon-carbon bonds. Lignin can be differentiated into three primary types; guaiacyl (G), syringyl (S), and hydroxyl benzyl (H), the latter being present in herbaceous lignin only, Figure 1-9. Softwoods only have the guaiacyl type, while both syringyl and guaiacyl can be found in hardwoods. Herbaceous lignins have all three types present[26].

The ratio of syringyl to guaiacyl lignin present in either hardwoods or grasses is important to know as it governs the delignification rate in both Kraft and organosolv pulping processes, see Table 1-3[27,28].

Table 1-3 Lignin composition in various plant types[29]

Biomass	Guaiacyl (G)	Syringyl (G)	Hydroxyphenyl (H)
Softwoods	>95%	0	<5%
Hardwoods	25-50%	45-75%	0-8%
Grasses	35-80%	20-55%	5-35%

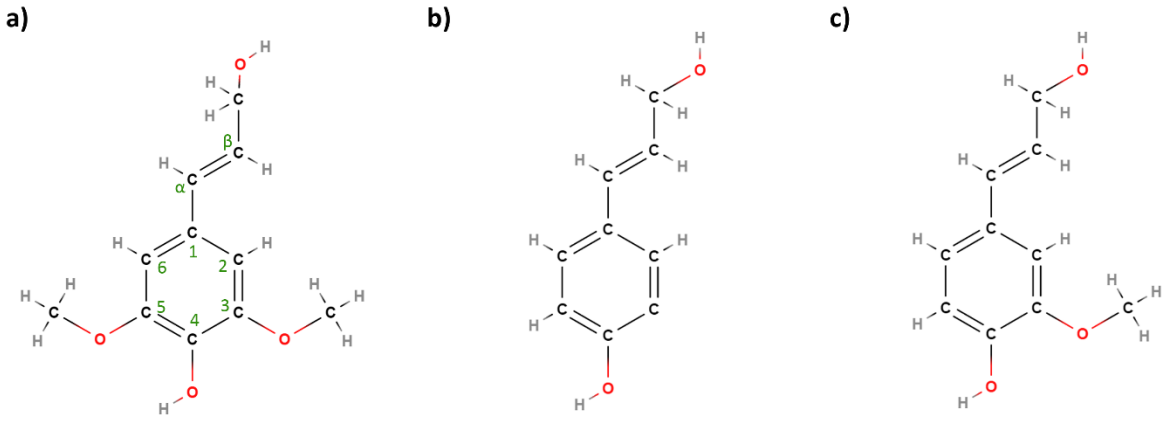

Figure 1-9. a) Syringyl, b) Guaiacyl, and c) Hydroxybenzyl Lignin

An important part of evaluating the potential of a lignocellulosic material is quantifying the carbonyl groups present. There are many methods for determining the carbonyl groups in the three

primary types of lignin[30]. Traditional methods involve titration based on oxidant consumption[31]. Various spectrophotometric methods are also available. Most recently methods have been developed to use head space gas chromatography[30].

1.2.3 Nanofibrillated Cellulose

Nanofibrillated cellulose, NFC, is composed of the smallest divisible unit containing both crystalline and amorphous regions of the cellulose matrix. Further division would result in fractionation into the cellulose oligomers. Nanofibrillated cellulose, NFC, and Cellulose nanofibrils, CNF, are used interchangeably to refer to fibrils having both amorphous and crystalline regions. Crystalline nanocellulose, CNC, refers to nanofibrils where the amorphous region has been significantly reduced or eliminated. The final form of nanofibers is generally as stable colloidal aqueous suspension of 1-3 weight %, blueish in hue, with increasing transparency as the surface charge increases. Above 4 weight % it begins to form a gel as shown in Figure 1-10

.

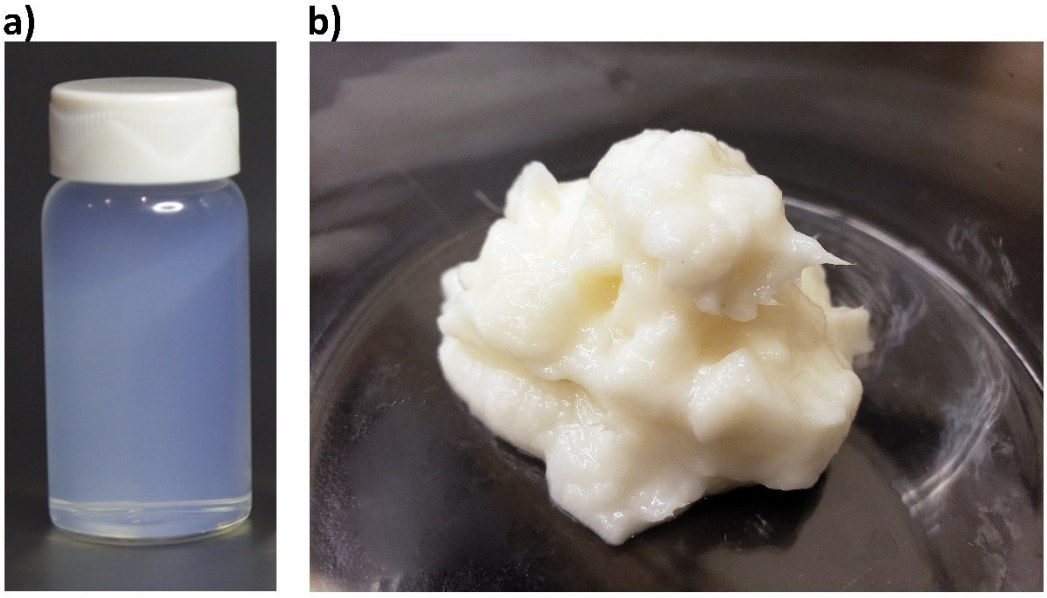

Figure 1-10.a) suspension of nanofibers, b) nanofiber gel

The Technical Association of the Pulp and Paper industry has proposed standardization of the terms used to describe nanocellulose materials based on their aspect ratio[32,33] , see the diagram in Figure 1-11 and Table 1-4. Throughout this text nanofibrillated cellulose will be referred to as NFC. This term will be utilized to reduce confusion between CNF and the abbreviation CNC. Despite this proposed naming convention, the range in dimensions can lead to nanocellulose suspensions of vastly different characteristics

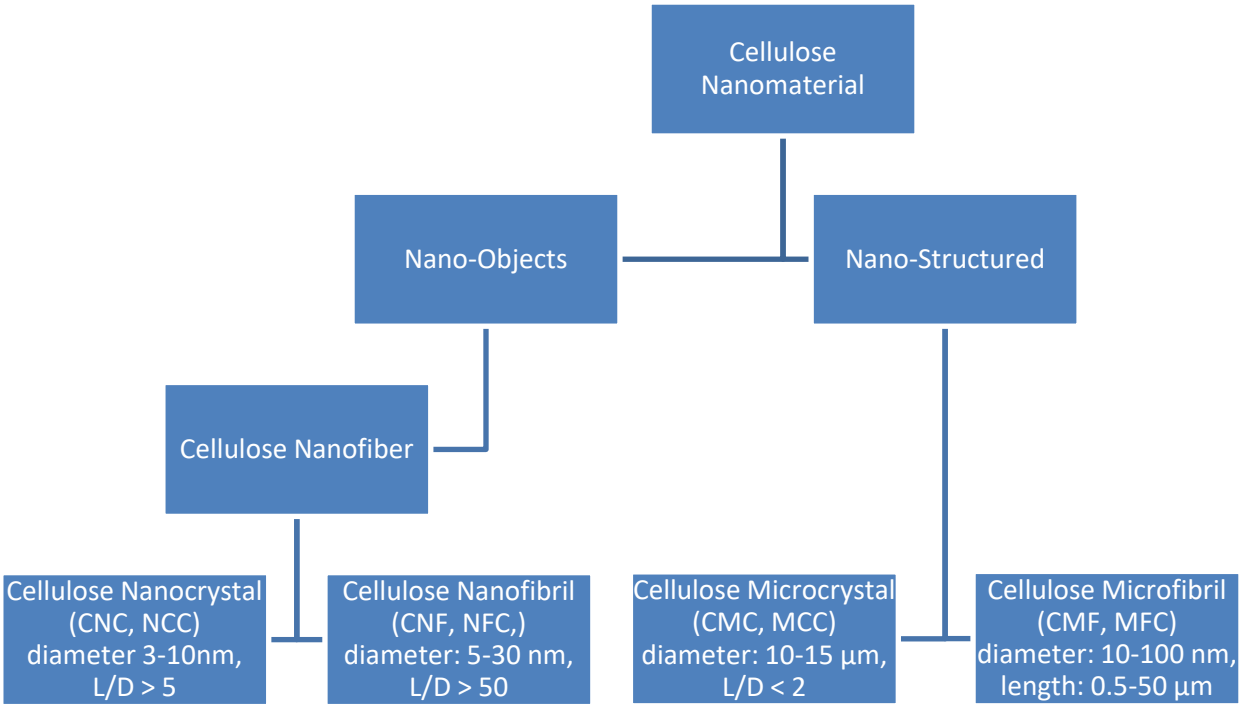

Figure 1-11. Hierarchy of nanofibers.

Table 1-4 Abbreviations used in cellulose nanomaterials - defined

Abbreviation		Diameter Range	Length	Aspect Ratio
NFC, CNF[34]	Nanofibrillated cellulose, Cellulose Nanofibrils	5-30 nm	> 1000 nm	> 50
CNC[35], NCC	Crystalline nanocellulose, nanocrystalline cellulose	3-10 nm	50-500 nm	< 5
MFC[34], CMF	Microfibrillated Cellulose, cellulose microfibril	10-100 nm	500-10,000 nm	50-100
CMC, MCC	Cellulose microcrystal, microcrystalline cellulose	>1000 nm	>1000 nm	<2
Tracheid	Wood cell	10-50 microns	1-3 mm	

Variations in nanofibers produced arise from three areas; 1) the source of the cellulose fibers, 2) the method used to extract and produce the nanofibers, and 3) the surface chemistry of the fibers[36]. The surface chemistry of the fiber dictates how the nano material will behave in suspension. While the morphology will effect how the material functions in a composite[37].

1.3 *Objective and Hypothesis*

The aim of this research is to develop a "green" method for producing nanofibrillated cellulose from either bleached or unbleached agricultural residues. The impact and contribution to knowledge this project has comes from the displacement of environmentally hazardous treatment methods with an environmentally non-hazardous, inexpensive, and tunable oxidant, ammonium persulfate – applied to agricultural residual biomass. Ammonium persulfate has been shown to be a suitable oxidant to produce nanofibrillated cellulose with indication that it may also be applied to lignin containing biomass. Through careful control of treatment conditions, ammonium persulfate oxidation of lignin and lignin-free fibers will produce nanofibers with specific morphological and chemical characteristics. This dissertation will expand on prior research in both chemical oxidation of cellulose fibers and utilization of agricultural residuals while working towards an environmentally green method.

1.4 *Reference Biomass*

The assessment of analytical methods and response to ammonium persulfate oxidation require a reference biomass that is suitably pure and provides a homogenous sample for testing. Bleached Northern Softwood Kraft has been selected as a reference material. It has been thoroughly

characterized and contains no components that would interfere with treatments. Bleached Northern Softwood Kraft, BNSWK, was supplied by the Westrock pulp mill in Tacoma, Washington. It is composed of Western hemlock, *Tsuga heterophylla*, and Douglas fir, *Pseudotsuga menziesii*. The mixture of fibers is approximately 50:50 by weight. The overall LWW fiber length of the mixture is approximately 3 mm. The lignin content of the fibers is not detectable.

Assessing Hop bine requires a suitable lignin containing reference biomass. Lignin containing Unbleached fiber (UB-NSWK, 4% lignin) was also supplied by the WestRock, Tacoma, WA pulp mill, taken prior to the bleaching. It represents an identical fiber composition to the bleached softwood reference biomass. Hop bine (*Humulus lupulus L.*) was kindly supplied by Roy Farms, Moxee, WA.

1.5 *Dissertation Overview*

Chapter 2 will evaluate the environmental impact that removal of hop bine residual has on the overall Hop cultivation and harvesting enterprise through a Life Cycle Assessment (LCA). The assessment will include modeling of soil organic carbon sequestration and denitrification, a sensitivity analysis, and a meta-analysis using the nearest relative to hop bine, industrial hemp. A step pursued in parallel to the LCA is to characterize the morphological features and chemical composition of the residual biomass from hop agriculture – results presented in Chapter 3..Analytical methods, SEM and XRAY-CT, will be utilized to elucidate the macro and micro structure of the bine. HPLC, IR, and UV will be employed to characterize the chemical composition. The fourth chapter presents the process, results, and discussion of the quantitative determination of the fiber response to oxidation with ammonium persulfate, a green chemistry, on

a lignin free benchmark biomass, bleached Northern Softwood Kraft, and on a lignin containing agricultural residual, Hop Bine. Response surface methodology (RSM) will be used to develop model equations for the response of crystallinity, fiber length and diameter, and surface charge. The physical response to varying the level of NFC fibers in a fiber composite, paper, from bleached Northern Softwood Kraft against varying the surface charge of the NFC fibers will be assessed in Chapter 5. The surface charge on the nanofibers can influence electrostatic repulsions between fibers and the interaction with high molecular weight polymer retention chemicals. The experiments will demonstrate the impact of engineered fibers on the physical structure and strength of NFC reinforced papers. Finally, Chapter 6 summarizes the results and conclusions of this work and discusses the extension of this research in future work.

References

[1] Caffrey, K. R., Veal, M. W.,Conducting an agricultural life cycle assessment: Challenges and perspectives. *The Scientific World Journal*, **2013**, 1–13. https://doi.org/10.1155/2013/472431

[2] Anwar, Z., Gulfraz, M., Irshad, M., Agro-industrial lignocellulosic biomass a key to unlock the future bio-energy: *A brief review. Journal of Radiation Research and Applied Sciences*, **2014**, 7(2), 163–173. https://doi.org/10.1016/j.jrras.2014.02.003

[3] Ragauskas, A. J., Williams, C. K., Davison, B. H., Britovsek, G., Cairney, J., Eckert, C. A., Frederick, W. J., Hallett, J. P., Leak, D. J., Liotta, C. L., Mielenz, J. R., Murphy, R., Templer, R., Tschaplinski, T., The path forward for biofuels and biomaterials. *Science*, **2006**, 311(5760), 484–489. https://doi.org/10.1126/science.1114736

[4] U.S. DOE. 2015. Lignocellulosic Biomass for Advanced Biofuels and Bioproducts: Workshop Report, DOE/SC-0170. U.S. Department of Energy Office of Science. (p. 3)

[5] The Freedonia Group. (2020). (rep.). Packaging Films: United States (pp. 1–32). Cleveland, OH: Freedonia Focus Reports.

[6] Gagliardi, M., Gobal markets and technologies for nanofibers., *BCC Research*, **2019**, NAN043E, 1–206.

[7] Varotto, A. (2015). (rep.). Cellulose Nanoparticles: Processing, Applications and Global Markets (Vol. AVM120A, pp. 1–166). Wellesley, MA: BCC Research.

[8] Springer, N., Kaliyan, N., Bobick, B., Hill, J., Seeing the forest for the trees: How much woody biomass can the Midwest United States sustainably produce? *Biomass and Bioenergy*, **2017**, 105, 266–277. DOI:10.1016/j.biombioe.2017.05.011

[9] Food and Agricultural Organization of the United Nations. (2017). Pulp and paper capacities capacités de la pâte et du papier capacidades de pasta y papel 2012-2017. Rome, Italy. ISSN 0255-7665

[10] Deleuran, L. C., Flengmark, P. K., Yield potential of hemp (cannabis satival.) cultivars in Denmark. *Journal of Industrial Hemp*, **2006**, 10(2), 19–31. DOI:10.1300/j237v10n02_03

[11] Devine, W. D., Harrington, T. B., Terry, T. A., Harrison, R. B., Slesak, R. A., Peter, D. H., Harrington, C. A., Shilling, C. J., Schoenholtz, S. H., Five-year vegetation control effects on aboveground biomass and nitrogen content and allocation in Douglas-fir plantations on three contrasting sites. *Forest Ecology and Management*, **2011**, 262(12), 2187–2198. DOI:10.1016/j.foreco.2011.08.010

[12] Food and Agriculture Organization of the United Nations. (2019). FAOSTAT Database. Rome, Italy: FAO. Retrieved July 7, 2021 from http://www.fao.org/faostat/en/#data/FO

[13] Zhuang, Z., Ding, L., & Li, H. (2008). China's Pulp and Paper Industry: A Review*. School of Economics Georgia Institute of Technology, 1–71.

[14] Tullis, Russell & Co. Ltd, Papermaking fibres. **1950**, Markinch Fife, Scotland.

[15] Reddy, N. (2009). Properties of natural cellulose fibers from hop stems. Carbohydrate Polymers, 77, 898-902. DOI: 10.1016/j.carbpol.2009.03.013

[16] Cim, A. (1905). Le livre : historique, fabrication, achat, classement, usage et entretien. Paris: Flammarion.

[17] Papier du guimauve | Graphic Arts. (2017, September 11). Retrieved January 03, 2018, from https://graphicarts.princeton.edu/2017/09/11/papier-du-guimauve/

[18] Yang, W. (2015). Elevating the fuel properties of Humulus lupulus, Plumeria alba and Calophyllum inophyllum L. through wet torrefaction. Fuel, 146, 88-94.

[19] Customer conference [Personal interview]. (2017, December 28).

[20] China Imports of Paper Pulp 1996-2018 | Data | Chart | Calendar. (n.d.). Retrieved January 07, 2018, from https://tradingeconomics.com/china/imports-of-paper-pulp

[21] Retrieved December 27, 2017, from https://nassgeodata.gmu.edu/CropScape/

[22] United States, United States Department of Agriculture, National Agricultural Statistics Servie. *National Hop Report*, **2016**, (pp. 1-8). Washington, DC: USDA.
ISSN: 2158-7825

[23] Medronho, B., Romano, A., Miguel, M.G., Stigsson, L., Lindman, B., Rationalizing cellulose (in)solubility: reviewing basic physicochemical aspects and role of hydrophobic interactions. *Cellulose*, **2012**,19:581–587

[24] French, A.D., Glucose, not cellobiose, is the repeating unit of cellulose and why that is important. *Cellulose*, **2017**, 24:4605-4609. doi 10.1007/s10570-017-1450-3

[25] ACD/ChemSketch, version 2021.1.3, Advanced Chemistry Development, Inc., Toronto, ON, Canada, www.acdlabs.com, 2021.

[26] Christakopoulos, P., Organosolv Fractionation of Softwood Biomass for Biofuel and Biorefinery Applications. *Energies*, **2018**, 11(50), 1-23.

[27] Nicholson, D. J., Estimation of the S/G ratios of lignins in three widely used North American Hardwoods. *TAPPI Journal*, **2016**,15(7), 449-457.

[28] Colodette, J. L., On the importance of raw material assessment and selection for low cost Eucalypt Kraft pulp production. *13th European Workshop on Lignocellulosics and Pulp*, **2014**, De Gruyter, Berlin

[29] Calvo-Flores, F., Lignin and Lignans As Renewable Raw Materials : Chemistry, Technology and Applications (1st ed.)., **2015**, John Wiley & Sons, Inc.

[30] Li, J., Rapid method for determination of carbonyl groups in lignin compounds by headspace gas chromatography. *Journal of Chromatography A*, **2015**, 1404, 39-43. DOI:10.1016/j.chroma.2015.05.055

[31] J. Gierer, Über die Carbonylgruppen des Lignins, Acta Chem. *Scand*., **1959**, 13 pp. 127-137

[32] TAPPI WI 3021 - Standard Terms and Their Definition for Cellulose Nanomaterial. (n.d.). 2013, Atlanta, GA.

[33] Osong, S.H., Norgren, S., Engstrand, P. Processing of wood-based microfibrillated cellulose and nanofibrillated cellulose, and applications relating to papermaking: a review. *Cellulose*, **2016**, 23, 93–123 DOI: 10.1007/s10570-015-0798-5

[34] Moon, R. J., Schueneman, G. T., Simonsen, J., Overview of Cellulose Nanomaterials, Their Capabilities and Applications. Jom, **2016**, 68(9), 2383–2394. DOI: 10.1007/s11837-016-2018-7

[35] Börjesson, M., Westman, G., Crystalline Nanocellulose — Preparation, Modification, and Properties. Cellulose - Fundamental Aspects and Current Trends., **2015**, DOI: 10.5772/61899

[36] Foster, E. J., Moon, R. J., Agarwal, U. P., Bortner, M. J., Bras, J., Camarero-Espinosa, S., Chan, K. J., Clift, M. J., Cranston, E. D., Eichhorn, S. J., Fox, D. M., Hamad, W. Y., Heux, L., Jean, B., Korey, M., Nieh, W., Ong, K. J., Reid, M. S., Renneckar, S., Youngblood, J., Current characterization methods for cellulose nanomaterials. *Chemical Society Reviews*, **2018**, 47(8), 2609–2679. DOI:10.1039/c6cs00895j

[37] Thomas, B., Raj, M. C., B, A. K., H, R. M., Joy, J., Moores, A., Drisko, G. L., Sanchez, C., Nanocellulose, a versatile green platform: From Biosources to materials and their applications. *Chemical Reviews*, **2018**, 118(24), 11575–11625. DOI:10.1021/acs.chemrev.7b00627

Chapter 2. Life Cycle Assessment of Humulus lupulus

2.1 Introduction

Low density biomass resources such as *Humulus lupulus* are handicapped by high transportation costs due to widely distributed – low density acreage and the need for densification of the biomass[1]. Fast pyrolysis to bio-oil has been proposed as once such method of densification[2]. Although Bio-oils are CO_2 – greenhouse gas neutral providing a significant environmental advantage over fossil fuels, densification assumes that local processing facilities exist and that the yield of the product is sufficient to produce an economically viable product[3].

Onsite bioconversion to nanocellulose using an ammonium persulfate oxidation where low biomass density and transportation costs result in high cost may be a viable alternative to composting. Bio-char produced from agricultural residuals, for example, can be utilized as a soil amendment[4]. Soils in the Columbia River Watershed may benefit from the returning carbon to the soil; however, the removal of nitrogen may increase the demand for inorganic fertilizers. A green process such as ammonium persulfate would allow not only carbon sequestration but could return nitrogen and sulfur to the soil. This study focuses instead on the impact removing hop bine from the agricultural enterprise has on soil carbon sequestration and denitrification. The outcome of this Life Cycle Assessment can be utilized to evaluate the potential for turning the agricultural residue, Humulus lupulus bine, into a specialty fiber using a green chemistry.

First, using remote sensing data, the cultivated areas specific to Roy Farms (Moxee, WA) was assessed for environmental conditions, soil viability, physical arrangement, and residual biomass yield potential.

This Life Cycle Assessment aims to assess the impact of segregating the residual woody waste (co-product) of an agricultural crop, hops (*Humulus lupulus)* on the greenhouse gas (GHG) emissions and on soil carbon sequestration. Humulus lupulus varieties are grown in eastern. Washington and account for over 79% of the total US production. Although hops cultivation is not the largest agricultural crop in the Yakima Valley; accounting in 2016 for only 1.2% of total cultivated acreage or 44,552 acres. An examination of geographical information system data for the Yakima valley has shown an 80% increase in cultivated acreage from 2014 to 2016,see Figure 2.1

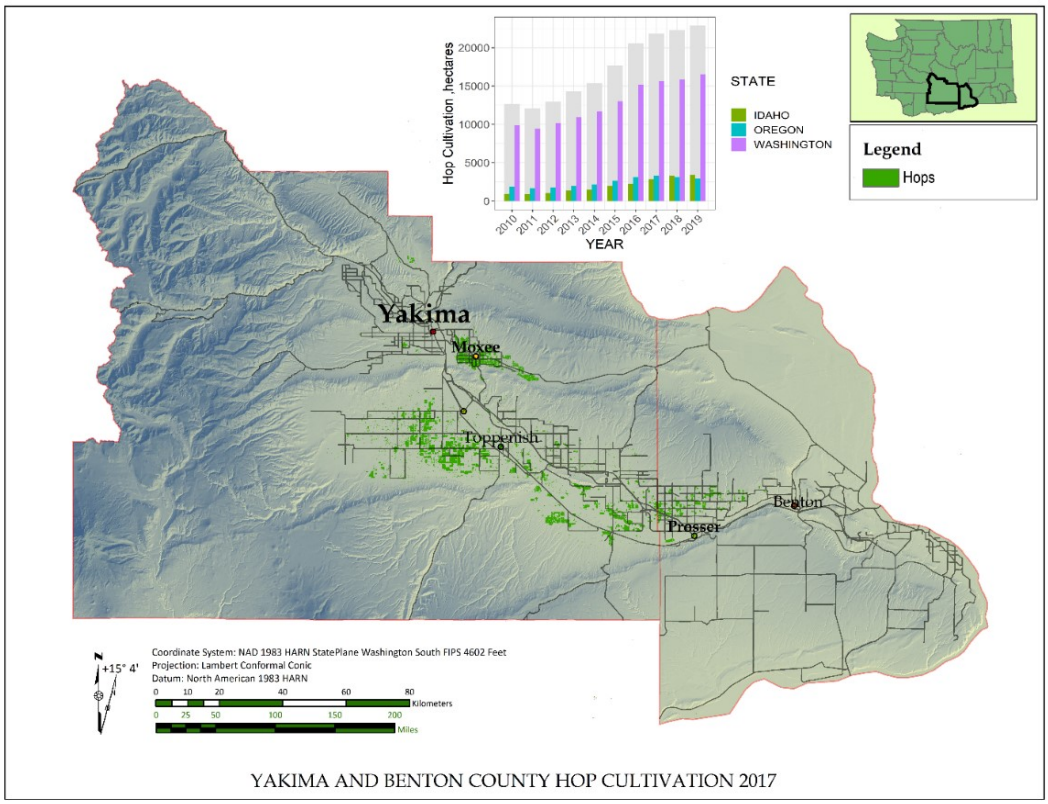

Figure 2.1. Yakima and Benton counties – hop cultivation in 2017.

The secondary biomass from hop cultivation is a mixture of non-woody residues (leaves and hop cone) and woody residue (bine). These end up as silage. The woody residue is the primary source of cellulosic fiber in the hop plant and with the increase in cultivated acreage may represent

a significant source of lignocellulosic biomass. Competition between agriculture dedicated to food production and dedicated to biofuel production has led to increases in food costs as land is turned over to the higher value crop. Unfortunately, low density biomass resources such as *Humulus lupulus* are handicapped by high transportation costs due to widely distributed – low density acreage and the need for densification of the biomass[1]. If this material could be utilized as a co-product, it is important to understand the impact that would have on the environment.

Published life cycle assessments focused on agricultural residues are dominated by biofuel crops[5], such as soy, corn, and wheat straw[6,7,8,9]. The only reference to hops found in published LCA's is limited to treatment as an input in life cycle assessments of beer production[10,11,12,13,14]. These agricultural residue Life Cycle Assessments however are relevant in consistent treatment of lignocellulosic biomass and form a model that can be applied to other lignocellulosic residues. Liu used a comprehensive assessment of environmental impacts; The Tool for the Reduction and Assessment of Chemical and other environmental Impacts (TRACI[15]) and defined the functional unit of well−to−wheels (WTW). Liu also used a hybrid model incorporating an economic analysis. Searcy discusses a gate-to-gate (GTG) LCA methodology that is likely more relevant in that it treats the harvesting and delivery of the raw material to the processing site. Both studies form a relevant basis of comparison as they both deal with the geographic areas of the mid-western United States. Shen used a different model to evaluate agricultural residue, GREET. None of these studies evaluated the positive or negative impact from that material being removed from the base system. Comparisons were made to other agricultural residues including forest residues.

2.2 Proposed LCA

There are several databases and models that can be used to provide and evaluate data that may be useful in the LCA study. Christensen evaluated the alternative treatment of waste streams using the EASEWASTE[16] composting module to model spreading of compost on farmland[17]. This is the practice Roy Farms engages in currently. Unfortunately, this database is no longer available having been replaced with a new model, EASETECH. The new model is available to researchers after completion of a 3-week course of study. Several other open access models were identified, but none provide all encompassing information. As a result, several models will be used to acquire the data necessary combined with literature and primary laboratory data. GREET, IPCC Inventory Software, DNDC model, and open LCA will be used to obtain foreground data. There is no need to model the reaction chemistries involved using programs such as Aspen as they are all first order reactions. Mass balances for determining allocation between products and co-products and stoichiometric balances for nutrients and emissions will be calculated using Microsoft Excel. USDA databases were not available at the time of this study due to the government shutdown[18].

The following environmental impact categories are proposed to be assessed; global warming (GWP), water cycle (WC), soil organic carbon (SOC), photochemical oxidant creation (POCP), eutrophication (EUT), and fossil fuel (FF).

The key difference between this LCA and those published in literature is that this proposal does not address production of a biofuel or energy conversion. It will examine removing this material from the existing lifecycle to use in other non-energy applications. The resulting LCA will have both open-loop and closed loop process flows. The subsequent treatment of residual hop bine as a co-product is open-loop, while the return of the non-woody residue after composting is considered close-loop. The secondary co-product will be an output of this life cycle assessment

to be then used as the raw material input in a second system. As stated by Olofsson (2018) it is the intersection of two LCA's[19].

2.2.1 Goal

This Life Cycle Assessment aims to apply methodologies to assess the impact of separating the residual woody waste (co-product) of an agricultural crop, hops (*Humulus lupulus)* from the total residual biomass. The non-woody waste separated will be spread on the fields after composting. Organic agriculture views this as a means of sequestering carbon in the soil and thus mitigating some aspects of climate change[20]. According to Petersen (2013) sequestering carbon in soils is not adequately addressed in current Life Cycle Assessments. Hop growers, their soil scientists, and those who manage this agricultural business need to understand the impact of backing up from organic agriculture to the conventional practices that may be required to offset the loss in nutrient potential caused by the removal of a portion of residual and substituted with inorganic fertilizers[21]. This Life Cycle Assessment will be used to make strategic decisions regarding the utilization of this lignocellulosic co-product and improve the understanding the residual biomass has on over-all soil carbon sequestration[22] and greenhouse gases (GHGs) emissions. The study area selected is the land cultivated by Roy Farms, Incorporated in the Yakima valley. Roy Farms is located in Moxee, Washington at 46°33′23″N, 120°23′14″W in Yakima County.

2.2.2 Scope

The existing process takes all residual biomass separated from the primary product, composts it, and then returns it to the field in a no-tillage manner. The composting process is

atmospheric – open ground composting. In the proposed process, the woody residual biomass is mechanically separated as a new co-product for use in a secondary application such as a feed for nanofibrillated cellulose or in the conversion to biochar. The system describing the existing and proposed production of hops is a combination of mechanical separation of primary plant product, hop cone, from the lignocellulosic co-product, thermal dehydration, composting, and physical transport functions. Utilization of the non-woody biomass as compost will reduce the demand for inorganic fertilizers[16]. The life span the hop plant is managed to is 5 years, at which point the fields are replanted with new rhizomes. The average volume of hops produced per hectare is 1960 kilograms[23].

2.2.3 Functional Unit

The functional unit will be 1 kilogram of good hop cone produced. The production from one hectare of land during a single growing season, a year, will be the basis for the analysis. This is consistent with the LCA report provided by Roy Farms[24]. The co-product will be expressed as kilograms/ kilogram of hop cone produced[25].

2.2.4 Geographic Region

The use of geographical information system (GIS) software, ArcGIS, adds a dimension to the life cycle assessment of hop cultivation[26]. Spatial data was categorized into three aspects; landscape features, climate, and land assignment. Landscape features include soil type and quality, and elevation. Climate features are composed of rain fall and temperature statistics. Land

assignment is data specific to county parcel maps designations and parcels dedicated to hop cultivation.

The study area selected is the land cultivated in 2017 by Roy Farms, Incorporated in the Yakima valley. Roy Farms is located in Moxee, Washington at 46°33′23″N, 120°23′14″W in Yakima County. Hop cultivation is predominantly in Yakima County with a small percentage in Benton counties. Hence, the layer displayed in Figure 2.2 shows the county boundary shape file over lay on a Washington state base map[27] for both Yakima and Benton counties. The Columbia River watershed boundary is depicted in light blue. Yakima and Benton counties are shown in light yellow[28]. The boundary of the Columbia River Watershed (Basin) feature layer represents the drainage area of the Columbia River. It was obtained from the Watershed Boundary Dataset (USGS) from the United States and Work Units from the Canadian National Hydrography Network (Base Mapping and Geomatic Service, Integrated Land Management Bureau, BC, Canada)[29]. The layer was projected to the spatial coordinate system WGS 1984 Web Mercator Auxiliary Sphere. The Yakima and Benton counties feature layer was projected to the common spatial coordinate system NAD 1983 HARN State Plane Washington South FIPS 4602 Feet. Using a definition query, Yakima and Benton counties were selectively displayed and shaded.

Figure 2.2 Columbia River Watershed with Yakima and Benton valley overlay.

2.2.5 Definition of co-product and waste residues, reference flows

Biomass residue will be defined either as a co-product or as a compostable residue based on the potential use as determined by the physical and chemical properties of the material. These properties are bulk density, carbohydrate composition, and % yield. Process economics will not be used to delineate a residual biomass as co-product as that is specific to the definition of the subsequent process.

Table 2.1. Reference Flows for one hectare of land

Input	**Unit**	**Quantity[23]**
Nitrogen[30,31]	Kg	203.47
Phosphorous[30,31]	Kg	33.91
Potasium[30,31]	Kg	135.65
Lime (CaCO)[32]	Kg	33.91
Coir Rope	Kg	131.23
Water[33]	Liters	2,746
Land Use[34]	Hectare	1
Diesel[35]	L	271.8
Gasoline[35]	L	143.32
Natural Gas[35]	kg	0.38
Magnesium[36]	kg	566.9
Sulfates	kg	113.4
Zinc	Kg	28.35
Iron	Kg	56.7
Manganese	Kg	22.68
Copper	Kg	6.8
Boron	kg	6.8

Output[37]	**Unit**	
Hop Residual Total	kg	4820
Woody-Residual	Kg	1520
Non-woody Residual	kg	3300
Hop Cone	kg	1960
Root System[53]	Kg	2305

The reference flows represent the average requirements for a hop grower to produce the USDA average yield of hop cones per hectare[23]. Co-product yield is based on the primary product yield. Although much of the soil amendments are less than 1% of the mass of product produced, they are essential to the agriculture and will not be included in any cutoffs, see Table 2.1.

.

2.2.6 *System Boundary*

The system boundary for this Life Cycle Assessment is the flows that encompass the boundary of the farm. Crop residue will be defined as the non-edible plant component separated from the hop cone. It will include the rope (coir or sisal) used in the trellis and hop cone losses. The process includes cultivation of hops, harvesting, soil treatment (fertilization), pesticide application, co-product separation/segregation, composting, compost return, drying, and transportation. The top cutter and bottom cutter tractor attachment remain in the field. Transportation of hop bines from the field to the processing plant is by ¾ ton pick-up trucks. The average transportation distance is 2 miles from field to processing plants. Roy farms locates its' processing points to minimize transportation and product losses. Processing will include the separation of hop cone from the bine, chipping of the residual biomass, and separation of the non-woody residual from the woody residual, see Figure 2.3 for LCA system boundary.

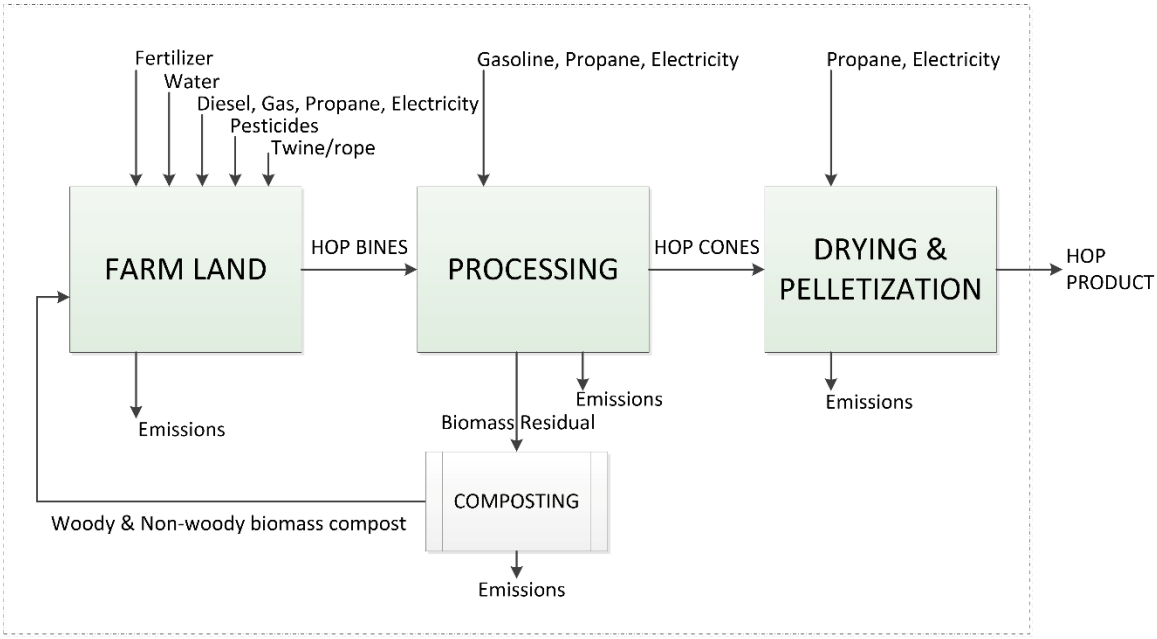

Figure 2.3. System boundary with removal of woody-residual co-product

The boundary will be farm gate-to-farm gate[38]. Using this as a guide for determining the allocation limits, there are a considerable number of inputs entering a farm, such as materials for repairing trellis, waste products from the maintenance of equipment, etc. These items are not bound by the temporal constraints of hop cultivation and represent a variable input to the farm. Variable inputs that represent less than 1% of the mass a kilogram of hop cone will be disregarded for this analysis. Variable inputs that are greater than 1% will be averaged and normalized against 1 kg of oven dry hop cone produced annually per acre over a period of 5 years (useful life of hop plant). Dividing the overall system boundary into modules will help manage the material balances and validate the allocation, see Figure 2.4.

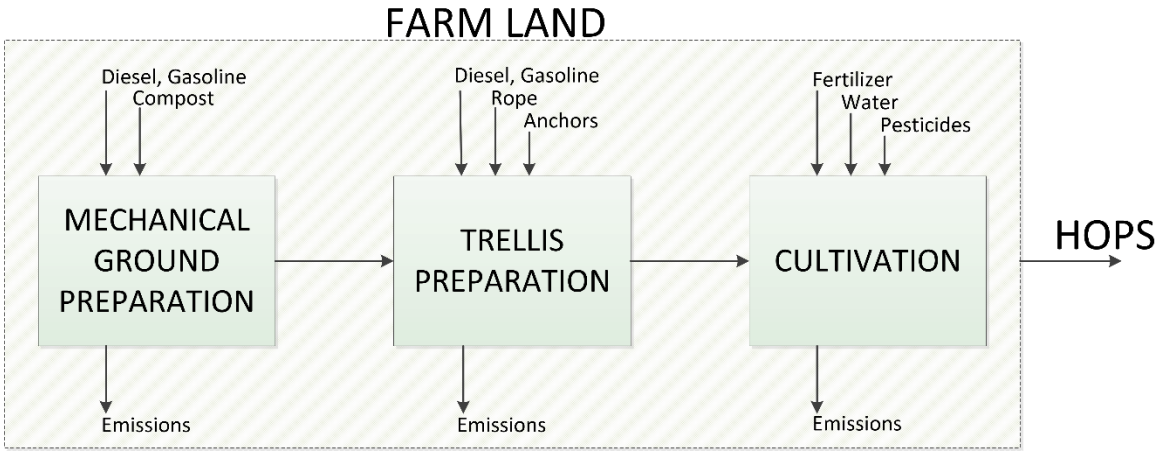

Figure 2.4. Farmland Module – subsystem boundary

2.2.7 *Methodology*

The impact assessment will utilize an attributional Life Cycle Analysis methodology to determine the environmental impacts of removing a portion of the residual biomass co-product from carbon sequestration in the soil. The linear algebraic mathematical model described in Heijungs will be used to construct the linear space describing both the technology matrix and

intervention matrix associated with the primary product, hop cone production, and the secondary co-product, residual biomass[39]. A process vector, Þ, will be defined to represent the flow of fertilizer, water, electricity, fossil fuels, and consumables using the convention that a negative coefficient indicates an input to the system and a positive an output of the process. A process matrix, P, will be defined for the set of process vectors described by Þ. The portioning of this matrix will follow the technology and intervention matrices, designated A and B respectively. This method will be applied to all process matrices developed in solving the resultant vector R.

GREET and ReCiPe will be used for background data for water, fossil fuel, and energy consumption. There are several crop residuals that could be used as a basis. Intergovernmental Panel on Climatic Change (IPCC) methods will be used for emission source data. The emission factor database will be utilized for greenhouse gas data. The ReCiPe database will also be used for toxicity analysis[40]. The significant number of midpoint indicators may be shortened for this analysis due to some regional climate and soil constraints. OpenLCA has some data specific to agricultural cultivation. Another tool – CTool, has been identified for evaluating the change in carbon sequestration. However, due to time constraints, this tool may not be realistically applied until a subsequent LCA. Additional investigation is required to determine geographic constraints of data required by the tool.

Global Warming Potential (GWP) for greenhouse gases will be expressed as kg CO_2-equivalents per kg for each gas[41].

$$GWP = \sum_i GWP_i * m_i \quad (2\text{-}1)$$

Eutrophication or nutrient enrichment potential (EP) of aquatic systems is primarily driven by nitrogen and phosphorous. The eutrophication potential will be expressed as an equivalent emission of the reference substance NO_3^-. Acidification Potential (AP) will be calculated based on SO_2 equivalents[42]. Acidification Potential refers to the emission of acidifying substances that impact soil, groundwater, and fresh water runoff. The equivalent factor (EF) is calculated based on stoichiometric chemical balances as follows;

$$EF = \frac{n}{2*MW} * 64.06 \qquad (2\text{-}2)$$

MW is the molecular weight of the substance emitted [g/mole], n is the number of hydrogen ions released by the target chemical, and 64.06 g/mole is the molecular weight of SO_2.

Table 2.2. Impact Categories.

Impact Category	Abbreviation	Unit
Global Warming Potential	GWP	CO_2-eq/kg
Eutrophication Potential	EP_N	N/kg
Eutrophication Potential	EP_P	P/kg
Acidification Potential	AP	SO_2-eq/kg
Carbon Sequestration	CS	kg C/acre/year
PMFP	P	PM2.5-eq/ kg

2.2.8 *Data Quality*

Agricultural yields are impacted by seasonal weather conditions and local soil quality. Data will be taken over several years to reduce the seasonal variability. Operational data will be drawn directly from Roy Farms. Compositional data will be taken directly from laboratory analysis performed on the residual biomass. Where data is unavailable for this crop, similar crops will be identified and utilized to provide missing information – for example industrial hemp

cultivation. Mass balance will be utilized to verify calculated data against published specifications for the product, for example the water consumption reported in the Roy Farms Sustainability report accounted for all water usage across all agricultural products and was not limited to hop production.

The two-tiered data quality analysis method for rating data presented by Cooper (2012) will be utilized,[43], see Table 2.3. Mass and energy balances will be applied as a data validation tool. Uncertainty will be described with statistics where possible. Geographic coverage will be established using ArcGIS software. A literature review on Humulus lupulus was performed focusing on impact category results and denitrification modeling to be used in a meta-analysis. Literature data will be normalized to 1 kg of oven dry raw biomass.

Table 2.3. Two-tiered data quality score[43]

Category	Requirements for a data quality score of A
1. Reliability and reproducibility	The flow data were based on measurements using a specified and standardized measurement method OR The flow data were estimated using methods and data described in specified archival or other consistently publicly available sources.
2. Flow data completeness	The flow data were collected over at least 3 years for agricultural (crop, livestock, forest and range) processes or other processes in which the data point varies for uncontrolled annual conditions (e.g., weather) AND The flow data balance the mass and energy in and out of the unit process.
3. Temporal coverage	The flow data represent operations that occurred between the unit process start and end dates without forecasting.
4. Geographical coverage	The flow data represent operations that occurred within the location of the unit process including nonagricultural process data that have been adapted to reflect logistics and market shares for the unit process location.
5.Technological coverage	The flow data represent the process(es) and/or material(s) specified without surrogacy or aggregation with other technologies.
6. Uncertainty	The flow data either include estimates of the first quartile, mean, median and third quartile values OR data or probability distribution from which these values can be estimated.
7. Precision	The relative standard error of the flow data is less than or equal to 25% OR the interquartile range divided by the median is less than or equal to 50% OR for a triangular distribution, the minimum flow data value is .75%, and maximum flow data value is .125% of the most likely value OR for a uniform distribution, the minimum flow data value is .75%, and maximum flow data value is .125% of the average of the minimum and maximum values.

2.3 Inventory Analysis

2.3.1 Data Collection

The data provided in the LCA's for the hop growers often included information for other crops produced by their farm. In these instances, hop agriculture guides were consulted in order to determine the specific requirements for the cultivation of the plant[30,36]. Nutrient requirements were calculated to produce 1960 kg of hop cone per hectare per year, see Table 2.4.

Table 2.4. Recommended nutrient levels for hop cultivation[36].

Nutrient		Minimum Level (PPM)	kg/Hectare
Nitrogen (Nitrates)	NO_3-N	40	181.4
Phosphorous	P	25	113.4
Potassium	K	120	544.3
Calcium	Ca	1800	7937.9
Magnesium	Mg	125	567.0
Sulfates (Sulfur)	SO_4-S	25	113.4
Zinc	Zn	6	28.3
Iron	Fe	12	56.7
Manganese	Mn	5	22.7
Copper	Cu	1.5	6.8
Boron	B	1.5	6.8

Table 2.5. Nutrient content of above ground biomass.

Allocation	Percentage	Units	Calculated Value - kg/Ha
Nitrogen (Cone)	3%	kg/Ha	60.81
Nitrogen (bine)	1%	kg/Ha	15.19
Nitrogen (leaves)	3%	kg/Ha	99.04

An initial nitrogen mass balance of the hop cycle for one year was performed using Microsoft Excel. The nitrogen content of the hop biomass was found in a Washington State Department of Ecology report published in 1994 by Hermanson[44]. The data reported were converted into mass per hectare using the allocated mass determination, see Table 2.5. Data for

the nutrient content for the coir rope, Table 2.6, came from a research report that examined the content of coir dust[45] and a report that examined its' application as a biofertilizer[46].

Table 2.6. Coir rope nutrient allocation.

Nutrient	Composition		Allocation	
Nitrogen[46]	0.033	%	4.3	kg/Ha
Phosphorous[45]	10	ppm	1.3 E-03	kg/Ha
Potassium[45]	299	ppm	3.9 E-02	kg/Ha

During the separation process, this material is segregated with the woody biomass co-product. This information was used to determine the contribution of nitrogen from each category of biomass and the amount of inorganic fertilizer required to make up the nitrogen uptake by the biomass and through other emissions, Figure 2.5.

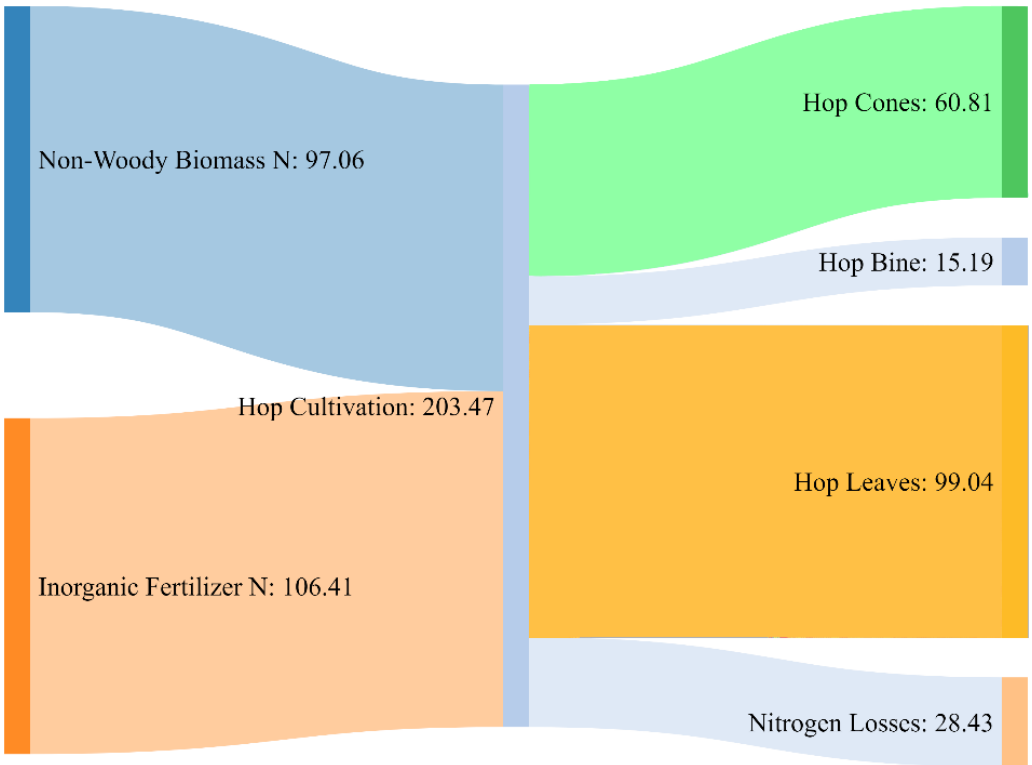

Figure 2.5. Initial nitrogen mass balance.

Data for irrigation life cycle assessments came from conference proceedings[47]. A drip line irrigation system is used in cultivation of hops which is reported to have the greatest impact on greenhouse gas emissions, 0.253 kg CO_2 per m^3. The Life Cycles for the production of urea-ammonium nitrate, phosphoric acid, potash, lime, diesel, gasoline, electricity, and natural gas were obtained using the GREET software. The application of lime was reported by Gingrich[32]. GREET was also used to determine the Life Cycle of each of the mineral nutrient soil amendments; magnesium, sulfates, zinc, iron, manganese and copper. The life cycle of boron could not be identified and so a hollow LCA was put in place. The Life Cycle of irrigation was established using ReCiPe2016[48], IPCC Inventory software, and data from the Hopsteiner LCA by Piroue[49]. The ReCiPe2016 model was used to determine the freshwater eutrophication from soil leachate.

Emissions generated from applying compost and inorganic fertilizer as soil amendments were modeled using the DeNitrification DeComposition (DNDC) agroecosystem model[50,51,52]. The model software was acquired from the Institute for the Study of Earth, Oceans, and Space at the University of New Hampshire[53]. Soil N_2O emissions vary with the type of nitrogen source applied to amend the soil. Denitrification and nitrification processes vary due to tillage practices and crop residue management. Goglio (2018) reported that applying the DNDC method resulted in data that was comparable to that derived from laboratory data produced for the same crop. Nutrient loss has been reported to have corresponding relationships with rainfall and the form of nitrogen input into the system[54].

Nitrification[55]

$$NH_4 + 1.5O_2 \xrightarrow{yields} NO_2^- + 2H^+ + H_2O$$

$$NO_2^- + 0.5O_2 \xrightarrow{yields} NO_3^-$$

Denitrification

$$5(CH_2O) + 4NO_3^- + 4H^+ \xrightarrow{yields} 5CO_2 + 2N_2 + 7H_2O$$

$$NO_3^- \rightarrow NO_2^- \rightarrow NO \rightarrow N_2O \rightarrow N_2$$

The library provided by the software included a hop crop data set. The data set included information for root biomass. This data was entered into the model for Roy Farms to update the biomass allocation. The library database in DNDC was then modified to match the yield data for one hectare of farm land for the Roy Farms basis. Soil nitrate and ammonium concentrations, 83.5 ppm and 21 ppm respectively, for eastern Washington soil were then entered into the model[56]. Additionally, the latitude and soil type were selected. A climate file was created for the Yakima valley and added to the model using data from US climate data for 2017[57]. Irrigation data was manually entered for the drip irrigation period for hop cultivation[58]. The scenario was then run for a one-year analysis.

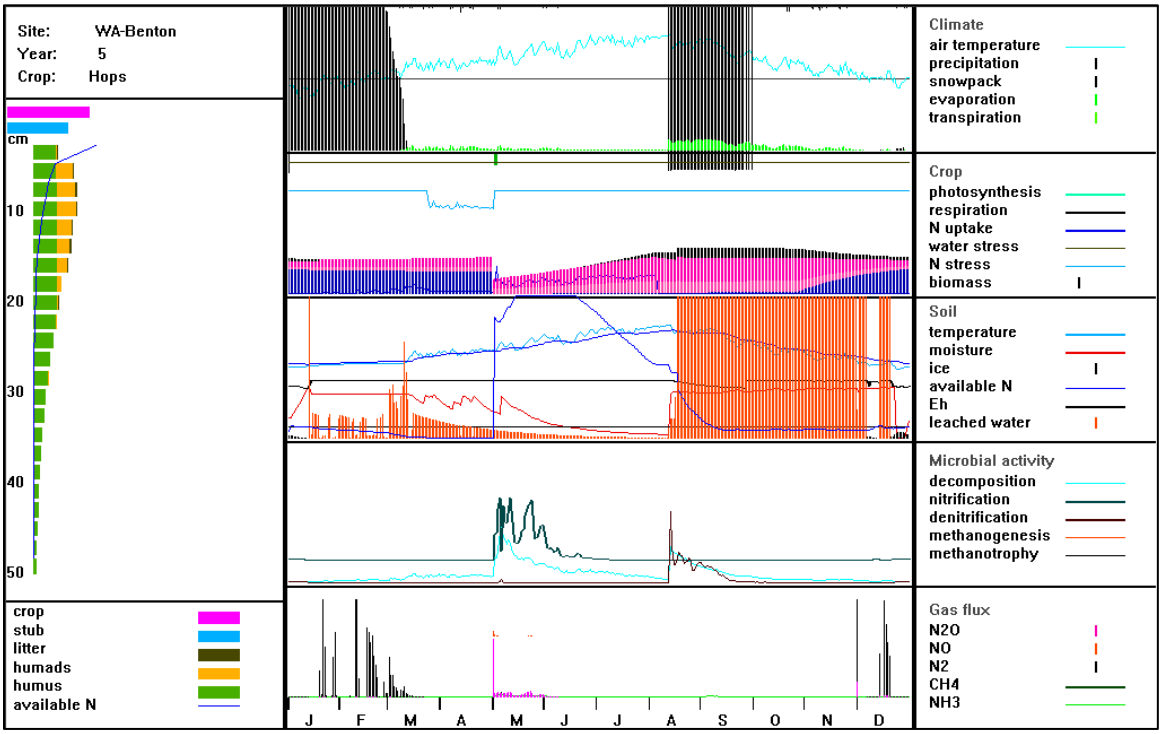

Figure 2.6. Simulation screen for hops grown in Benton County, Washington.

The regional input GIS file, usa6_53, provided by the software was selected that contained information by county GIS identifier[59] for Yakima (53077) and Benton (53005) counties.

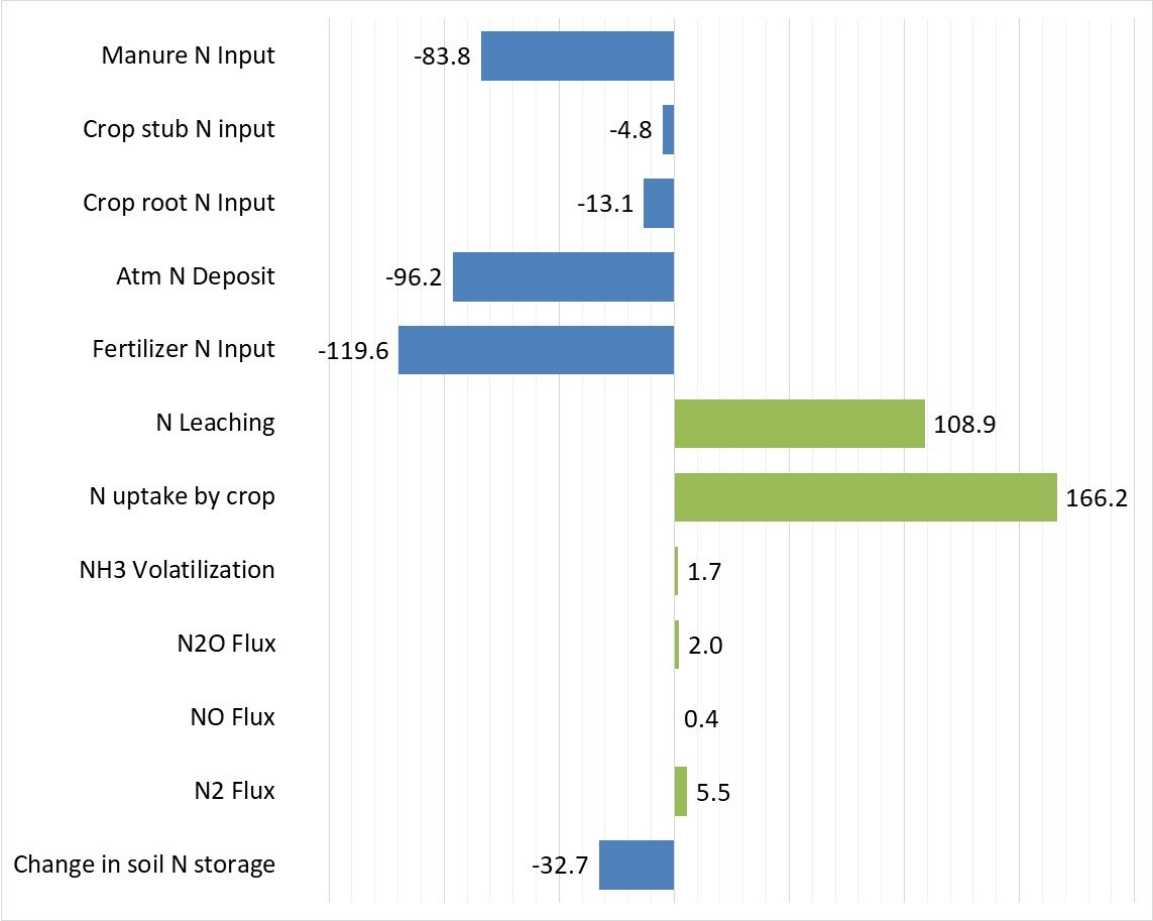

Figure 2.7. DNDC simulation result for Nitrogen (negative values indicate inputs)

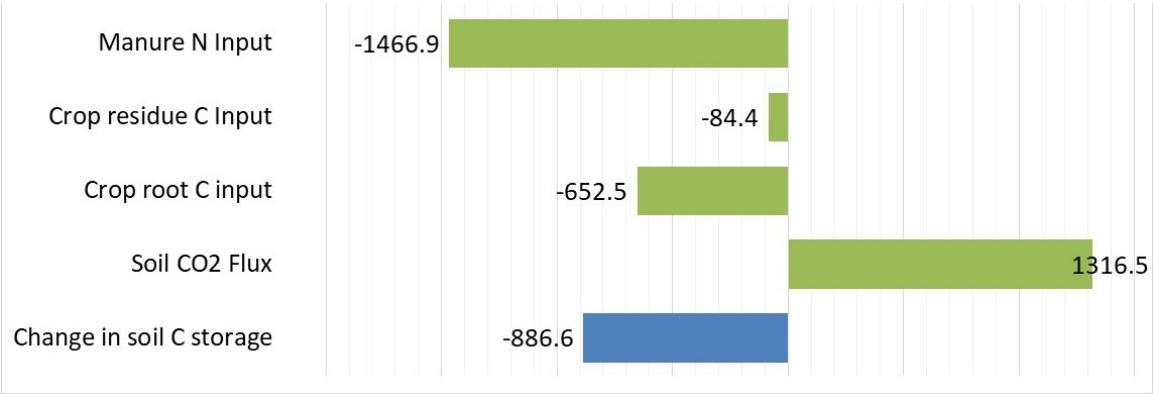

Figure 2.8 DNDC simulation result for carbon

2.4 Soil Analysis

Soil feature layers were sourced from the U.S. Department of Agriculture, Natural Resources Conservation Service. The layer contains information on soil type, the acreage attributed to that soil type, the soil class, and the National Commodity Crop Productivity Index (NCCPI) model rating. The average NCCPI index can then be determined for each specific field. The NCCPI index can be utilized to evaluate crop yields based on soil conditions for that field. NCCPI index data was acquired from reports generated on AcreValue website, see Table 2.7[60].

The parcel shapefile for Yakima County was obtained from the Yakima County GIS service[61]. A query was setup to select only those attributes matching the county assessor number for parcels owned by Roy Farms. 46 parcels (fields) owned by Roy Farms in Yakima County, a total of 2032 acres, was examined. Eight parcels accounting for 320 acres is designated as non-cropland. The parcels designated as cropland are a mixture of various crops, see Table 2.8.

Using the arctoolbox clip tool, the soils layer was set as the input, and the clip feature was the shapefile displaying only Roy farm parcels. The resulting shapefile isolated the soil data for Roy Farms. An example of 5 parcels is displayed in Figure 2.9.

Table 2.7. NCCPI data and soil type for Roy Farms parcels

Soil Description	Soil Code	Acres	%	NCCPI
Willis silt loam, 2 to 5 percent slopes	187	294.42	14.5	13.6
Ritzville silt loam, basalt substratum,	105	278.77	13.7	18.6
Moxee silt loam	83	156.8	77	9.9
Ritzville silt loam, basalt substratum	106	150.57	7.4	14.6
Willis silt loam, 8 to 15 percent slopes	189	118.40	5.8	13.1
Moxee cobbly silt loam	85	113.62	5.6	8.4
Willis silt loam, 5 to 8 percent slopes	188	102.20	5.0	13.5
Ritzville silt loam, 8 to 15 percent slopes	101	94.51	4.7	20.5
Ritzville silt loam, 2 to 5 percent slopes	99	88.58	4.4	21.3
Sinloc silt loam, 2 to 5 percent slopes	140	84.69	4.2	5.8
Starbuck-Rock outcrop complex	143	83.48	4.1	1.8
Warden silt loam, 0 to 2 percent slopes	176	55.67	2.7	15.3
Quincy loamy fine sand	95	46.91	2.3	10.6
Harwood-Burke-Wiehl silt loams	53	40.31	2.0	8.4
Kiona stony silt loam	65	36.59	1.8	4.3
Wanser loamy fine sand	171	36.29	1.8	3.3

Warden silt loam, 2 to 5 percent slopes	177	35.38	1.7	15.2
Ritzville silt loam, 30 to 60 percent slopes	103	31.91	1.6	4.9
Esquatzel silt loam, 0 to 2 percent slopes	32	28.71	1.4	20.6
Warden silt loam, 5 to 8 percent slopes	178	28.62	1.4	15.0
Harwood-Burke-Wiehl silt loams, 5 to 8 percent slopes	51	25.12	1.2	10.9
Harwood-Burke-Wiehl stony silt loams, 15- 30 % slopes	55	21.61	1.1	6.5
Outlook fine sandy loam	91	21.47	1.1	7.1
Sinloc fine sandy loam, 0 to 2 percent slopes	138	21.11	1.0	5.8
Harwood-Burke-Wiehl silt loams, 30- 60 percent slopes	54	18.77	0.9	2.6
Wanapum complex, 5 to 10 percent slopes	195	5.50	0.3	4.8
Scooteney cobbly silt loam, 0 to 5 percent slopes	127	3.74	0.2	9.3
Outlook silt loam	92	3.42	0.2	7.1
Sinloc silt loam, 0 to 2 percent slopes	139	2.41	0.1	5.8
Water	197	1.64	0.1	
Harwood-Burke-Wiehl silt loams, 8 to 15 percent slopes	52	0.53	0.0	10.6
		2030.12	**99.99**	**12.7**

Table 2.8. Parcel data for Roy Farms, Moxee, WA

Crop	2017	2016	2015
Hops	30.0%	29.5%	22.0%
Apples	26.5%	31.6%	30.5%
Non-cropland	28.0%	27.6%	26.7%
Fallow	2.7%	1.7%	12.1%
Cherries	4.1%	2.2%	1.6%
Grapes	2.5%	2.0%	1.4%
Grass/Pasture	0.4%	0.2%	0.5%
Other	5.8%	4.6%	2.6%

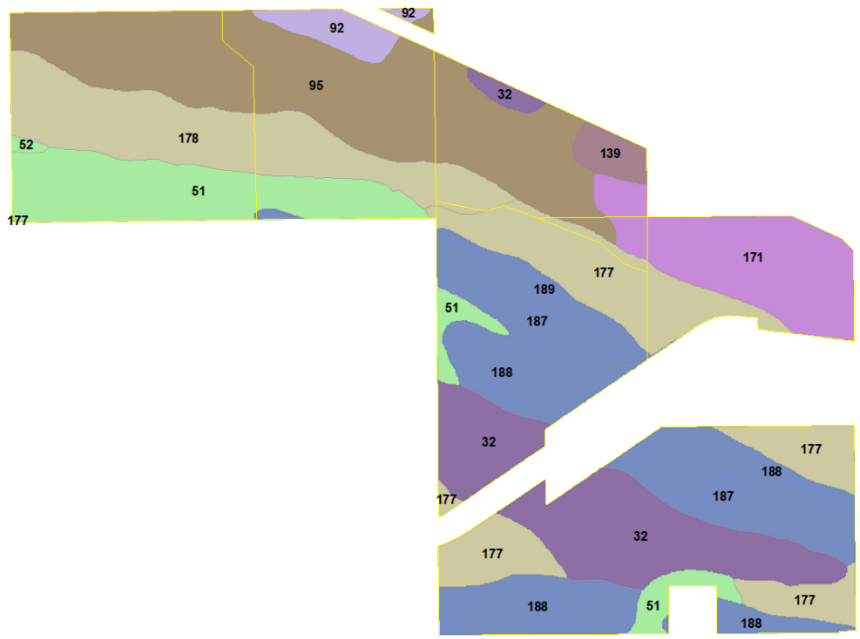

Figure 2.9. Parcels at 12N 20E-9 showing soil types.

2.5 Compost Emission Factors

Emission factors for estimating the composting of the residual biomass from hop cultivation are taken from the 2006 IPCC guidelines Chapter 4, see Table 2.9. The CO_2 emissions from the degradation of the agricultural residue are biogenic[62]. The global warming potential from these emissions are typically not accounted for since biogenic CO_2 is considered to be carbon neutral[69]. This study will consider the change in emissions due to the removal of residual biomass from the compost process.

Table 2.9. Default Emission Factors for CH_4 and N_2O Emissions from Biological Treatment of Waste[69].

Type of biological treatment	**CH_4 Emission Factors (g CH_4/kg waste treated)**	**N_2O Emission Factors (g N_2O/kg waste treated)**
Composting	10 (0.08 - 20)	0.6 (0.2 - 1.6)

Assumptions on the waste treated: 25-50% DOC in dry matter, 2% N in dry matter, moisture content 60%. The emission factors for dry waste are estimated from those for wet waste assuming a moisture content of 60% in wet waste.
Sources: Arnold, M.(2005) Personal communication; Beck-Friis (2002); Detzel et al. (2003); Petersen et al. 1998; Hellebrand 1998; Hogg, D. (2002); Vesterinen (1996). Note: Default emission factors for CH4 for anaerobic digestion already account for CH4 recovery.

2.6 Identification & Allocation of Co-Products

The economic flow data for allocating hop production across the co-products was derived from primary laboratory and field data[30,36], discussion with Roy Farms representatives, from models[53], and from several published hop grower life cycle assessments[24,33,33], see Table 2.10. Biophysical allocation method was used to distribute inputs and outputs across the product, co-product and residual biomass based on the physical relationship between and within the products[63].

Table 2.10. Mass allocation – one hectare of cultivated farm land[53,64].

Biomass	Mass Allocation per Hectare		% Total
Hope Cone	1961	kg	21%
Wood Residual	1519	kg	16%
Non-woody Residual	3301	kg	36%
Rope	131	kg	1%
Roots	2305	kg	25%

Due to the variation in yield between hop varieties and differences due to soil conditions, and possible differences in agricultural practices, the production reported per hectare by Roy Farms was not used. The USDA crop data for the state of Washington for 2017 was used as it represents data for all hop production in Yakima and Benton counties. Analysis was also performed using ArcGIS software. The layers were projected to the spatial coordinate system WGS 1984 Web Mercator Auxiliary Sphere. The Yakima and Benton counties feature layer was projected to the common spatial coordinate system NAD 1983 HARN State Plane Washington South FIPS 4602 Feet. Using a definition query, Yakima and Benton counties were selectively displayed and shaded. These counties were then extracted and established the boundaries for the WSDA crop layers[65]. The crop xy data shape file was accessed using a definition query to display only the crop hops. Using the attribute table, data was summarized for total acres for hop production. Using the summation of total production, an average yield per acre was determined. This was then converted to metric units.

The environmental flows associated with composting of the non-woody residue were determined from data provided by ACRIBALYSE[66], GREET, and IPCC Inventory software. The flows were normalized to the allocated mass for non-woody residual.

2.7 Assumptions & Limitations

The pH ranges for the Yakima River valley vary during the year from 6.5 to 8.5[67]. Data could not be pulled from the available literature regarding average and median measurements during the months relevant to hop cultivation. Therefore, a default value of 7.0 was used in the DNDC model. The pH was found to not impact the outputs of the DNDC model for this LCA's system by varying the pH and rerunning the simulation.

The various life cycle assessments specific to hop cultivation included other crops that confounded back calculation of water consumption. The Yakima Hop Union reported values were determined to include rain water but were the only ones not including non-Hop crops, therefore this was removed and the irrigation per hectare was back calculated then normalized to the 2017 average hop yield.

The proportion of mass attributed to the underground biomass of the plant, the roots, was provided by the DNDC model software[53]. Assuming that the ratio of above ground biomass to below ground biomass is consistent across geographic regions, this was used to calculate the theoretical below ground biomass for this LCA's geographic region.

The initial mass balance for nitrogen assumes that all emissions are accounted for in the loss value. It assumes that the contribution of weeds is negligible relative to the total mass of hops present.

Data for soil quality was sampled from two specific croplands. The soil sample that represents the closest to the Roy Farms was selected, see Figure 2.10. The assumption is that this is a representative average for an operating hop cropland[56]. Proposed changes to agricultural practices require a time frame that allows for the measurement of changes to carbon sequestration in soils[20,68]. This may not be measurable until new carbon equilibrium has been attained. The

time frame is often 20 to 30 years. Additionally, there is a spatial boundary that must be considered; soil depth defined by the Intergovernmental Panel on Climate Change (IPCC) as 0-25cm (topsoil)[69]. For this analysis, it is assumed that the system is at equilibrium and that the soil depth is consistent with the IPCC specification.

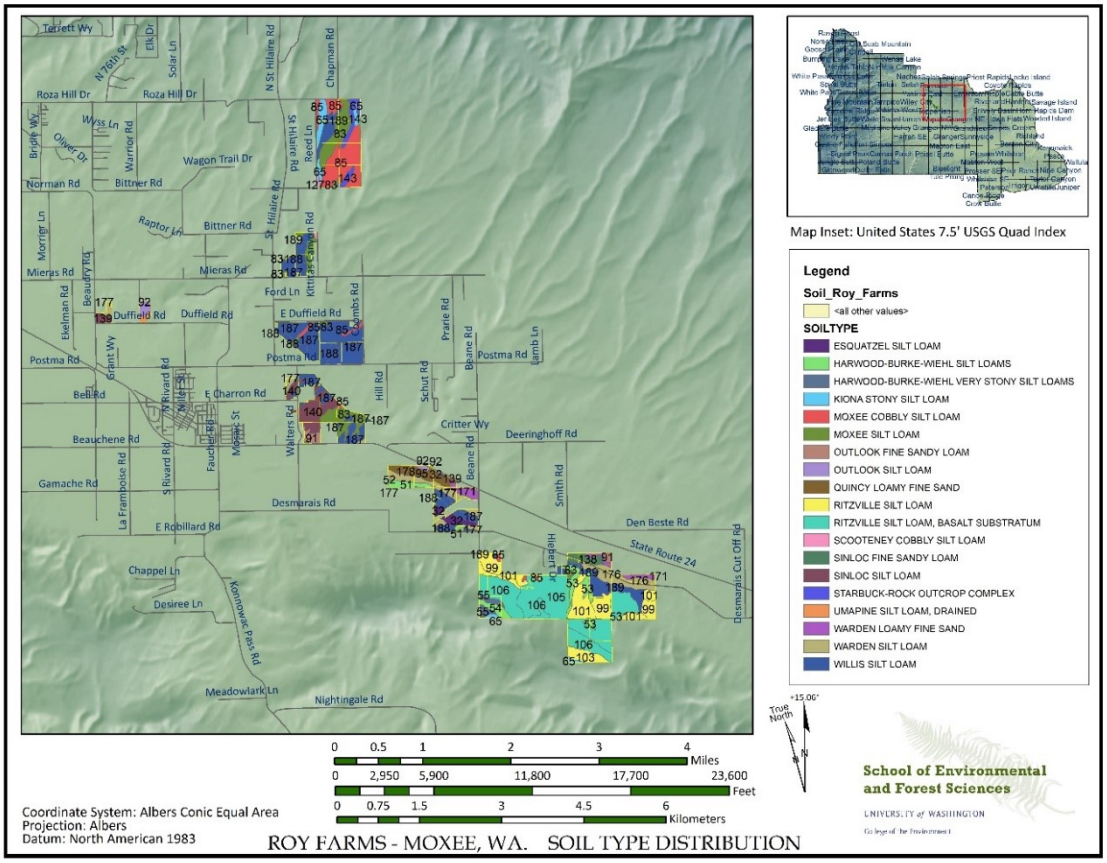

Figure 2.10. Soil types for Roy Farms

2.8 Data Quality Assessment

The following table indicates the data quality estimated for the various databases and models used[43].

Table 2.11. Data Quality Assessment

		QUALITY CATEGORY						
Unit Process	Data Source	1	2	3	4	5	6	7
Mass Allocated Production of Hop Cone	USDA	A	A	A	A	A	B	B
Separation Process of Woody Residue	PRIMARY	A	B	A	A	A	A	A
Composting	PRIMARY	A	B	A	A	A	A	A
Production of Urea-Ammonium Nitrate Solution	GREET	A	B	B	B	A	B	B
Production of Phosphoric Acid (as P)	GREET	A	B	B	B	A	B	B
Production of Potash (as K)	GREET	A	B	B	B	A	B	B
Production of Lime	GREET	A	B	B	B	A	B	B
		QUALITY CATEGORY						
Unit Process	Data Source	1	2	3	4	5	6	7
Production of Electricity	GREET	A	B	B	B	B	B	B
Production of Natural Gas	GREET	A	B	B	B	B	B	B
Application of Urea	IPCC	A	B	A	B	B	B	B
Application of Lime	IPCC	A	B	B	B	B	B	B
Managed Soils	IPCC	A	B	B	B	B	B	B
Operation of Mobile Equipment	GREET	A	B	B	B	B	B	B
Compost - Residual biomass	AGRILABYSE	A	A	A	A	B	B	B
Carbon Sequestration	DNDC	A	A	A	B	A	B	B

2.9 Impact Assessment

2.9.1 CharacterizationTable 2.12

The contribution of an intervention to the selected impact categories for this LCA are calculated on a mass basis using characterization factors for global warming potential, eutrophication, acidification, sequestration of carbon, ecotoxicity, and particulate matter. The midpoint characterization factors were drawn from GREET, ReCiPe 2016, IPCC2013, and openLCA which included factors from BEES. The economic flows sorted by effect that they have on the environment are multiplied by the characterization factor and represent a portion of the impact category.

2.9.2 Impact Contribution Analysis

Two scenarios were established in this study. The first was removal of the woody residual biomass from the compost stream as a co-product and the second represented the current state with all residual biomass returned to the field as compost[70]. The life cycle assessments for each process were categorized into five-unit operations. The contribution vector was determined by partitioning the unit processes, then determining a vector that describes the contribution of the environmental flow to the partial intervention.

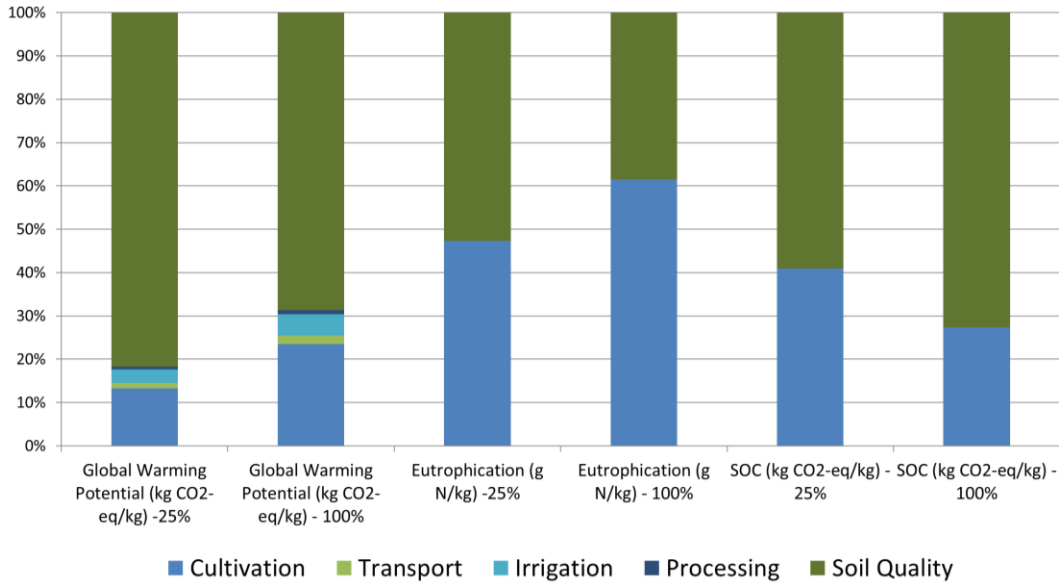

Figure 2.11. Contribution analysis – 100% hop bine separated

These vectors were then multiplied by the characterization factor discussed in the previous section an aggregated into the impact category, see Figure 2.11. Unit process were partitioned into several pseudo unit operations selected in part on the process function but also on the method used for sensitivity analysis, see Table 2.12.

Therefore, soil quality and fertilization were treated separately in order to improve the visibility of measured responses to perturbations of the model.

Table 2.12. Partitioning of process flows for contributional analysis

Process Flow	Contribution
Cultivation	Production of Hop Cone
	Separation Process of Woody Residue
	Composting Non-woody residue
	Life Cycle of the Production of Coir Rope
Transportation	Life Cycle of the Production of Diesel
	Life Cycle of the Production of Gasoline
Fertilization	Life Cycle of the Production of Urea-Ammonium Nitrate Solution (as nitrogen)
	Life Cycle of the Production of Potash (as K)
	Life Cycle of the Production of Phosphoric Acid (as P)
	Life Cycle of the Production of Lime
Irrigation	Life Cycle of Irrigation
Processing	Life Cycle of the Production of Electricity
	Life Cycle of the Production of Natural Gas
Soil Quality	Life Cycle of Production of Magnesium
	Life Cycle of Production of Sulfates
	Life Cycle of Production of Zinc
	Life Cycle of Production of Iron
	Life Cycle of Production of Manganese
	Life Cycle of Production of Copper
	Life Cycle of Production of Boron

Five-unit operations were identified; cultivation, transport, irrigation, processing, fertilization, and soil quality. The cultivation process included the production of hop cone, separation of woody residue, composting of non-woody residue, and the life cycle of coir rope. Transportation included all vehicles used in the removal from the fields and delivery to the processing plant. Irrigation was limited to the LCA for crop irrigation. Processing involved all processes using electricity and natural gas. Fertilization was the life cycle assessments for the components associated with inorganic fertilizers. Soil quality referred to amendments to the soil such as compost and mineral additives. Transport was tractor and truck use in field and at the processing facility.

2.9.3 Sensitivity Analysis

The sensitivity analysis is conducted to evaluate the variation in output and input flow to the system. This study examines the difference in input and output flow for separation of woody biomass and changes in the percentage of woody biomass separated. The mass balance around biomass was first performed at two different levels of hop bine removal, 25% and 50%. The associated carbon and nitrogen content as well as the inorganic fertilizer required was calculated for input into the DNDC model. The model was then run for each of the segregation levels and compared to the LCA study model. The Table 2.13 summarizes the overall balance data input into the model.

Table 2.13. Sensitivity analysis mass data

Biomass	Kg	100% Bine	50% Bine	20% Bine
Hop Cone	1961	1961	1961	1961
Hop Bine	1519	1519	759	304
Rope	131	131	65	26
Non-woody	3301	3301	3301	3301
Compost Bine		0.0	759	1216
Compost Rope		0.0	65	105
Total Compost		3301	4127	4622
Inorganic Fertilizer		119.61	103.43	93.72
Compost N		83.86	100.04	109.75
C/N		17.50	21.05	22.67
Carbon		1467	2106	2488

The base scenario in this analysis is the removal of all hop bine as a co-product. By varying the percentage of hop bine removed as co-product, the influence on soil organic carbon sequestration can be observed, see Table 2.14. Nitrogen eutrophication had the greatest variance which follows the reduction in inorganic fertilizers as a greater percentage of the bine is returned as compost. Soil carbon sequestration has the next greatest variance, again decreasing as bine is removed from the field, see Figure 2.12. The phosphorous eutrophication was also varied corresponding to the reduction in inorganic fertilizers. Ecotoxicity had the lowest variation. Acidification and

particulate matter had very little change in each scenario. The emission is primarily due to tractor and truck use which is independent of scenario selected. Each perturbation required a recalculation of the inorganic fertilizer demand, the C/N ratio of the compost, and the amount of Carbon being returned as compost. These were entered for each scenario and the DNDC model run. The output of the model was then entered into the LCA model to determine the effect on the impact categories.

Table 2.14. Soil Type and Weighting – DNDC model outputs

Hop Bine Co-Product	100% Bine			
Soil Nitrogen Balance (kg N/ha/yr)	4.28% Loamy Sand	2.19% Sandy Loam	93.52% Silt Loam	Totals
Manure N Input	-83.8	-83.8	-83.8	-83.8
Crop stub N input	-4.9	-4.8	-4.8	-4.8
Crop root N input	-13.0	-13.1	-13.1	-13.1
Weeds N input	0.0	0.0	0.0	0.0
Atm N deposit	-96.2	-96.2	-96.2	-96.2
Fertilizer N input	-119.6	-119.6	-119.6	-119.6
N fixation	0.0	0.0	0.0	0.0
N leaching	113.4	113.2	108.6	108.9
N runoff	0.0	0.0	0.0	0.0
N uptake by crop	165.3	166.3	166.3	166.2
N uptake by weeds	0.0	0.0	0.0	0.0
NH3 volatilization	1.5	1.4	1.7	1.7
N2O flux	2.0	2.0	2.0	2.0
NO Flux	0.4	0.4	0.4	0.4
N2 flux	2.0	2.2	5.7	5.5
Change in soil N storage	-32.7	-32.0	-32.7	-32.7
Soil Carbon Balance (kg C/ha/yr)				
Manure N Input	-1467.0	-1467.0	-1467.0	-1466.9
Crop residue C input	-86.8	-84.3	-84.3	-84.4
Crop root C input	-648.8	-652.6	-652.7	-652.5
Weeds C input	0.0	0.0	0.0	0.0
Soil CO2 flux	1187.6	1277.5	1323.4	1316.5
DOC Leaching	0.0	0.0	0.0	0.0
CH4 Emission	0.0	0.0	0.0	0.0
Change in soil C storage	-1012.0	-926.4	-880.0	-886.6

A 10% reduction in hop bine removed resulted in a 2.4% increase in global warming potential as kg CO2-eq/kg of hops, a 6.9% decrease in Eutrophication (g N/kg) and an increase of 5.4% in soil carbon sequestration (SOC).

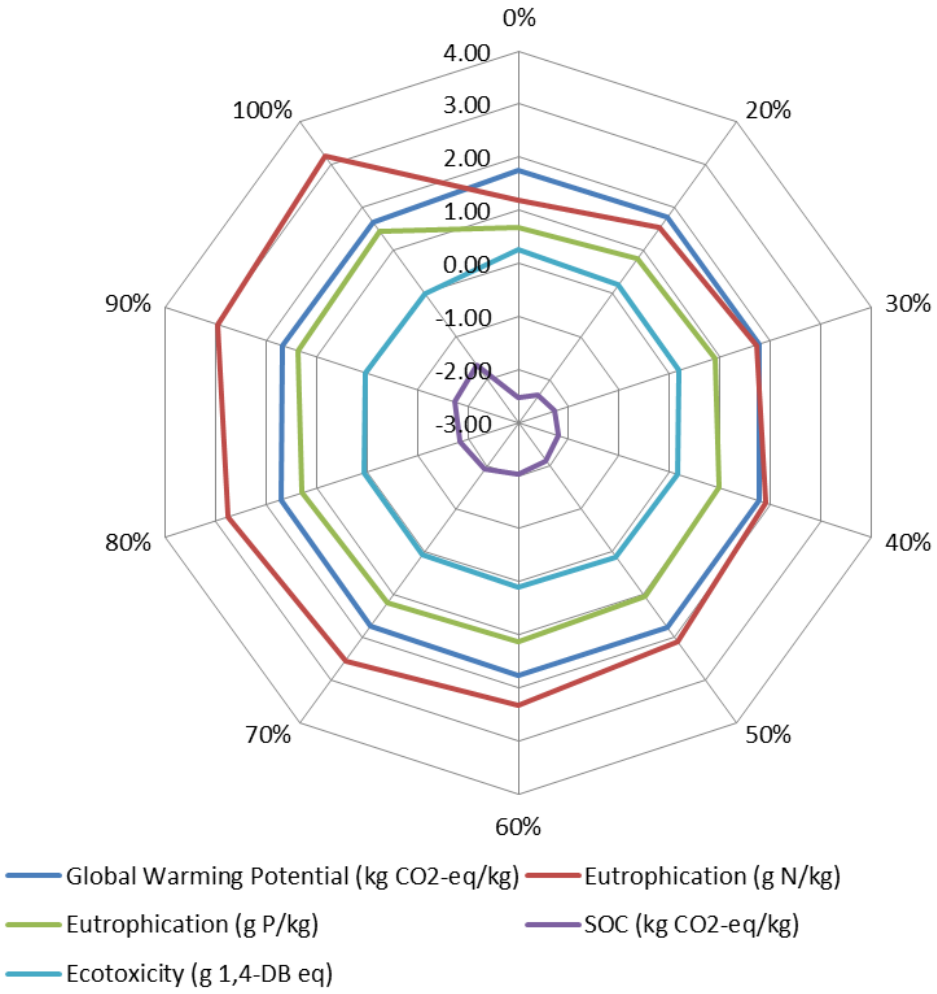

Figure 2.12. Sensitivity analysis for impact factors with varying levels of bine separation

2.10 Identification of Significant Issues

It is not fully understood what factors in the DNDC model may influence emission of methane. It may be that the model assumes that biological oxidation to nitrogen dominates the reaction and therefore once compost is returned to the fields, methane is no longer emitted. Further investigation is needed to determine how the model treats methane emissions.

The factors contributing to acidification are significantly low compared to other crop residues which may indicate that there is either a missing process or that a data point may be

wrong. Fuel data was drawn from GREET and converted from emission per MJ of energy using the standard conversion factors of 35.9 MJ/liter of diesel and 32.6 MJ/liter of gasoline.

2.11 Completeness & Data Quality

Data quality was assessed using the description given in Table 2.11. A data quality index of "B" was given to most data as meta data was either unavailable or the literature source did not share the uncertainty details for their data. Future work should involve returning to these data sets to determine if uncertainty information can be determined.

The impact of weeding and insect control is not addressed in this LCA study. Using the defaults for weed management from the DNDC model, the impact to soil organic carbon was a decrease of 9.6% and a decrease in eutrophication of 43% as weeds take up additional nitrogen from the soil. Ecotoxicity results were quite low. This may be due to incorrect impact characterization factors being utilized. Future work should include a review of impact characterization factors with a comparison to other biomass residues.

2.12 Meta-Analysis: Comparison to Prior Life Cycle Assessments

The challenge was finding suitable crops to compare where the impacts of the life cycle of the biomass could be separated and converted to the same base unit. Most agricultural residuals focused on conversion to energy fuels and most did not document the inherited life cycle of producing the biomass. Table 2.15 illustrates a comparison to other common residuals.

A survey of literature found that the only life cycle assessments available for hops were isolated to studies performed by hop growers where the objective was to illustrate the positive aspect of hop cultivation or were studies on breweries. Neither of these areas treated the residual bine. The nearest cousin to *Humulus lupulus* is *Cannibis sativa* (industrial hemp). The meta-analysis focused on harmonizing the results from life cycle assessments for industrial hemp[71]. Sixteen papers were identified that included impact category data for industrial hemp residual biomass and had separated the industrial hemp data.

Table 2.15. LCA Comparison – 100% bine removal

	Hops (1kg)	Wheat Straw Pellets[72] (1kg)	Wheat Straw (Biofuel)	Corn Stover (Biofuel)
Global Warming Potential (kg CO2-eq/kg)	1.65	1.86	1.30	1.37
Eutrophication (g N/kg)	3.21	-	-	-
Eutrophication (g P/kg)	1.44	0.54	0.39	0.52
SOC (kg C/kg)	-0.88	-0.97	-	-0.35
Acidification (g SO2-eq/kg)	1.07E-03	-	7.80-01	9.30E-01
Ecotoxicity (g 1,4-DB eq)	9.71E-05	-	2.80E-01	2.20E-0.1

The majority of papers identified did not break out the data separately. The gap in these papers was how the biomass was fractionated and how the biomass fractions were allocated. This allocation was not evident in most papers and could be the source of the distribution in results. None of the papers surveyed addressed the impact of residual removal on the denitrification of the soils and carbon soil sequestration. The data from these papers is summarized in Table 2.16.

Table 2.16. Summary impact category data for industrial hemp residuals

		Min	Mid	Max
Eutrophication, Ep	kg PO_4-eq/MT	0.00	0.90	3.05
Climate Change, GWP100	kg CO_2-eq/MT	78.87	183.97	409.23
Acidification, AP	kg SO_2-eq/MT	0.30	0.94	2.18
Ecotoxicity, air	PAF m^3 d/MT	0.41	0.41	0.41
Ecotoxicity, water	PAF m^3 d/MT	0.33	0.33	0.33
Terrestrial Ecotoxicity, TETP	kg 1,4 DCB/MT	0.00	0.17	0.34
Energy Use	MJ/MT	0.00	300.90	2490.00
Land Use	Ha/year/MT	0.15	0.15	0.15
Ozone Depletion	g CFC11 -eq/MT	0.02	0.02	0.02
Human Toxicity, HT	kg 1,4 DCB/MT	0.00	1.17E+04	2.33E+04
Marine Aquatic Ecotoxicity, ME	kg 1,4 DCB/MT	0.00	0.00	0.00
Photochemical Oxidation, POF	kg C2H2 eq/MT	0.07	0.11	1.60
Ecotoxicity,	kg 1,4 DCB/MT	1130.00	1130.00	1130.00

Table 2.17. Meta analysis of Life Cycle Assessments concerning industrial hemp

	kg_Ha	PARTITIONED	EUT kg PO_4-eq/MT	GWP100 kg CO_2-eq/MT	AP kg SO_2-eq/MT
Gonzalez-Garcia [73]	1500	Yes	0.08	109.1	0.30
Gonzalez-Garcia [74]	2600	Yes	0.26	115.9	0.40
Gonzalez-Garcia (2010)	3000	Yes	4.28	271.4	1.30
Gonzalez-Garcia [75]	6000	Yes	2.43	266.7	1.57
van der Werf (2004)	6720	No	3.05	346.7	1.46
Vieira (2010)	6720	No	0.10	409.2	0.74
van der Werf (2007)	8000	No	0.90	398.3	2.18
Buck (2016)	8750	Yes	0.00	213.9	0.94
John Finnan (2013)	10000	No	-	300.0	-
Zampori (2013)	15000	Yes	-	104.4	-
Andrianandraina (2015)		No	1.90	154.0	1.47
Gonzalez-Garcia (2010)		Yes	2.37	103.6	0.86

2.13 Recommendations and Conclusions

Removal of biomass from a perennial crop normally used as a soil amendment in the form of compost requires an increase in inorganic fertilizer application to make up for the nutrient demand of the plant. The results of this LCA show the carbon sequestered in the soil (SOC) is reduced as hop bine is removed. Global warming potential, however, rises as the hop bine is

returned to soil as compost. This is likely due to emission from the increased carbon pool. Eutrophication is reduced as compost is returned which follows the reduction of inorganic fertilizer applied.

The primary driver behind the global warming potential, soil carbon sequestration, and ecotoxicity associated with hop bine removal was identified as soil quality. Changing inorganic fertilization practices by studying and controlling the surplus of nitrogen in the soil may be another strategy to help offset the impact of removal of hop bine from the compost[76]. Not taking into account the starting concentration of nitrogen in the soil, the mass balance indicates an excess of 28kg/Ha of nitrogen in applied to the soil. Research has indicated that above 11kg/Ha, nitrogen dioxide flux can be impacted[77].

Nitrous oxide emissions were found to decrease with added organic fertilizer in this study. This is contrary to documented observation that increased organic carbon in the soil favors the NO_2 flux. In this model – the quality of the soil nutrient content and moisture level in eastern Washington may explain this impact on nitrous oxide emissions and warrants further study. The methane emissions from soils in this model was also found to be significantly lower than expected. Soil emission of methane is estimated to be 10g/ kg N[78]. The model may simply reflect the uncertainty associated with emissions from fertilized soils[79]. In comparison to the LCA of wheat straw and corn stover, the order of magnitude difference in eutrophication in hop cultivation was slightly less than the difference in nitrogen demand for these crops.

It has been documented that approximately 60% of residues decompose during the first year, with a gradual decrease in following years. Combine this with addition of pesticides and treatment of weeds, the model could be more robust if run for the life cycle of a hop plant, 5 years. Additionally, data quality could be improved through primary data on soils analysis obtained and

accurate evaluation of losses in the field and in processing. The primary data in this study was acquired through survey work and laboratory research, while secondary data came from database and literature reviews. A robust model of the entire life cycle of the hop plant will require a complete understanding of how the DNDC software is handling the inputs and may require primary soil, weed, and pesticide data rather than utilization of the program defaults.

[1] Mueller-Warrant, G., Banowetz, G., Whittaker, G., Geospatial identification of optimal straw-to-energy conversion sites in the Pacific Northwest. *Biofuels, Bioprod. Biorefin*., **2010**, 4(4), 385-407. DOI: 10.1002/bbb.230

[2] Wright, M., Brown, R., Boateng, A., Distributed processing of biomass to bio-oil for subsequent production of Fischer-Tropsch liquids. *Biofuels, Bioprod. Biorefin.*, **2008**, 2(3), 229-238. DOI: 10.1002/bbb.73

[3] Mohan, D. U., Pittman Jr., C. H., Steele, P., Pyrolysis of wood/biomass for bio-oil: A critical review. *Energy Fuels*, **2006**, 20(3), 848-889. DOI: 10.1021/ef0502397

[4] Buss, G., Shepherd, M., Suitability of marginal biomass-derived biochars for soil amendment. *Sci. Total Environ.*, **2016**, 547(C), 314-322. DOI: 10.1016/j.scitotenv.2015.11.148

[5] SciFinder; Chemical Abstracts Service: Columbus, OH; corn and wheat stover, soy bean, agricultural residue; https://scifinder.cas.org (accessed January 13,**2019**).

[6] Liu, C., Huang, Y., Wang, X., Tai, Y., Liu, L., Liu, H., Total environmental impacts of biofuels from corn stover using a hybrid life cycle assessment model combining process life cycle assessment and economic input-output life cycle assessment. *Integr. Environ. Assess. Manage.*, **2017**, 14(1), 139-149. DOI:10.1002/ieam.1969

[7] Searcy, E., Flynn, P. C., Processing of Straw/Corn Stover: Comparison of Life Cycle Emissions. *Int. J. Green Energy*, **2008**, 5(6), 423-437. DOI:10.1080/15435070802498010

[8] Shen, X., Kommalapati, R., Huque, Z., The Comparative Life Cycle Assessment of Power Generation from Lignocellulosic Biomass. *Sustainability*, **2015**, 7(10), 12974-12987. DOI:10.3390/su71012974

[9] Jeong, S. T., Cho, S. R., Lee, J. G., Kim, P. J., Kim, G. W., Composting and compost application: Trade-off between greenhouse gas emission and soil carbon sequestration in whole rice cropping system. *J. Cleaner Prod.*, **2019**, 212, 1132-1142. DOI:10.1016/j.jclepro.2018.12.011

[10] Scholl, G. U., Nisius, S., The environmental benefits to German companies through application of LCA. *J. Cleaner Prod.*, **1998**, 6(3-4), 247-252. DOI:10.1016/s0959-6526(98)00025-0

[11] Cordella, M., Tugnoli, A., Spadoni, G., Santarelli, F., Zangrando, T., LCA of an Italian lager beer. *The International Journal of Life Cycle Assessment*, **2007**, 13(2), 133-139. DOI:10.1065/lca2007.02.306

[12] Cimini, A., Moresi, M., Carbon footprint of a pale lager packed in different formats: Assessment and sensitivity analysis based on transparent data. *J. Cleaner Prod.*, **2016**, 112, 4196-4213. DOI:10.1016/j.jclepro.2015.06.063

[13] Saxe, H., LCA-based comparison of the climate footprint of beer vs. wine & spirits. Fødevareøkonomisk Institut, Københavns Universitet. **2010**, Report, No. 207

[14] The Climate Conservancy. The Carbon Footprint of Fat Tire® Amber Ale., **2008**, Retrieved January 10, 2019, from http://www.ess.uci.edu/~sjdavis/pubs/Fat_Tire_2008.pdf

[15] Bare, J., TRACI 2.0: The tool for the reduction and assessment of chemical and other environmental impacts 2.0. *Clean Technol. Environ. Policy*, **2011**, 13(5), 687-696. DOI:10.1007/s10098-010-0338-9

[16] Boldrin, A., Andersen, J. K., Møller, J., Christensen, T. H., Favoino, E., Composting and compost utilization: Accounting of greenhouse gases and global warming contributions. *Waste Manage. Res.*, **2009**,27(8), 800-812. DOI:10.1177/0734242x09345275

[17] Christensen, T. H., Simion, F., Tonini, D., Møller, J., Global warming factors modelled for 40 generic municipal waste management scenarios. *Waste Manage. Res.*, **2009**, 27(9), 871-884. DOI:10.1177/0734242x09350333

[18] USDA Updates Available Functions During Lapse in Funding. (n.d.). Retrieved from https://www.usda.gov/media/press-releases/2018/12/29/usda-updates-available-functions-during-lapse-funding. Antideficiency Act (31 U.S.C. §§1341 et seq.) The United States federal government shutdown of 2018–2019 occurred from midnight EST on December 22, 2018 until January 25, 2019 (35 days).

[19] Olofsson, J., Börjesson, P., Residual biomass as resource – Life-cycle environmental impact of wastes in circular resource systems. *J. Cleaner Prod.*, **2018**, 196, 997-1006. DOI:10.1016/j.jclepro.2018.06.115

[20] Petersen, B. M., Knudsen, M. T., Hermansen, J. E., Halberg, N., An approach to include soil carbon changes in life cycle assessments. *J. Cleaner Prod.*, **2013**, 52, 217-224. DOI:10.1016/j.jclepro.2013.03.007

[21] Boldrin, A., Andersen, J. K., Møller, J., Christensen, T. H., Favoino, E., Composting and compost utilization: Accounting of greenhouse gases and global warming contributions. *Waste Manage. Res.*, **2009**, 27(8), 800-812. DOI:10.1177/0734242x09345275

[22] Taghizadeh-Toosi, A., Christensen, B. T., Hutchings, N. J., Vejlin, J., Kätterer, T., Glendining, M., Olesen, J. E., C-TOOL: A simple model for simulating whole-profile carbon storage in temperate agricultural soils. *Ecol. Modell.*, **2014**, 292, 11-25. DOI:10.1016/j.ecolmodel.2014.08.016

[23] United States, United States Department of Agriculture, National Agricultural Statistics Servie. (**2016**). National Hop Report (pp. 1-8). Washington, DC: USDA.
ISSN: 2158-7825

[24] Roy Farms Corporation. (**2015**). Sustainability Report (Vol. 1, Rep.).

[25] Cooper, J. S., Specifying functional units and reference flows for comparable alternatives. *The International Journal of Life Cycle Assessment*, **2003**, 8(6), 337-349. DOI:10.1007/bf02978507

[26] Young, S., Harris, R., Changing patterns of global-scale vegetation photosynthesis, 1982–1999. *International Journal of Remote Sensing*, **2005**, 26(20), 4537-4563.

[27] World Imagery - Source: Esri, DigitalGlobe, GeoEye, Earthstar Geographics, CNES/Airbus DS, USDA, USGS, AeroGRID, IGN, and the GIS User Community [Map]. (n.d.).

[28] LNI_RegionsByCounty - AppServ. (April 12, 2016). In WA State Dept of Labor and Industries; WA Dept of Ecology. Feature layer displaying the individual counties in Washington State. [June 2018] URL: <https://services2.arcgis.com/J4VMdGWiZXReffvo/arcgis/rest/services/LNI_RegionsByCounty/FeatureServer>

[29] Pacific States Marine Fisheries Commission, Columbia Basin Watershed Boundary, Streamnet [**June 2018**] URL: https://www.streamnet.org/data/interactive-maps-and-gis-data/

[30] Brown, D. (n.d.). Fertilizers and nutrient management for hops. Retrieved January 20, 2019, from https://www.canr.msu.edu/ipm/uploads/files/IPMA/fertilizer_and_nutrient_requirements_for_hops.pdf

[31] Carter, P. R., Oelke, E. A., Kaminski, A. R., Hanson, C. V., Combs, S. M., Doll, J. D., . . . Oplinger, E. S. (**1990, September**). Alternative Field Crops Manual: Hop. Retrieved January 20, 2019, from https://hort.purdue.edu/newcrop/afcm/hop.html

[32] Gingrich, C., Hart, J., Christensen, N. (**1994, July**). Hops; Fertilizer Guide FG79. Retrieved February 12, 2019, from https://ir.library.oregonstate.edu/xmlui/bitstream/handle/1957/20648/fg79-e.pdf

[33] Yakima Chief Hopunion. (**2016**). Sustainability Report

[34] Acre Value agricultural parcel database, [**June 2018**] URL: https://www.acrevalue.com/

[35] Roy Farms Corporation. (**2015**). Sustainability Report (Vol. 1, Rep.).

[36] Godin, R. (n.d.). Calendar of Hops Field Work. In Colorado State University Extension. http://thehopyard.com/wp-content/uploads/2012/06/COState_Soil.pdf

[37] Haunreiter, K. J., Dichiara, A., Gustafson, R., Structural and chemical characterization of hop bine fibers and their applications in the paper industry. *Ind. Crops Prod*. **2021**,

[38] Caffrey, K. R., Veal, M. W., Conducting an Agricultural Life Cycle Assessment: Challenges and Perspectives. *Sci. World J.*, **2013**, 1-13. DOI:10.1155/2013/472431

[39] Heijungs, R., Suh, S. (2011). The Computational Structure of Life Cycle Assessment. Vol. 11. Eco-Efficiency in Industry and Science. Dordrecht: Springer Netherlands, **2002**. DOI: 10.1007/978-94-015-9900-9

[40] Goedkoop, M., Heijungs, R., Huijbregts, M., De Schryver, A., Struijs, J., Van Zelm, R., ReCiPE 2008: A life cycle impact assessment method which comprises harmonised category indicators at the midpoint and the endpoint level. **2008**

[41] Stranddorf, H., Hoffman, L., Schmidt, A., Update on Impact Categories, Normalisation and Weighting in LCA (Ser. 995) (Denmark, Environmental Protection Agency) *Danish Environmental Protection Agency*. **2005**.

[42] Stranddorf, H., Hoffman, L., Schmidt, A. Impact categories, normalisation and weighting in LCA. (Ser. 78) (Denmark, Environmental Protection Agency). *Danish Environmental Protection Agency*. **2005**.

[43] Cooper, J. S., Kahn, E., Commentary on issues in data quality analysis in life cycle assessment. *The International Journal of Life Cycle Assessment*, **2012**, 17(4), 499-503. DOI:10.1007/s11367-011-0371-x

[44] Hermanson, R., Pan, W., Perillo, C., Stevens, R., Stockle, C., Nitrogen Use by Crops and the Fate of Nitrogen in the Soil and Vadose Zone, **1994**, (Publication No. 00-10-015 ed., Interagency Agreement No. C9600177) (United States, Washington State Department of Ecology). Olympia, WA. page3-50

[45] Meerow, A. (**1997, January**). Coir Dust, A Viable Alternative to Peat Moss - ResearchGate. Retrieved from https://www.researchgate.net/publication/239530350_Coir_Dust_A_Viable_Alternative_to_Peat_Moss

[46] Dagde, K., James, S., Production of Biofertilizer from Coconut Coir Pith by Solid State Fermentation Using Micro-organism (Aspergillus Niger). *J. Sci. Eng. Res. (Shriganganagar, India)*, **2016**, 3(3), 448-456.

[47] Guiso, A., Ghinassi, G., Spugnoli, P., Carbon footprint of the three different irrigations systems., Montpellier, France: International Commission on Irrigation and Drainage. 26th Euro-mediterranean Regional Conference and Workshops, **2015**, Innovate to improve Irrigation performances

[48] Huijbregts, M.A.J., Steinmann, Z.J.N., Elshout, P.M.F., Stam, G., Verones, F., Vieira, M., Van Zelm, R., ReCiPe2016. A harmonized life cycle impact assessment method at midpoint and

endpoint level. Report I: Characterization. Department of Environmental Science, Radboud University Nijmegen, **2016**.

[49] Piroue, P., Gehde, J., Hopsteiner Sustainability Report, Simon H. Steiner, Hopfen GmBH, Mainburg, Germany (**2014**)

[50] Goglio, P., Smith, W. N., Grant, B. B., Desjardins, R. L., Mcconkey, B. G., Campbell, C. A., Nemecek, T., Accounting for soil carbon changes in agricultural life cycle assessment (LCA): A review. *J. Cleaner Prod.*, **2015**, 104, 23-39. DOI:10.1016/j.jclepro.2015.05.040

[51] Goglio, P., Smith, W., Grant, B., Desjardins, R., Gao, X., Hanis, K., Williams, A., A comparison of methods to quantify greenhouse gas emissions of cropping systems in LCA. *J. Cleaner Prod.*, **2018**, 172, 4010-4017. DOI:10.1016/j.jclepro.2017.03.133

[52] Gilhespy, S. L., Anthony, S., Cardenas, L., Chadwick, D., Prado, A. D., Li, C., Yeluripati, J. B., First 20 years of DNDC (DeNitrification DeComposition): Model evolution. *Ecol. Modell.*, **2014**, 292, 51-62. DOI:10.1016/j.ecolmodel.2014.09.004

[53] Li, C., Salas, W., Zhang, R., Krauter, C., Rotz, A., Mitloehner, F., Manure-DNDC: A biogeochemical process model for quantifying greenhouse gas and ammonia emissions from livestock manure systems. *Nutr. Cycling Agroecosyst.*, **2012**, 93(2), 163-200. DOI:10.1007/s10705-012-9507-z

[54] Leon, A., Kohyama, K., Estimating nitrogen and phosphorus losses from lowland paddy rice fields during cropping seasons and its application for life cycle assessment. *J. Cleaner Prod.*, **2017**, 164, 963-979. DOI:10.1016/j.jclepro.2017.06.116

[55] Powers, S.E., Quantifying Cradle-to-Farm Gate Life-cycle Impacts Associated with Fertilizer used for Corn, Ssoybean, and Stover production, National Renewable Energy Laboratory, **2005**. (http://www1.eere.energy.gov/biomass/pdfs/37500.pdf)

[56] United States, Environmental Protection Agency, U.S. EPA Region 10., Relation Between Nitrate in Water Wells and Potential Sources in the Lower Yakima Valley, Washington, **2012**, (EPA-910-R-12-003, p. 70). EPA.

[57] Data, U. C. (n.d.). Temperature - Precipitation - Sunshine - Snowfall. Retrieved February 24, 2019, from https://www.usclimatedata.com/climate/yakima/washington/united-states/uswa0502/2017/12

[58] O'Neal, S., Pest Management Strategic Plan for U.S. Hops (Publication). Prosser, WA: Washington State University Irrigated Agriculture Research and Extension Center. **2015**.

[59] Geographic Codes. Retrieved from Washington State Office of Financial Management P.O. Box 43113 Olympia, WA 98504- 113
http://www.ofm.wa.gov/pop/geographic/codes/geographic_codes.xlsx

[60] Acre Value agricultural parcel database, [**June 2018**] URL: https://www.acrevalue.com/

[61] Yakima County Open Data Portal, Land records, [**June 2018**] URL: https://gis-yakimacounty.opendata.arcgis.com/

[62] Sánchez, A., Artola, A., Font, X., Gea, T., Barrena, R., Gabriel, D., Mondini, M., Greenhouse gas emissions from organic waste composting. *Environ. Chem. Lett.*, **2015**, 13(3), 223-238. DOI: 10.1007/s10311-015-0507-5

[63] Mackenzie, S. G., Leinonen, I., Kyriazakis, I., The need for co-product allocation in the life cycle assessment of agricultural systems—is "biophysical" allocation progress? The *International Journal of Life Cycle Assessment*, **2016**, 22(2), 128-137. DOI:10.1007/s11367-016-1161-2

[64] USDA National Agricultural Statistics Service Cropland Data Layer. 2017 Washington Cropland Data Layer. Available at https://nassgeodata.gmu.edu/CropScape/ (accessed 2018). USDA-NASS, Washington, DC.

[65] WSDACrop_2017: polygons representing individual crop field borders with attributes including crop, irrigation, TRS, county, source, and acres. Attributes are updated by WSDA staff via ground surveys or by using outside sources such as USDA's NASS Cropland Data Layer. Projected Coordinate System: NAD_1983_HARN_StatePlane_Washington_South_FIPS_4602

[66] Koch P., Salou T. 2016. AGRIBALYSE®: Rapport Méthodologique – Version 1.3. November 2016. Ed ADEME. Angers. France. 335 p.

[67] Rinella, J. F., McKenzie, S. W., Fuhrer, G. J., Surface-water-quality assessment of the Yakima river basin, Washington: Analysis of available water-quality data through 1985 water year. **1992**, (Tech. No. 91-453). Portland, OR: US Geological Survey.

[68] Lal, R., Crop residues as soil amendments and feedstock for bioethanol production. *Waste Management*, **2008**, 28(4), 747-758. DOI:10.1016/j.wasman.2007.09.023

[69] IPCC 2006, 2006 IPCC Guidelines for National Greenhouse Gas Inventories, Prepared by the National Greenhouse Gas Inventories Programme, Eggleston H.S., Buendia L., Miwa K., Ngara T. and Tanabe K. (eds). Published: IGES, Japan. IPCC National Greenhouse Gas Inventories Programme Technical Support Unit % Institute for Global Environmental Strategies.

[70] Cooper, J., Godwin, C., Hall, E. S., Modeling process and material alternatives in life cycle assessments. *The International Journal of Life Cycle Assessment*, **2007**,13(2), 115-123. DOI:10.1065/lca2007.06.341

[71] Pizzol, M., Laurent, A., Sala, S., Weidema, B., Verones, F., Koffler, C., Normalisation and weighting in life cycle assessment: Quo Vadis? *The International Journal of Life Cycle Assessment*, **2016**, 22(6), 853-866. DOI:10.1007/s11367-016-1199-1

[72] Li, X., Mupondwa, E., Panigrahi, S., Tabil, L., Adapa, P., Life cycle assessment of densified wheat straw pellets in the Canadian Prairies. *The International Journal of Life Cycle Assessment*, **2012**, 17(4), 420-431. DOI:10.1007/s11367-011-0374-7

[73] González-García, S., Luo, L., Moreira, M. a. T., Feijoo, G., Huppes, G., Life cycle assessment of hemp hurds use in second generation ethanol production. Biomass and Bioenergy, **2012**, 36, 268–279. DOI: 10.1016/j.biombioe.2011.10.041

[74] González-García, S., Teresa Moreira, M., Artal, G., Maldonado, L., Feijoo, G., Environmental impact assessment of non-wood based pulp production by soda-anthraquinone pulping process. *J. Cleaner Prod.*, **2010**,18(2), 137–145. DOI:10.1016/j.jclepro.2009.10.008

[75] González-García, S., Hospido, A., Feijoo, G., Moreira, M. T., Life cycle assessment of raw materials for non-wood pulp mills: Hemp and flax. Resources, *Conserv. Recycl.*, **2010**, 54(11), 923–930. DOI: 10.1016/j.resconrec.2010.01.011

[76] Van Groenigen, J. W., Oenema, O., Van Groenigen, K. J., Velthof, G., Van Kessel, C., Best Nitrogen Management Practices to Decrease Greenhouse Gas Emissions. *Better Crops*, **2011**, 95(2), 13-17.

[77] Smith, K., Watts, D., Way, T., Torbert, H., Prior, S., Impact of Tillage and Fertilizer Application Method on Gas Emissions in a Corn Cropping System. *Pedosphere*, **2012**, 22(5), 604-615. DOI:10.1016/s1002-0160(12)60045-9

[78] Cherubini, F., Ulgiati, S., Crop residues as raw materials for biorefinery systems – A LCA case study. *Applied Energy*, **2010**, 87(1), 47-57. DOI:10.1016/j.apenergy.2009.08.024

[79] Chapter 14. Greenhouse Gas Biogenic Sources. Supplement B, 14.1 Emission from Soils -- Greenhouse Gases (5th ed., Vol. 1, AP42). (**1996**). Environmental Protection Agency.

Chapter 3. STRUCTURAL AND CHEMICAL CHARACTERIZATION OF HOP BINE FIBERS AND THEIR APPLICATIONS IN THE PAPER INDUSTRY.

3.1 Abstract

The growth in the *Humulus lupulus L.* or hops industry, a perennial species, driven by demand from brewers has had annual revenue growth of 11.3% since 2015 making it one of the fastest growing agricultural commodities in the Pacific Northwest(PNW)[1]. There is currently 85,000 MT per year of hop bine in the Pacific Northwest (PNW) available for paper making. The land dedicated to hop agriculture increased by 68% from 2010 to 2019 in the Yakima Valley. The plant *Humulus lupulus L.* belongs to the same family as *Cannabis sativa L*, industrial hemp, which has seen practical use in both the paper industry and in the bioproduct development. The bulk density of the hop bine is low, 0.296 g/cm^3 and only 1.5 metric tons of bine is produced per acre each year. However, as crops allocated to production of renewable resources compete for land previously dedicated to food crops, the residual biomass from hop cultivation offers an inexpensive alternative source of renewable lignocellulosic biomass without cannibalizing a food crop. *Humulus lupulus* was characterized to evaluate the acceptability for use as a paper making fiber and for hydrolytic conversion to biobased products. The high carbohydrate content, 58%, is similar to other lignocellulosic materials suitable for bioenergy feedstocks. The fiber has morphological characteristics similar to hardwood with length and width centered around 0.85 mm and 16.5 μm, respectively. The tensile strength of the hop-made papers was 61% greater than the industrial hemp at the same refining level. This fiber presents a sustainable multi-use commodity with excellent application in biobased products and paper making which would otherwise be lost.

3.2 Introduction

Hop varieties are grown in eastern Washington and account for over 79% of the total U.S. production. Hops cultivation is a modest agricultural crop in the Yakima Valley; accounting in 2016 for only 1.2% of total cultivated acreage or 18,029 hectares. An examination of geographical information system data for the Yakima valley has shown an 68% increase in cultivated acreage from 2010 to 2019, as shown in Figure 1. Of the 26 crops that represent 98% of the cultivated land in the Yakima Valley, the cultivation of hops has the second largest growth, with a 9% increase since 2014[2]. The agricultural residual biomass from hop cultivation is the bine, which ends up being returned to the fields and may take several years before it begins to compost, see Figure 3.1.

Figure 3.1. a) bine and leafy material being discharged, b) compost pile of bine and leaf.

This is the primary source of cellulosic fiber in the hop plant and the increase in cultivated acreage may represent a significant source of fiber for use in paper making or for conversion into various bioproducts. The average mass of hop bine produced per hectare is 1.5 MT[3], as listed in Table 3.1. The yield of hop bine is quite low compared to other agricultural residuals, such as wheat straw (2.5 MT/hectare), or bagasse (9 MT/hectare)[4]. This yield equates to 85,000 MT of bine that

would potentially be available from the Northwest region annually. With this much material potentially available it is important to characterize its structural and chemical properties for use as a papermaking fiber or as feedstock for new material development, such as nano fibrillated cellulose.

Table 3.1. Hop plant woody and non-woody mass allocation for above ground and belowground biomass based on one hectare of cultivated farm land[5,6,7].

Biomass	Mass Allocation per Hectare		% Total
Hope Cone	1961	kg	21%
Hop Bine Residual	1519	kg	16%
Non-woody Residual	3301	kg	36%
Rope	131	kg	1%
Roots	2305	kg	25%

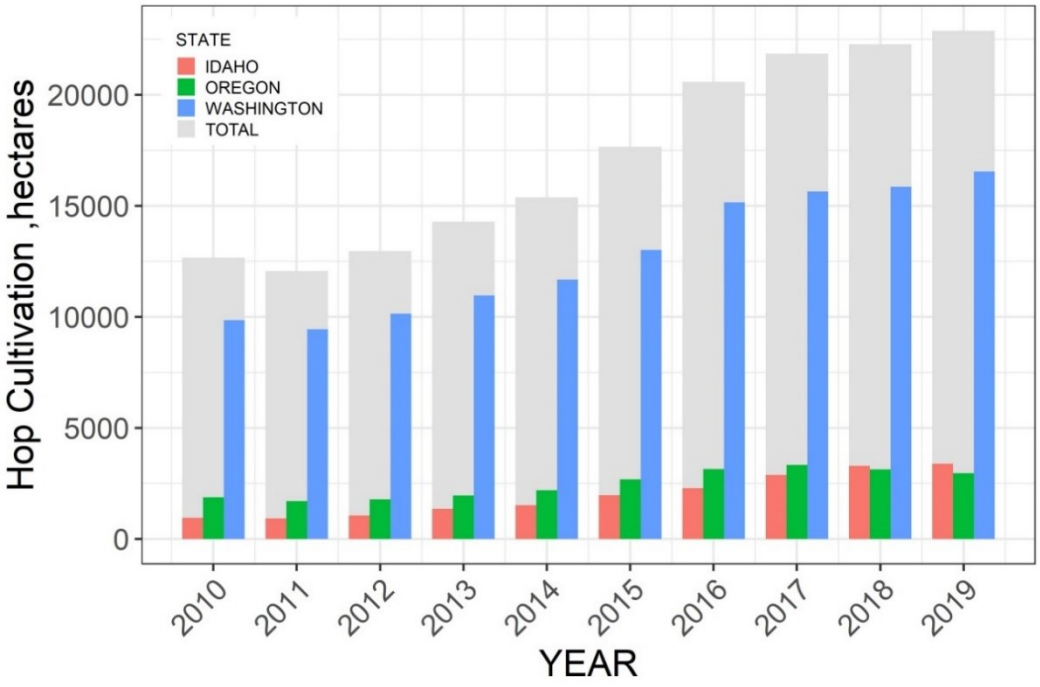

Figure 3.2. Hop cultivation in the United States. Gray bars represent the totals of all three states combined[8].

Humulus lupulus, hops, is a member of the *Cannabaceae* family of which *Cannabis sativa*, industrial hemp, belongs[9]. Industrial hemp is a well-documented source of biomass for use in papermaking[10,11,12,13,14]. Before determining if hop bine can provide suitable fibers for papermaking or for carbohydrate bioconversion, it needs to be thoroughly characterized.

Engineering an efficient method for converting residual biomass to value-add products requires knowledge of the chemical composition and physical structure of the material. Physical factors include the biomass' bulk density, pore structure, and fiber quality, which defines its suitability as a papermaking fiber. The chemical composition provides insight into potential yield of cellulose, hemicellulose and lignin. These details will provide information for determining the pretreatment required for efficient fractionation of the biomass into value-added chemicals and products.

In this study, a combination of chemical, gravimetric, spectroscopic, and microscopic analytical techniques are utilized to characterize the *Humulus lupulus* bine. The bine is subsequently delignified in a Kraft pulping process and paper hand sheets are produced to assess potential as a paper making fiber. For comparison purposes, pulp and paper produced from industrial hemp under similar conditions are also prepared to gauge the hop bine feedstock performance and value.

3.3 Experimental Method

3.3.1 Biomass Pretreatment

Residual bine combined with coir rope was supplied by Roy Farms (Moxee, Washington). Hop bine was separated from any leafy material or residual rope material and segregated into three lots for specific pretreatment for chemical analysis, morphological analysis, and pulp production. The chemical analysis lot 1 was dried in an oven for 24 hours at 105°C. The oven dry bine was milled in a Wiley mill with a 40-mesh screen. The material then was sieved to remove dust and fine particles, see Figure 3.3. Accepts were retained between 40 and 100 mesh screens.

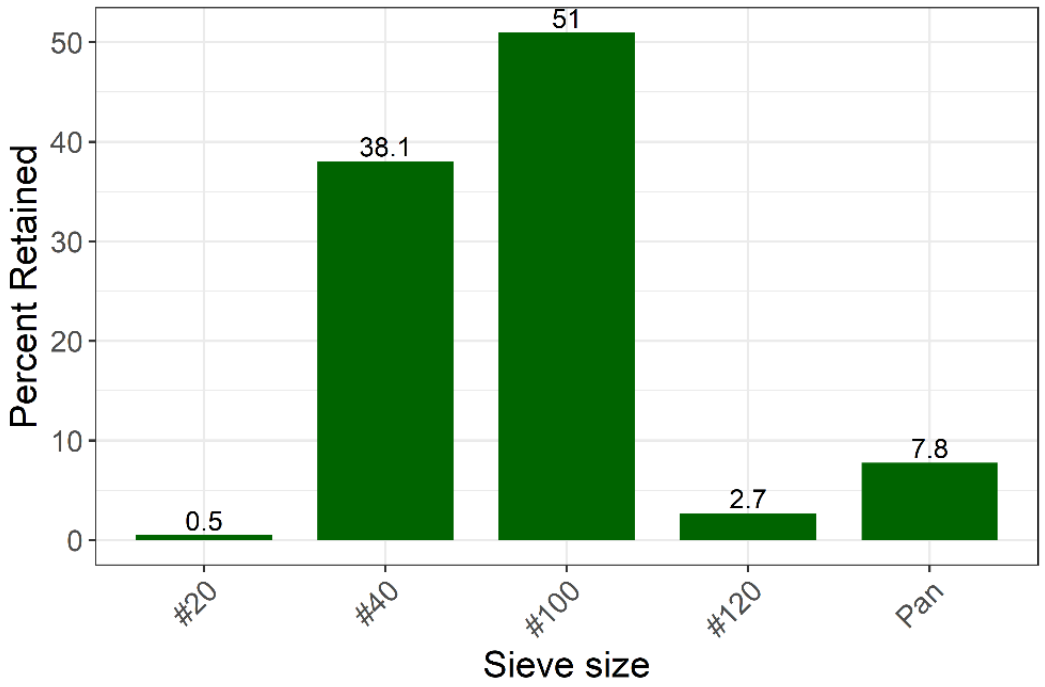

Figure 3.3. Sieve analysis of milled hop bine - % Retained on each screen.

Lot 2 and lot 3 for fiber morphology and pulping were cut into 2 cm lengths for further morphological analysis and pulp production.

Approximately 50 grams of lot 2 was macerated in a solution of 1 part water, 4 parts hydrogen peroxide, and 5 parts acetic acid at 70°C for three days for subsequent fiber quality analysis. This is a modification of a method first reported by Franklin[15]. It is known that acetic acid in the presence of an oxidizer will solubilize lignin mainly through hydrolysis of α-aryl ether bonds and β-aryl ether bonds of the lignin macro molecule[16]. One of the possible reaction mechanisms for the cleavage of α-aryl ether bonds is illustrated in Figure 3.4.

Although the mild maceration solution requires a significant digestion time it does not result in damage to the fibers. Pulping liquor assays found that there was no change in the concentration of acetic acid as delignification progressed. Acetic acid's main role is as a solvent for lignin dissolution. Using more traditional pulping conditions will result in cellulose fiber

fragmentation and skew the fiber length distribution[17]. The resulting pulp was then placed in a laboratory disintegrator for 1 minute to break apart fibrous components.

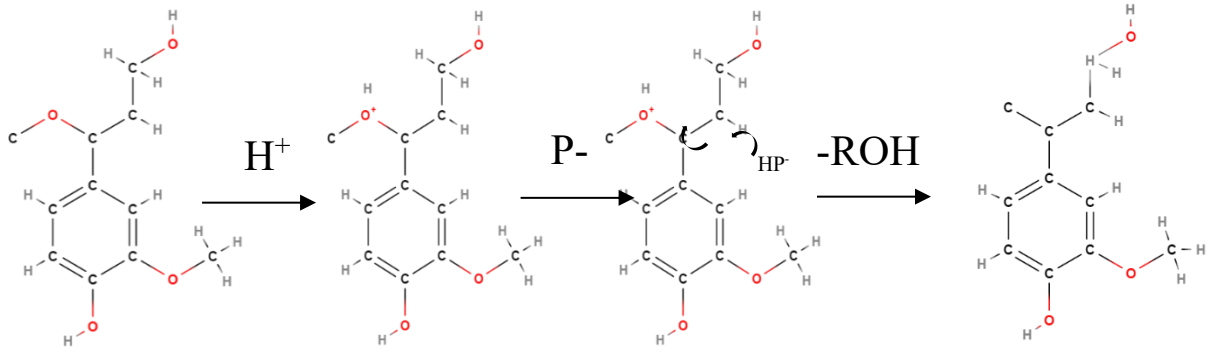

Figure 3.4. Cleavages of α-aryl ether bonds by nucleophilic substitution, R=H or CH3; P=HO– or CH3COO–[18]

The 2-cm fraction not used for morphological analysis was stored in a cooler until moisture content could be determined prior to Kraft pulping. Industrial hemp used in the Kraft pulping study was pretreated under the same conditions as the hop bine for comparison purposes.

3.3.2 Pulping

Kraft pulping of hop bine and industrial hemp was conducted under the same conditions described below. 1000g of lot 3 was placed in a 10.0-L M/K digester. White liquor was prepared at 12% EA as Na_2O and 25% sulfidity on oven dry biomass. The liquor to wood ratio was set to 10:1 (kg/kg) due to the bulk of the biomass. This ensured full coverage of biomass by cooking liquor during the process. The digester was operated until an H-factor of 2,500 was attained at a top cooking temperature of 170°C[14]. The cook was quenched using non-contact cooling water. The digested biomass was subsequently placed into a laboratory waring blender to mechanically break it apart and separate out the spent cooking liquor. It was then washed and screened on a 0.008" laboratory slotted vibratory screen. Klason lignin analysis was performed on the screened

pulp to determine the final lignin content. The accept fraction was refined in a PFI mill then formed into hand sheets for physical testing.

3.4 Characterization

3.4.1 Structural Characterization

The bulk density of hop bine, defined as the measurement of solid material per unit volume, was determined based on the maximum water absorption method[19,20]. Bine was sectioned into 1-2 cm lengths producing a cylindrically shaped section from a random selection of air dry bine. Both length and diameter were measured with a micrometer. Samples were then placed in a 30.0 ml scintillation vial to which 10.0 ml of deionized water was added. The vials were subsequently placed in a vacuum dessicator. A vacuum pump pulled 18 in. Hg for 10 minutes, then the vent was closed to maintain vacuum. Samples were allowed to equilibrate for 1 hour. The vacuum was then broken to produce a positive pressure differential between the exterior and interior of the hop bine, a motive force for liquid penetration. This was repeated twice more followed by soaking for 24 hours under vacuum. The samples were assumed to be fully saturated after 24 hours based on extended treatments of several samples. The samples undergoing an extended treatment of one week indicated identical saturation levels as the one-day treatments. Samples were then removed from the vial and water adhering to the surface of the bine was removed with a tissue. The saturated weight was measured immediately, then the samples were placed in a 105 °C drying oven for 24 hours. The oven dry mass was measured and the length and diameter were measured again with a micrometer to evaluate shrinkage. The bulk density, D in g•cm^{-3}, was determined using equation 3.1 that accounts for the relationship between moisture content, MC in % and basic specific gravity[21]. The basic specific gravity, G_b in g•cm^{-3}, is defined as the density of the biomass

(M_d/V_g), where M_d is the oven dry weight of biomass in g and V_g is the green volume of biomass in cm^3, divided by the density of water, p_w.

$$D = p_w * G_b * \left(1 + \frac{\%MC}{100}\right) \quad (3\text{-}1)$$

$$G_b = \frac{\frac{M_d}{V_g}}{\rho_W} \quad (3\text{-}2)$$

The basic specific gravity equation 3-2, G_b in g/cm3, is defined as the density of the biomass (M_d/V_g), where Md is the oven dry weight of biomass in g and V_g is the green volume of biomass in cm^3, divided by the density of water, p_w.

X-ray tomography was used to provide anatomical detail of the hop bine[22,23]. 2D and 3D results were yielded using an NSI X5000 CT scanner with a resolving power of 10 µm. This non-destructive technique maps the variation in x-ray attenuation within the sample by scattering or absorption to create a three-dimensional visualization of the internal morphology of the plant[24,25]. This was then utilized to calculate the relative area of the lumen to the cross section of hop bine by analyzing each slice taken.

Scanning electron microscopy was performed using a Sirion XL30 operated at 5 kV. The samples were sputter-coated with approximately 4 nm of platinum using a Leica EM ACE600 sputter coater[26]. Preparation of the biomass to preserve the structures and features for morphological characterization first require dehydration of the biomass followed by embedding with a suitable fixative. The hop bine biomass samples were sectioned then dehydrated using a stepped ethanol solution series[27,28];

- *½ day with 50% ethanol: 50% deionized water*
- *½ day with 70% ethanol: 30% deionized water*
- *½ day in 90% ethanol: 10% deionized water*
- *½ day in 100% ethanol*

At each stage, samples were placed under vacuum to infiltrate the cells with the solution[29]. The samples were then dried in an oven at 60°C. They were set into polyethylene glycol 1450 (PEG) under vacuum and left in an oven at 60°C for 2 days. A Leitz 1512 rotary microtome fitted with 170 mm by 35 mm blades secured at angle of 20 degrees to the sample was utilized for sectioning the hop bine. It has been found that significant damage occurs to wood biomass at angles less than 20 degrees[30]. 30 nanometer sections were prepared in the tangential, cross, and lateral directions. SEM images were colorized for clarity purposes based on previously reported method[31].

An OpTest Fiber Quality Analyzer (FQA) was used to measure the length distribution, fines content, vessel elements, and coarseness of cellulose fibers in a dilute fiber suspension. It uses a hydraulic, optical, and image processing system to evaluate dilute suspensions of fibers. Pulp fibers are oriented into the middle portion of the sheath by two sheath currents located to either side. The samples were washed three times with deionized water. It has been reported that the impact of fines on the length weighted average fiber length is not significant, therefore samples were left unscreened[32]. The FQA provides three calculations; arithmetic mean, length weighted average, and weight weighted average[33].

Arithmetic mean (Ln) $$l_n = \frac{\sum_i n_i l_i}{\sum_i n_i} \quad (3\text{-}3)$$

Length Weighted Average (Lw) $$l_{lw} = \frac{\sum_i n_i l_i^2}{\sum_i n_i l_i} \quad (3\text{-}4)$$

Weight Weighted Average (Lww) $$l_{ww} = \frac{\sum_i n_i l_i^3}{\sum_i n_i l_i^2} \quad (3\text{-}5)$$

The FQA-360 groups fibers into bins or length classes denoted by l_i. The number of fibers in each bin is denoted by n_i. The arithmetic mean is influenced by the presence of fines in the fiber slurry

and can produce a skewed result. The length weighted average fiber length calculation is influenced less by the fines content of the sample.

3.4.2 Chemical Composition

Moisture content was determined by weight difference before and after heating at 105°C according to method TAPPI T264[34]. Hop bine being a very dry woody material, a two-part extraction process was not necessary. The milled bine was extracted with 150 ml of a 1:1 dichloromethane; acetone mixture[35]. 3.0 grams of milled oven dry bine was weighed out and placed into a tared glass thimble. The bine was extracted in a soxhlet extraction apparatus fitted with an Alihn condenser for 24 hours. The solid was allowed to air dry. The liquid extract was concentrated down to approximately 20 mls, then transferred to a tared crucible and dried in a 105°C oven. The percentage of ash was determined gravimetrically[36]. Dry hop bine was placed in a crucible and covered. The contents were ignited in a muffle furnace at 575°C for 18 hours. The results are compared in Table 3.4 to published literature for hop bine and for industrial hemp[37]. The primary components of lignocellulosic materials are cellulose, hemicellulose, and lignin. Extractives and ash make up the minor components. To evaluate the potential of hop bine to produce value added products, such as fibers and biofuels, these minor components must first be removed. The quantification of these components is important as their presence may have a significant impact on the performance of a full-scale bio refinery.

A Klason extraction of the solvent extracted biomass was conducted according to a modified NREL method[38,39]. Acid soluble and insoluble lignin were determined by gravimetric and UV-Vis absorption spectroscopy procedures. Measurement of acid soluble lignin was performed using a Shimadzu UV1800 spectrophotometer with a spectral resolution of 1 nm[40]. Residual biomass was digested with 72% H_2SO_4 following the Klason procedure. 0.2g of residual

biomass was mixed with 3.0 milliliters of 72% H_2SO_4 for 120 minutes. After digestion, the sample was diluted with water to a total volume of 115 milliliters. Prior to autoclaving, a 1.0 milliliter aliquot was removed for later determination of the sugar degradation. The sample was autoclaved for 60 minutes at 121 °C. The hydrolysate was filtered through a medium porosity fritted glass crucible in order to separate the acid insoluble lignin component from the soluble lignin and sugar component. The crucible was then placed in an oven to dry and the dry solids removed for FTIR analysis and extinction coefficient determination. The filtrate was set aside for UV spectrophotometer lignin determination according to TAPPI UM-250 and HPLC monomeric and oligomeric soluble carbohydrate analysis according to NREL LAP TP-510 42618[41]. The soluble lignin was extracted from the Klason liquor with methyl isobutyl ketone (MIBK). The extract was then dried and the isolated lignin was dissolved in ethanol to produce a concentration of 1 mg/ml. A series of standards were then produced from serial dilutions of the stock solution. A full spectrum reading was taken for each standard and absorbance values were recorded at 205 nm and 240 nm A quartz cuvette was used with a 1 cm path length. The extinction coefficient for hop bine was determined from the slope of the calibration line of lignin standard solutions produced from extracted hop bine lignin.

The percentage of ash was determined gravimetrically[42]. Empty crucibles were placed in a muffle furnace for two hours at 575 °C prior to use. They were then placed in a desiccator and allowed to cool to room temperature. The tare weight of each crucible was then determined. 1 gram of oven dry hop bine was placed in a crucible and covered. The contents were ignited in a muffle furnace at 575 °C for 18 hours. The crucibles were then removed and placed in a desiccator until cool to room temperature.

The concentration of monomeric sugars (arabinose, galactose, glucose, xylose and mannose) in the acid hydrolysates were measured on a Dionex (Sunnyvale, CA) HPLC (ICS-3000) system equipped with an AS auto sampler, ED electrochemical detector, dual pumps, and anion exchange column (Dionex, CarboPac PA1) according to ASTM method E1758-01 . The Dionex Carbopac PA1 is designed for separating mono and di-oligosaccharides by high pH anion exchange chromatography. The resins consist of 10 μm diameter nonporous beads covered with a fine latex of functionalized Thermo Scientific™ Dionex™ MicroBead™ resin. Deionized water at 1 ml/min was used as an eluent, and post-column addition of 0.2 M NaOH at a flow rate of 0.5 ml/min ensured optimization of baseline stability and detector sensitivity. After each analysis, the column was reconditioned with 0.25 M NaOH[43].

Stock solutions were created for arabinose, galactose, glucose, xylose and mannose by dissolving the sugar in deionized water. Calibration standards were produced from the stock solution by subsequent dilution to produce concentrations that would bracket the sample. Five standard solutions were produced for each sugar. Linearity of response was determined using peak areas versus concentration for each set of calibration standards. Linear regression analysis of peak area versus concentration was performed in Excel to construct a >95% correlation coefficient equation. Arabinose, Galactose, and Mannose were linear from 0.004 mg/ml to 0.072 mg/ml. Glucose and Xylose were linear from 0.070 mg/ml to 1.394 mg/ml.

Fucose was selected as the internal standard as it is similar to the sugars of interest and produces a peak that does not overlap with target sugars . A stock solution was produced at 5.0 mg/ml. Samples were diluted as appropriate, fucose was spiked at 0.870 mg/ml as an internal standard and filtered through 0.22 μm syringe filters (Restek Corp., Bellefonte, PA, U.S.). Sugar calibration standards were treated in the same manner as the samples. Twenty microliters of each

sample were injected into the HPLC column. The response of the target sugar, A_S, was then normalized to the response of the internal standard, A_{IS}. The ratio of the peak area of the target sugar to the peak area of the internal standard in each sample was then compared to the ratio of the peak area of the calibration standard, C_S, to the peak area of the internal standard, C_{IS}. The response factor, RF, is calculated as follows;

$$RF = (A_S * C_{IS})/(A_{IS} \& C_S) \quad (3\text{-}6)$$

A Shimadzu IRPrestige 21 Fourier Transform spectrometer equipped with an attenuated total reflectance (ATR) system was employed to characterize the main functional groups present in the extracted hop bine. It performed 25 scans per measurement in the 600 to 4000 cm^{-1} range and at a resolution of 8 cm^{-1}. Spectra were normalized and scaled to 100% using the intensity at 1516 cm^{-1}, which corresponds to the carbon-carbon double bond stretching of the lignin aromatic ring. Each pooled sample set represented ten replicates. The standard normal variate (SNV) was selected as the normalization method as it weighs intensities that deviate from the individual sample mean more heavily than those values that are nearer the mean [44,45,46,47,48]. It is also very effective at reducing variability caused by scattering effects common in solid samples. The most prevalent types of light scattering are Rayleigh and Lorentz-Mie – mostly caused by the fine particle surface roughness and fibrous structure typical of lignocellulosic biomass. In the case of bine – Lorentz-Mie is likely the dominant scattering effect as particle sizes are larger than the wavelength and dependent on the size and shape of the material.

S_i indicates the signal parameter, intensity, of the peak in the spectral region of 600 to 4000 cm^{-1}. The corrected spectrum (SNV) is calculated by equation 1[48,49].

$$\hat{S}_i = (S_i - \text{mean}(S_{1516}))/ \text{std}(S_{1516}) \quad (3\text{-}7)$$

$\hat{S}_i$ represents the corrected signal of spectra i.

The resulting z-value vector were then scaled so that the intensity at 1516 cm^{-1} was 100% with a standard deviation of 1. Subtraction of the means serves to project the intensity of the spectra at 1516 cm^{-1} orthogonal to a vector of ones. The resultant transformed reference peak will have a z-vector mean of zero. Dividing by the standard deviation transforms the spectra so that all have the same length. The resulting z-vector produced by the transformation has a squared length.

3.5 Papermaking

The response of the fibers to mechanical refining was evaluated using a laboratory pulp refiner (Papirindustriens Forskningsinstitutt (PFI) mill method)[50]. Pulp fibers were disintegrated using a British disintegrator. Excess water was removed from the pulp slurry until a consistency of 10% was achieved. Fiber was placed into the PFI mill and refined to specific number of revolutions. The Canadian Standard Freeness (CSF) was determined at each corresponding revolution level; 0, 500, 1000, and 2500[51].

3.6 Mechanical Testing

Hand sheets with 60 $g \cdot m^{-2}$ grammage were produced from both hop bine and industrial hemp pulps at each refining level[50,52]. Hand sheets were conditioned in a humidity and temperature-controlled laboratory for physical testing[53]. Tensile index, tensile energy absorbed, and elongation were examined using a uniaxial Thwing-Albert tensile tester[54].

3.7 Results

3.7.1 Morphology

1-kilogram samples of the unscreened biomass were placed in an oven at 105 °C until a constant weight was attained prior to classification. Classification was performed on a laboratory chip screen with 45mm, 8mm, 6mm bar, and 7mm perforated screens, Figure 3.5. The pan contained all non-woody biomass. Woody biomass was 33% of the total oven-dry mass. Non-woody biomass accounted for 67% of the total oven dry mass. The woody biomass had a moisture content of 47% while the non-woody biomass was 64%.

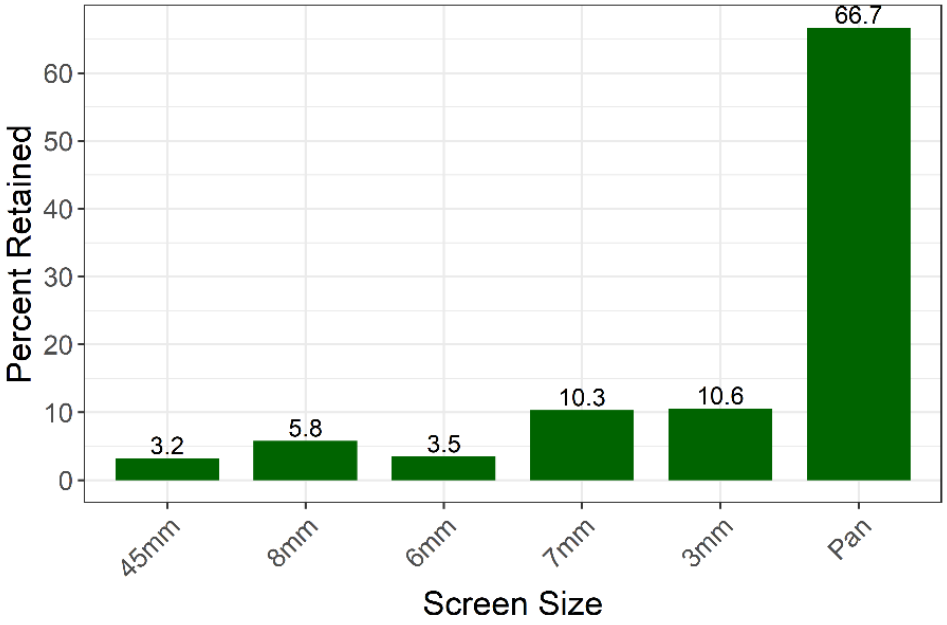

Figure 3.5. Hop residual biomass classification, 45mm hole, 8mm bar, 6 mm bar, 7 mm hole, 3mm hole.

Roy farms provided production data from 2017 for three hop varieties. Using this data, production of residual biomass was determined on a per acre basis for woody and non-woody components, Table 3.2. Relative percent composition is illustrated for the Cascade hops variety in Figure 3.6.

Table 3.2. Biomass production by component – ODMT/acre

	Hop Cone (ODMT/acre)	Bine Biomass (ODMT/acre)	Rope – Biomass (ODMT/acre)	Non-woody Biomass (ODMT/Acre)
Cascade	1.8 (28.4%)	1.5 (22.0%)	0.118 (1.9%)	3.1 (47.8%)
Centennial	1.4 (28.4%)	1.0 (22.0%)	0.079 (1.9%)	2.0 (47.8%)
Chinook	1.9 (28.6%)	1.6 (21.9%)	0.127 (1.9%)	3.1 (47.6%)

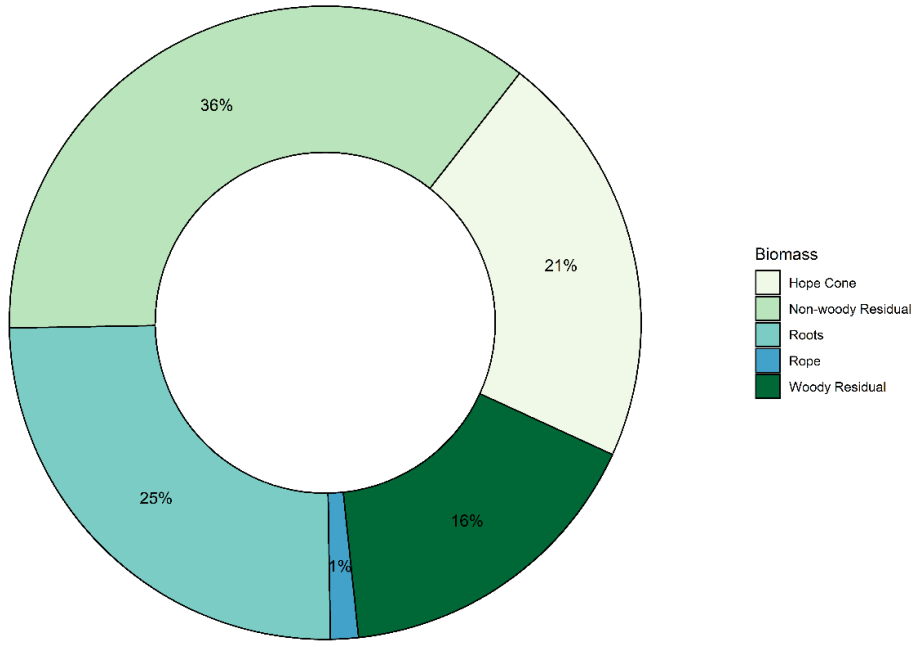

Figure 3.6. Percent composition of total biomass per acre – Cascade Hops

The images in Figure 3.7 were prepared using a microtome with neither a PEG nor a resin such as Epon-812 embedding mix[55]. The resulting 3d image reconstructed from X-ray-CT scan correspond to variations in object density, Figure 3.7b. The slices were utilized to calculate the relative area of the lumen to the cross section of hop bine by analyzing each slice taken shown in Figure 3.7a,c. The lumen accounted for 13.6% of the total area of the hop bine cross section. The average density was 0.296 g/cm^3. Shrinkage in diameter and length were 5.28% and 0.47% respectively for oven dry compared to green bine. The bine absorbed 0.984 grams of water per gram of biomass.

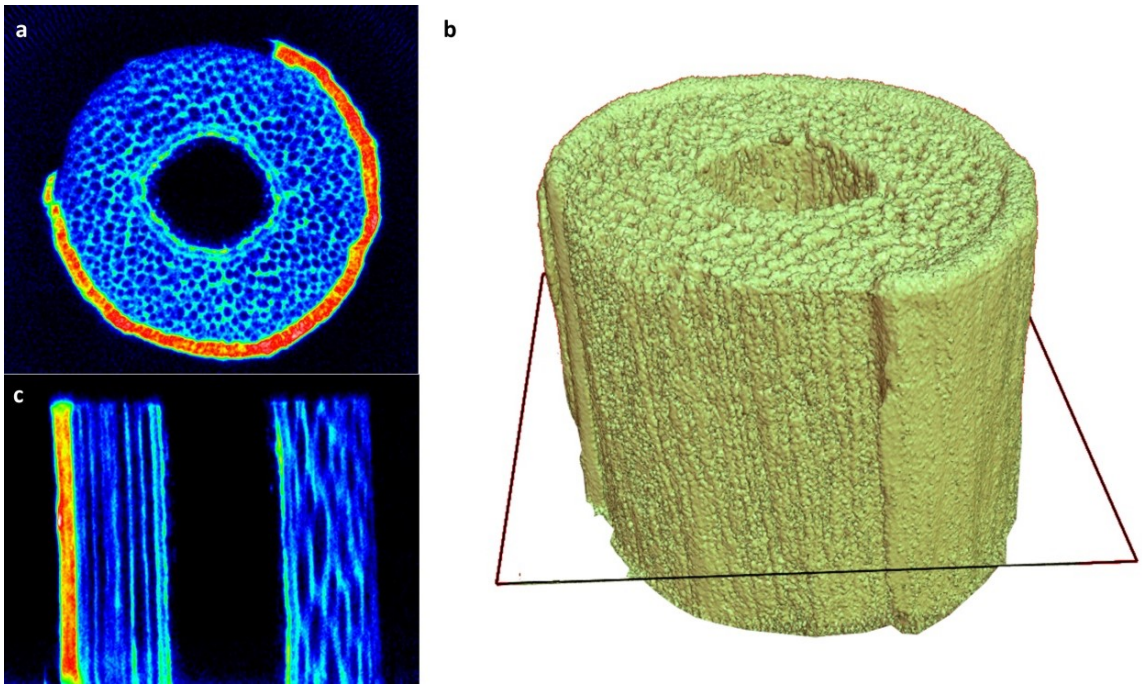

Figure 3.7. a) cross section slice b) 3d construct of X-ray CT scan, c) longitudinal section slice.

Table 3.3. Bulk density of hop bine and reduction in bine diameter.

	Density g/cm^3	Shrinkage Diameter	Shrinkage Length	Water absorbed (g/g)
Average	0.295	5.28%	0.47%	0.984
SD	0.032	0.9%	0.23%	0.077

The SEM The SEM transverse cross section shows the outer epidermis, porous bast fibers, inner hurd, and hollow center consistent with previous work[56]. The hurd layer reveals the significant disruption of the fiber wall without the use of an embedding matrix shown in Figure 3.8. The porous are diffuse across the face of the bine. A magnification of the transverse section shows that vessel elements are grouped around a dominant vessel, Figure 3.10. The reticulated wall structure of the vessel element shown in Figure 3.10 is similar in structure to what is found in black walnut (*Juglans nigra L*). Figure 3.12a is an example of a longitudinal tracheid with diffuse pitting on all sides. This is likely a sclereid fiber based on the abundant pitting. The angular intervessel pitting is crowded and exhibits a structure comparable to that of hard wood American Hornbeam

(*Carpinus caroliniana*). A transverse view of an individual vessel element separated using an acetic acid/hydrogen peroxide maceration solution is illustrated in in the inset of Figure 3.12b.

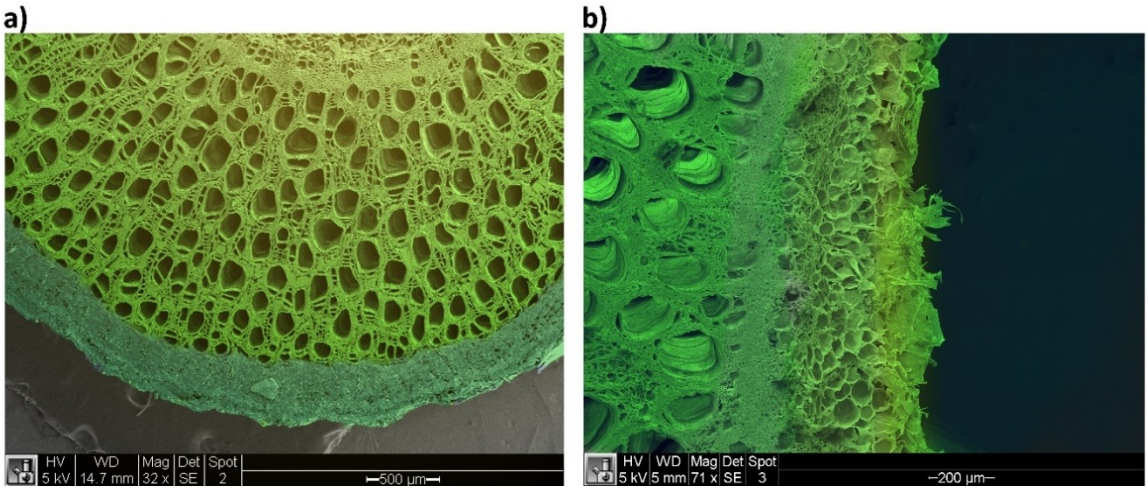

Figure 3.8. a) SEM transverse cross section image in false colors showing outer epidermis, b) porous bast fibers, inner hurd, and the hollow center.

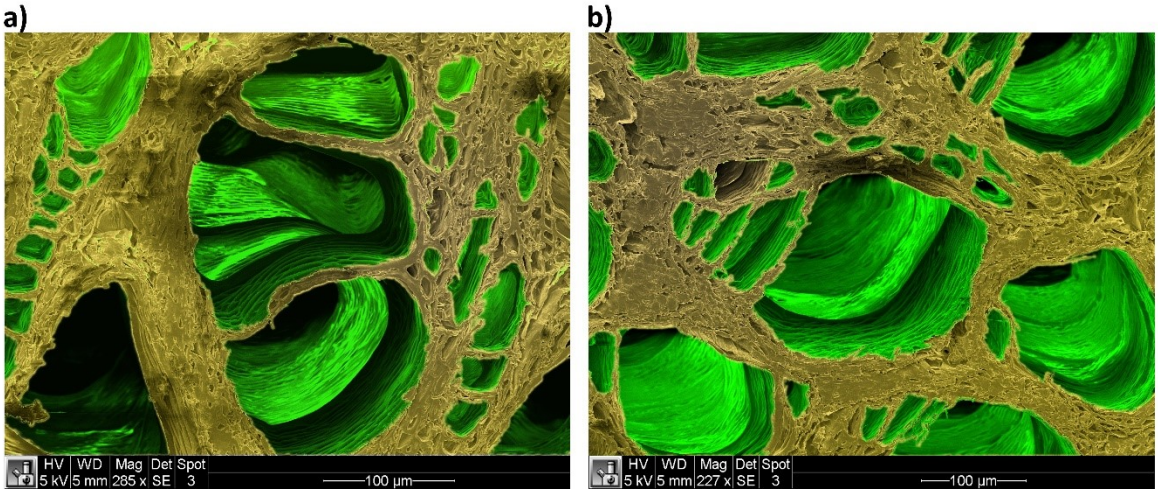

Figure 3.9. a-b) Transverse cross-section of diffuse distribution and coupling of vessel elements.

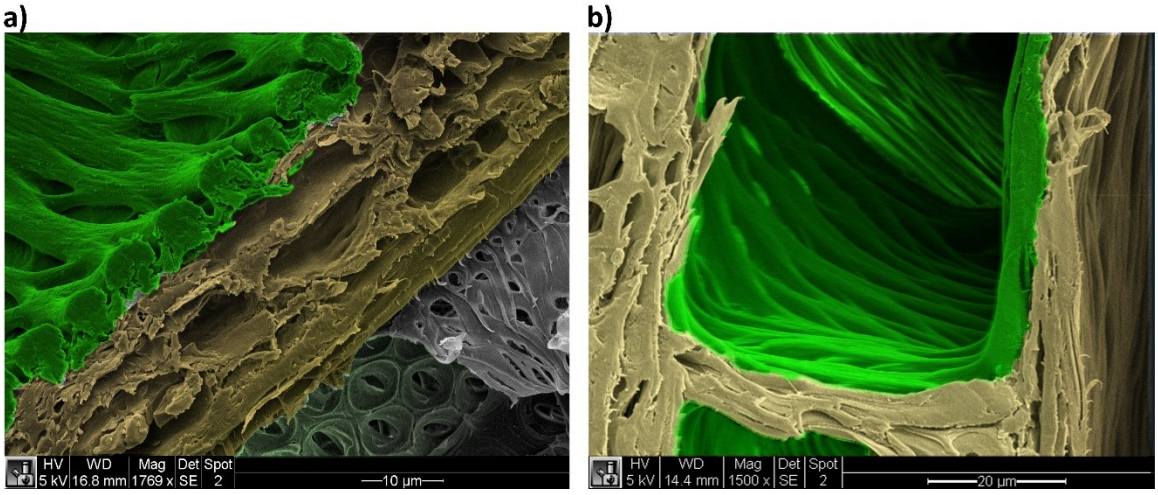

Figure 3.10.a) Longitudinal cross-sectional closeup view of vessel elements and ray parenchyma with reticulated wall structure of a vessel element. b) Transverse close up of vessel elements located near the transition from bast fibers to hurd fibers.

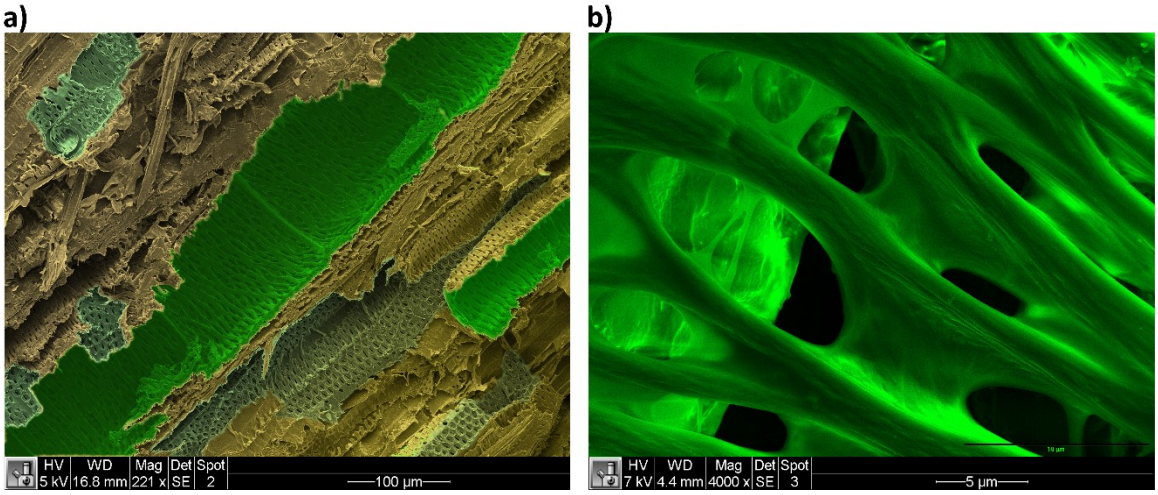

Figure 3.11. a) Longitudinal cross section of vessel elements. and ray parenchyma with b) closeup of the reticulated wall structure a vessel element

Isolated vessel elements show an open-ended structure with simple perforation plate, Figure 3.12. Figure 3.13 is a close-up of porous vessels in the bast fibers. A radial cross section view of the vessel elements indicates simple perforation plates between vessel elements. The longitudinal fibers are long and appear to be tracheids. Consistent with prior work these will be identified as tracheids[56]. The lateral contact between the vessel wall and adjoining tracheids is very heavily pitted. The pitting is an irregular diagonal arrangement of scalariform-like gaps in the cell wall.

Also visible in the micrograph are longitudinal tracheids with alternate pitting. These pits are approximately 0.5 µm in size, as depicted in Figure 3.13.

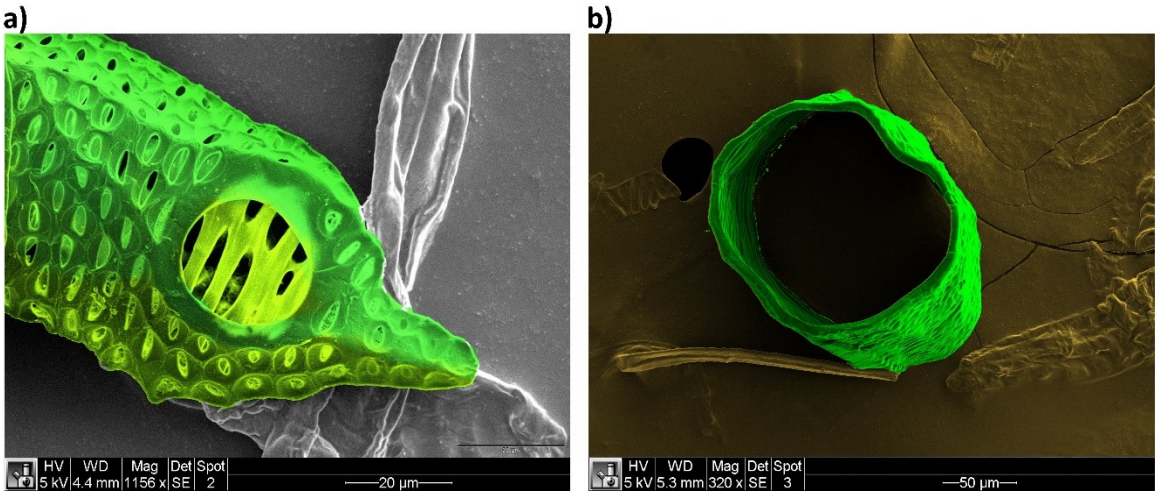

Figure 3.12. a) Isolated vessel element showing surface pitting. Scalariform structure visible on inside of element. b) transverse view of isolated vessel element.

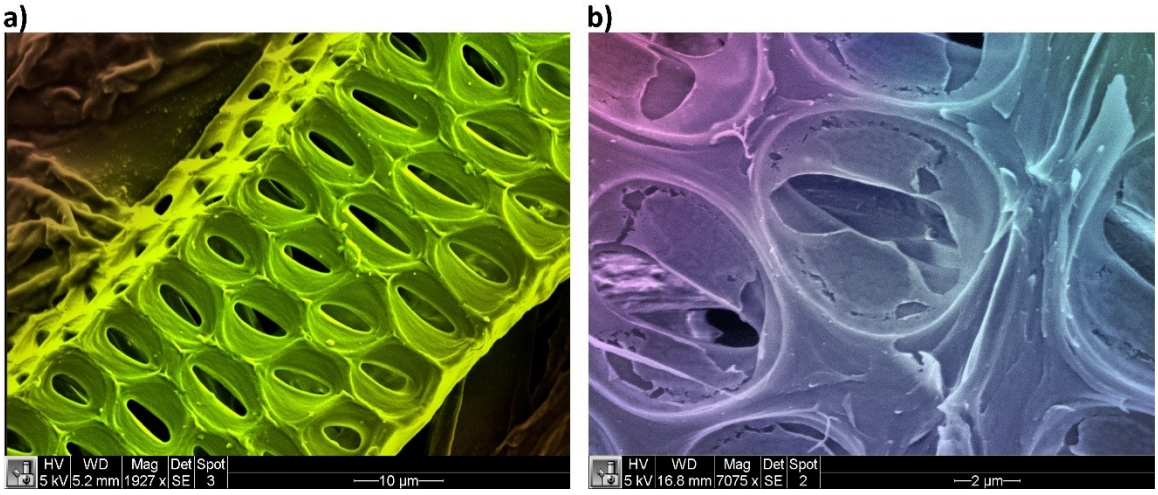

Figure 3.13. a) pitting in tracheid cell wall, b) closeup of pits.

The initial scans indicate the PEG is interfering with the resolution of features using the SEM. In a discussion with Wai Pang Chan, Research Coordinator, Biology, College of Arts & Sciences, Division of Natural Science, considering the fragility of the bine, it may not be necessary to embed the material either in PEG or a resin such as Epon-812, a glycerin based aliphatic epoxy resin[57].

The images were not prepared using an embedding mix but cut by hand using a microtome knife. The magnified image of the hurd layer indicates significant disruption of the fiber wall without the use of an embedding matrix.

3.7.2 Fiber Quality

The length weighted average plotted in Figure 3.14 shows two distinct peaks. The first dominant peak appears at a fiber length of 0.1 mm, while the second peak appears at a fiber length of 1.3 mm. The fines content (*i.e.,* length < 0.2 mm) was quite high at 19.56% likely due to the numerous vessel elements. The length weighted average fiber length was 0.85 mm. As a comparison, Eucalyptus fibers are in the range of 0.7 to 0.8 mm, as reported in Table 3.4.

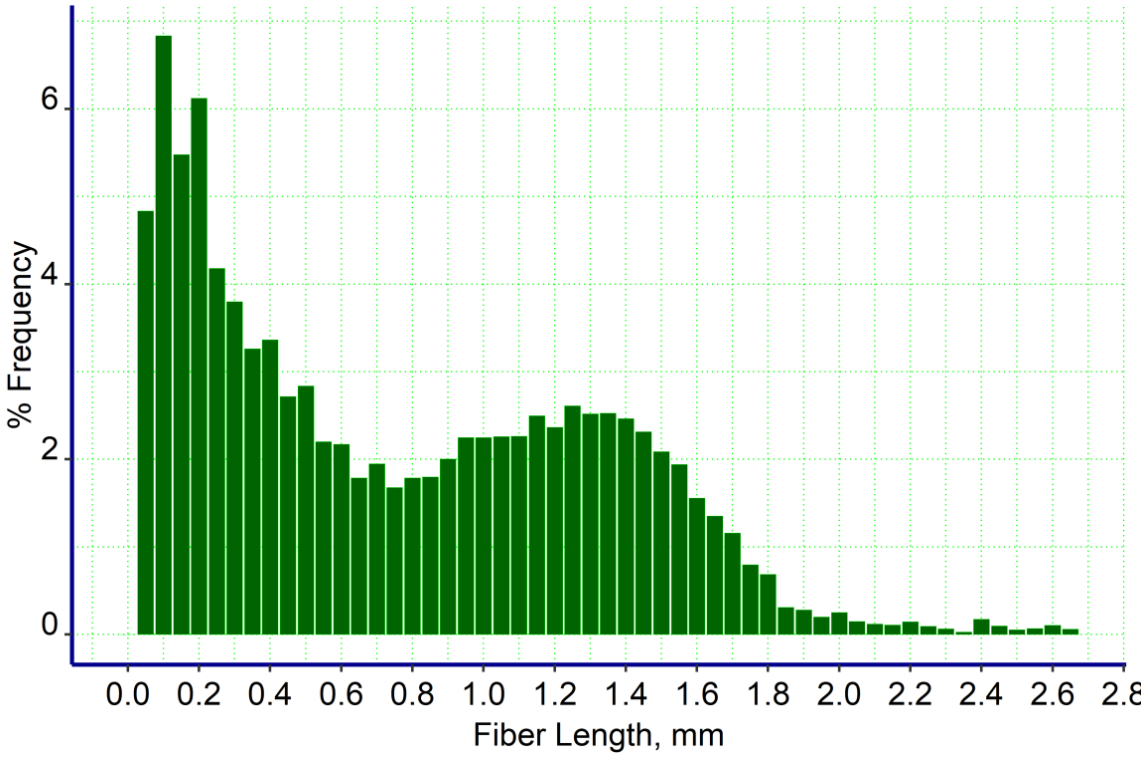

Figure 3.14. Pareto diagram produced from length weighted average data produced by Fiber Quality Analyzer of macerated hop bine fibers.

Table 3.4 Comparison of morphological properties of hop stems to other non-wood and wood fibers[58,59,60].

Fiber	Length (mm)	Width (µm)
Hop - bine	0.85-1.3	11-22
Hemp	0.9-2.3	20-24
Douglas Fir	3.5-4.5	35-45
W. Hemlock	2.5-4.2	30-40
Eucalyptus	0.8-1.1	15-19

3.7.3 Chemical Composition

Results of chemical compositional analysis are summarized in Table 3.5 and Table 3.6. The composition data for other lignocellulosic biomass reported in the literature is also provided for comparison purposes with the hop bine and industrial hemp results.

Table 3.5. Comparison of composition of hop stems to other non-wood and wood fibers[37,61,62,63].

Fiber	Cellulose	Hemicellulose	Lignin	Ash	Extractives
Hop bine	32.9%	26.0%	25.9%	3.4%	12.0%
Industrial Hemp	42.5-44.0%	22.2-25.1%	23.4-24.8%	1.2-3.3%	1.1%
Grape Stalk	36.3%	24.5%	40.6%	3.9%	8.2%
Wheat Straw	43-46.4%	21.5-28.9%	20.8-21.2%	6.5-7.6%	2.8-5.0%
Bagasse	41.9-45.0%	28.8-29.1%	17.7-22.1%	1.1-2.1%	2.5%
Poplar	29.6-43.8%	9.2-21.2%	25.2-32.0%	3.2%	

Table 3.6. Carbohydrate composition of residual biomass[64,46,65,37,61,66,67,63,68,69,70]

Sample	Arabinose	Galactose	Glucose	Xylose	Mannose	AIL	ASL
Hop Bine	9.0%	1.2%	32.9%	15.2%	0.6%	20.9%	6.4%
Industrial Hemp	0.4%	1.0%	41.7%	14.6%	0.0%	21.0%	2.4%
Grape stalk	3.7%	3.9%	36.3%	14.9%	2.0%	39.6%	1.0%
Wheat Straw	2.1%	0.5%	34.6%	21.5%	0.2%	15.1%	1.0%
Bagasse	1.7%	11.1%	44.3%	22.1%	ND		
Poplar	0.6%	1.0%	43.8%	14.9%	3.9%		

The hop bine has similar amount of total lignin, hemicellulose and ash when compared to industrial hemp. The cellulose content is significantly lower than *Cannibis sativa L* but falls into the lower range of Poplar and grape stalks, *Vitis vinifera*. Extractives were significantly higher

relative to industrial hemp likely due to higher condensed tannin content as is found in grape stalk, see the HPLC graph of the sugars in Figure 3.15[63].

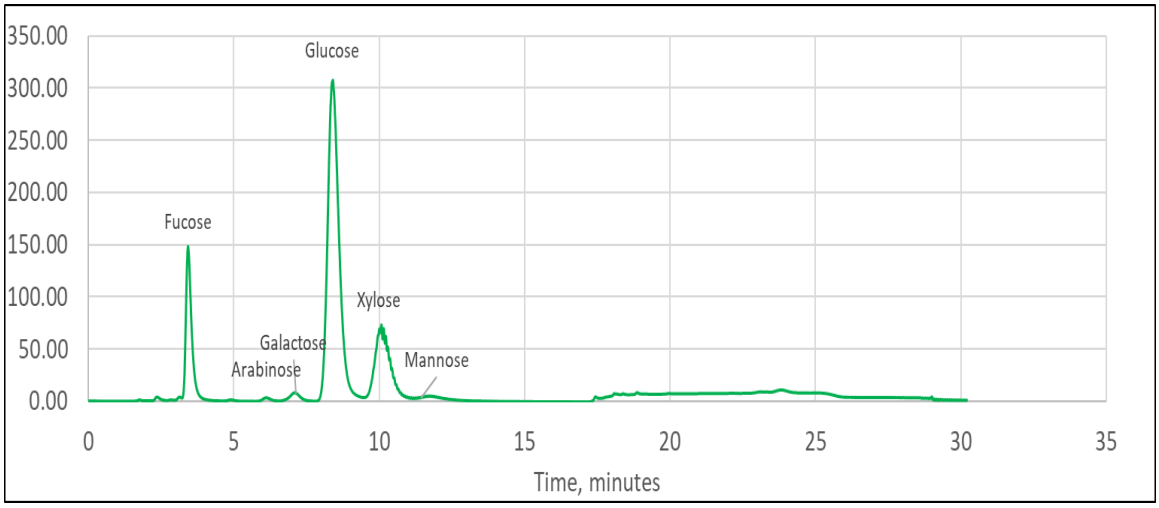

Figure 3.15. HPLC graph of sugars in industrial hemp hydrolysis sample

The extinction coefficient for hop bine was determined from the slope of the calibration line of the lignin standard solutions. At 205 nm, the extinction coefficient was 60.3 L/g-cm and at 240nm was 25.7 L/g-cm, see Figure 3.17.

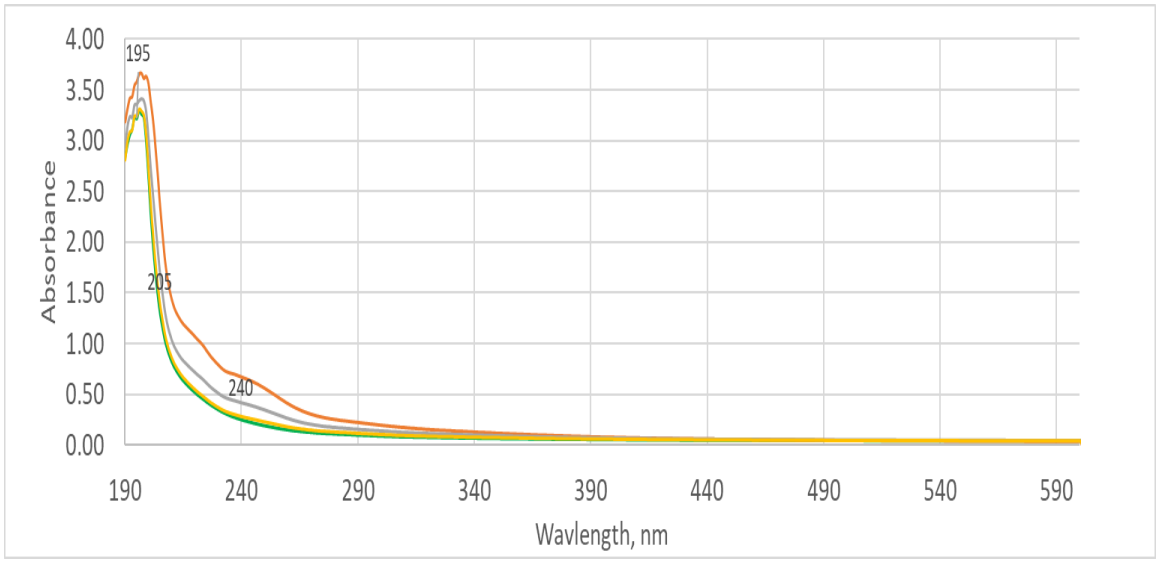

Figure 3.16 UV absorbance spectrum for industrial hemp.

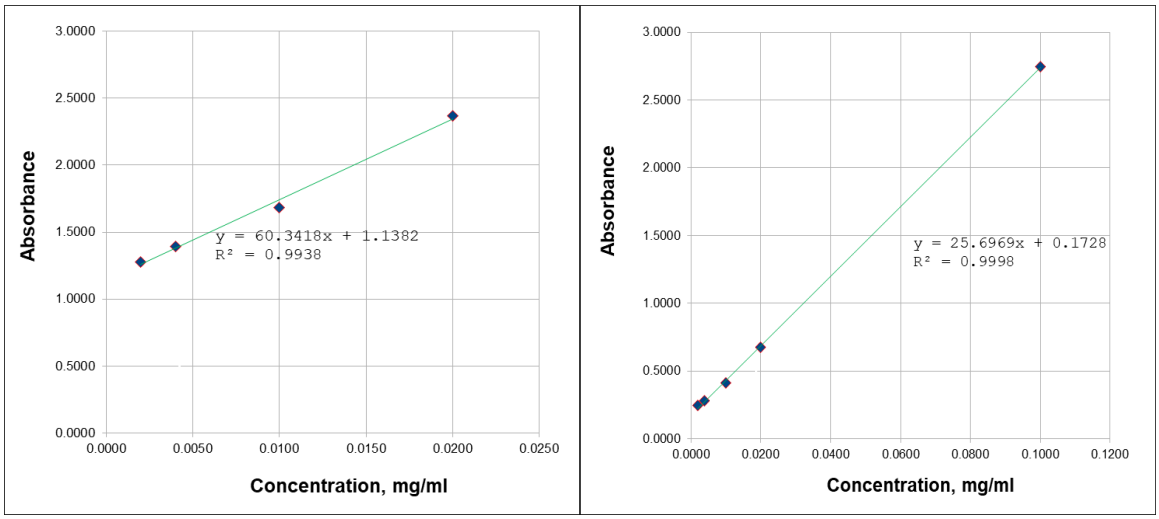

Figure 3.17. Determination of the extinction coefficient at 205nm and 204nm

The primary functional groups of hop bine and industrial hemp samples were identified by FT-IR spectroscopy. The peaks highlighted in Figure 3.18 are the fingerprint for cellulose, hemicellulose, and lignin[71,72,73,74,75,76,77,78,79]. The spectra indicate similar chemical composition in hop bine compared to industrial hemp. Note that the high intensity at 1616 cm^{-1}, corresponding to OH bending, is likely due to the high-water absorbance capacity of the hop bine relative to the industrial hemp.

The spectra indicate lignin by the O-H peak at 3450 cm^{-1} and the C-H in aliphatic side chains at 2932-2842cm^{-1}, see Table 3.7 [80,81,82,83,84, 85]. The peak at 1423 cm^{-1} can be attributed to symmetric CH_2 bending vibration attributed to crystalline cellulose[86]. The small peak at 1724 cm^{-1} is attributed to stretching of the C=O carbonyl in hemicellulose and lignin. The peak at 1234 cm^{-1} is characteristic of the C-O aryl group in lignin. These peaks are the fingerprint for hemicellulose and lignin in the extracted hop bine. Taking the ratio of the peak at 1327 cm^{-1} and the peak at 1267 cm^{-1} the calculated value of syringyl to guaiacyl lignin may be determined[83], see Table 3.7.

Table 3.7 FT-IR Peak Assignments

PEAK CM−1	ASSIGNMENT
3435	O–H stretching
2932 - 2842	Aliphatic C-H
1759	Aryl–O-Acetal
1731	Alkyl–O-Acetal
1707-1691	Unconjugated carbonyl stretching of aldehyde and ketone groups
1660	C=O stretch conjugation
1616	OH - water
1600-1615	C=C stretching of aromatic ring in lignin
1567	C=O stretching (ionic compounds)
1515 - 1505	C=C stretching of aromatic ring in lignin
1463 - 1459	C-H ending of methyl and methylene groups
1425 - 1423	C-H Deformation in Lignin
1423	CH2 bending vibration of cellulose
1366	Aliphatic C–H stretching in CH3
1328 - 1323	C=O stretching of Syringyl unit
1267	C-O stretching of Guaiacyl unit
1234 - 1230	C–O aryl group stretch in lignin
1219 - 1211	C-C, C-O, C=O stretching of Guaiacyl unit
1167 - 1162	C–O stretch in ester group
1126 - 1110	Aromatic C-H deformation of Syringyl units
1033	Aromatic CH in plane deformation G + S
1031 - 1015	C-O stretching of primary alcohols
983	CH=CH bending
911	CH Bending of Syringyl units, aromatic rings
899	C-H deformation vibration of cellulose
835 - 815	C-H bending of Syringyl unit
755	asymmetric bending of HCCH group

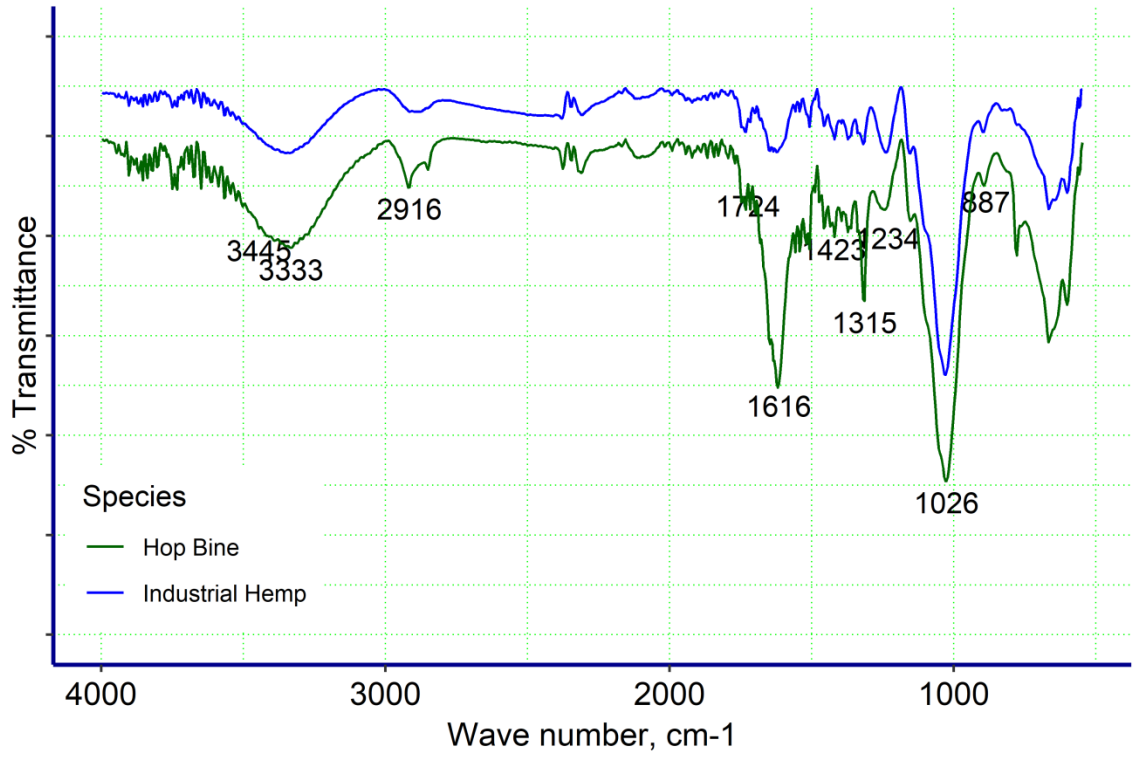

Figure 3.18. Comparison of unextracted hop bine to industrial hemp.

3.8 Pulp and Paper

After pulping, the average lignin content for the industrial hemp was 3.31% and that for the hop bine was 3.93%, suggesting that hop bine and industrial hemp responded similarly to the Kraft process and could be easily pulped together in a mill. The initial drainage rate of the hop bine, 480 Canadian Standard Freeness (CSF), was 100 points higher than the industrial hemp pulp cooked to the same H-factor. This measured difference is likely due to the contribution of smaller core fibers (~0.5 mm) and the longer bast fibers from whole hemp pulping[67]. The bulk density of the hop bine was the driver behind the high liquor to wood ratio. Densification of the biomass would allow significant reduction of the liquor to wood ratio, thereby allowing for reduced H-factor.

3.8.1 Paper Testing

As-prepared hand sheets were tested to determine the impact of refining intensity on paper mechanical properties using a uniaxial Thwing-Albert tensile tester. The hop bine developed a higher strength at a given refining level than the industrial hemp, as demonstrated in Figure 3.19. Hop bine achieved approximately 7.4 points of tensile (N-m/g) for every 100-point drop in Canadian Standard Freeness(ml), whereas the industrial hemp only developed 6.4 points of tensile per 100-point CSF drop. The average percentage difference was 61% at a given CSF. The variability of the tensile index measurements was somewhat higher in the hop bine than in the industrial hemp. In unrefined pulps, vessel elements contribute little to paper strength rather harming the performance of the final product. Refining reduces the content of vessel elements in the pulp, increasing the fines content and flexibility of these fibers. The increased range in measured tensile index for hop bine is likely due to the higher content of vessel elements in the hop bine producing a wider range of fines at increasing refining levels. The tensile energy absorption (TEA) for hop bine is also higher for a given amount of stretch. This indicates that the extensibility and inter fiber bonding of the hop bine fibers developed during refining is greater than the industrial hemp[87]. The shorter fiber contribution from the industrial hemp core likely lowers the tensile development from refining. A plot of the normalized stretch as a function of normalized TEA (N-m/g) (Figure 3.19d) was found to have proportionality factors of 1.36 and 1.41 for hop bine and industrial hemp, respectively. Typical proportionality factors of unbleached pine range from 1.31 to 1.39[88]. The linear relationship between TEA and the product of tensile strength and stretch depicted in Figure 3.19c is consistent with other reports in the literature[89,90].

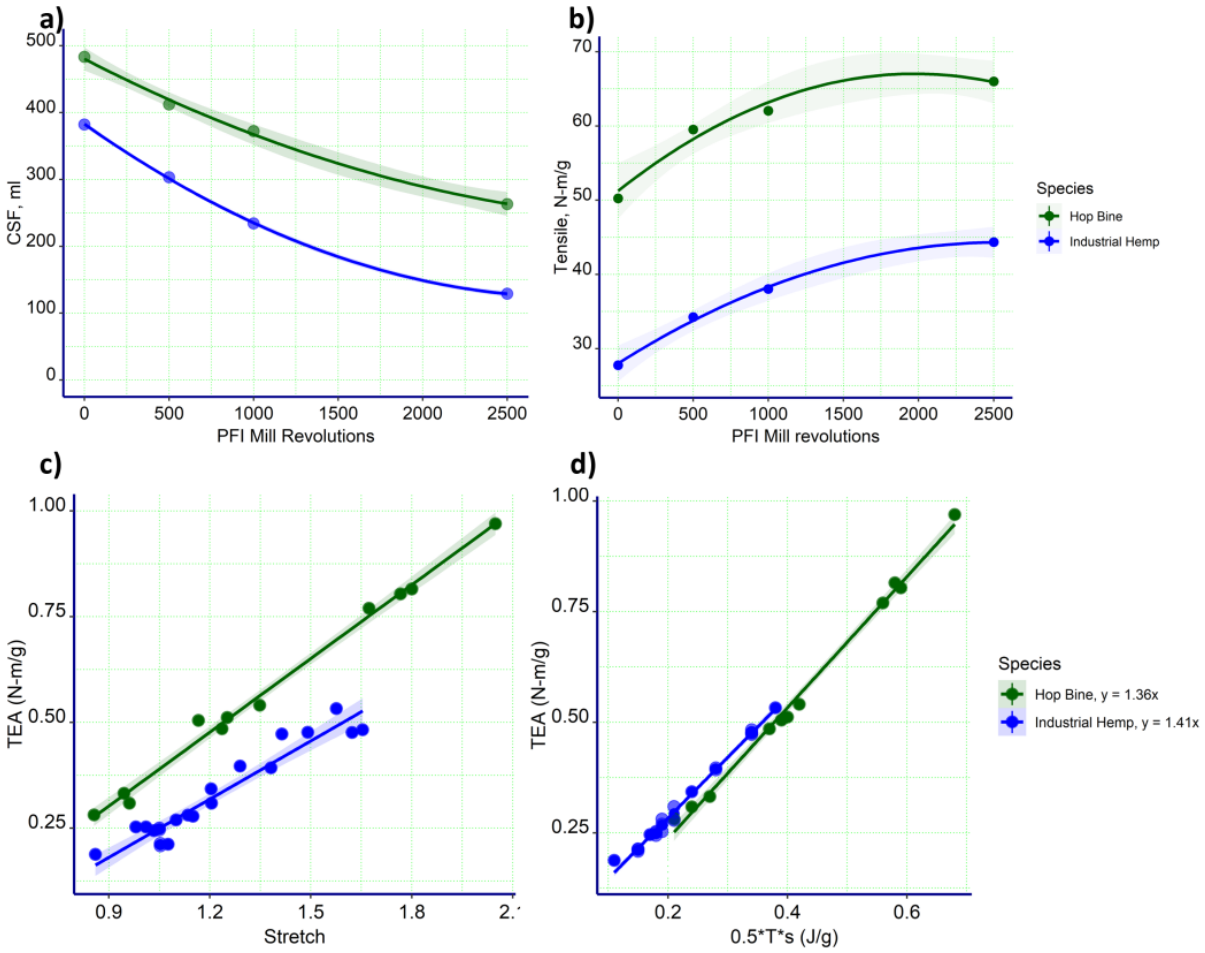

Figure 3.19 . (a-b) PFI mill curve – CSF vs PFI Mill revolutions and Tensile Index vs revolutions with 95% confidence interval shaded in blue. (c-d) TEA Index versus stretch (elongation) and against the product of tensile index and stretch for refined hand sheets.0.5*T*s

3.9 Conclusion

We investigated morphological, chemical, and papermaking qualities of hop bine to assess whether this residual crop material could serve as an opportunistic feedstock for the pulp and paper industry. The low bulk density, 0.296 g•cm^{-3}, and low yield per hectare, 1.5 MT, of cultivated land suggest an on-location densification process would be needed to address transportation costs. Despite the high content of vessel elements, the mechanical strength of the fibers developed during refining was higher than industrial hemp. Strength development and hardwood like fiber quality indicate good promise as a paper making fiber. The carbohydrate composition of hop bine is

similar to other woody bio-mass, such as wheat straw and industrial hemp, indicating that it may also be suitable for conversion to value-added products, such as nanocellulose. The high extractives content, 12%, may represent an opportunity for recovery of organic non-structural components from the perennial biomass crop residual worthy of further investigation. To obtain a more accurate assessment of the paper making potential, a series of trials investigating the interaction of this fiber with softwood fibers and an expansion of the physical testing, such as tear, burst, and permeability should be undertaken in the future. Additionally, consideration must be given to the agricultural concern regarding the ecosystems impact to soil carbon sequestration, global warming potential, and water as this fiber is removed from the system.

ACKNOWLEDGMENTS
The authors express sincere thanks to Roy Farms, Moxee, Washington for financial and material support of this research.

References

[1] Madigan, J., Hops Farming: Hop to it: Volatile demand is expected to slow industry growth (INDUSTRY REPORT OD6150, pp. 1-31, Rep. No. INDUSTRY REPORT OD6150 Hops Farming). *IBIS World*. **2020**

[2] National Agricultural Statistics Service, CropScape - Cropland Data Layer, Retrieved December 27, 2017, from https://nassgeodata.gmu.edu/CropScape/

[3] United States, United States Department of Agriculture, National Agricultural Statistics Servie. (**2016**). National Hop Report (pp. 1-8). Washington, DC: USDA.
ISSN: 2158-7825

[4] Paavilainen, L., Torgilsson, R., Reed Canary Grass – A New Nordic Papermaking Fiber, *Proceedings of TAPPI Pulping Conference*, **1994**, San. Diego, CA., p611-618

[5] Meerow, A. (1997, January). Coir Dust, A Viable Alternative to Peat Moss - ResearchGate. Retrieved from https://www.researchgate.net/publication/239530350_Coir_Dust_A_Viable_Alternative_to_Peat_Moss

[6] United States, Environmental Protection Agency, U.S. EPA Region 10., Relation Between Nitrate in Water Wells and Potential Sources in the Lower Yakima Valley, Washington **2012**, (EPA-910-R-12-003, p. 70). EPA.

[7] USDA National Agricultural Statistics Service Cropland Data Layer. **2017** Washington Cropland Data Layer. Available at https://nassgeodata.gmu.edu/CropScape/ (accessed 2018). USDA-NASS, Washington, DC.

[8] United States, United States Department of Agriculture, National Agricultural Statistics Service., **2019**. National Hop Report (pp. 1-8). Washington, DC: USDA.ISSN: 2158-7825

[9] Sytsma, K. J., Morawetz, J., Pires, J. C., Nepokroeff, M., Conti, E., Zjhra, M., Chase, M. W., Urticalean rosids: circumscription, rosid ancestry, and phylogenetics based on rbcL, trnL-F, and ndhF sequences. *Am. J. Bot.*, **2002**, 89(9), 1531–1546. DOI: 10.3732/ajb.89.9.1531

[10] Dutt, D., Upadhyaya, J., Tyagi, C., Kumar, A., Lal, M., Studies on Ipomea carnea and Cannabis sativa as an alternative pulp blend for softwood: An optimization of kraft delignification process. *Ind. Crops Prod.*, **2008**, 28(2), 128–136. DOI: 10.1016/j.indcrop.2008.02.001

[11] Groot, B. D., Dam, J. E. V., Riet, K. V. 'T., Alkaline Pulping of Hemp Woody Core: Kinetic Modelling of Lignin, Xylan and Cellulose Extraction and Degradation. *Holzforschung*, **1995**, 49(4), 332–342. DOI: 10.1515/hfsg.1995.49.4.332

[12] Danielewicz, D., Surma-Slusarska, B., Processing of Industrial Hemp into Papermaking Pulps Intended for Bleaching. *Fibers & Textiles in Eastern Europe*, **2010**, 18(6), 110–115.

[13] Tutuş, A., Karataş, B., Çiçekler, M., Pulp and Paper Production from Hemp by Modified Kraft Method. *1st International Mediterranean Science and Engineering Congress* (IMSEC **2016**), 1036–1042.

[14] Abdul-Karim, L. A., Rab, A., Polyànszky, É., Rusznàk, I., Kinetics of delignification in kraft pulping of wheat straw and hemp. *Tappi J.*, **1995**, 78(8), 161–164.

[15] Franklin, G. L., Preparation of Thin Sections of Synthetic Resins and Wood-Resin Composites, and a New Macerating Method for Wood. *Nature*, **1945**, vol. 155, p. 51., DOI:10.1038/155051a0.

[16] Zhao, X., Liu, D., Kinetic Modeling and Mechanisms of Acid-Catalyzed Delignification of Sugarcane Bagasse by Aqueous Acetic Acid. *BioEnergy Res.*, **2012**, 6(2), 436-447. DOI:10.1007/s12155-012-9265-4

[17] Ring, G. J. F., Bacon, A. J., Multiple component anlysis of fiber length distributions , *International Paper Physics Conference*, Niagara-on-the-Lake ON, **1995**, pp. P75-P85.

[18] McDonough, T. J., The chemistry of organosolv delignification. *Tappi J.*, **1993**, 76(8):186–193

[19] Smith, D. M. (1954). Maximum moisture content method for determining specific gravity of small wood samples. Madison, WI: U.S. Dept. of Agriculture, Forest Service, Forest Products Laboratory.

[20] Usta, I., Comparative study of wood density by specific amount of void volume (porosity). *Turk. J. Agric. For.*, **2003**, 27(1), 1-6.

[21] Simpson, W., Specific gravity, moisture content, and density relationship for wood, **1993**, (General technical report FPL ; 76). Madison, WI (One Gifford Pinchot Dr., Madison 53705-2398): U.S. Dept. of Agriculture, Forest Service, Forest Products Laboratory.

[22] Brereton, N. J. B., Ahmed, F., Sykes, D., Ray, Michael J., Shield, I., Karp, A., Murphy, R. J., X-ray micro-computed tomography in willow reveals tissue patterning of reaction wood and delay in programmed cell death. *BMC Plant Biol.*, **2015**, 15(1), 83. DOI: 10.1186/s12870-015-0438-0

[23] Gomez, F. E., Carvalho, G., Shi, F., Muliana, A. H., Rooney, W. L., High throughput phenotyping of morpho-anatomical stem properties using X-ray computed tomography in sorghum. *Plant Methods*, **2018**,14(1), 59. DOI: 10.1186/s13007-018-0326-3

[24] Flannery, B., Deckman, H., Roberge, W., D'Amico, K., Three-Dimensional X-ray Microtomography. *Science* (New York, N.Y.), **1987**, 237(4821), 1439-44. DOI: 10.1126/science.237.4821.1439

[25] Ketcham, R., Carlson, W., Marschallinger, R., Johnson, S. E., Acquisition, optimization and interpretation of X-ray computed tomographic imagery; applications to the geosciences. *Comput. Geosci.*, **2011**, 27(4), 381-400. DOI: 10.1016/S0098-3004(00)00116-3

[26] Ghosh, N., Smith, D., Characterization of some biological specimens using TEM and SEM. *Proceedings of SPIE*, **2009**, 7378(1), 73781N-73781N-8. DOI:10.1117/12.821825

[27] Jansen, S., Preparation of Wood Specimens for Transmitted Light Microscopy and Scanning Electron Microscopy, *Belg. Journ. Bot.*, **1998**,131: 41:49

[28] Rapp, A.O., Preparation of Wood for Microscopitc Analysis after Decay Testing, *Holz als Roh-und Werkstoff*, **1998**, 56: 277-278. DOI:10.1007/s001070050319

[29] Kuo J., Processing Plant Tissues for Ultrastructural Study. In: Kuo J. (eds) Electron Microscopy. Methods in Molecular Biology™, vol 369. *Humana Press*, **2007**, pp35-45, DOI:10.1007/978-1-59745-294-6_3

[30] Brown, F. B. H., The Preparation and Treatment of Woods for Microscope Study, *Bulletin of the Torrey Botanical Club*, **1919**,Vol 4, No.4, pp127-150

[31] Miller, E.J.,. Basic Photoshop for Electron Microscopy. NUANCE Center, Northwestern University. **2013**

[32] Nanko, H., The World of Market Pulp. Atlanta,, GA: *TAPPI Press*, **2005**.

[33] Robertson, G., Olson, P., Allen, B., Chan, Seth, R., Measurement of fiber length, coarseness, and shape with the fiber quality analyzer, *Tappi J.*, **1999**, 82:10

[34] TAPPI Method T264 cm-97, Preparation of wood for chemical analysis. *Test methods of the Technical Association of the Pulp and Paper Industry* **1997**.

[35] TAPPI Method T204 cm017., Solvent extractives of wood and pull, *Test methods of the Technical Association of the Pulp and Paper Industry*, **2007**.

[36] Sluiter A, Ruiz R, Scarlata C, Sluiter J, Templeton D. Determination of extractives in biomass: laboratory analytical procedure (LAP). Jefferson: National Renewable Energy Laboratory; **2008**.

[37] Reddy, N. Properties of natural cellulose fibers from hop stems. *Carbohydr. Polym.*, **2009**, 77, 898-902. DOI: 10.1016/j.carbpol.2009.03.013

[38] Bura R, Mansfield SD, Saddler JN, Bothast RJ., SO2-catalysed steam explosion of corn fibre for ethanol production. *Appl. Biochem. Biotechnol.*, **2002**, 98–100:59–72. DOI: 10.1007/978-1-4612-0119-9_5

[39] NREL Laboratory Analytical procedure, "Determination of Total Solids in Bio-mass and Total Dissolved Solids in Liquid Process Samples" NREL/TP-510 (**2008**)

[40] TAPPI Method T222 om-11. :Acid-insoluble lignin in wood and pulp, *Test methods of the Technical Association of the Pulp and Paper Industry* Atlanta; **2001**.

[41] Sluiter, A., Hames, B., Ruiz, R., Scarlata, C., Sluiter, J., Templeton, D., Crocker, D., Determination of Structural Carbohydrates and Lignin in Biomass; NREL/TP-510-42618, US National Renewable Energy Laboratory, Golden, Colorado, **2008**

[42] Sluiter A, Ruiz R, Scarlata C, Sluiter J, Templeton D. Determination of extractives in biomass: laboratory analytical procedure (LAP). Jefferson: National Renewable Energy Laboratory; **2008**.

[43] Ewanick S, Bura R. The effect of biomass moisture content on bioethanol yields from steam pretreated switchgrass and sugarcane bagasse. *Bioresour Technol*. **2011**;102:2651–8. DOI: 10.1016/j.biortech.2010.10.117

[44] Randolph, Timothy W., Scale-based normalization of spectral data, University of Washington, Department of Biostatistics , 16 Nov. 2005.

[45] Fearn, T., Riccioli, C., Garrido-Varo, A., Guerrero-Ginel, J. E., On the geometry of SNV and MSC. *Chemom. Intell. Lab. Syst.*, **2009**, 96(1), 22-26. DOI:10.1016/j.chemolab.2008.11.006

[46] Shin, S.-J., Han, G.-S., Choi, I.-G.,Han, S.-H., Chemical characterization of industrial hemp (Cannabis sativa) biomass as biorefinery feedstock, *Korean J. Plant Res*. **2008**, 21(3): 222-225.

[47] Bi, Y., Yuan, K., Xiao, W., Wu, J., Shi, C., Xia, J., Zhou, G., A local pre-processing method for near-infrared spectra, combined with spectral segmentation and standard normal variate transformation. *Anal. Chim. Acta*, **2016**, 909, 30-40. DOI:10.1016/j.aca.2016.01.010

[48] Rinnan, Å, Berg, F. V., Engelsen, S. B., Review of the most common pre-processing techniques for near-infrared spectra. *TrAC, Trends Anal. Chem.*, **2009**, 28(10), 1201-1222. DOI:10.1016/j.trac.2009.07.007

[49] Bi, Y., Yuan, K., Xiao, W., Wu, J., Shi, C., Xia, J., Zhou, G., A local pre-processing method for near-infrared spectra, combined with spectral segmentation and standard normal variate transformation, *Anal. Chim. Acta*, **2016**, 909, 30-40. DOI:10.1016/j.aca.2016.01.010

[50] TAPPI Method T248 sp-00. Laboratory beating of pulp (PFI mill method). *Test methods of the Technical Association of the Pulp and Paper Industry* **2000**.

[51] TAPPI Method T227 om-99 , Freeness of pulp (Canadian standard method). *Test methods of the Technical Association of the Pulp and Paper Industry*.**1999**.

[52] TAPPI Method T205 sp-95. Forming handsheets for physical tests of pulp, *Test methods of the Technical Association of the Pulp and Paper Industry* **1995**.

[53] TAPPI Method T402 sp-13. Standard Conditioning and Testing Atmos-phere for Paper, Board, Pulp Handsheets and Related Products. *Test methods of the Technical Association of the Pulp and Paper Industry* **2013**.

[54] TAPPI Method T401 cm-92. Tensile breaking strength and elongation of paper and paperboard (using pendulum type tester), *Test methods of the Technical Association of the Pulp and Paper Industry* **1992**.

[55] Mascorro, J., Novel choices for formulating embedding media kits. *Proc. SPIE*, **2009**, 7378(1), 73780F-73780F-12. DOI:10.1117/12.821821

[56] Miller, R., Anatomy and Morphology of Humulus lupulus, ProQuest Dissertations and Theses, **1954**.

[57] Mascorro, J., Novel choices for formulating embedding media kits. *Proc. SPIE*, **2009**, 7378(1), 73780F-73780F-12. DOI:10.1117/12.821821

[58] Ellis, R. L., Ideal fibers for pulp and paper products, *21st Southern Forest Tree Improvement Conference*, **1991**, pp. 295-302.

[59] Dutt, D., Comparison of various eucalyptus species for their morphological, chemical, pulp and paper making characteristics. *Indian J. Chem. Technol.*, **2011**, 18, 145-151.

[60] Danielewicz, D., Surma-Ślusarska, B., Properties and fibre characterisation of bleached hemp, birch and pine pulps: a comparison. *Cellulose*, **2017**,24, 5173–5186. DOI:10.1007/s10570-017-1476-6

[61] Bura, R., Chandra, R., Saddler, J., Influence of xylan on the enzymatic hydrolysis of steam-pretreated corn stover and hybrid poplar. *Biotechnol. Prog*., **2009**,25(2), 315–322. DOI:10.1002/btpr.98

[62] Huijgen, W. J., Reith, J. H., Uil, H. D., Pretreatment and Fractionation of Wheat Straw by an Acetone-Based Organosolv Process. *Ind. Eng. Chem. Res.*, **2010**, 49(20), 10132-10140. DOI:10.1021/ie101247w

[63] Ping, L., Brosse, N., Sannigrahi, P., Ragauskas, A., Evaluation of grape stalks as a bioresource. *Ind. Crops Prod.*, **2011**, 33(1), 200–204. DOI:10.1016/j.indcrop.2010.10.009

[64] Sanjuán, R., Anzaldo, J., Vargas, J., Turrado, J., Patt, R., Morphological and Chemical Composition of Pith and Fibers from Mexican Sugarcane Bagasse. *Holz Als Roh- Und Werkstoff*, **2001**, 59(6), 447–450. DOI:10.1007/s001070100236

[65] Dutt, D., Upadhyaya, J., Tyagi, C., Kumar, A., Lal, M., Studies on Ipomea carnea and Cannabis sativa as an alternative pulp blend for softwood: An optimization of kraft delignification process. *Ind. Crops Prod.*, **2008**, 28(2), 128–136. DOI:10.1016/j.indcrop.2008.02.001

[66] Ai, J., Tschirner, U., Fiber length and pulping characteristics of switchgrass, alfalfa stems, hybrid poplar and willow biomasses. *Bioresour. Technol.*, **2010**, 101(1), 215–221. doi: 10.1016/j.biortech.2009.07.090

[67] Barberà, L., Pèlach, M., Pérez, I., Puig, J., Mutjé, P., Upgrading of hemp core for papermaking purposes by means of organosolv process. *Ind. Crops Prod.*, **2011**, 34(1), 865–872. DOI:10.1016/j.indcrop.2011.02.005

[68] Singh, S., Dutt, D., Tyagi, C. H., Complete Characterizaton of Wheat Straw (Triticum Aestivum PBW-343 L. Emend.Fiori&Paol.) – A renewable Source of Fibers for Pulp and Paper Making., *BioResources*, **2011**, 6(1), 154-177. DOI: 10.15376/biores.6.1.154-177

[69] Gandolfi, S., Ottolina, G., Riva, S., Fantoni, G. P., Patel, I., Complete Chemical Analysis of Carmagnola Hemp Hurds and Structural Features of Its Components. *BioResources*, **2013**, 8(2). DOI:10.15376/biores.8.2.2641-2656

[70] Torres, L. A. Z., Woiciechowski, A. L., Tanobe, V. O. D. A., Karp, S. G., Lorenci, L. C. G., Faulds, C., Soccol, C. R., Lignin as a potential source of high-added value compounds: A review. *J. Cleaner Prod.*, **2020**, 263, 121499. DOI:10.1016/j.jclepro.2020.121499

[71] Abidi, N., Hequet, E., Cabrales, L., Applications of Fourier Transform Infrared Spectroscopy to Study Cotton Fibers. Fourier Transforms - New Analytical Approaches and FTIR Strategies. **2011**, DOI:10.5772/15829

[72] Fan, M., Dai, D., & Huang, B., Fourier Transform Infrared Spectroscopy for Natural Fibres. Fourier Transform - Materials Analysis. **2012**, DOI:10.5772/35482

[73] Xu, F., Yu, J., Tesso, T., Dowell, F., Wang, D., Qualitative and quantitative analysis of lignocellulosic biomass using infrared techniques: A mini-review. *Appl. Energy*, **2013**, 104, 801-809. DOI:10.1016/j.apenergy.2012.12.019

[74] Garside, P., Wyeth, P., Identification of Cellulosic Fibres by FTIR Spectroscopy Differentiation of flax and hemp by polarized ATR FTIR. *Stud. Conserv.*, **2006**, 51(3), 205–211. DOI:10.1179/sic.2006.51.3.205

[75] Jayapal, N., Samanta, A., Kolte, A. P., Senani, S., Sridhar, M., Suresh, K., Sampath, K., Value addition to sugarcane bagasse: Xylan extraction and its process optimization for xylooligosaccharides production. *Ind. Crops Prod.*, 2013, 42, 14–24. DOI:10.1016/j.indcrop.2012.05.019

[76] Li, X., Sun, C., Zhou, B., He, Y., Determination of Hemicellulose, Cellulose and Lignin in Moso Bamboo by Near Infrared Spectroscopy. *Scientific Reports (Nature Publisher Group)*, **2015**, 5(1), 17210. DOI: 10.1038/srep17210

[77] Magaton, A. D. S., Piló-Veloso, D., Colodette, J. L., Caracterização das O-acetil-(4-O-metilglicurono)xilanas isoladas da madeira de Eucalyptus urograndis. *Química Nova*, **2008**, 31(5), 1085–1088. DOI:10.1590/s0100-40422008000500027

[78] Popescu, C.-M., Popescu, M.-C., Singurel, G., Vasile, C., Argyropoulos, D. S., Willfor, S., Spectral Characterization of Eucalyptus Wood. *Appl. Spectrosc.*, **2007**, 61(11), 1168–1177. DOI:10.1366/000370207782597076

[79] Tipson, R., Infrared spectroscopy of carbohydrates; a review of the literature (NBS monograph ; 110). Washington: U.S. Dept. of Commerce, National Bureau of Standards; for sale by the Supt. of Docs., U.S. Govt. Print. Off. **1968**.

[80] Kline, L. M., Simplified Determination of Lignin Content in Hard and Soft Woods via UV-Spectrophotometric Analysis of Biomass Dissolved in Ionic Liquids. *BioResources*, **2010**, vol. 5, no. 3, pp. 1366–1383.

[81] El Hage, R., Characterization of Milled Wood Lignin and Ethanol Organosolv Lignin from Miscanthus. *Polym. Degrad. Stab.*, **2009**, vol. 94, no. 10, , pp. 1632–1638., DOI:10.1016/j.polymdegradstab.2009.07.007.

[82] Yáñez-S, M., Physicochemical Characterization of Ethanol Organosolv Lignin (EOL) from Eucalyptus Globulus: Effect of Extraction Conditions on the Molecular Structure. *Polym. Degrad. Stab.*, **2014**, vol. 110, pp. 184–194., DOI:10.1016/j.polymdegradstab.2014.08.026.

[83] Labbé, N., Chemical Structure of Wood Charcoal by Infrared Spectroscopy and Multivariate Analysis., *J. Agric. Food Chem*., **2006**, vol. 54, pp. 3492–3497., DOI:10.1021/jf053062.

[84] Yang, Q., Shi, J., Lin, L., Characterization of structural changes of lignin in the process of cooking of bagasse with solid alkali and active oxygen as a pretreatment for Lignin Conversion. *Energy Fuels*, **2012**, 26(11), 6999-7004. DOI:10.1021/ef300983h

[85] Popescu, C., Popescu, M., Singurel, G., Vasile, C., Argyropoulos, D. S., Willfor, S., Spectral characterization of eucalyptus wood. *Applied Spectroscopy*, **2007**, 61(11), 1168-1177. DOI:10.1366/000370207782597076.

[86] Zhao, W.J., In situ inorganic flame retardant modified hemp and its polypropylene composites, *RSC Adv.*, **2017**, 7, 32236, DOI:10.1039/c7ra04078d

[87] Seth, R. S., Understanding sheet extensibility. *Pulp Pap. Can.*, **2005**,106(2), 33-40.

[88] El-Hosseiny, F., The Effect of Sheet Densification on the Shape of its Stress-Strain Curve. *J. Pulp Pap. Sci.*, **1994**, 20(12), 432-436.

[89] Shallhorn, P, Gurnagul, N., A Semi-empirical model of the tensile energy absorption of sack Kraft paper, *BioResources*, **2010**, 5(1), 455-476. DOI: 10.15376/biores.5.1.455-476

[90] Gurnagul, N., Ju, S,, Shallhorn, P., Miles, K., Optimising High-consistency Refining Conditions for Good Sack Paper Quality. *Appita J.*, **2006**, 59(6), 476-480.

Chapter 4. Nanocellulse by Ammonium Persulfate Mediated Oxidation, an alternative to TEMPO.

4.1 Abstract

Ammonium persulfate mediated oxidation used in conjunction with acids under extended reaction times have produced highly crystalline nanocellulose with varying surface chemistry and morphological properties. Subtle and dramatic changes in treatment conditions have produced nanocellulose with varied properties. Predictable and reproducible physical and chemical properties are needed for engineering fibers with desired functionality. We applied response surface methodology to control and assess the effect of varying treatment conditions on the oxidation of bleached and unbleached northern softwood Kraft, changing the applied ammonium persulfate on fiber, duration of oxidation, and temperature. Atomic force microscopy (AFM), X-ray diffraction (XRD), chemical titration, and gravimetric analysis were used to systematically characterize the oxidized nanocellulose fibers produced. As-prepared materials exhibited surface charge and crystallinity index ranging from 0.6 mmol/g to 1.4 mmol/g carboxylic acid and 72 to 88%, respectively. The morphological characteristics varied from 48 to 80 for the aspect ratio, from 2.7 to 4.5 nm for the diameter, and from 146 to 247 nm for the length. The response surface model developed in this research allows for designing nanocelluloses with targeted surface charge, crystallinity and aspect ratio. We demonstrate that the environmentally friendly ammonium persulfate, opposed to TEMPO-mediated oxidation, is effective at producing similar surface chemistry in lignin containing wood and non-wood fibers without pretreatment or adjustment of experimental conditions.

4.2 Introduction

Nanofibrillated cellulose may be produced by mechanical methods or a combination of chemical and mechanical homogenization[1]. Nanofibers are described interchangeably as either cellulose nanofibers (CNF) or as nanofibrillated cellulose (NFC), crystalline nanocellulose (CNC), and microfibrillated cellulose (MFC). The nanofibers produced are on the order of 2-20 nm in diameter and 30 to 900 nm in length[2,3] as shown in Table 4.1.

Table 4.1 Abbreviations used in cellulose nanomaterials - defined

Abbreviation	Description	Diameter Range	Length
NFC, CNF[4]	Nanofibrillated cellulose, Cellulose Nanofibrils	5–15 nm	> 1μ
CNC[5]	Crystalline nanocellulose	2-20 nm	0.05-0.5 μ
MFC[4]	Microfibrillated Cellulose	10-50 μ	10-50 μ
Tracheid	Wood cell	10-50 μ	1-3 mm

The qualification of nanofibers characterize the morphological characteristics of diameter and length as well as the crystallinity and surface chemistry[6]. Nanocellulosic fibers present a sustainable material with broad application in material science[7]. A significant amount of research has been conducted in modification of the nanocellulose surface[8,9], composite applications[10,11], rheology of nanocellulose suspensions[12,13], and preparation methods[14,15].

Chemical methods are dominated by acidic processes designed to penetrate the cellulose fibers, break the hydrogen bonds between fiber bundles, and modify the surface chemistry. Sulfuric acid, oxone, periodate, chlorite, enzymatic[16], TEMPO, and ammonium persulfate are a few of the chemical treatments used to produce nanofibers[17]. TEMPO is the most commonly used in research as it produces very homogenous and predictable results, however it is both costly, involves complex reaction chemistry, and has a negative environmental footprint[18]. TEMPO is classified as an H412 chemical, harmful to aquatic life, by the Globally Harmonized System (GHS)[19]. Sulfuric acid is scalable and economically attractive; however, it results in a sulfonated

surface that may require subsequent treatment. Oxone® (Potassium peroxymonosulfate) and periodate require multiple steps achieving similar surface chemistry and aspect ratios to other methods. Periodate has been capable of achieving surface charge as high as 1.75 mmol/g[20] as it is not limited to reaction with the C6 hydroxyl. Chlorite oxidation of cellulose is capable of achieving aspect ratios similar to those achieved with ammonium persulfate (APS) oxidation, albeit with a chlorinated chemistry[21]. APS is economical, selective for cellulose, and environmentally safe, however the oxidation process has not been well characterized. The focus has been primarily on the final product, thus the characteristics of nanofibers produced have varied from laboratory to laboratory and researchers have reported difficulty in controlling results[22,23]. As such, treatment conditions are similar; extended oxidation time, > 10 hours, and high dosage of APS, > 2000% on fiber, see Table 4.2.

Table 4.2. Summary of selected published research using APS oxidation to produce nanocellulose.

Author	*Biomass*	*Time, min*	*mols APS/g*	*APS, %*	*Temp, °C*	*Consistency, %*	*mmol Carb/g*	*DO*
Zhang[24]	Bagasse	960	0.100-0.200	2282-4564	60	1	0.560-0.990	-
Leung[25]	Flax	960	0.100	2282	60	1	-	0.180
Leung	Hemp	960	0.100	2282	60	1	-	0.170
Leung	Wood	960	0.100	2282	60	1	-	0.190
Castro-Guerro[26]	Wood	480	Unk	Unk	60	Unk	0.900	0.130
Du[38]	Bagasse	480	0.100	2282	65	1	-	0.190
Filipova[37]	Birch	240	0.050	1140	70	2	-	-
Vecbiskena[27]	Birch	240	0.004	100	70	2	-	-
Rozenberga[28]	Brich	240	0.004	100	70	2	-	-
Cheng[29]	Cotton	960	0.100	2282	70	1	-	-
Jiang[30]	Poplar	960	0.100	2282	70	1	-	0.163
Mascheroni[43]	Cotton	960	0.100	2282	75	1	0.160	0.150
Oun[31]	Cotton	960	0.100	2282	75	1	-	0.150
Cheng[29]	Cotton	240-1440	0.05-0.2	1141-4564	80-90	1	-	0.058-0.132

Less total active chemistry is required using the TEMPO mediated oxidation method compared to APS to achieve the same level of surface charge. The high cost of TEMPO combined with hazardous chemistry, however, makes APS an attractive alternative. TEMPO sells for $248.00/kg while ammonium persulfate can be purchased for $0.60/kg. Sodium borohydride, sodium hypochlorite cost $3.90/kg and $1.10/kg, respectively. Several authors have reported the cost of producing a kg of cellulose nanofibrils, see Table 4.3. Energy consumption values provided by Filipova[32] were used as the basis and adjusted for current Washington state energy prices, $0.144/kWh[33]. Note that Filipova applied TEMPO at a level 88% lower than Serra (0.016 vs 0.002 g/g fiber). Delgado's cost appears to be the price for analytical-grade chemical, not bulk price. All reported chemistry was relativized for comparison. The cost results provide a relative cost in laboratory but do not represent a true cost as provided in a techno-economic study.

Table 4.3. Relativized cost data using current market prices and Washington state energy costs.

Treatment	*$/kg CNF as published*	*$/kg CNF relativized*	*mmol Carb/g*
TEMPO (Filipova 2020)[32]	$7.20	$18.05	0.149
APS (Filipova 2020)	$6.91	$8.02	0.133
TEMPO (Serra 2017)[78]	$9.02	$106.29	0.881
TEMPO (Delgado 2015)[34]	$205.73	$105.97	0.840
APS (Haunreiter)	-	$5.35	0.881

Ammonium persulfate is the most cost-effective and has the greatest efficiency when considering the surface charge developed, 293 mmol of carboxylic acid/$ cost. TEMPO averaged 0.12 mmol of carboxylic acid/$. APS is an environmentally non-toxic oxidizer and may be used with biomass containing up to 20% lignin to produce NFC or CNC[35]. The formation of furfural and 2-hydroxymethylfurfural, commonly formed when carbohydrates are hydrolyzed with strong

acids, have been shown to not be present in the spent APS liquor[36]. Research indicates that it may be hampered, however, by non-homogenous oxidation results[37,38].

APS is an environmentally nontoxic oxidizer[39] and may be used with biomass containing up to 20% lignin to produce NFC or CNC[40]. The formation of furfural and 2-hydroxymethylfurfural, commonly formed when carbohydrates are hydrolyzed with strong acids, has been shown to not be present in the spent APS liquor[41].

APS decomposes in aqueous solution through two reaction pathways that occur simultaneously. The homolysis of the peroxide bond in ammonium persulfate using heat activates the S_2O_8 anion in equation 1[42, 43]. The maximum amount of ammonium persulfate applied is limited by a desired pH of greater than 0.3 ([H+] < 0.5M). Increasing the concentration of hydronium ion will increase the rate of peroxydisulfate anion decomposition and result in the formation of Caro's acid[44]. The pH for this investigation was between 0.5 and 0.8. The first step, equation 1, is fast decomposition of the peroxydisulfate to form $SO_4^{\bullet-}$, the sulfate free radical[45,46,47]. The sulfate free radical penetrates the amorphous region of the cellulose chain to co-hydrolyze the β-1,4 bond between glucose units, reducing the overall chain length and increasing the crystallinity of the nanofiber. The subsequent decomposition reactions, equation 2 and 3, is rapid formation of hydrogen sulfate, HSO_4^- , sulfate free radical $SO_4^{\bullet-}$, and peroxyl radical, $HO^{\bullet}$. The sulfate free radical oxidizes the C6 to its' aldehyde form, followed by peroxyl radical oxidation to form carboxylic acid groups on the nanofiber surface[48,49]. The peroxyl radical may also form carbonyl's with secondary alcohols, ultimately contributing to the formation of hemiacetal cross-links when dried, however, Leung demonstrated using FTIR and NMR that this reaction does not occur[50,51]. The byproduct of the oxidation reaction is the formation of sulfate ion and sulfuric acid. Leung determined that these were in the molar ratio of 4 to 6 in the residual liquor. The formation of

peroxide under acidic conditions, equation 4, leads to oxidation of lignin, which may be improved through possible formation of peroxymonosulfate in secondary reactions with sulfate radical[52,53].

$$S_2O_8^{-2} \xrightarrow[heat]{} 2SO_4^{\bullet -} \quad (4\text{-}1)$$

$$SO_4^{\bullet -} + H_2O \xrightarrow[heat]{} HSO_4^- + HO^\bullet \quad (4\text{-}2)$$

$$S_2O_8^{-2} + HO^\bullet \xrightarrow[heat]{} HSO_4^- + SO_4^{\bullet -} + \frac{1}{2}O_2 \quad (4\text{-}3)$$

$$2HO^\bullet \xrightarrow[heat]{} H_2O_2 \quad (4\text{-}4)$$

$$SO_4^{\bullet -} + HO^\bullet \xrightarrow[heat]{} HSO_4^- + \frac{1}{2}O_2 \quad (4\text{-}5)$$

Evaluation of the ammonium persulfate must consider the effect of lignin on the response to treatment. Chemical processes for oxidizing cellulose, such as TEMPO, to nanofibers require a lignin free biomass to prevent increased consumption of reactants[54,55]. The insoluble lignin content of unbleached pulps has been shown to consume hypochlorite in TEMPO mediated oxidation reactions[56]. A multi-step process is required to remove the lignin. Published research has reported that ammonium persulfate is selective for cellulose and thus can be effective at oxidizing cellulose with less than 20% lignin content.

Response surface methodology is applied to assess the effect of varying oxidation conditions on bleached and unbleached residual biomass. Ammonium persulfate application on fiber, time, and temperature are adjusted using a central composite design. Oxidation conditions are mild in our process compared to previous literature. This novel response surface model will allow for synthesizing nanofibers with a range of morphological and chemical characteristics. In some applications, nanocellulose with high surface charge are desired, such as the dispersion of carbon nanomaterials like nanotubes and graphene in water , while in other cases, a high charge

density makes cellulosic materials more sensitive to water and hinders their strength in wet conditions . The proposed approach can serve to tailor the nanocellulose properties based on targeted applications by the fine-tuning of the APS oxidation conditions.

4.3 Materials & Methods

The base fiber used is bleached Northern softwood Kraft (B-NSWK), supplied by WestRock, Tacoma, WA. Unbleached fiber (UB-NSWK, 4% lignin) was also supplied by the WestRock, Tacoma, WA pulp mill, taken prior to the bleaching. The two furnished pulps are an approximately 50:50 Douglas fir (*Pseudotsuga menziesii*) and Western Hemlock (*Tsuga heterophylla*) blend. Hop bine (*Humulus lupulus L.*) was kindly supplied by Roy Farms, Moxee, WA.

4.3.1. Preparation of NFC by APS Oxidation.

2.5 grams of oven dry fiber is weighed out and disintegrated in a waring disintegrator. The fiber is then transferred to a 500 ml Erlenmeyer flask where a volume of 2M ammonium persulfate solution (228.18 g/500ml) are added based on experimental design levels to achieve a 0.5% consistency. Low consistency was selected to minimize the interaction of mass transfer with treatment conditions. A stir bar set to 250 rpm is used for continuous agitation. The flask is heated on a hot plate with a thermocouple placed into the solution. The oxidation reaction is quenched by placing the beaker in an ice bath to rapidly drop the temperature. After quenching the reaction, the sample is transferred to a Spectra/Por 4 molecular porous membrane tube, MWCO: 12-14kD. It is then placed into a tank of deionized water for seven days to dialyze or until a pH greater than 3.4 is achieved. Post dialysis, the oxidized fibers require treatment with mechanical energy. Samples were ultra-sonicated with 14,000 J of energy for 2 minutes. After samples had been

mechanically treated, they were centrifuged for 20.0 minutes at 2950 RPM (1720 relative centrifugal force). The nanofibrillated cellulose fibers remained suspended in the supernatant while partially oxidized fibers were deposited on the bottom of the centrifuge tube.

The carboxylic acid concentration of the fibers was measured using a conductometric titration method which is described in the following section. The fibers were then sonication using a 750 W Sonics Vibracell VCX probe sonicator equipped with a 13 mm stepped tip to break up the nanofibrillated cellulose aggregates[57],[58]. There is evidence that ultrasonication may reduce the degree of polymerization of the nanofibers[59]. Therefore, time, consistency, probe position, and amplitude were held constant. The fiber was transferred to a 150 mL beaker and diluted to a consistency of 1.5%. The temperature is controlled by placing the beaker in an ice/water bath[60]. The probe is placed into the beaker so that it is approximately in the middle of the suspension[61]. Amplitude was set at 90% for 4 minutes of treatment for a total of 26,000 J. The ultrasonicated fiber is transferred to 50.0 mL centrifuge vials and centrifuged for 20.0 minutes at 2950 RPM (1720 relative centrifugal force). The supernatant, containing the nanofibrillated cellulose, is then transferred to a clean 50.0 mL centrifuge vial.

4.3.2 Factorial Design; Preliminary Investigation.

A factorial design, 2^3 ,was used to conduct an initial investigation to guide the selection of treatment conditions for more rigorous experimentation as shown in Table 4.4. Consistency was set at two levels (2% and 5%), two reaction temperatures (70, and 90 °C), and two ammonium persulfate (APS) dosages (0.0022 and 0.0044 mol/g fiber). Time was held constant at 240 minutes. The data from this initial experiment will be used to construct an experimental design to evaluate the kinetics, see the experimental details in Table 4.5. Kinetic Study and a central composite design (CCD) experiment for the primary investigation.

Table 4.4. Initial Experimental Design

Trial	*Consistency*	*mols APS/g*	*Temp* °C	*AxB*	*AxC*	*BxC*	*AxBxC*
1	2%	0.0022	70	1	1	1	-1
2	2%	0.0022	90	1	-1	-1	1
3	2%	0.0044	70	-1	1	-1	1
4	2%	0.0044	90	-1	-1	1	-1
5	5%	0.0022	70	-1	-1	1	1
6	5%	0.0022	90	-1	1	-1	-1
7	5%	0.0044	70	1	-1	-1	-1
8	5%	0.0044	90	1	1	1	1

Table 4.5. Kinetic Study

Trial	*Time, min*	*Level 1 mols APS/g*	*Level 2 mols APS/g*	*Temp* °C	*M[APS]$_0$*
1	60	0.044	-	70	0.221
2	120	0.044	0.066	70	0.221
3	180	0.044	-	70	0.221
4	240	0.044	0.066	70	0.221
5	300	0.044	-	70	0.221
6	360	0.044	0.066	70	0.221
7	420	0.044	-	70	0.221
8	480	0.044	0.066	70	0.221
9	540	0.044	-	70	0.221
10	600	0.044	0.066	70	0.221

4.3.3 Central Composite Design.

Response surface methodology (RSM) was used to assess the effect of varying treatment conditions on ammonium persulfate oxidation (APS) of bleached softwood, unbleached softwood and hop bine pulps. RSM is an empirical modeling method that evaluates the effect of the independent variables and their interactions on the process[62]. Specifically, five APS dosages (i.e. 0.032, 0.039, 0.049, 0.058, and 0.065 mols APS/g fiber), five reaction times (i.e. 158, 240, 360, 480, and 562 min) and five temperatures (i.e. 63, 70, 80, 90, and 97 °C) was examined using the central composite design reported in Table 4.6, in which the three variables are converted to dimensionless ones with the coded values at five levels: -1.682, -1, 0, 1, and 1.682. Four replicates of the centroid conditions were conducted for statistical soundness. The surface charge,

crystallinity, diameter, and length of the resulting nanocellulose fibers prepared based on the various combinations listed in Table 2 were systematically characterized. R-Studio software was used to evaluate the response surface model[63].

Table 4.6. Experimental matrix of the Central Composite Design with four replicates of the central point (i.e. factor #15).

Factor	*Time, min*	*mols APS/g*	*Temp, °C*	*A*	*B*	*C*
1	240	0.039	70	-1	-1	-1
2	240	0.039	90	-1	-1	1
3	240	0.058	70	-1	1	-1
4	240	0.058	90	-1	1	1
5	480	0.039	70	1	-1	-1
6	480	0.039	90	1	-1	1
7	480	0.058	70	1	1	-1
8	480	0.058	90	1	1	1
9	158	0.049	80	-1.682	0	0
10	562	0.049	80	1.682	0	0
11	360	0.032	80	0	-1.682	0
12	360	0.065	80	0	1.682	0
13	360	0.049	63	0	0	-1.682
14	360	0.049	97	0	0	1.682
15	360	0.049	80	0	0	0
15	360	0.049	80	0	0	0
15	360	0.049	80	0	0	0
15	360	0.049	80	0	0	0

The model was applied to test the response of lignin containing fibers to ammonium persulfate mediated oxidation. The bleached and unbleached fibers were supplied by the same mill and comprise identical fiber blends. The unbleached fibers contained 3% lignin (20 Kappa number). Treatment conditions were selected from the central composite design with the addition of a midpoint, see Table 4.6, to compare shifts in response between the oxidized fibers.

Hop bine containing lignin was also evaluated to investigate the response of non-woody feedstock as this would be a strong candidate for commercial NFC production. Hop bine was pulped in a 10-liter M/K digester to a final lignin content of 4%. Hop bine was treated using the conditions in Table 4.7.

Table 4.7. Treatment Conditions – Unbleached pulp and hop bine oxidation experiment

Run Order	*Time, min*	*mols APS/g*	*Temp, °C*
1	240	0.058	70
2	240	0.058	90
3	480	0.058	70
4	480	0.058	90
5	360	0.058	70
6	360	0.058	90

The central composite design (CCD) methodology was used to fit a second order polynomial to a response surface using RSM. The best fit predicted second order quadratic equation is used to estimate the response for the validation experiments, equation 4-6. Y is the response variable; β_0 is the intercept; β_i, β_{ij} and β_{ii} are coefficients of the linear double interactions; x_i, are the factors mols APS/g, temperature, and time[64].

$$Y = \beta_o + \sum_{i=1}^{3} \beta_i x_i + \sum_{i=1}^{3} \sum_{j=1}^{3} \beta_{ij} x_i + \sum_{i=1}^{3} \beta_{ii} x_{ii}^2 \qquad (4\text{-}6)$$

4.3.4 Carboxylic Acid Determination.

APS oxidation reactions introduce carboxylic acid functional groups via nucleophilic substitution reactions at the C6 carbon[65,66]. The hydroxymethyl conformation at C6 is trans-gauche in the crystalline regions and gauche-gauche in the amorphous regions resulting in intramolecular hydrogen bonding between the O2 and O6 and the O3 and O5 hydroxyl groups[67]. This produces a helical twist in the cellulose chain results in the C6 hydroxymethyl group pointing outwards on alternating glucopyranose units. Determination of the theoretical number of hydroxyls exposed on the surface of the cellulose chain uses the height and width of the cellulose nanocrystal and dividing by the crystal plane (110 and 110 planes) spacings perpendicular to the faces of the crystal, see Figure 4.1[68,69,70].

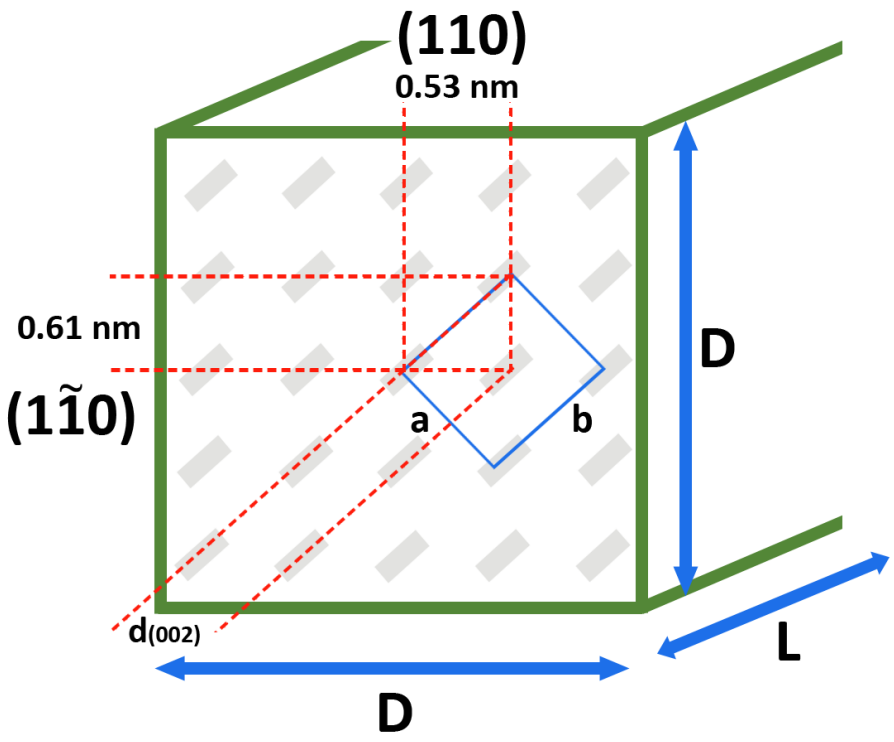

Figure 4.1 . Nanocrystal model representation

The mass of nanofibrils produced of a length L, with B (36) cellulose chains, and C (20) chains exposed on the surface is given by equation 4-7[68,71]. N_A is Avogadro's constant and the length of a cellobiose unit is 1.03 nm. The molecular weight of a hydroglucose ring is 162. The number of hydroxyl groups available for reaction is given by equation 4-8. The theoretical moles of carboxylic acid produced is given by equation 4-9.

$$\frac{L}{1.03} \text{x } 2 \text{ x } B \text{ x } \frac{162}{N_A} = \frac{314.555LB}{N_A} \tag{4-7}$$

$$C \text{ x } \frac{L}{1.03} \text{x } 2 \text{ x } \frac{1}{2} = 0.9709LC \tag{4-8}$$

$$n_{-COOH} = \frac{0.9709LC}{N_A} x10^3 \text{ mmol} \tag{4-9}$$

Rearranging equations 4-8 and 4-9, the theoretical carboxylic acid concentration (mmol/g) is given by equation 4-10.

$$[-COOH] = \frac{0.9709LC}{N_A} \text{x } 10^3 \text{ x } \frac{N_A}{314.555LB} = \frac{3.0865C}{B} \text{ mmol/g} \tag{4-10}$$

The carboxylate content of the NFC is one of the most critical determinations. A modification of previously published conductometric titration methods using 0.01 molar NaOH was used[7273,74,75]. Approximately 0.1 grams of oven-dried fiber are added to a 40.0mL scintillation vial to which 10 mL of 0.01M HCl is added. Deionized water makes up the remaining volume. The vials are then either sonicated for 15 minutes or allowed to sit for 2 hours during which the Na cations bound to the carboxylic acid groups are exchanged by H^+ ions[76]. The samples are then transferred to a 400 mL beaker and the volume brought up to 200 mL with deionized water. Conductivity is recorded using an Orion Star A212 meter for every 0.250 mL of titrant delivered by an Arduino controlled peristaltic pump. The corrected conductivity is plotted versus the volume of titrant added, see Figure 4.2.

Once the titration is complete, the oven dry mass of fiber is determined by filtering the solution through Whatman 589/2 ashless membranes and drying at 105 °C for three hours. The carboxyl content is determined by equation 4-11[77];

$$C = \frac{c*(V_2 - V_1)}{m} \tag{4-11}$$

C is the mmol/g of carboxyl, V_1 and V_2 is the amount of NaOH (mL) corresponding to the first and second equivalence points. *c* is the mol/L of NaOH. *m* is the oven dry mass of pulp (g). The degree of oxidation, eauaation 12, (DO) is determined by a modification of this equation[78];

$$DO = \frac{162*c*(V_2 - V_1)}{m - 36*c*(V_2 - V_1)} \tag{4-12}$$

The molecular weight of anhydro-glucose units (AGU) is 162. The molecular weight difference between an AGU and the sodium salt of a glucuronic acid is 36.

Previous TEMPO and APS-mediated oxidation studies on wood cellulose have achieved carboxylic acid content of 1.64 and 1.55meq/g respectively[79,80,81].

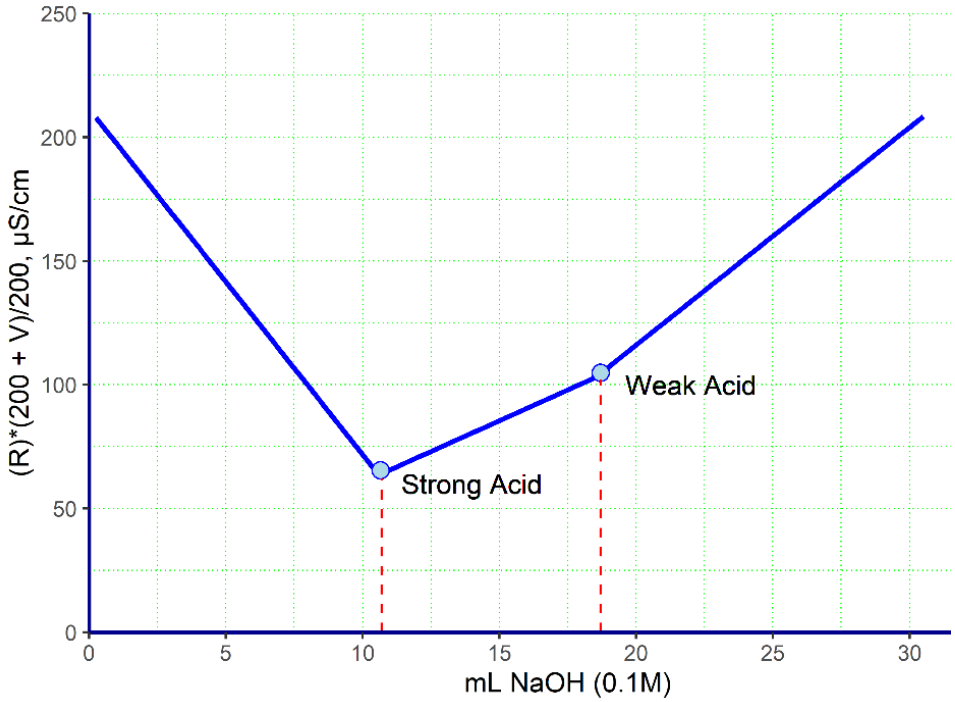

Figure 4.2. Adjusted conductivity titration curve, R is measured conductivity.

Spent oxidation liquor was collected after the reaction was quenched. 5.0 mL of the ammonium persulfate liquor (V_s) was diluted to 50.0 mL with deionized water for a 10:1 dilution. 7.0 mL of a 0.1N ferrous ammonium sulfate (FAS) solution was added to the sample providing an excess of ferrous ions. After 40 minutes, the solution was titrated with 0.5 N potassium permanganate solution (V_t)[82]. Equation 4-13 is used to calculate the concentration of residual ammonium persulfate. V_{mb} is the volume of titrant for the method blank.

$$\frac{g}{L}APS = \frac{(V_{mb}-V_t)N_{KMnO_4}*114}{V_s} \quad (4\text{-}13)$$

4.3.5 X-Ray Diffraction.

X-ray diffraction profiles of as-prepared nanocellulose films were collected using a Bruker D8 Discovery X-ray diffraction (XRD) system equipped with a high-efficiency Cu (1.54 Å) anode, a microfocus X-ray source, and a Pilatus 100 K large-area 2D-detector. A sample of the supernatant for each sample was dried in an oven at 50 °C to produce a flat thin film. Cellulose may produce up to five distinct peaks, however these peaks are influenced by the amorphous region in the fibers[83, 84]. The Segal method was used to interpret the XRD profiles by evaluating the ratio between the difference in peak height for the intensity at I_{200} and I_{am} and the total intensity at I_{002} , using equation 4-14, after back ground subtraction as illustrated in Figure 4.3[,85,86].

$$\% C = \frac{I_{200} - I_{am}}{I_{200}} \quad (4\text{-}14)$$

While this method provides a good basis for relative comparison between samples, it tends to overestimate the crystallinity index of cellulose because of the somewhat arbitrary determination of the amorphous region that can induce error in crystallinity estimation[85,86].

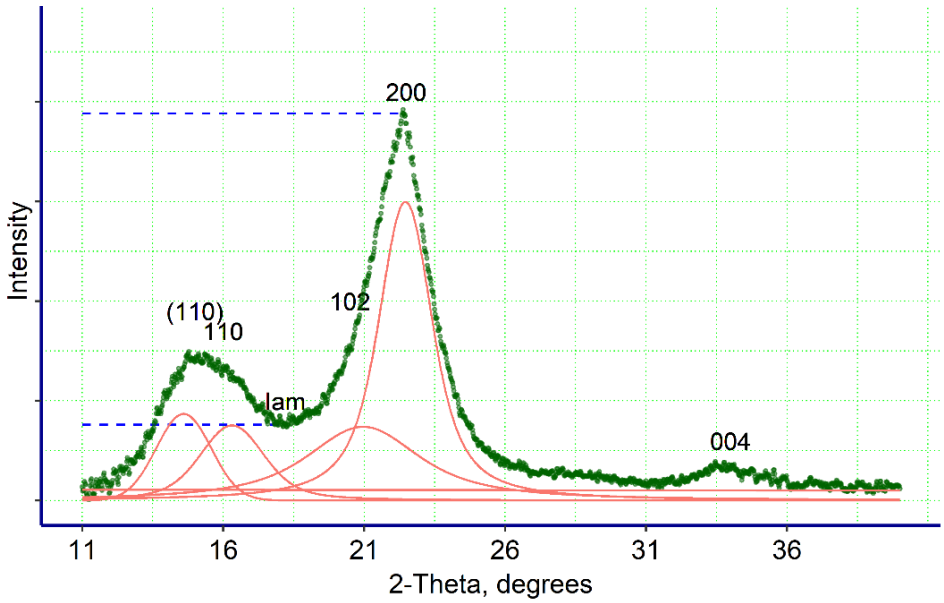

Figure 4.3. X-Ray diffraction scan of nanofilm. Peak deconvolution indicated in red.

Peak deconvolution using Bragg's law was applied to determine the crystallite size using the Fityk software package[87]. Voigt functions produce the best fit of deconvoluted peaks being aware that the amorphous region causes these peaks to broaden[88]. This function is a combination of Gaussian and Lorentzian functions. Applying the Scherrer equation, the width of the peak (200) at half height can be used to calculate the crystallite size. A two-point linear background subtraction was applied, which brought the peaks to a baseline. A Levenburg-Marquardt non-linear peak function was used to deconvolute the peaks. A weakness of this method is that the function is driven to obtain the best coefficient of determination. The fitted intensities that did not coincide with the two theta intensities required manual manipulation[89]. An improvement in the crystallinity determination would be to apply an amorphous subtraction method utilizing a standard chosen from the same cellulose source[85].

4.3.6 Atomic Force Microscopy (AFM).

Prior to AFM observations, nanocellulose dispersions were chemically bonded to the surface of a mica wafer using lysine based on a previously established procedure[90]. NFC was diluted to produce a 0.001 mg/ml solution. 100 ul of this solution was added to mica that had been cleaved to produce an atomically clean surface and treated with the protein lysine. The solution was allowed to sit on the mica surface for 30 seconds and then washed with deionized water to immobilize the nanofibers on the mica substrate. Nitrogen gas was utilized to dry the sample.

Topography images were produced by scanning 5 μm^2 regions of the different samples at a scan rate of 0.977 Hz using a Bruker ICON AFM operated in tapping mode with a bluedrive photothermal excitation. The scan required leveling due to the piezo effect of the scan method and

any raster artifacts in the image were eliminated. Gwyddion software was used to level the surface, analyze the resulting scan, and determine the fiber diameters[91], while ImageJ was employed to measure the fiber lengths, as depicted in Figure 4.5[92]. Profilm was utilized as a backup method for leveling the image when Gwyddion was not capable[93].

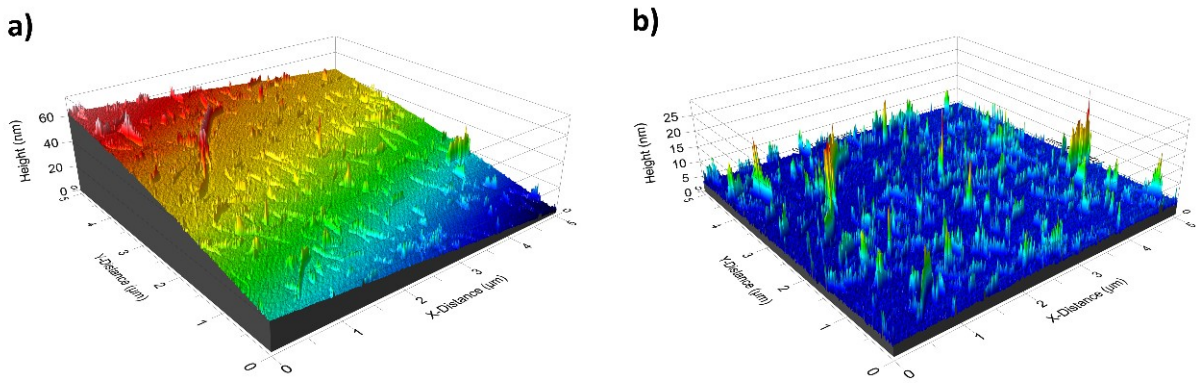

Figure 4.4. a) raw surface image, b) leveled surface with raster defects removed using Profilm.

The aspect ratio was calculated by dividing the measured length by the diameter of the fiber.

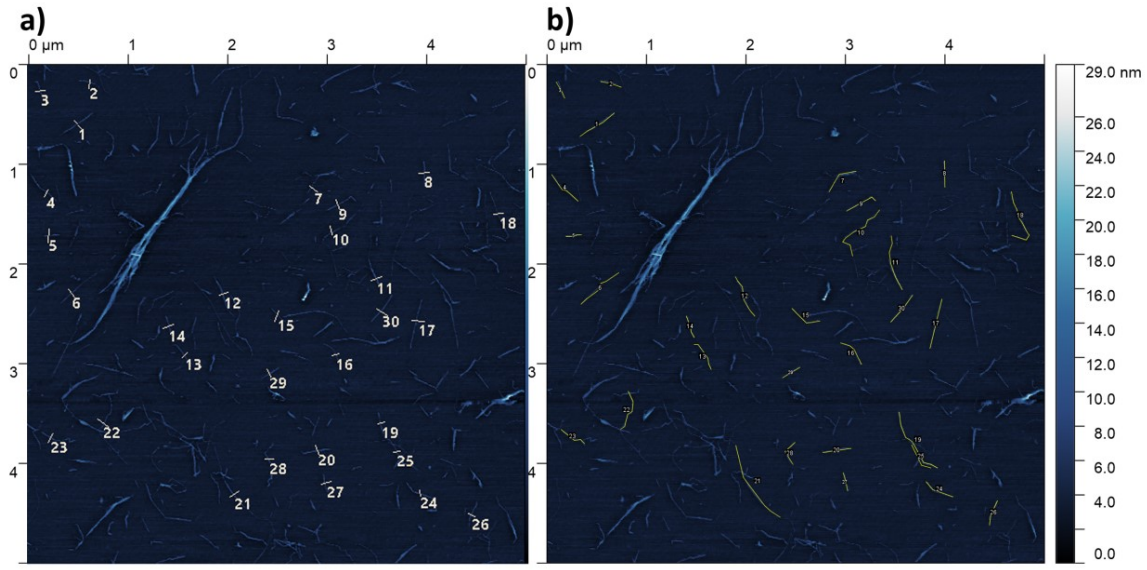

Figure 4.5. Representative AFM image of nanocellulose produced from ammonium persulfate oxidation of bleached northern softwood pulp used for; (a) height measurement in Gwyddion software, and (b) fiber length in ImageJ software.

The minimum number of fibers in each sample required for the diameter measurement to be in the 95% confidence interval was calculated using a formula, equation 4-15, introduced by Cochran[94]. Due to the small population of useable fibers in each scan, the number was modified using equation 4-16.

$$n_o = \frac{Z^2\sigma(1-\sigma)}{\alpha^2}, \text{ Z is the Z-statistic} \quad (4\text{-}15)$$

$$n = \frac{n_o}{1+\left(\frac{n_o-1}{N}\right)} \text{ , N is the population size} \quad (4\text{-}16)$$

At the 95% confidence level, z-value of 1.96, a population of 240 fibers, and standard deviation of 0.25 nm, the Cochran number n_o was determined to be 288 using equation 4-15. The average number of useable fibers is estimated to be far less than 288 in a scan. Using equation 4-15, adjusting for small population size, n was determined to be 27 fibers. Additional segments were measured until the minimum number of fibers were identified.

4.3.7 Data Analysis

The effect of ammonium persulfate liquor concentration, applied ammonium persulfate per gram of fiber in moles, and temperature on the chemical and morphological aspects of nanofibrillated cellulose was evaluated using permutational multivariate analysis of variance (Permanova). Permanova was applied to the non-parametric multivariate data using the R software package[95]. The ordination of the data set was performed using the explanatory data. The data was relativized by the maximum for each measured response in order to adjust for differences in the spread of values[96]. This was followed by Euclidean distance calculation for all three response variables. The permutational multivariate analysis of variance (PERMANOVA) tested the overall

affect each explanatory variable had on these response variables[97]. Partitioning of variance within treatments and between treatments was performed on the raw and summarized data sets. The data does not contain zero values so a Euclidean distance for the dissimilarity measure is appropriate. Bray-Curtis dissimilarity may be sensitive to differences in the frequency of diameters. It was stated by Ricotta that Bray-Curtis will weigh abundant species more than rare which may be advantageous in diameter-based response variables where large low frequency diameters can skew results[98]. A multivariate regression tree was created to visualize the relationship between the explanatory variables and the response variables. Principle component analysis was used to visualize the interaction of each treatment on the response variables. Non-metric Multi-Dimensional Scaling (NMDS) was utilized to visualize the impact of ammonium persulfate liquor concentration on the response variables.

4.4 Results

4.4.1 Initial Investigation

Evaluating the impact to morphological features of the nanofibrillated celluloses in the initial investigation a plot of diameters versus the % ammonium persulfate applied on fiber is illustrated in Figure 4.6. The change in diameter at each level is small versus the % applied APS. The trend indicates that as the % of APS is increased in combination with temperature and molar concentration of APS, the diameter of the nanofibrillated cellulose fibers is reduced. A plot of diameter versus molar concentration of APS by temperature shows an asymptotic relationship.

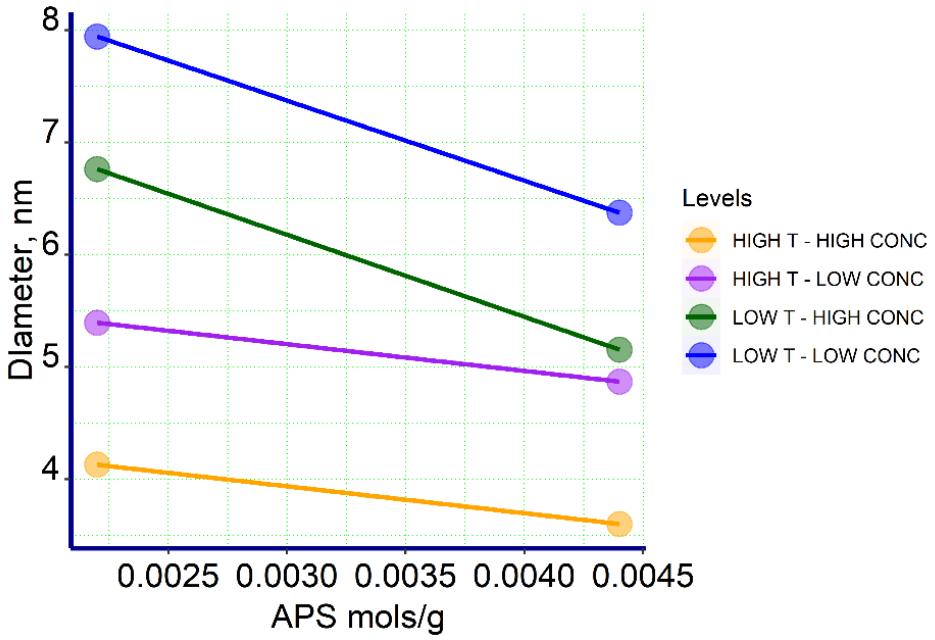

Figure 4.6. Plot of Diameter (nanometer) versus % applied ammonium persulfate by combined factors temperature (Celsius) and molar concentration of APS (M).

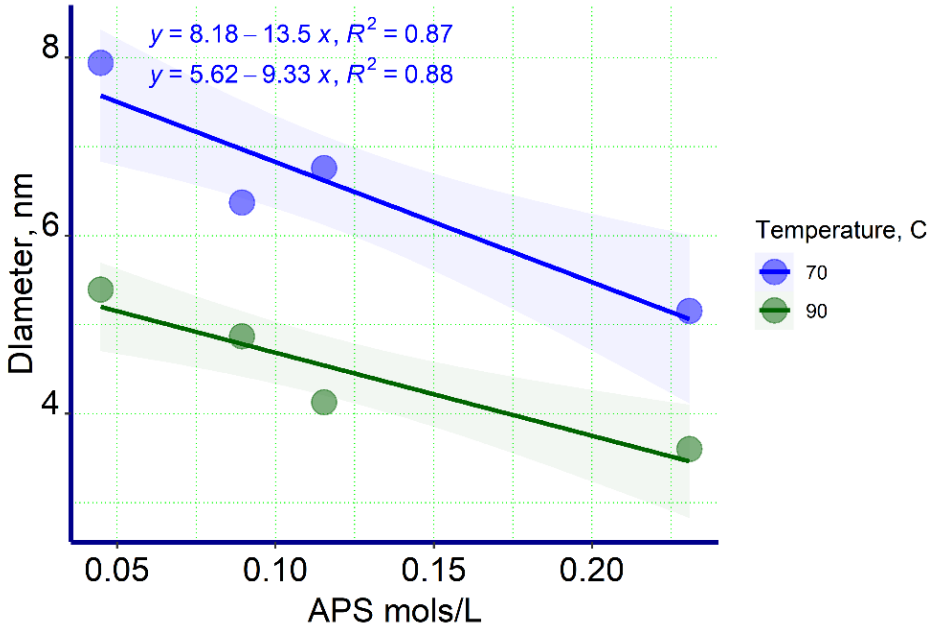

Figure 4.7. Plot of Diameter (nanometers) versus molar concentration of APS by temperature (Celsius).

These plots do not provide information on the effect of each treatment independent of the others or their interaction with one another on the response variables. A permanova analysis of

the data show that the effect of ammonium persulfate applied accounted for 42% of the variance in measured diameters. Temperature and APS liquor concentration by themselves were not significant contributors, however the interaction of these treatments with the applied APS accounted for 23.3% and 23.9% of the total variance respectively at the 90% confidence level, see Table 4.8.

Table 4.8. Multivariate analysis for nanofibrillated cellulose diameter examining effect of each treatment and interaction between treatments.

Treatment	Df	SumOfSqs	R2	F	Pr(>F)
Temperature, °C	1	0.02732	0.01535	3.8817	0.280
Mole APS/g	1	0.83531	0.42162	121.2194	0.066
[APS], M	1	0.15871	0.07843	22.5501	0.135
Mole APS/g:[APS], M	1	0.48532	0.23984	68.9567	0.081
Mole APS/g: Temperature	1	047166	0.23309	67.0165	0.083
[APS],M : Temperature	1	0.02031	0.01004	2.8863	0.338
Residual	1	0.00704	0.00348		
Total	7	2.02351	1.00000		

The difference in length of fibers between treatments was not statistically significant as determined by permutational multivariate analysis of variance (PERMANOVA). and Tukey test using the ghlt function in Rstudio[99]. The only significant difference was between factor 4 and factor 2. The aspect ratio, ratio of length to diameter, varied from 90 to 125 with a standard deviation of +/- 50.

Table 4.9. Tukey Test Results – comparing fiber length by factor

	Estimate	Std. Error	t value	Pr(>|t|)
FACTOR 3 - FACTOR 2 == 0	85.758	52.014	1.649	0.720
FACTOR 4 - FACTOR 2 == 0	161.240	52.694	3.060	0.052
FACTOR 5 - FACTOR 2 == 0	176.050	51.391	3.426	0.018
FACTOR 6 - FACTOR 2 == 0	32.178	52.694	0.611	0.999
FACTOR 7 - FACTOR 2 == 0	59.195	52.014	1.138	0.947
FACTOR 8 - FACTOR 2 == 0	95.858	52.014	1.843	0.592
FACTOR1 - FACTOR 2 == 0	51.767	53.440	0.969	0.978
FACTOR 4 - FACTOR 3 == 0	75.482	52.694	1.432	0.841
FACTOR 5 - FACTOR 3 == 0	90.292	51.391	1.757	0.650
FACTOR 6 - FACTOR 3 == 0	-53.579	52.694	-1.017	0.971
FACTOR 7 - FACTOR 3 == 0	-26.562	52.014	-0.511	1.000
FACTOR 8 - FACTOR 3 == 0	10.101	52.014	0.194	1.000
FACTOR1 - FACTOR 3 == 0	-33.990	53.440	-0.636	0.998
FACTOR 5 - FACTOR 4 == 0	14.810	52.079	0.284	1.000
FACTOR 6 - FACTOR 4 == 0	-129.061	53.366	-2.418	0.240
FACTOR 7 - FACTOR 4 == 0	-102.045	52.694	-1.937	0.528
FACTOR 8 - FACTOR 4 == 0	-65.382	52.694	-1.241	0.918
FACTOR1 - FACTOR 4 == 0	-109.472	54.102	-2.023	0.469
FACTOR 6 - FACTOR 5 == 0	-143.871	52.079	-2.763	0.113
FACTOR 7 - FACTOR 5 == 0	-116.855	51.391	-2.274	0.315
FACTOR 8 - FACTOR 5 == 0	-80.192	51.391	-1.560	0.773
FACTOR1 - FACTOR 5 == 0	-124.282	52.833	-2.352	0.272
FACTOR 7 - FACTOR 6 == 0	27.017	52.694	0.513	1.000
FACTOR 8 - FACTOR 6 == 0	63.680	52.694	1.208	0.928
FACTOR1 - FACTOR 6 == 0	19.589	54.102	0.362	1.000
FACTOR 8 - FACTOR 7 == 0	36.663	52.014	0.705	0.997
FACTOR1 - FACTOR 7 == 0	-7.428	53.440	-0.139	1.000
FACTOR1 - FACTOR 8 == 0	-44.091	53.440	-0.825	0.991

A violin plot, a variation of Tukey's box plot, of the measured fiber length distribution for each factor in the initial experimental design illustrates the scatter in the preliminary data shown in Figure 4.8. The symmetrical density plot shows the shape of this distribution. The circle indicates the median of the sample set, and the solid vertical bar indicates the upper and lower quartiles.

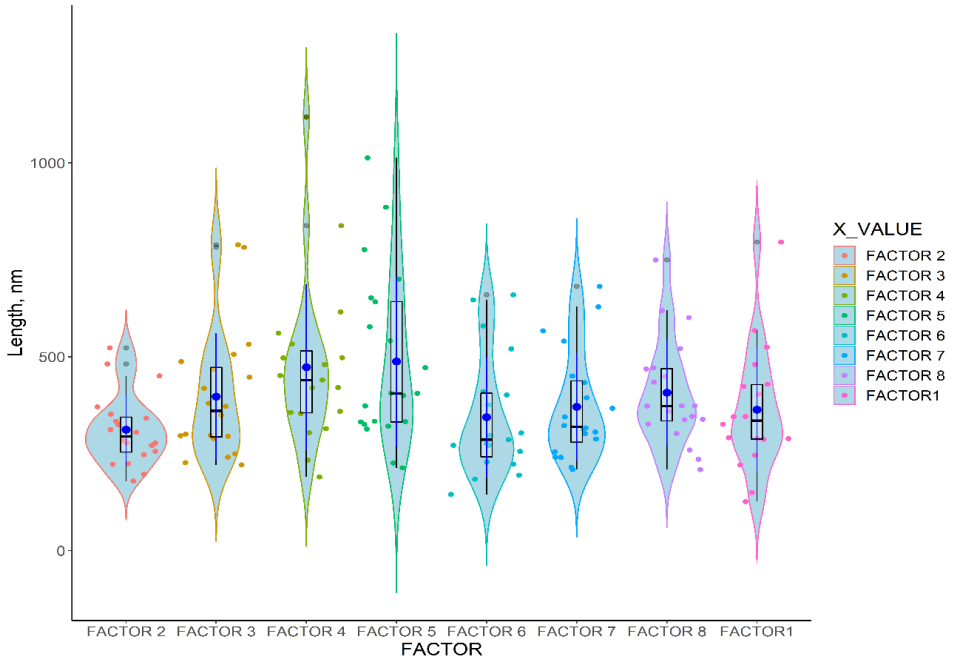

Figure 4.8. Violin-Plot of fiber lengths by factor[100]

Crystallinity was driven by the application of APS on fiber, 25.6% of the variance and the concentration of APS accounted for 8.6% of the variance, see Table 4.10. The interaction between applied APS and concentration accounted for 62.9% of the total variance. Temperature did not have an impact on the reduction in crystalline regions but did interact with the concentration of APS slightly.

Table 4.10. Multivariate analysis for nanofibrillated cellulose crystallinity.

Treatment	Df	SumOfSqs	R2	F	Pr(>F)
Temperature, *°C*	1	0.000021	0.00036	1.8863	0.374
Mole APS/g	1	0.015051	0.25566	1343.9591	0.052
[APS], M	1	0.005048	0.08575	450.7910	0.048
Mole APS/g:[APS], M	1	0.037074	0.62974	3310.4284	0.017
Mole APS/g: Temperature	1	0.000946	0.01607	84.4823	0.110
[APS],M : Temperature	1	0.000720	0.01223	64.2955	0.053
Residual	1	0.000011	0.00019		
Total	7	0.058872	1.00000		

Overall, crystallinity did not significantly change. This coupled with the statistically insignificant different lengths between treatments may indicate that ammonium persulfate serves

to stabilize the carbohydrate reducing end similar to the polysulphide mechanism. As the reducing end group hemiacetal is hydrolyzed to open the ring and form an aldehyde, the ammonium persulfate may reduce the aldehyde group to carboxyl group, stopping the peeling reaction.

Ammonium persulfate applied was very conservative resulting in no significant measured difference in nanofiber lengths or crystallinity. At medium consistency, 5%, mixing became problematic. The surface charge and diameter response even at the low level of ammonium persulfate in the experimental design was likely aided by the higher consistencies, molar concentration in the liquor, not used in previously published research.

4.4.2 Kinetics.

The rate of ammonium persulfate consumption was evaluated holding temperature, molar concentration of APS in the liquor and the mols of APS per gram constant. Samples were taken at ten-minute intervals during a two-hour oxidation and the concentration of ammonium persulfate was measured. The consumption of ammonium persulfate was determined to be second order with a rate constant of 0.0898 $M^{-1}min^{-1}$, see Figure 4.9a .

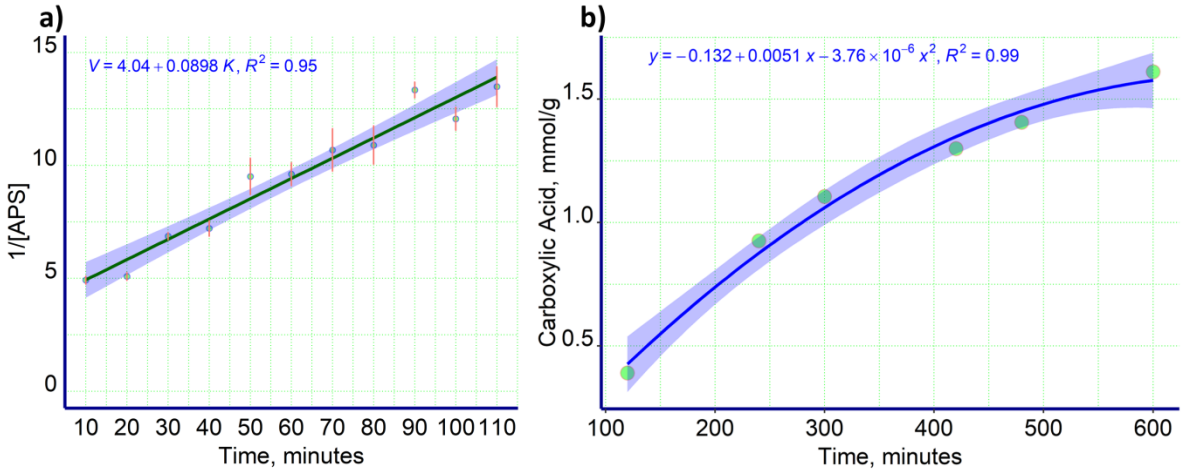

Figure 4.9. a) Residual ammonium persulfate over time. b) Plot of carboxylic acid mmol/g versus time at 70°C, and 0.044 mol/g APS applied. Shaded area indicates the 95% confidence interval.

A plot of carboxylic acid versus time at a temperature of 70 °C, ammonium persulfate of 0.044 mol/g fiber and an APS liquor concentration of 0.221 M is shown in Figure 4.9b. The development of carboxylic acid content approach an asymptotic limit at approximately 1.5 mmol/g after ten hours of oxidation. This is close to the theoretical maximum of 1.71 mmol/g using the 110 and (110) plane dimensions reported by Nishiyama for the unit cell and the average length and diameter for the nanofibers produced in this investigation[101,102,103,104,105,106]. A plot of residual ammonium persulfate overlay with the surface acidity is shown in Figure 4.10.

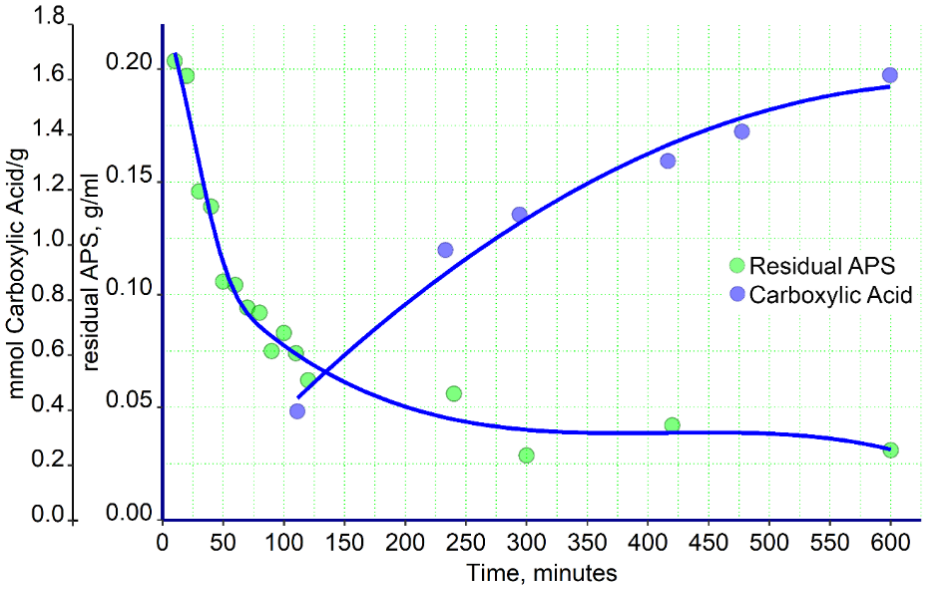

Figure 4.10. Residual ammonium persulfate over time and a plot of carboxylic acid mmol/g versus time at 70 °C, and 0.044 mol/g APS applied.

4.4.3 Response Surface – Primary Investigation.

Three independent variables were used in the study in a central composite design; moles of ammonium persulfate applied per gram of fiber (A), temperature of the oxidation reaction °C, (B), and duration of the reaction in minutes (C). The responses measured were mmol of carboxylic acid per gram produced (W), length (X), diameter (Y), and crystallinity index (Z). The empirical models in terms of the coded factors for the responses are shown in equations 4-17 to 4-20.

$$W = 1.178 + 0.254A + 0.150B + 0.224C + 0.299AB + 0.121AC - 0.150BC - 0.340A^2 - 0.083B^2 - 0.446C^2 \quad (4\text{-}17)$$

$$X = 181.000 + 51.300A + 15.000B + 0.740C - 97.600AB + 110.400AC - 18.433BC + 7.001A^2 - 13.465B^2 + 23.200C^2 \quad (4\text{-}18)$$

$$Y = 3.932 + 0.092A + 0.466B + 0.419C - 0.359AB + 0.726AC + 0.152BC + 0.457A^2 - 0.387 - 0.154C^2 \quad (4\text{-}19)$$

$$Z = 0.798 + 0.012A + 0.033B + 0.024C + 0.017AB + 0.034AC + 0.026BC - 0.032A^2 - 0.003B^2 - 0.049C^2 \quad (4\text{-}20)$$

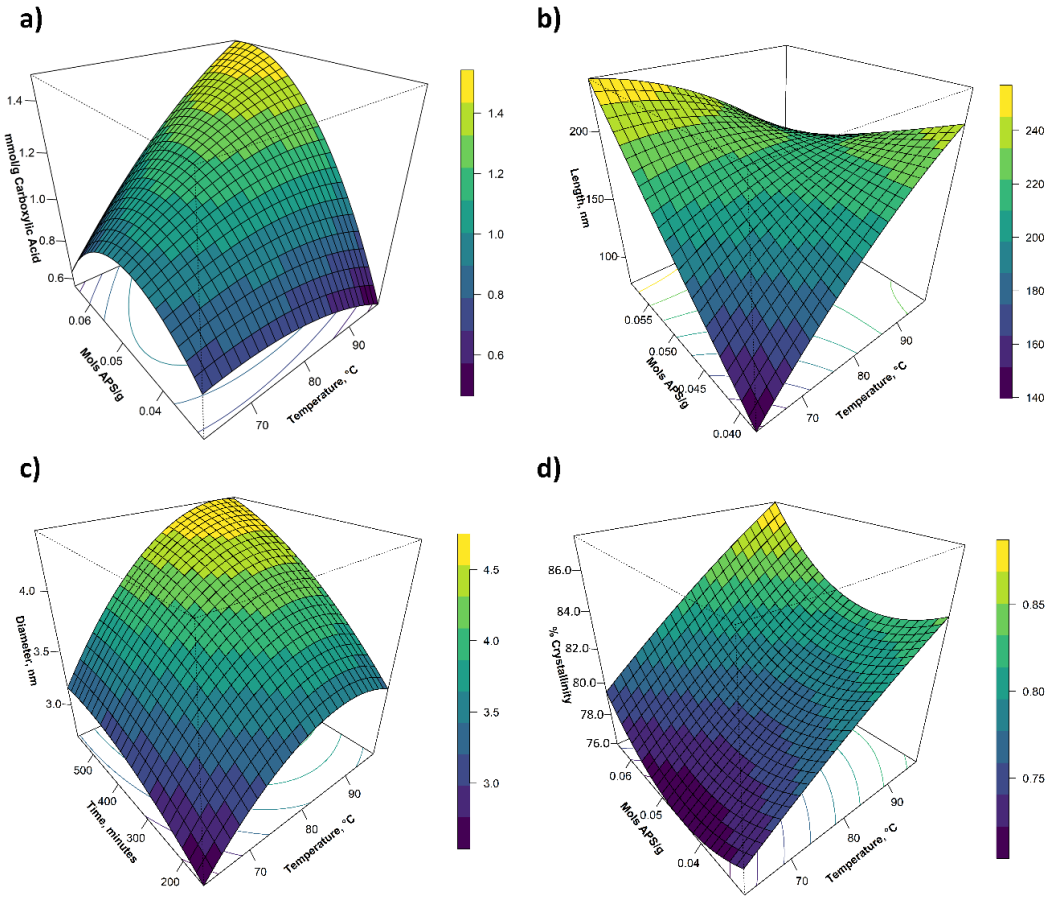

Figure 4.11. Response surface plots; a) carboxylic acid $R^2 = 0.81$, b) length $R^2 = 0.93$, c) diameter $R^2 = 0.61$, and d) crystallinity index $R^2 = 0.66$.

The interaction between time, temperature, and applied ammonium persulfate had a significant influence on the development of carboxylic acid content, the crystallinity, crystallite size, and

aspect ratio of nanocellulose fibers produced. The best fit for the models was a second order quadratic, see Figure 4.11.

Applied APS, time and temperature have significant influence on the surface chemistry. The carboxylate content of the NFC produced ranged from 0.64 mmol/g to 1.44 mmol/g as measured by conductometric titration. Higher charge developed with increasing time, temperature, and applied ammonium persulfate. The turbidity of the NFC solutions decreased as the surface charge increased, see Figure 4.12.

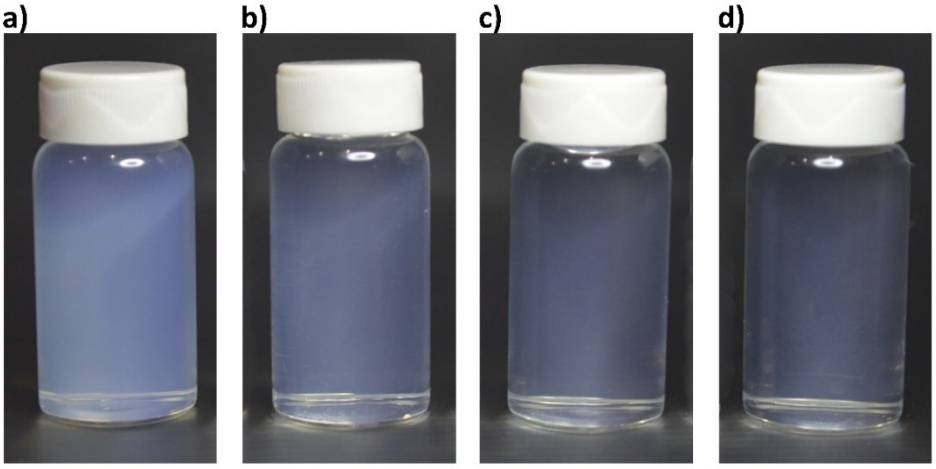

Figure 4.12. Left to right increasing carboxylic acid content of the NFC; a) 0.6, b) 0.8, c) 1.2, d) 1.5 mmol/g.

The density plot distribution was not a normal or Gaussian shape, instead skewing toward the fiber with smaller lengths shown in Figure 4.13[107].

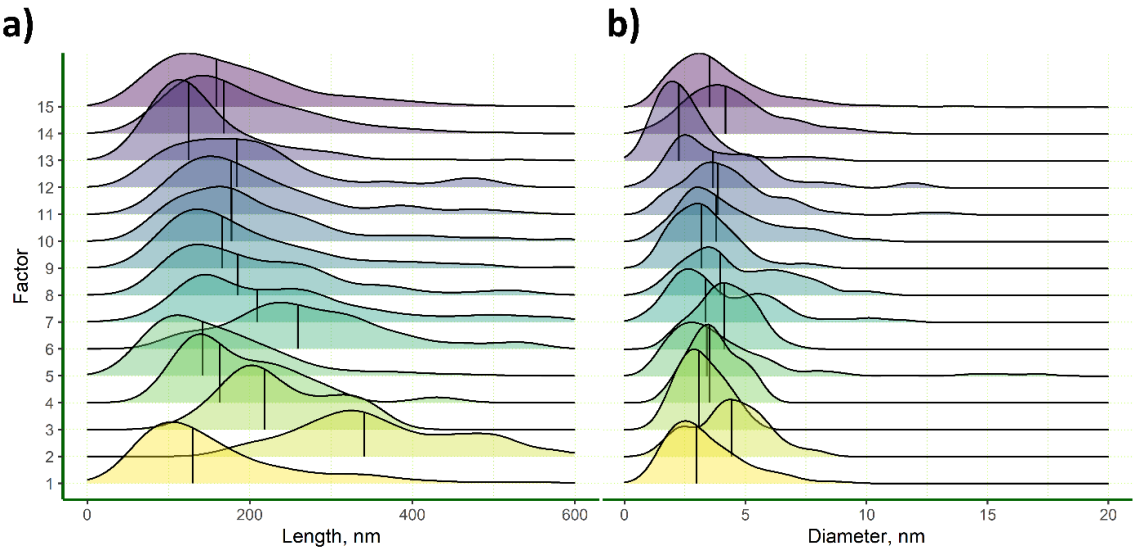

Figure 4.13. Density plots of the probability distributions of fiber a) length (nm) for each model factor (color selected to distinguish curves) and b) diameter (nm) for ammonium persulfate oxidized bleached northern softwood pulp.

Nanofiber lengths were strongly impacted by applied APS and temperature, see Figure 4.14. Average fiber length ranged from 145 to 247 nm with an r^2 of 0.93. NFC diameters increased slightly with increasing time and temperature, however, the range in diameters as measured by AFM, was narrow, 2.7 to 4.6 nm. The model did not have a good fit, $r^2 = 0.61$ likely due to the similar non-Gaussian shape.

The crystallinity index determined by the Segal method ranged from 73 to 88%. It increased with increasing temperature as the amorphous regions were hydrolyzed by APS. The model correlation coefficient for crystallinity was poor, $r^2 = 0.65$. Crystallite was governed by applied APS and time. The model produced a better correlation when considering the change in crystallite size, $r^2 = 0.93$, see Figure 4.15. The crystallite size of the NFC increased as the temperature and applied APS increased, which may indicate increased swelling of the fibers as measured by XRD[108]. A decrease in crystallite size after 350 minutes was measured which may indicate crystalline structure disruption associated with the steep rise in crystallinity measured[109].

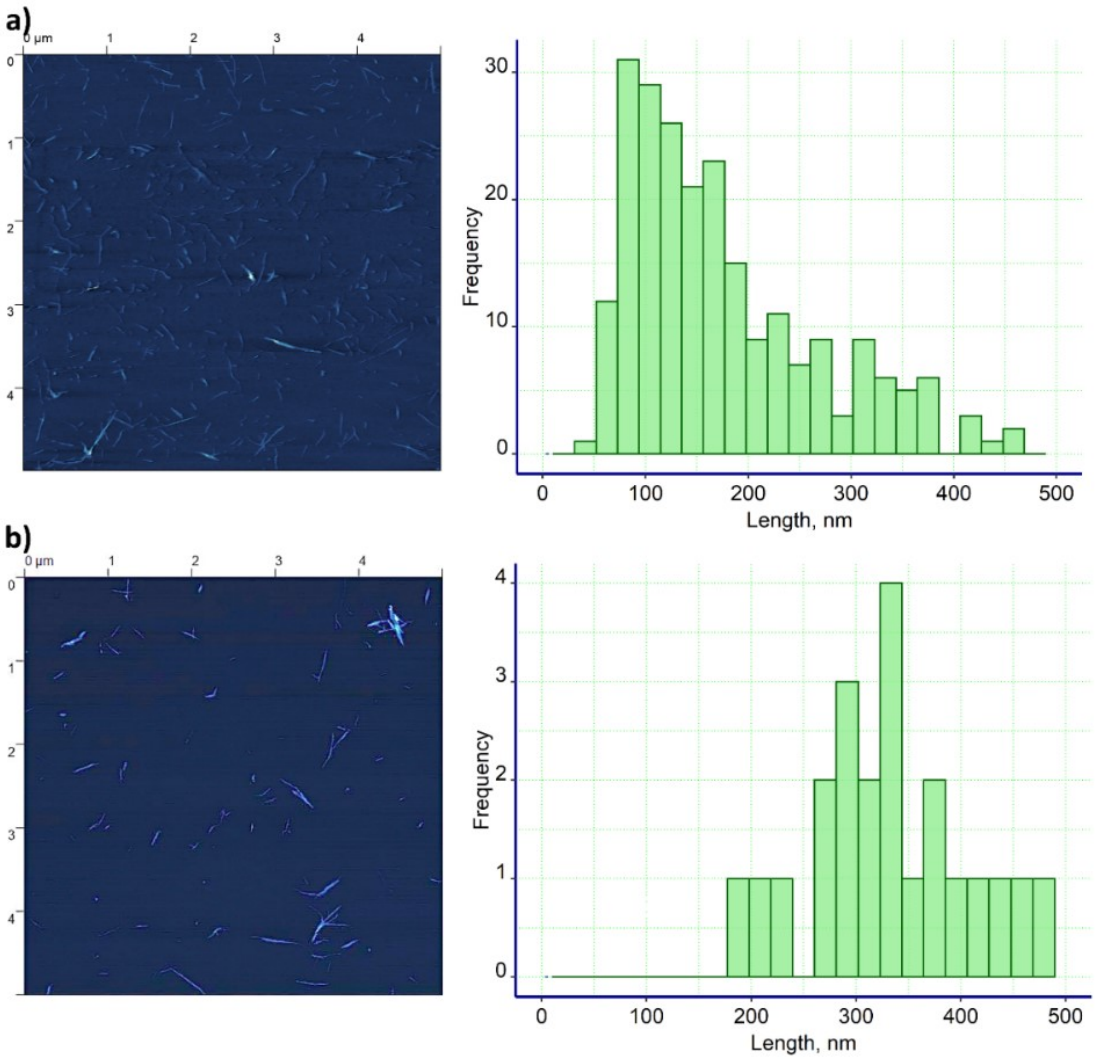

Figure 4.14. AFM images and length distribution histograms for a) treatment 1 (70C, 240 minutes, 0.039 mols APS/g, b) treatment 2 (90C, 240 minutes, 0.039 mols APS/g).

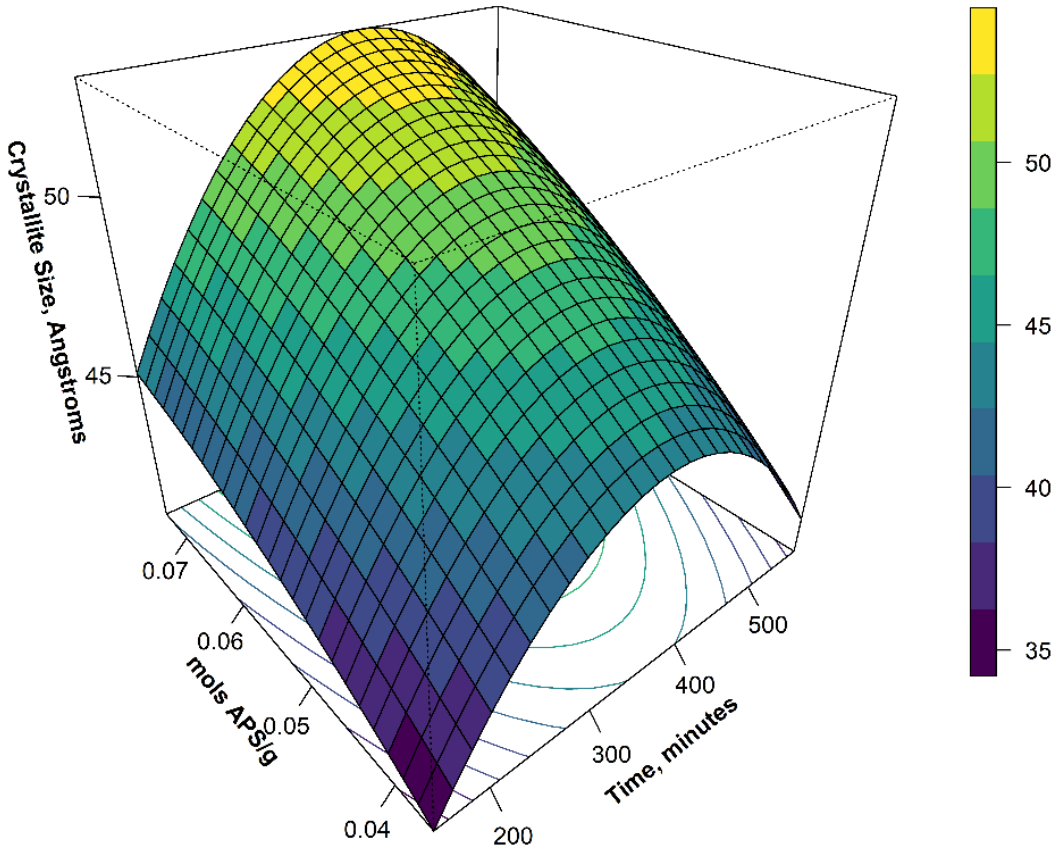

Figure 4.15. Response surface plot of crystallite size, $R^2 = 0.93$.

A plot of intensities normalized to the 002 peak is unremarkable and does not indicate the measured changes in crystallinity, see Figure 4.16. The amorphous region obscures any peak differentiation.

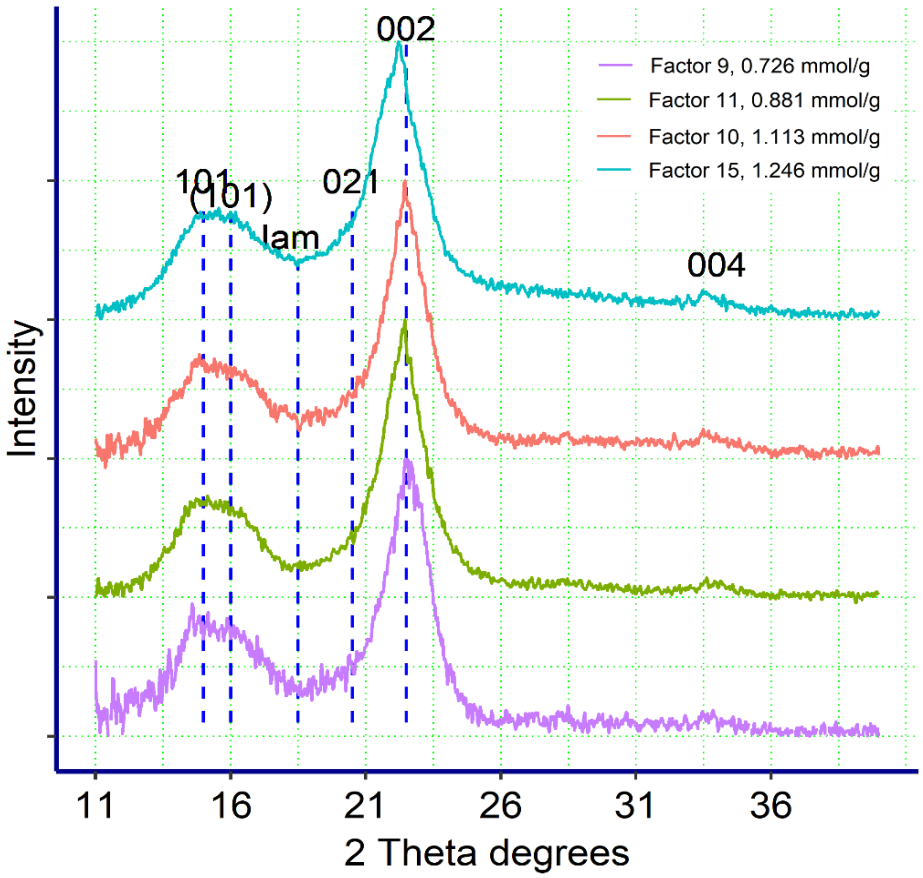

Figure 4.16. XRD scans of NFC films for several treatment condition with increasing surface charge.

4.4.4 Response Surface – Model Validation.

The model, equation 4-17, was validated using three oxidation experiments. One was within the boundaries of the design and two were outside of the experimental boundary. Results of the validation of the model are outlined in Table 4.11. Two validation tests were outside the model experimental space as shown by the red frame in Figure 4.17. The difference between the model prediction, equation 4-16, and the actual measured carboxylic acid content was 4% or less demonstrating the model's good estimation capability.

Table 4.11. Validation test results, Treatment (mols APS/g, Temperature, Time). * Treatments that were outside the experimental model.

Treatment	Predicted mmol/g	Actual mmol/g	% Difference
0.039/ 70/ 360	0.878	0.845	4.0%
0.039/ 70/ 120	0.443*	0.461	4.0%
0.058/ 70/ 120	0.294*	0.299	1.7%

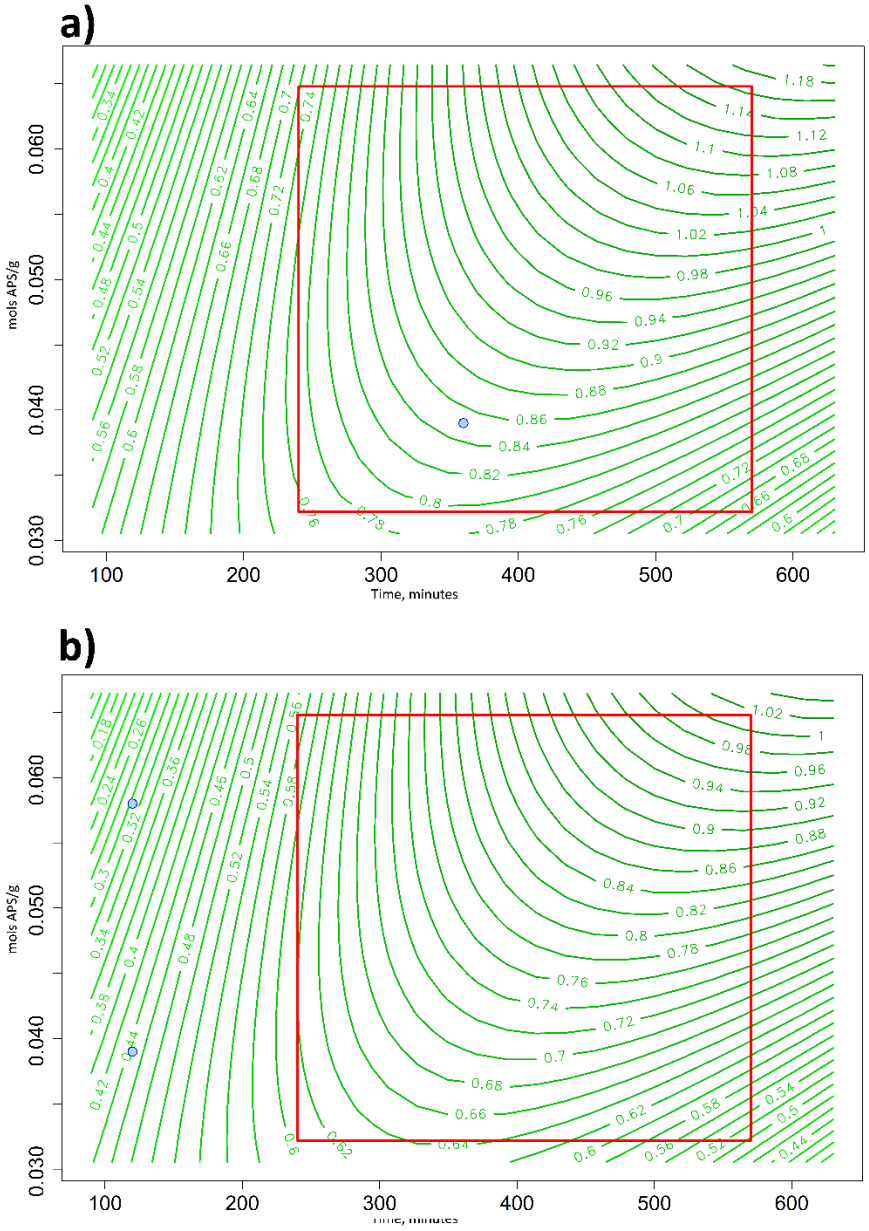

Figure 4.17 Experimental validation points a) within the boundaries of the response surface model, b) outside the boundaries of the response surface model. Red square indicates boundaries of experimental design.

Reproducibility of the experiments was confirmed using eleven replicates spread across two months and at two levels. These were analyzed using a pooled variance t procedure – Tukey test using the R glht function[110]. No statistically significant difference between samples within factors was determined. There was a statistically significant difference between samples across different factors. Factors were grouped by month and compared in a butterfly plot, see Figure 4.18b. A Tukey analysis was also performed on these blocks.

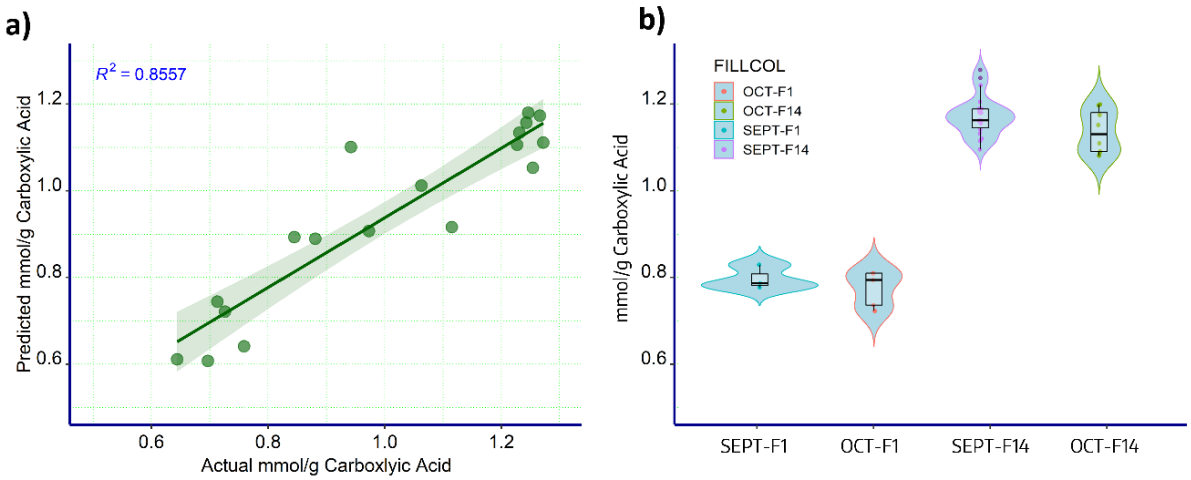

Figure 4.18. a) Predicted vs Actual surface chemistry, b) Box plot with butterfly overlay – groups by month and factor.

The block-to-block analysis indicate no statistical difference within levels between blocks (months). There was still significant difference between factors within a month.

4.4.5 Lignin Selectivity.

The color change was rapid as APS reacted with the lignin, see Figure 4.19a. It has been reported that reactive functional groups in lignin can be oxidized in TEMPO mediated oxidation reactions[111]. A portion of the carboxylic acid content produced during APS oxidation may be from reactions with lignin as was found with TEMPO mediated oxidation of thermo-mechanical pulp. However, to achieve a similar carboxylic acid content on high lignin (25.3%) thermomechanical pulp as with a lignin-free fiber, Okita demonstrated that a three-fold increase in hypochlorite was

required[112]. The treatment of wheat straw fines with lower lignin (0.42%) content, at the same hypochlorite addition, resulted in a 45% decrease in carboxylic acid development[113].

The ammonium persulfate (APS) mediated oxidation produced similar surface charge in unbleached fibers (4% lignin) by extending only reaction time as shown in Figure 4.19b. Surface charge developed on the bleached northern softwood Kraft (B-NSWK) at the same rate for both 70°C and 90°C treatments. Increasing the temperature by 20 degrees increased the surface charge of the bleached fiber by 13%. The rate of surface charge development on the unbleached northern softwood Kraft (UB-NSWK) was considerably flatter. At 90°C the unbleached fiber surface charge was 52% lower than for the bleached fiber and lower than the 70°C treatment. The rate of $SO_4^{\bullet-}$ radical β-O-4 cleavage reactions with Guaiacyl lignin will be slower than acidolysis reactions such as sulfuric acid due to the lower pKa of the conjugate base[114]. In persulfate systems reinforced with hydrogen peroxide, high degradation of lignin and hemicellulose has been observed similar to Fenton-like reactions[115,116]. In the described process, formation of the sulfate anion is rapid reacting preferentially with amorphous cellulose and forming carboxylic acid groups. The results indicate that a portion of the sulfate radical is consumed in delignification reactions but with increasing temperature, the delignification reactions are favored.

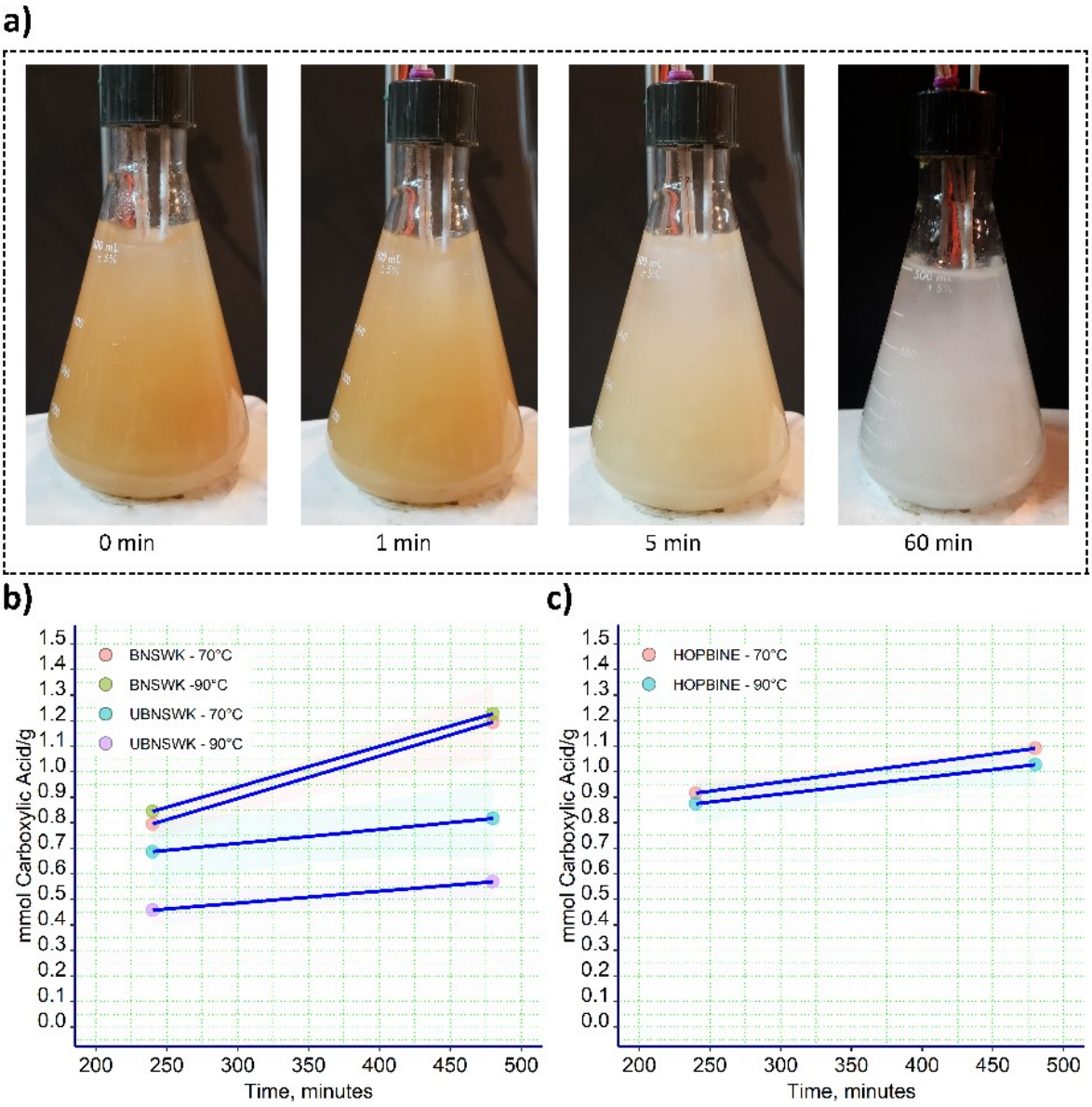

Figure 4.19. a) Photographs showing the visual evolution of the APS oxidation of unbleached pulp over a one-hour period. b) Surface charge of bleached (BNSWK) wood pulp and unbleached (UB-NSWK) c) Surface charge of non-wood hop bine fibers (HOPBINE).

To demonstrate the applicability of this approach on non-wood fibers, APS oxidation of low lignin (4%) hop bine developed close to the same rate as the unbleached softwood pulp (UB-NSWK), however, it achieved a higher carboxylic acid content closer to that of the bleached softwood (B-NSWK), Figure 4.19c. Note that the RSM conditions selected did not result in the lignin

containing fibers approaching an asymptotic limit for carboxylic acid development. There was also a measured decrease in carboxylic acid content as temperature was increased. Hop bine (HOPBINE) surface charge at 90 °C was 5% lower than at 70 °C, see Table 4.12. This may be due to the Guaiacyl, Syringyl, and p-coumaryl lignin present in non-wood species. Higher delignification rates have been shown to correlate with the ratio of Syringyl to Guaiacyl (S/G) lignin present in hardwoods[117]. Although the S/G ratio of hop bine lignin has not been studied, the ratio of S/G in industrial hemp has been experimentally determined to be 0.64[118]. A previous study has demonstrated that hop bine delignifies at the same rate as industrial hemp therefore we hypothesize that hop bine likely contains a similar S/G ratio[119].

Table 4.12. Experimental matrix for the APS oxidation of bleached and unbleached softwood pulp, and residual hop bine fibers.

Sample	Time	mols APS/g	Temperature, °C	mmol Carb/g
B-NSWK-70	240	0.0582	70	0.796
B-NSWK-90	240	0.0582	90	0.845
B-NSWK-70	480	0.0582	70	1.194
B-NSWK-90	480	0.0582	90	1.227
UB-NSWK-70	240	0.0582	70	0.687
UB-NSWK-90	240	0.0582	90	0.458
UB-NSWK-70	480	0.0582	70	0.817
UB-NSWK-90	480	0.0582	90	0.570
HOPBINE-70	240	0.0582	70	0.916
HOPBINE-90	240	0.0582	90	0.874
HOPBINE-70	480	0.0582	70	1.091
HOPBINE-90	480	0.0582	90	1.027

The color of the hop bine fiber initially was darker and bleaching of the fibers did not occur as rapidly or to the extent that the UB-NSWK proceeded.

4.4.6 Mechanical Treatment.

Prior to mechanical homogenization of the oxidized fibers, fibers were isolated and analyzed with scanning electron microscope. The solid precipitate after mechanical

homogenization and centrifugation was also isolated and examined by scanning electron microscopy. The scans show an intact but collapsed fiber surface, see Figure 4.20.

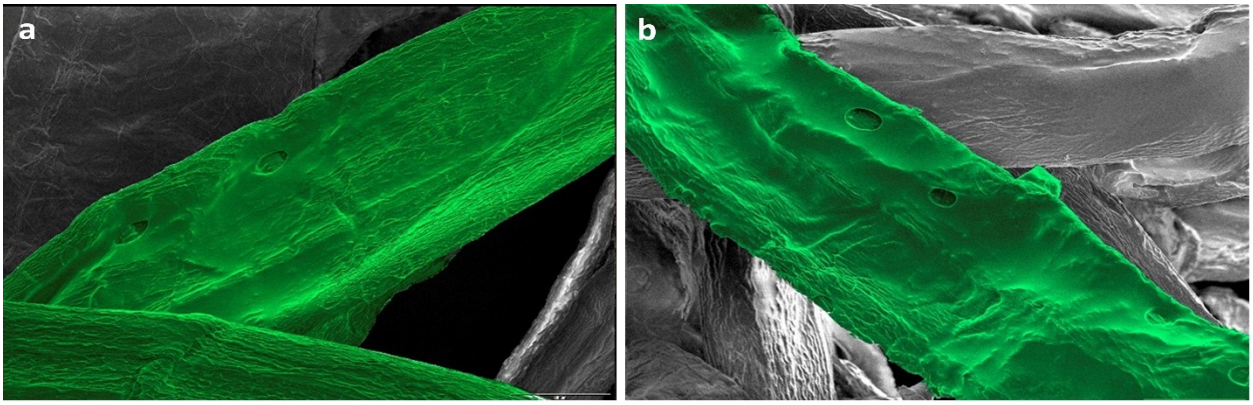

Figure 4.20. a) Unoxidized softwood fiber, b) APS oxidized softwood fiber.

After sonication and centrifugation, the precipitate was isolated and scans were taken with an SEM. The images show collapsed fiber fragments and fiberous material coating the substrate likely microcrystalline cellulose shown in Figure 4.21a. Bordered pitting is still visible in the small fragments enlarged in Figure 4.21b.

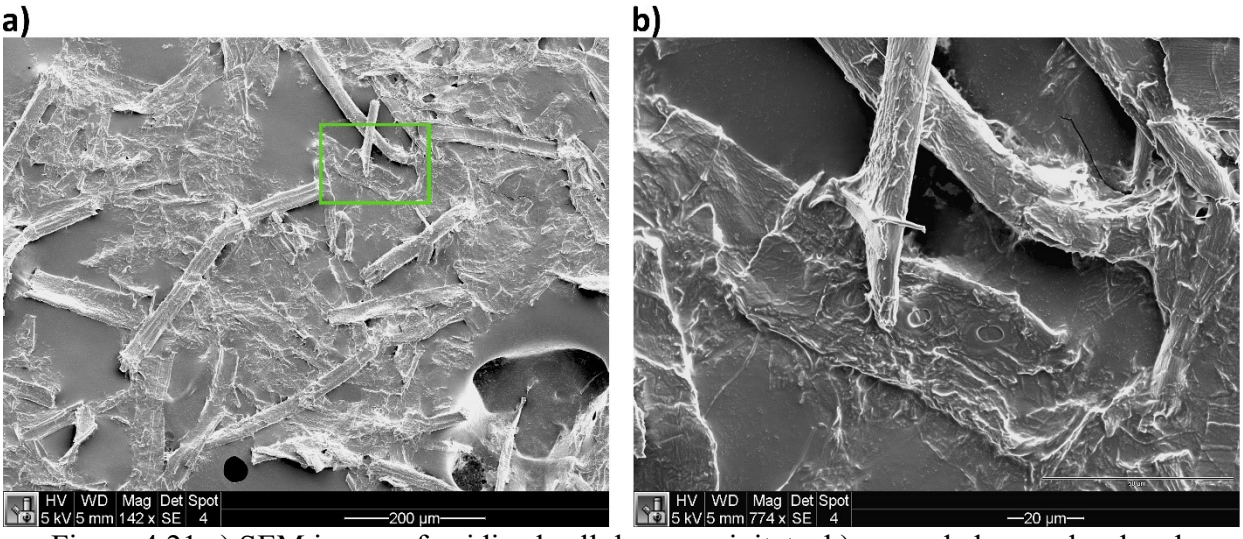

Figure 4.21 a) SEM image of oxidized cellulose precipitate, b) expanded green bordered inset showing fiber fragments and bordered pits.

Low surface charge samples did not disintegrate well. The standard 4-minute sonication used in the standard method for TEMPO-mediated oxidation was insufficient resulting in significant MFC retained after centrifugation. Amplitude is the primary control. A test sample of Northern bleached softwood kraft pulp was prepared at 70 °C for 4 hours to produce approximately 25 g of oxidized fiber for evaluation at a charge of 0.85 mmol carboxylic acid/g. Amplitude was held constant at 90%, consistency held constant at 1.0%, volume of 150ml. The more viscous a solution, the greater the power demand on the probe. Time was varied in increments; 5, 7.5, 10, 12.5, 15, and 20 minutes, see Table 4.13. The tip was replaced prior to this treatment.

Table 4.13. AFM results of mechanical treatment response

Experiment	mol APS/g	Temp °C	Time hrs	Time, min sonic	Joules	Yield %	Length (nm)	Diamter (nm)	Aspect Ratio
CCD - 3	0.059	70	4				219 (sd=159)	3.4 (sd=1.8)	80.16
1	0.059	70	4	5	33000	4%	197 (sd=131)	3.1 (sd=1.2)	70.09
2	0.059	70	4	7.5		6%	223 (sd=141)	3.3 (sd=1.2)	73.80
3	0.059	70	4	10	66800	9%	224 (sd=165)	3.9 (sd=1.9)	69.14
4	0.059	70	4	12.5	85000	8%	241 (sd=158)	3.8 (sd=1.7)	77.06
5	0.059	70	4	15	100200	4%	230 (sd=136)	3.7 (sd=1.4)	69.48
6	0.059	70	4	20	129200	10%	225 (sd=138)	2.8 (sd=1.4)	93.95

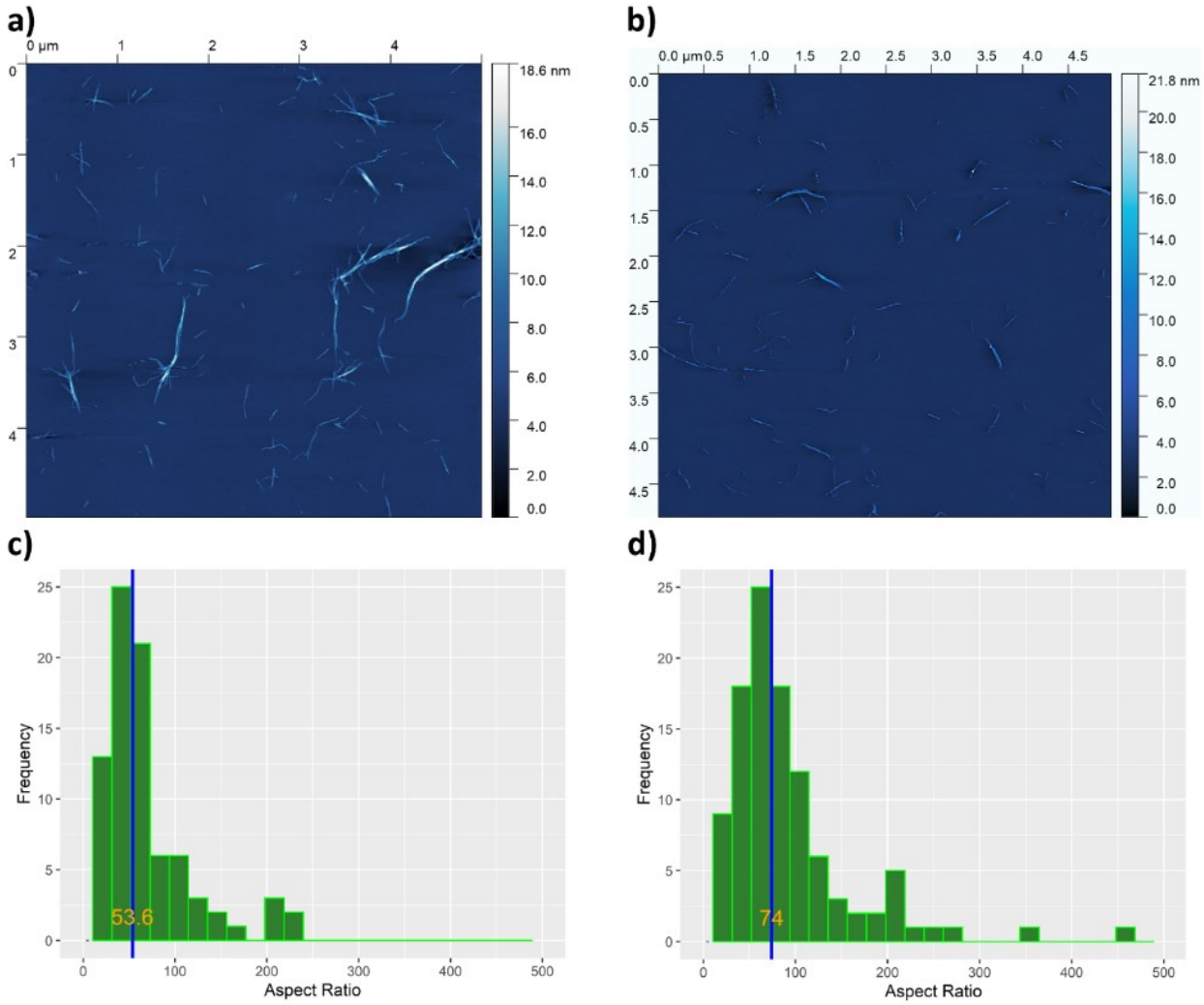

Figure 4.22 a) AFM scan of 5-minute treatment, b) AFM scan of 20 minute treatment, c) histogram of 5 minute scan with median value indicated by blue line, d) frequency plot of 20 minute scan.

A Tukey test indicates that all samples are identical with the exception of the 20-minute treatment. This treatment is statistically different then each of the other treatment times. The 20-minute test produced virtually no fiber aggregates and median aspect ratio was higher – likely due to the disruption of the fiber aggregates, see Figure 4.22a. The supernatant of the 20-minute treatment was also twice the concentration of NFC compared to the 5-minute treatment. Yield is likely low for a number of reasons. First, volumes are small and a significant mass of MFC remains

at the bottom of the centrifuge tube after sonication. Prior to this filtration methods used are not intended for yield determination likely resulting in losses.

A second set of APS oxidized samples were produced using different consistencies to evaluate the impact of molar concentration on resulting yield. Yield increased with increasing molar concentration while surface charge decreased.

Table 4.14. Yield at varying APS molar concentrations and resulting surface charge development.

Sample	Time minutes	Temp *°C*	Consistency	mols APG/g	[APS] M	mmol Carb/g	Yield %
1	180	70	0.5%	0.048	0.244	0.771	2.38%
2	180	70	1.0%	0.024	0.245	0.632	-
3	180	70	2.0%	0.024	0.497	0.477	21.5%

The production of quantities of NFC required for paper amendment would require several days of ultrasonication. A more suitable approach would be use of a microfluidizer. Samples were processed and XRD analysis performed as shown in Figure 4.23 and Table 4.15. As the number of passes increased the MFC precipitating after centrifugation eventually became negligible. Increasing the number of passes resulted in increasing concentration of NFC in the supernatant and increasing crystallinity. Crystallinity began to reach an asymptotic limit at approximately 5 passes.

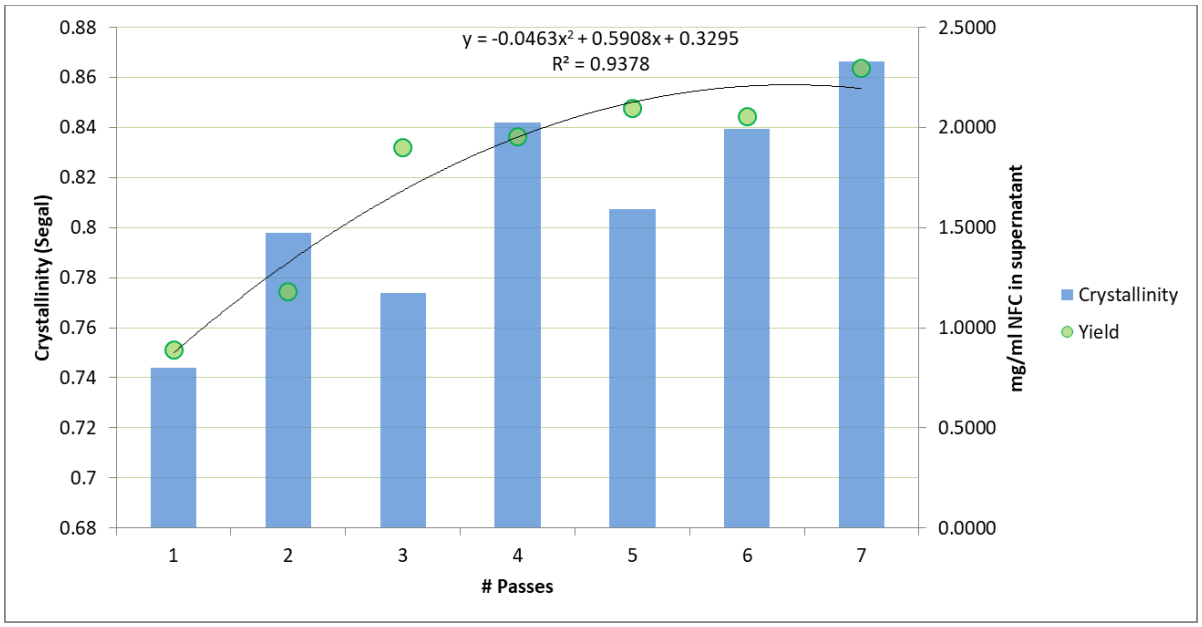

Figure 4.23. Crystallinity and yield with increasing passes through microfluidizer.

Table 4.15. Concentration of NFC in supernatant and crystallinity response to increasing the number of passes through microfluidizer.

Sample	Passes	mg/ml NFC	Crystallinity
1	1	0.8867	0.744
2	2	1.1800	0.798
3	3	1.9000	0.774
4	4	1.9533	0.842
5	5	2.0933	0.807
6	6	2.0533	0.839
7	7	2.2933	0.866

4.5 Conclusions

The response surface model developed using a central composite design demonstrates that ammonium persulfate oxidation of cellulose fibers under controlled conditions of temperature, time, and applied oxidant will produce nanofibrillated cellulose with specific surface chemistry, crystallinity, and aspect ratio. Selecting conditions outside and within the experimental design, RSM was used to predict the carboxylic acid content for the various treatments, which was then validated experimentally. Extending the response surface model, nanofibrillated cellulose fibers

was produced from lignin containing fibers from both softwood and an agricultural residual, hop bine. While increased temperature significantly reduced the development of surface chemistry in unbleached softwood fibers, the surface charge obtained with the higher lignin content agricultural residual demonstrate the model is not limited to lignin-free fibers. Renewable fibers from agricultural residues, such as hop bine, combined with a "green" oxidant represent a significant step in producing lignocellulosic nanofibers (LNF) for advanced materials. These results demonstrate that the reactivity of ammonium persulfate can be controlled to engineer specific nanofibrillated cellulose fiber characteristics in both bleached and unbleached fibers. Where measured, yields, defined as the extent of reaction for the conversion of cellulose fibers to NFC were below 10% as a result of the dilution factor (400:1) selected. Preliminary experimentation reducing the liquor to wood ratio to 19:1 has achieved yields of up to 57% without affecting the product properties. While process yield was not selected as one of the responses of the RSM design being outside the scope of this investigation, process optimization will be undertaken in future research to optimize the yields of APS-oxidized nanocellulose with specific characteristics. Additionally, consideration will be given to the spent reaction liquor produced, which may provide both sulfur, nitrogen, and carbon as a soil amendment, an opportunity to reduce inorganic fertilizer requirements and increase soil carbon sequestration.

References

[1] Abraham, E, Deepa, B, Pothan, L.A, Jacob, M, Thomas, S, Cvelbar, U, & Anandjiwala, R. Extraction of nanocellulose fibrils from lignocellulosic fibres: A novel approach. *Carbohydr. Polym.*, **2011,** 86(4), 1468-1475. DOI: 10.1016/j.carbpol.2011.06.034

[2] Stelte, W., Sanadi, A. R. Preparation and Characterization of Cellulose Nanofibers from Two Commercial Hardwood and Softwood Pulps. *Ind. Eng. Chem. Res.*, **2009**, 48(24), 11211-11219. DOI: 10.1021/ie9011672

[3] Klemm, D., Kramer, F., Moritz, S., Lindström, T., Ankerfors, M., Gray, D., & Dorris, A., Nanocellulosen: Eine neue Familie naturbasierter Materialien. *Angew. Chem.,* **2011**, 123(24), 5550-5580. DOI: 10.1002/ange.201001273

[4] Moon, R. J., Schueneman, G. T., & Simonsen, J. (2016). Overview of Cellulose Nanomaterials, Their Capabilities and Applications. Jom, 68(9), 2383–2394. doi: 10.1007/s11837-016-2018-7

[5] Börjesson, M., & Westman, G. (2015). Crystalline Nanocellulose — Preparation, Modification, and Properties. Cellulose - Fundamental Aspects and Current Trends. doi: 10.5772/61899

[6] Foster, E. J., Moon, R. J, Agarwal, U. P, Bortner, M.l J, Bras, J., Camarero-Espinosa, S., Youngblood, J., Current characterization methods for cellulose nanomaterials. *Chem. Soc. Rev.*, **2018**, 47(8), 2609-2679. DOI: 10.1039/C6CS00895J

[7] Lam, E., Male, K. B, Chong, J. H, Leung, A. C.W, & Luong, J. H.T. Applications of functionalized and nanoparticle-modified nanocrystalline cellulose. *Trends Biotechnol.* (Regular Ed.), **2012**,30(5), 283-290. DOI: 10.1016/j.tibtech.2012.02.001

[8] Habibi, Y., Lucia, L. A, Rojas, O. J. Cellulose Nanocrystals: Chemistry, Self-Assembly, and Applications. *Chem. Rev. (Washington, DC, U. S.)*, **2010**, 110(6), 3479-3500. DOI: 10.1021/cr900339w

[9] Missoum, K., Belgacem, M. N., Bras, J., Nanofibrillated Cellulose Surface Modification: A Review. *Materials*, **2013**, 6(5), 1745-1766. DOI: 10.3390/ma6051745

[10] Hubbe, M. A., Rojas, O. J, Lucia, L. A., Sain, M., Cellulosic nanocomposites. A review. *Bioresources*, **2008**, 3(3), 929-980.

[11] Moon, R. J, Martini, A., Nairn, J., Simonsen, J., Youngblood, J., Cellulose nanomaterials review: Structure, properties and nanocomposites. *Chem. Soc. Rev.*, **2011**, 4(7), 3941-3994. DOI: 10.1039/c0cs00108b

[12] Okita, Y., Saito, T., Isogai, A., Entire Surface Oxidation of Various Cellulose Microfibrils by TEMPO-Mediated Oxidation. *Biomacromolecules*, **2010**, 11(6), 1696-1700. DOI: 10.1021/bm100214b

[13] Capron, I., Rojas, O. J, Bordes, R., Behavior of nanocelluloses at interfaces. *Curr. Opin. Colloid Interface Sci.,* **2017**, 29, 83-95. DOI: 10.1016/j.cocis.2017.04.001

[14] Qing, Y., Sabo, R., Zhu, J.Y, Agarwal, U., Cai, Z., Wu, Y., A comparative study of cellulose nanofibrils disintegrated via multiple processing approaches. *Carbohydr. Polym.*, **2013**, 97(1), 226-234. DOI: 10.1016/j.carbpol.2013.04.086

[15] Saito, T., & Isogai, A.,TEMPO-Mediated Oxidation of Native Cellulose. The Effect of Oxidation Conditions on Chemical and Crystal Structures of the Water-Insoluble Fractions. *Biomacromolecules*, **2004**, 5(5), 1983-1989. DOI: 10.1021/bm0497769

[16] Yan, J., Hu, J., Yang, R., Zhang, Z., Zhao, W., Innovative Nanofibrillated Cellulose from Rice Straw as Dietary Fiber for Enhanced Health Benefits Prepared by a Green and Scale Production Method. *ACS Sustainable Chem. Eng.*, **2018**, 6(3), 3481-3492. DOI: 10.1021/acssuschemeng.7b03765

[17] Nechyporchuk, O., Belgacem, M. N., Bras, J., Production of cellulose nanofibrils: A review of recent advances. *Ind. Crops Prod.*, **2016**, 93, 2-25. DOI: 10.1016/j.indcrop.2016.02.016

[18] Environmental Protection Agency. (n.d.). TOXVAL_V5 EPA: Toxicity Values Version 5 (**Aug 2018**). EPA. Retrieved November 8, 2021, from https://comptox.epa.gov/dashboard/dsstoxdb/results?abbreviation=TOXVAL_V5&search=DTXSID2073300#safety.

[19] National Center for Biotechnology Information (**2021**). PubChem Compound Summary for CID 2724126, Tempo. Retrieved November 8, 2021 from https://pubchem.ncbi.nlm.nih.gov/compound/Tempo.

[20] Liimatainen, H., Visanko, M., Sirviö, J. A., Hormi, O. E. O, Niinimaki, J., Enhancement of the Nanofibrillation of Wood Cellulose through Sequential Periodate–Chlorite Oxidation. *Biomacromolecules*, **2012**,13(5), 1592-1597. DOI: 10.1021/bm300319m

[21] Matsuki, S., Kayano, H., Takada, J., Kono, H., Fujisawa, S., Saito, T., Isogai, A., Nanocellulose Production via One-Pot Formation of C2 and C3 Carboxylate Groups Using Highly Concentrated NaClO Aqueous Solution. *ACS Sustainable Chem. Eng.*, **2020**, 8(48), 17800-17806. DOI: 10.1021/acssuschemeng.0c06515

[22] Filipova, I., Fridrihsone, V., Cabulis, U., Berzins, A., Synthesis of Nanofibrillated Cellulose by Combined Ammonium Persulphate Treatment with Ultrasound and Mechanical Processing. *Nanomaterials*,**2018**, 8(9), 640. DOI: 10.3390/nano8090640

[23] Du, C., Liu, M., Li, B., Li, H., Meng, Q., Zhan, H., Cellulose Nanocrystals Prepared by Persulfate One-Step Oxidation of Bleached Bagasse Pulp. *Bioresources*, **2016**, 11(2). DOI: 10.15376/biores.11.2.4017-4024

[24] Zhang, K., Sun, P., Liu, H., Shang, S., Song, J., Wang, D., Extraction and comparison of carboxylated cellulose nanocrystals from bleached sugarcane bagasse pulp using two different

oxidation methods. *Carbohydrate Polymers*, **2016**,138, 237-243. DOI:10.1016/j.carbpol.2015.11.038

[25] Leung, A. C., Hrapovic, S., Lam, E., Liu, Y., Male, K. B., Mahmoud, K. A., Luong, J. H., Characteristics and Properties of Carboxylated Cellulose Nanocrystals Prepared from a Novel One-Step Procedure. *Small*, **2010**, 7(3), 302-305. doi:10.1002/smll.201001715

[26] Castro-Guerrero, C. F., Gray, D. G., Chiral nematic phase formation by aqueous suspensions of cellulose nanocrystals prepared by oxidation with ammonium persulfate. *Cellulose*, **2014**, 21(4), 2567-2577. DOI:10.1007/s10570-014-0308-1

[27] Vecbiskena, L., Rozenberga, L.,Nanocelluloses obtained by ammonium persulfate (APS) oxidation of bleached kraft pulp (BKP) and bacterial cellulose (BC) and their application in biocomposite films together with Chitosan. *Holzforschung*, **2017**, 71(7-8), 659-666. DOI:10.1515/hf-2016-0187

[28] Rozenberga, L., Vikele, L., Vecbiskena, L., Sable, I., Laka, M., Grinfelds, U., Preparation of nanocellulose using ammonium persulfate and method's comparison with other techniques. *Key Engineering Materials*, **2016**, 674, 21-25. DOI:10.4028/www.scientific.net/kem.674.21

[29] Cheng, M., Qin, Z., Liu, Y., Qin, Y., Li, T., Chen, L., Zhu, M., Efficient extraction of carboxylated spherical cellulose nanocrystals with narrow distribution through hydrolysis of lyocell fibers by using ammonium persulfate as an oxidant. *J. Mater. Chem. A*, **2014**, 2(1), 251-258. doi:10.1039/c3ta13653a

[30] Jiang, H., Wu, Y., Han, B., Zhang, Y., Effect of oxidation time on the properties of cellulose nanocrystals from hybrid poplar residues using the ammonium persulfate. *Carbohydrate Polymers*, **2017**,174, 291-298. DOI:10.1016/j.carbpol.2017.06.080

[31] Oun, A. A., Rhim, J., Characterization of carboxymethyl cellulose-based nanocomposite films reinforced with oxidized nanocellulose isolated using ammonium persulfate method. *Carbohydrate Polymers*, **2017**,174, 484-492. DOI:10.1016/j.carbpol.2017.06.121

[32] Filipova, I., Serra, F., Tarrés, Q., Mutjé, P., Delgado-Aguilar, M., Oxidative treatments for cellulose nanofibers production: a comparative study between TEMPO-mediated and ammonium persulfate oxidation. *Cellulose*, **2020**, 27(18), 10671–10688. DOI:10.1007/s10570-020-03089-7

[33] U.S. Bureau of Labor Statistics. (2021, October 19). Average energy prices, Seattle-tacoma-bellevue – September 2021 : Western Information Office. U.S. Bureau of Labor Statistics. Retrieved November 8, 2021, from https://www.bls.gov/regions/west/news-release/2021/averageenergyprices_seattle_20211019.htm.

[34] Delgado-Aguilar, M., González Tovar, I., Tarrés, Q., Alcalá, M., Pèlach, M. À., Mutjé, P., Approaching a Low-Cost Production of Cellulose Nanofibers for Papermaking Applications. *BioResources*, **2015**, 10(3), 5345–5355. DOI: 10.15376/biores.10.3.5345-5355

[35] Zhao, Z. Q., Ouyang, X. P., Effect of Oxidation on the Structures and Properties of Lignin. *Advanced Materials Research,* **2012**,550-553, 1208-213. DOI: 10.4028/www.scientific.net/AMR.550-553.1208

[36] Leung, A.C.W.; Hrapovic, S.; Lam, E.; Liu, Y.; Male, H.B.; Mahmoud, K.A.; Luong, J.H.T. Characteristics and properties of carboxylated cellulose nanocrystals prepared form a novel one-step procedure. *Small*, **2010**, 7, 302–305. DOI: 10.1002/smll.201001715

[37] Filipova, I., Fridrihsone, V., Cabulis, U., Berzins, A., Synthesis of Nanofibrillated Cellulose by Combined Ammonium Persulphate Treatment with Ultrasound and Mechanical Processing. *Nanomaterials*,**2018**, 8(9), 640. DOI: 10.3390/nano8090640

[38] Du, C., Liu, M., Li, B., Li, H., Meng, Q., Zhan, H., Cellulose Nanocrystals Prepared by Persulfate One-Step Oxidation of Bleached Bagasse Pulp. *Bioresources*, **2016**, 11(2). DOI: 10.15376/biores.11.2.4017-4024

[39] Block, P., SIDS Initial Assessment Report for SIAM 20. United Nations Environment Programme (UNEP) Publications, **2005**, Paris, France.

[40] Zhao, Z. Q., Ouyang, X. P., Effect of Oxidation on the Structures and Properties of Lignin. *Advanced Materials Research,* **2012**,550-553, 1208-213. DOI: 10.4028/www.scientific.net/AMR.550-553.1208

[41] Leung, A.C.W.; Hrapovic, S.; Lam, E.; Liu, Y.; Male, H.B.; Mahmoud, K.A.; Luong, J.H.T. Characteristics and properties of carboxylated cellulose nanocrystals prepared form a novel one-step procedure. *Small*, **2010**, 7, 302–305. DOI: 10.1002/smll.201001715

[42] FMC, Persulfates: Technical Information, Retrieved June 05, 2020., from https://www.peroxychem.com/media/90826/AOD_Brochure_Persulfate.pdf, Brussels, Belgium. **2001**.

[43] Mascheroni, E., Rampazzo, R., Ortenzi, M. A., Piva, G., Bonetti, S., Piergiovanni, L., Comparison of cellulose nanocrystals obtained by sulfuric acid hydrolysis and ammonium persulfate, to be used as coating on flexible food-packaging materials. *Cellulose*, **2016**, 23(1), 779-793. DOI: 10.1007/s10570-015-0853-2

[44] Goulden, P. D., Anthony, D. H. J., Kinetics of uncatalyzed peroxydisulfate oxidation of organic material in fresh water. *Analytical Chemistry*, **1978**, 50(7), 953–958. DOI: 10.1021/ac50029a032

[45] Winkler, C. A., Eager, R. L., The oxidation of mercaptans by potassium persulfate in homogenous solution. *Can. J. Res., Sect. B*, **1948**, 26b(7), 527–540. DOI: 10.1139/cjr48b-054

[46] House, D. A., Kinetics and Mechanism of Oxidations by Peroxydisulfate. *Chem. Rev. (Washington, DC, U. S.)*, **1962**, 62(3), 185–203. DOI: 10.1021/cr60217a001

[47] Liang, C., Clifford J B., Thermally Activated Persulfate Oxidation of Trichloroethylene: Experimental Investigation of Reaction Orders., *Ind. Eng. Chem. Res.* **2008**, 47, no. 9 : 2912-918. DOI: 10.1021/ie070820l

[48] Kislenko, V.N., Berlin, A.A., Litovchenko, N.V., Kinetics of oxidation of glucose by persulfate ions in the presence of Mn(II) ions. *Kinet. Catal.*, **1997**, 38(3):391-396.

[49] Koshani, R., Van de Ven, T. G., Madadlou, A.,Characterization of carboxylated cellulose nanocrytals isolated through catalyst-assisted H2O2 oxidation in a one-step procedure. *J. Agric. Food Chem.*, **2018**, 66(29), 7692-7700. DOI: 10.1021/acs.jafc.8b00080

[50] Martinsson, A., Hasani, M., Theliander, H., Hardwood kraft pulp fibre oxidation using acidic hydrogen peroxide. *Nord. Pulp Pap. Res. J.*, **2021**, 36(1), 166-176. DOI: 10.1515/npprj-2020-0088

[51] Leung, A.C.W., Green synthesis, modification, and properties of carboxylated cellulose nanocrystals using ammonium persulfate, *Production and Application of Cellulose Nanomaterial*, **2013**, TAPPI Press

[52] Springer, E. L., Delignification of aspen wood using hydrogen peroxide and peroxymonosulfate. *TAPPI Journal*, **1990**, January, 175–178.

[53] Springer, E. L., Potential uses for peroxymonosulfate in pulping and bleaching. *Proceedings of the 1989 and 1990 AIChe Forest Products Symposium* : **November 5-10, 1989**, San Francisco, California ; **November 11-16, 1990**, Chicago, Illinois. Atlanta, GA : TAPPI Press, 1992: pages 113-120.

[54] McDonagh, Birgitte Hjelmeland, & Chinga-Carrasco, Gary. (2020). Characterization of Porous Structures of Cellulose Nanofibrils Loaded with Salicylic Acid. Polymers, 12(11), 2538.

[55] Chinga-Carrasco, G., Ehman, N. V., Pettersson, J., Vallejos, M. E., Brodin, M. W., Felissia, F. E., Håkansson, J., Area, M. C., Pulping and pretreatment affect the characteristics of bagasse inks for three-dimensional printing, *ACS Sustainable Chem. Eng.*, **2018**, 6 (3), 4068-4075, DOI: 10.1021/acssuschemeng.7b04440

[56] Ehman, N., Lourenço, A., McDonagh, B., Vallejos, M., Felissia, F., Ferreira, P., Area, M., Influence of initial chemical composition and characteristics of pulps on the production and properties of lignocellulosic nanofibers. *Int. J. Biol. Macromol.*, **2020**, 143, 453-461. doi:10.1016/j.ijbiomac.2019.10.165

[57] Gicquel, E., Bras, J., Rey, C., Putaux, J.-L., Pignon, F., Jean, B., Martin, C., Impact of sonication on the rheological and colloidal properties of highly concentrated cellulose nanocrystal suspensions. *Cellulose*, **2019**, 26(13–14), 7619–7634. DOI: 10.1007/s10570-019-02622-7

[58] Chen, W., Yu, H., Liu, Y., Chen, P., Zhang, M., Hai, Y., Individualization of cellulose nanofibers from wood using high-intensity ultrasonication combined with chemical pretreatments. *Carbohydr. Polym.*, **2011**, 83(4), 1804–1811. DOI: 10.1016/j.carbpol.2010.10.040

[59] Cheng, Q., Wang, S., Han, Q., Novel process for isolating fibrils from cellulose fibers by high-intensity ultrasonication. II. Fibril characterization. *J. Appl. Polym. Sci.*, **2010**, 115(5), 2756–2762. DOI: 10.1002/app.30160

[60] Flint, E. B, Suslick, K. S., The Temperature of Cavitation. *Science (American Association for the Advancement of Science)*, **1991**, 253(5026), 1397-1399. DOI: 10.1126/science.253.5026.1397

[61] Wang, S., Cheng, Q., A novel process to isolate fibrils from cellulose fibers by high-intensity ultrasonication, Part 1: Process optimization, *J. Appl. Polym. Sci.*, **2009**, 113(2), 1270–1275. DOI: 10.1002/app.30072

[62] Basri, M., Abd Rahaman, Z.N., Ebrahimpour, A., Salleh, A.B., Gunawan, E.R., Rahman, M.B.A., Comparison of estimation capabilities of response surface methodology (RSM) with artificial neural network (ANN) in lipase-catalyzed synthesis of palm-based wax ester *BMC Biotechnol*, **2007**, 7, p. 53

[63] Lenth, R. V., Response-Surface Methods in R, Using rsm. *Journal of Statistical Software*, **2009**, 32(7), 1–17.

[64] Marget, W. M., Morris, M. D., Central composite experimental designs for multiple responses with different models. *Technometrics*, **2019**, 61(4), 524-532. DOI: 10.1080/00401706.2018.1549102

[65] Peng, B. L., Dhar, N., Liu, H. L., Tam, K. C., Chemistry and applications of nanocrystalline cellulose and its derivatives: A nanotechnology perspective. The Canadian *Journal of Chemical Engineering*, **2011**, 89(5), 1191–1206. DOI: 10.1002/cjce.20554

[66] Filipova, I., Fridrihsone, V., Cabulis, U., Berzins, A., Synthesis of nanofibrillated cellulose by combined ammonium persulphate treatment with ultrasound and mechanical processing. *Nanomaterials*, **2018**, 8(9), 640. DOI: 10.3390/nano8090640

[67] Eyley, S., Thielemans, W., Surface modification of cellulose nanocrystals. *Nanoscale*, **2014**, 6(14), 7764–7779. DOI:10.1039/c4nr01756k

[68] Sun, X., He, Q., Yang, Y., Preparation of dicarboxyl cellulose nanocrystals from agricultural wastes bysequential periodate-chlorite oxidation. *Journal of Renewable Materials*, **2020**, 8(4), 447–460. DOI: 10.32604/jrm.2020.09671

[69] Song, L., Pei, X., Chen, H., Sun, X., Preparation of cellulose nanofibrils by multi-site regioselective oxidation. *Journal of Renewable Materials*. **2020**, 8, 10.

[70] Funahashi, R., Okita, Y., Hondo, H., Zhao, M., Saito, T., Isogai, A., Different conformations of surface cellulose molecules in native cellulose microfibrils revealed by layer-by-layer peeling. *Biomacromolecules*, **2017**, 18(11), 3687–3694. https://doi.org/10.1021/acs.biomac.7b01173

[71] Nishiyama, Y., Structure and properties of the cellulose microfibril. *Journal of Wood Science*, **2009**, 55(4), 241–249. DOI:10.1007/s10086-009-1029-1

[72] Katz S, Beatson RP, The determination of strong and weak acidic groups in sulfite pulps. *Sven Papperstidning*, **1984**, 87:48–53

[73] Yu, H., Zhang, D., Lu, F., Yao, J., New approach for single-step dxtraction of carboxylated cellulose nanocrystals for their use as adsorbents and flocculants. *ACS Sustainable Chem. Eng.*, **2016**, 4(5), 2632-2643. DOI: 10.1021/acssuschemeng.6b00126

[74] Araki, J., Wada, M., Kuga, S., Steric Stabilization of a Cellulose Microcrystal Suspension by Poly(ethylene glycol) Grafting. *Langmuir*, **2001**, 17(1), 21-27. DOI: 10.1021/la001070m

[75] Arola, S., Tammelin, T., Setälä, H., Tullila, A., Linder, M. B., Immobilization–Stabilization of Proteins on Nanofibrillated Cellulose Deriva-tives and Their Bioactive Film Formation. *Biomacromolecules*, **2012**, 13(3), 594-603. doi:10.1021/bm201676q.

[76] Mascheroni, E., Rampazzo, R., Ortenzi, M. A., Piva, G., Bonetti, S., Piergiovanni, L., Comparison of cellulose nanocrystals obtained by sulfuric acid hydrolysis and ammonium persulfate, to be used as coating on flexible food-packaging materials. *Cellulose*, **2016**, 23(1), 779-793. DOI: 10.1007/s10570-015-0853-2

[77] Jiang, H., Wu, Y., Han, B., Zhang, Y., Effect of oxidation time on the properties of cellulose nanocrystals from hybrid poplar residues using the ammonium persulfate. *Carbohydr. Polym.*, **2017**, 174, 291-298. DOI: 10.1016/j.carbpol.2017.06.080

[78] Serra, A., González, I., Oliver-Ortega, H., Tarrès, Q., Delgado-Aguilar, M., & Mutjé, P. (2017). Reducing the Amount of Catalyst in TEMPO-Oxidized Cellulose Nanofibers: Effect on Properties and Cost. Polymers, 9(11), 557. doi:10.3390/polym9110557

[79] Brodin, F., Theliander, H. Absorbent materials based on Kraft pulp: preparation and material characterization., *Bioresources*, **2012**, 7(2), 1666-1683. DOI: 10.15376/biores.7.2.1666-1683
[80] Patiño-Masó, J., Serra-Parareda, F., Tarrés, Q., Mutjé, P., Espinach, F. X., Delgado-Aguilar, M., TEMPO-Oxidized Cellulose Nanofibers: A Potential Bio-Based Superabsorbent for Diaper Production., *Nanomaterials*, **2019**, 9(9), 1271. DOI: 10.3390/nano9091271

[81] Bashar, M. M., Zhu, H., Yamamoto, S., Mitsuishi, M., Highly carboxylated and crystalline cellulose nanocrystals from jute fiber by facile ammonium persulfate oxidation. *Cellulose*, **2019**, 26(6), 3671-3684. DOI: 10.1007/s10570-019-02363-7

[82] Eastman Kodak Company., Titrimetric Determination of Persulfate in Persulfate Bleach, ECR-1125B. *Processing KODAK Motion Picture Films*, **1999**, Module 3, Analytical Procedures, pp. 235–236.

[83] French, A. D., Idealized powder diffraction patterns for cellulose polymorphs. *Cellulose*, **2013**, 21(2), 885–896. DOI: 10.1007/s10570-013-0030-4

[84] González-García, S., Teresa Moreira, M., Artal, G., Maldonado, L., Feijoo, G., Environmental impact assessment of non-wood based pulp production by soda-anthraquinone pulping process. *J. Cleaner Prod.*, **2010**, 18(2), 137–145. DOI: 10.1016/j.jclepro.2009.10.008

[85] Ahvenainen, P., Kontro, I., Svedström, K.,vComparison of sample crystallinity determination methods by X-ray diffraction for challenging cellulose I materials. *Cellulose*, **2016**, 23(2), 1073–1086. DOI: 10.1007/s10570-016-0881-6

[86] Fawcett, T. G., Crowder, C. E., Kabekkodu, S. N., Needham, F., Kaduk, J. A., Blanton, T. N., Petkov, V., Bucher, E., Shpanchenko, R., Reference materials for the study of polymorphism and crystallinity in cellulosics. *Powder Diffr.*, **2013**, 28(1), 18–31. DOI: 10.1017/s0885715612000930

[87] Wojdyr, M., Fityk: A General-purpose Peak Fitting Program, *J. Appl. Crystallogr.* **2010**, 43, no. 5-1: 1126-128. DOI: 10.1107/S0021889810030499

[88] Park, S., Baker, J. O., Himmel, M. E., Parilla, P. A., Johnson, D. K., Cellulose crystallinity index: measurement techniques and their impact on interpreting cellulase performance. *Biotechnol. Biofuels*, **2010**, 3(1), 10. DOI: 10.1186/1754-6834-3-10

[89] Yao, W., Weng, Y., & Catchmark, J. M., Improved cellulose X-ray diffraction analysis using Fourier series modeling. *Cellulose*, **2020**, 27(10), 5563–5579. DOI: 10.1007/s10570-020-03177-8

[90] Canadian Standards Association (CSA), Cellulosic nanomaterials – Test methods for characterization (CSA Z5100-14), Report, 2017.

[91] Nečas, D., Klapetek, P., Gwyddion: an open-source software for SPM data analysis, *Cent. Eur. J. Phys*., **2021**, 10(1) 181-188, DOI: 10.2478/s11534-011-0096-2

[92] Schneider, C. A.; Rasband, W. S., Eliceiri, K. W., NIH Image to ImageJ: 25 years of image analysis, *Nat. Methods*, **2012**, 9(7): 671-675, DOI: 10.1038/nmeth.2089

[93] ProfilmOnline. (2017, December 17). Filmetrics, Inc. San Diego, CA, Retrieved from https://www.profilmonline.com/

[94] Cochran, W. G. (1977). Sampling techniques. 3.ed. New York, NY: Wiley.

[95] Anderson, M. J. (2001). A new method for non-parametric multivariate analy-sis of variance. Austral Ecology, 26(1), 32–46. doi: 10.1111/j.1442-9993.2001.01070.pp.x

[96] Anderson, M. (2003). Analysis of Ecological Communities: Bruce McCune and James B. Grace, MjM Software Design, Gleneden Beach, USA, 2002, ISBN 0 9721290 0 6, US$ 35 (Pbk). Journal of Experimental Marine Biology and Ecology, 289(2), 303-305.

[97] Anderson, M. J. (2017). Permutational Multivariate Analysis of Variance (PERMANOVA). Wiley StatsRef: Statistics Reference Online, 1–15. doi: 10.1002/9781118445112.stat07841

[98] Ricotta, C., & Podani, J., On some properties of the Bray-Curtis dissimi-larity and their ecological meaning. *Ecological Complexity*, **2017**, 31, 201–205. doi: 10.1016/j.ecocom.2017.07.003

[99] Hothorn T, Bretz F, Westfall P., Simultaneous Inference in General Parametric Models. *Biometrical Journal*, **2008**, 50(3), 346–363

[100] Hintze, J. L., & Nelson, R. D. (1998). Violin Plots: A Box Plot-Density Trace Synergism. The American Statistician, 52(2), 181. doi: 10.2307/2685478

[101] Eyley, S., Thielemans, W., Surface modification of cellulose nanocrystals. *Nanoscale*, **2014**, 6(14), 7764–7779. DOI: 10.1039/c4nr01756k

[102] Sun, X., He, Q., Yang, Y., Preparation of Dicarboxyl Cellulose Nanocrystals from Agricultural Wastes bySequential Periodate-Chlorite Oxidation. *J. Renewable Mater.*, **2020**, 8(4), 447–460. DOI: 10.32604/jrm.2020.09671

[103] Song, L., Pei, X., Chen, H., Sun, X., Preparation of Cellulose Nanofibrils by Multi-Site Regioselective Oxidation. *Tech Science Press*, **2020**, 8(10), 1269–1282. DOI: 10.32604/jrm.2020.010923

[104] Habibi, Y., Chanzy, H., Vignon, M. R., TEMPO-mediated surface oxidation of cellulose whiskers. *Cellulose*, **2006**, 13(6), 679–687. DOI: 10.1007/s10570-006-9075-y

[105] Nishiyama, Y., Structure and properties of the cellulose microfibril. *J. Wood Sci.*, **2009**, 55(4), 241–249. DOI: 10.1007/s10086-009-1029-1

[106] Funahashi, R., Okita, Y., Hondo, H., Zhao, M., Saito, T., Isogai, A., Different Conformations of Surface Cellulose Molecules in Native Cellulose Microfibrils Revealed by Layer-by-Layer Peeling. *Biomacromolecules*, **2017**, 18(11), 3687–3694. DOI: 10.1021/acs.biomac.7b01173

[107] Wilke CO (2018) Ggridges: Ridgeline plots in'ggplot2'. R package version 05.

[108] Gong, J., Li, J., Xu, J., Xiang, Z., Mo, L., Research on cellulose nanocrystals produced from cellulose sources with various polymorphs. *RSC Adv.*, **2017**, 7(53), 33486-33493. DOI:10.1039/c7ra06222b

[109] del Cerro, D.R., Koso, T.V., Kakko, T., Crystallinity reduction and enhancement in the chemical reactivity of cellulose by non-dissolving pre-treatment with tetrabutylphosphonium acetate. *Cellulose*, **2020**, 27, 5545–5562 . DOI: 10.1007/s10570-020-03044-6

[110] Hothorn, T., Bretz, F., Westfall, P., Simultaneous Inference in General Parametric Models, *Biom. J.*, **2008**, 50(3), 346-363

[111] Ma, P., Fu, S., Zhai, H., Law, K., Daneault, C., Influence of tempo-mediated oxidation on the lignin of Thermomechanical Pulp. *Bioresour. Technol.*, **2012**, 118, 607-610. DOI: 10.1016/j.biortech.2012.05.037

[112] Okita, Y., Saito, T., Isogai, A., Tempo-mediated oxidation of softwood thermomechanical pulp. *Holzforschung*, **2009**, 63(5). DOI: 10.1515/hf.2009.096

[113] Hulten, A. H., Basta, J., Samuelsson, M., Greschik, T., Ander, P., Daniel, G., Aspects on bleaching and TEMPO-mediated oxidation of wheat straw pulp fractions, *Bioresources*, **2012**, 7, no. 3: 3051-063.

[114] Imai, T., Yokoyama, T., Matsumoto, Y., Revisiting the mechanism of β-O-4 bond cleavage during acidolysis of lignin IV: Dependence of acidolysis reaction on the type of acid. *J. Wood Sci.*, **2011**, 57(3), 219-225. DOI:10.1007/s10086-010-1166-6

[115] Jeong, S.-Y., Lee, J.-W., Sequential Fenton oxidation and hydrothermal treatment to improve the effect of pretreatment and enzymatic hydrolysis on mixed hardwood. *Bioresour. Technol*., **2016**, 200, 121–127. DOI:10.1016/ j.biortech.2015.10.015.

[116] Davaritouchaee, M., Chen, S., Persulfate oxidizing system for biomass pretreatment and process optimization. *Biomass Bioenergy*, **2018**, 116, 249-258. DOI:10.1016/j.biombioe.2018.06.021

[117] Santos, R., Capanema, E., Balakshin, M., Chang, H., Jameel, H., Effect of hardwoods characteristics on kraft pulping process: Emphasis on lignin structure. *BioResources*. **2011**, 6. 3623. DOI: 10.15376/biores.6.4.3623-3637.

[118] Gutiérrez, A., Rodríguez, I. M., Del Río, J. C., Chemical characterization of lignin and lipid fractions in industrial hemp bast fibers used for manufacturing high-quality paper pulps. *J. Agric. Food Chem.*, **2006**, 54(6), 2138-2144. DOI:10.1021/jf052935a

[119] Haunreiter, K. J., Dichiara, A., Gustafson, R., Structural and chemical characterization of hop bine fibers and their applications in the paper industry. *Industrial Crops and Products*, **2021**,174, 114217. DOI: 10.1016/j.indcrop.2021.114217

Chapter 5. Ammonium persulfate oxidized nanofibrillated cellulose for reinforcement of paper; morphological and mechanical evaluation.

5.1 Introduction

With the increasing rate of recycled pulp being utilized in the production of printing and packaging materials, paper manufacturing employs larger quantities of chemical additives, up to 30% of the material composition, to maintain and optimize the properties of the final products[1]. In particular, silica nanoparticles have been used to improve drainage and retention in paper through a bridging mechanism with other polyelectrolytes such as cationic polyacrylamide (cPAM) or cationic starch[2,3]. High molecular weight cationic polymers combined with anionic nanoparticles, such as anionic silica, improve the dispersion and bridging between fibers and particles in suspensions, while demonstrating resistance to high-shear deflocculation. These wet end chemistry systems however can be expensive, result in low intrinsic strength and do not biodegrade in the environment.

Nanofibrillated cellulose (NFC), produced from abundant natural biomass exhibit high specific surface area and share a similar composition as pulp fibers, providing a renewable and biodegradable alternative to traditional fillers used for paper quality improvements. The incorporation of NFC in paper has been effective in enhancing mechanical and barrier characteristics[4.5,6].

Mechanically produced NFC and TEMPO-oxidized NFC have been used to increase the strength properties and reduce the permeability of paper[7,8,9]. However, the direct addition of NFC to pulp suspensions is limited by coulombic repulsions between NFC and pulp fibers (i.e both structures present anionic charges on their surface) and by drainage issues due to the high-water

retention capacity of the hygroscopic network[10]. In addition, when NFC is used in combination with cationic polymers and/or inorganic fillers in dual component retention systems [11], flocculation issues may arise, hindering the reinforcing effect of NFC.

The flocculation of fine materials may further improve with control of surface charge. Mechanically produced NFC and TEMPO-NFC have been utilized as a reinforcement in paper to improve the strength properties and to reduce the permeability of paper[12,13,14,15]. As a result, the introduction of NFC into paper either as an amendment or coating is growing and has potential in commercial application as shown in Table 5.5

The aspect ratio and surface charge of nanocellulose influence their ability to form a cross-linked network through hydrogen bonding and electrostatic interactions between the different paper components, all of which are important to improved function of dual component retention chemistry. Despite the increasing number of reports on the utilization of NFC in papermaking, comprehensive studies examining the effect of NFC characteristics on paper properties remain scarce. The use of retention chemistry required to form stable dispersions and promote bridging between the polydispersed NFC and paper fibers is rare[16], but instead favor formation of aggregates according to percolation theory[17]. Where charged NFC is used, the effect of NFC surface charge cannot be assessed as it is not decoupled from variation in NFC morphology[18], see Table 5.5. In this work, NFC with similar morphologies but different carboxylic contents were synthesized based on the economically attractive ammonium persulfate (APS) mediated oxidation method, to assess specifically the influence of surface charge and NFC content on the physical performance of the resulting materials. Principal component analysis (PCA) will be used to uncover interactions between treatment conditions and response variables. This research provides a method for reinforcing cellulose paper fibers in dual component retention systems with a

sustainable and cost-effective alternative nano cellulose product derived from lignocellulosic biomass.

5.2 Materials and Methods

The base fiber used is bleached Northern softwood Kraft (B-NSWK) supplied by Westrock, Tacoma, WA. The mixture is approximately 50:50 Douglas fir (*Pseudotsuga menziesii*) and Western Hemlock (*Tsuga heterophylla*). Cationic polyacrylamide (cPAM) was supplied by BASF, Florham Park, New Jersey. Poly-DADMAC was supplied by Aldrich Chemical. Ammonium persulfate (APS) was supplied by VWR Chemicals LLC, CAS: 7727-54-0. Sodium sulfate was obtained from Sigma Aldrich, St. Louis, MO, USA, CAS 7757-82-6.

5.2.1 Preparation of NFC by APS Oxidation.

NFC were synthesized from bleached softwood pulp using a previously reported ammonium persulfate (APS) oxidation procedure[19]. 15 grams of oven dried pulp was added to 300 ml of deionized water and disintegrated in a waring blender. The pulp slurry was then transferred to an Erlenmeyer flask containing 480 g of 2M ammonium persulfate solution. The degree of oxidation was controlled by carefully adjusting the reaction time and temperature as follows: the high charge NFC was oxidized at 80 °C for 420 minutes, while the low charge NFC was prepared at 70 °C for 180 minutes, as shown in Table 5.1. These conditions were determined based on response surface models for APS oxidation of NFC, as reported elsewhere[19]. The oxidation reactions were conducted under constant agitation and terminated by quenching the mixture in an ice bath to rapidly drop the temperature. The resulting suspensions were then

transferred to a Spectra/Por 4 molecular porous membrane tube, MWCO: 12-14 kD for dialysis against deionized water until a pH greater than 3.4 was achieved.

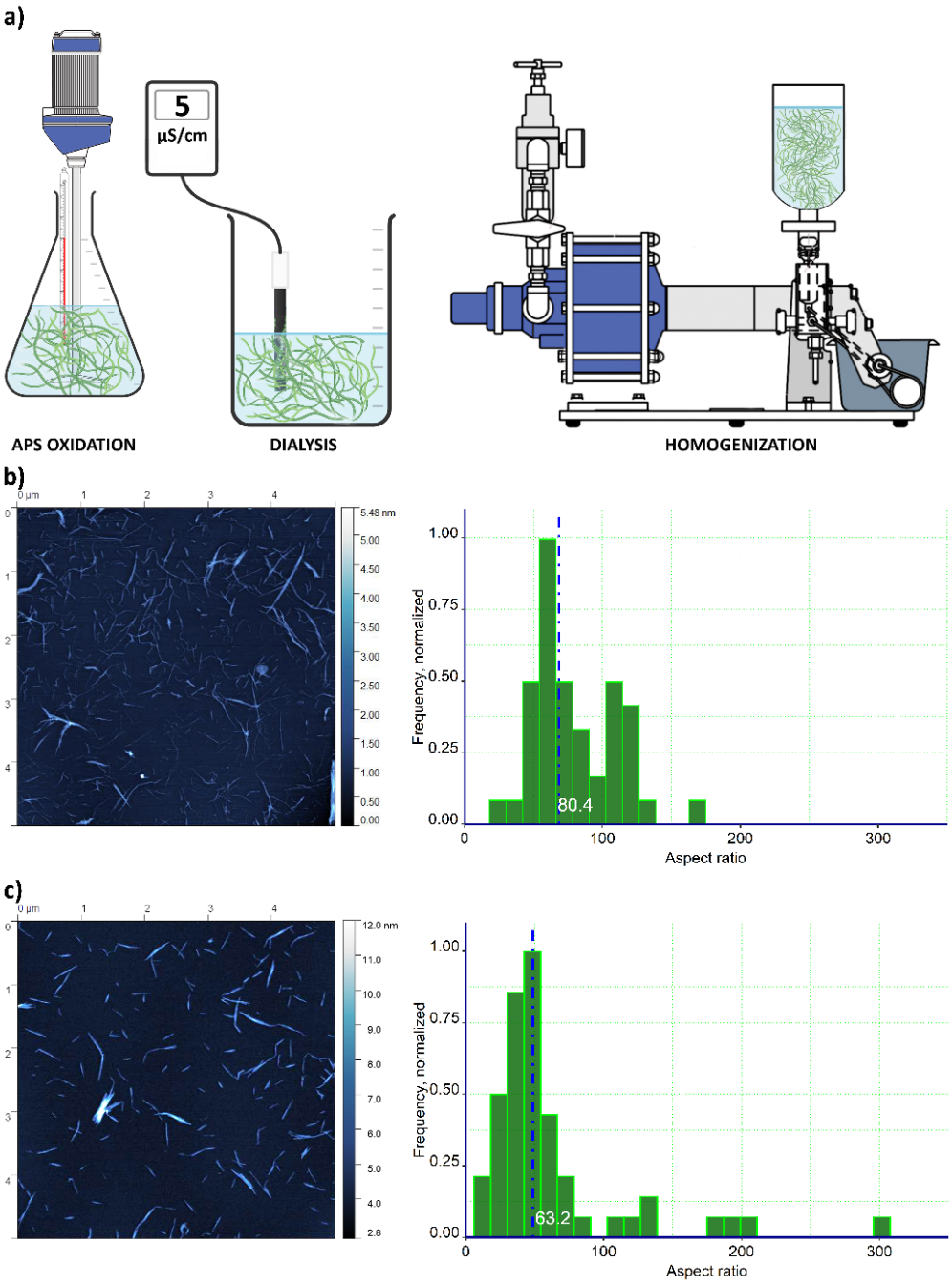

Figure 5.1. a)Schematic representation of the oxidation, dialysis, homogenization, . b-c) AFM plot and aspect ratio distribution of nanofibers for low carboxylic acid surface charge and high carboxylic acid surface charge respectively.

A 2^2 factorial design summarized in Table 5.1was selected to examine the two levels of surface charge and two levels of NFC amendment relative to a base sheet.

Table 5.1. Experimental Design

Condition	% NFC	mmol Carb/g
1	0	0.00
2	5%	0.88
3	10%	0.88
4	5 %	1.34
5	10%	1.34

After dialysis, the oxidized materials were subjected to mechanical energy from a microfluidizer M110-S, Microfluidics Corporation, Westwood, Massachussetts[20]. A 0.3% dispersion was passed through an 80 µm diameter z-type interaction chamber five times at an operating pressure of 95 MPa. The processed materials were transferred to 50.0 mL vials and centrifuged for 20.0 minutes at 2950 rpm (1720 relative centrifugal force). The supernatant, containing the NFC, was then collected into a clean 50.0 mL centrifuge vial prior to further testing[21,22,23].

5.2.2 Nanofiber Characterization.

The morphology of NFC prepared under different conditions was characterized by atomic force microscopy (AFM). Prior to AFM observations, nanocellulose dispersions were chemically bonded to the surface of a mica wafer based on a previously established procedure[24]. Topography images were produced by scanning 5 μm^2 regions of the different samples at a scan rate of 0.977 Hz using a Bruker ICON AFM equipped with a bluedrive photothermal excitation and operated in tapping mode. Gwyddion software was used to level the surface, analyze the resulting scan, and determine the fiber diameters[25], while ImageJ was employed to measure the NFC length

distribution[26]. The aspect ratio was calculated by dividing the measured length by the diameter of the fiber.

The carboxylate content of the NFC is determined by a modification of previously published conductometric titration conductometric titration using 0.01 molar NaOH[27,28,29].. Approximately 0.1 grams of oven-dried fiber are added to a 40.0 mL scintillation vial to which 10 mL of 0.01M HCl are added. Deionized water makes up the remaining volume. The vials are then either sonicated for 15 minutes or allowed to sit for 2 hours during which the Na cations bound to the carboxylic acid groups are exchanged by H+ ions[30].. The samples are then transferred to a 400 mL beaker and the volume brought up to 200 mL with deionized water. Conductivity is recorded using an Orion Star A212 meter for every 0.250 mL of titrant delivered by an Arduino controlled peristaltic pump.

The specific surface area (SSA) of as-synthesized materials was determined using Congo Red (CR) adsorption on the NFC surface[31,32,33]. The fine structure of nanofibers may be characterized through the use of direct dye, Congo red, as they are physically absorbed on the cellulose in a method described by Ingelsby[34]. The specific surface area (SSA) was determined using Congo red (CR) adsorption of the nanofibers after dialysis[34]. The CR molecule diffuse into the fiber as shown in Figure 5.2.

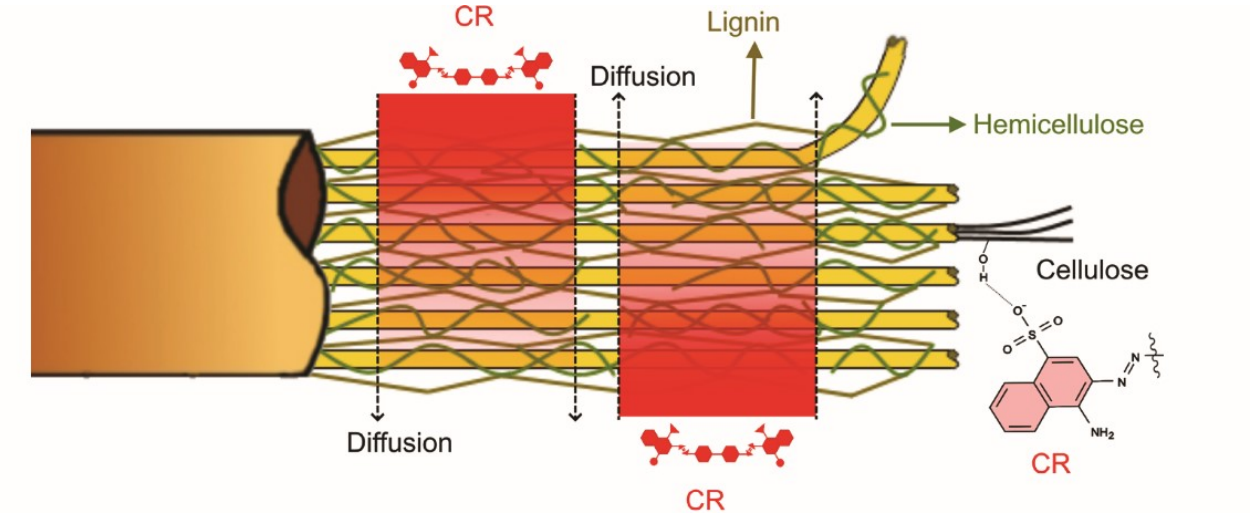

Figure 5.2. Schematic of the adsorption of Congo red (CR) on the cellulose fibers[37].

Nanofibers typically range in size from 91 to 282 m^2/g determined by the CR method as shown in Table 5.2.

Table 5.2. Nanofiber size comparisons using Congo red dye adsorption.

Nanofiber type	**SSA, m^2/g**
Bacterial Cellulose (BC) [32]	91
Microcrystalline Cellulose (MFC)[32]	35-160
Nanofibrillated Cellulose (NFC)[35,36]	132-282
Cellulose[37]	2.9-22.1

The NFC suspension for each charge was dyed with a 5% to 15% W/W Congo Red solution at 50 C for 24 H. Prior to treatment with CR, 0.08% (W/W) sodium sulfate buffer (0.1M) is added to the dialyzed supernatant. NaCl (0.1M) was added at 0.0005% (W/W) to each sample to neutralize the negative charge on the nanofibers[38]. If this is neutralization is not performed, the dye will not adsorb[39]. Congo red is an inorganic anionic dye making it challenging to approach the surface of the cellulose nanofiber. The Na^+ gathers around the carboxylic acid charge on the surface and neutralizes it facilitating adsorption of the dye. The samples were then centrifuged for 10 minutes followed by UV absorbance measurement of the supernatant at 488 nm using a

Shimadzu UV1880 spectrophotometer with a spectral resolution of 1 nm. The adsorption of Congo red on the nanofibers was calculated using the Langmuir isotherm equation 5-1 because it forms a mono-layer on the surface of the nanofibers[40,41,42,43]. $[C]_t$ is the concentration of dye in solution at adsorption equilibrium (mol/L). $[A]_a$ is the equilibrium concentration of the applied dye adsorbed on nanofiber (mg/g). $[A]_{t,max}$ is the maximum amount (mg/g) of dye adsorbed onto the nanofiber. K_L is the Langmuir adsorption equilibrium constant (L/mol)[44,45].

$$[A]_a = \frac{[A]_{max} K_L [C]_t}{1 + K_L [A]_{max}} \tag{5-1}$$

The specific surface area of the nanofiber can be calculated from equation 2 where N_A is Avogadro's constant, SA_{CR} is the surface area of one molecule of Congo red (1.73 nm^2) and MW is the molecular weight of Congo red (696.7 g/mol).

$$SSA_{nanofiber} = [A]_{max} \; x \; N_A \; x \; \frac{SA_{CR}}{MW \; x \; 10^{21}} \tag{5-2}$$

5.2.3 Preparation of Hand-sheets.

Bleached softwood kraft pulp was slurried in a British disintegrator then dewatered to form a 10% pulp consistency. The pulp slurry was placed in a PFI mill and refined until a Canadian Standard Freeness (CSF) of 150 was achieved[46]. The electrical conductivity of the refined bleached softwood pulp was adjusted to 1000µs/cm using sodium sulfate in a method described by Lenze[4]. Charged nanofibrillated cellulose (NFC) was subsequently added at the prescribed amendment level with water to bring slurry consistency to 0.3%, see Table 5.1.

Poly-DADMAC, prepared as a solution of 0.25% in water, was added to the 0.3% consistency pulp slurry at 0.05% (W/W) prior to addition of cationic polyacrylamide (cPAM).

Poly-DADMAC, prepared as a solution of 0.25% in water, was added to the 0.3% consistency pulp slurry at 0.05% (W/W) before the addition of cationic polyacrylamide (cPAM). The pulp slurry was continuously stirred at 500 rpm. The poly-DADMAC addition promotes the bridging mechanism over the patch mechanism of the cPAM. The negative counterions introduced by the polyelectrolyte reduce the Stern layer and stabilize the dispersion as depicted in Figure 5.3[47,48]. After five minutes, cPAM, prepared as a 0.1% solution in water, was added to the slurry at 0.05% (W/W) as shown in Figure 5.3, followed by an additional five minutes of agitation. Hand sheets were produced to 60 gsm according to TAPPI T220[49].

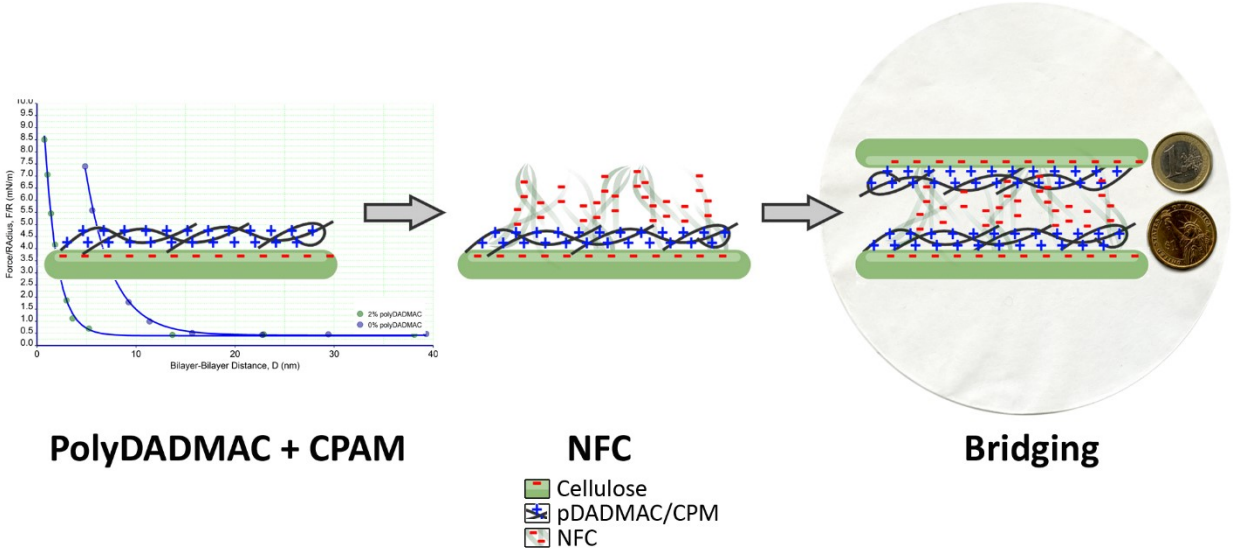

Figure 5.3. Schematic representation of Fiber-CPAM-NFC bridging network.

5.2.4 Fines Retention.

Fine retention was performed using a dynamic drainage tester, Britt jar, with four different screens, 125M, 100P, 60W, and 125W according to TAPPI test method T261[5051]. Agitation was set to 500 RPM[52,53]. The filtrate was collected and subsequently passed through a 2.5µ filter paper. The solids retained were then determined by weight on the mesh screen and filter paper according to TAPPI method T261[54].

5.2.5 Physical Testing.

Hand sheets were conditioned according to TAPPI method T402 for 24 hours[55]. Non-destructive testing of opacity, light scattering and absorbence, L*a*b* color[56], and permeability[57] were conducted followed by tensile[58] and tear evaluation[59]. SEM images were taken with a Sirion XL30 scanning electron microscope (5 kV), and all samples were platinum-sputtered with a Leica EM ACE600 to a depth of 4 nm before observation.

5.2.6 Data Analysis.

R-studio was used to perform statistical analysis, principle component analysis, and to visualize the data[60,61,62]. Matlab was utilized to construct average plots of the elongation curves for each sample[63,64].

5.3 Results and Discussion

5.3.1 Nanocellulose Characterization.

NFC fibers were produced with surface charge of 0.88 and 1.34 mmol carboxylic acid/g with aspect ratio of 80.4 and 63.2, respectively and shown Figure 5.1b-c. The mean fiber length was determined to be 237 nm and 195 nm and mean fiber diameter to be 3.2 nm and 3.6 nm respectively.

There was a significant increase in specific surface area, 47%, of the nanofiber for the low charge versus the high charge, see Table 5.3. This is in contrast to increasing specific surface area (SSA) and decreasing fiber diameter with increasing carboxylic acid content found in prior studies, see Figure 5.4[65,72].

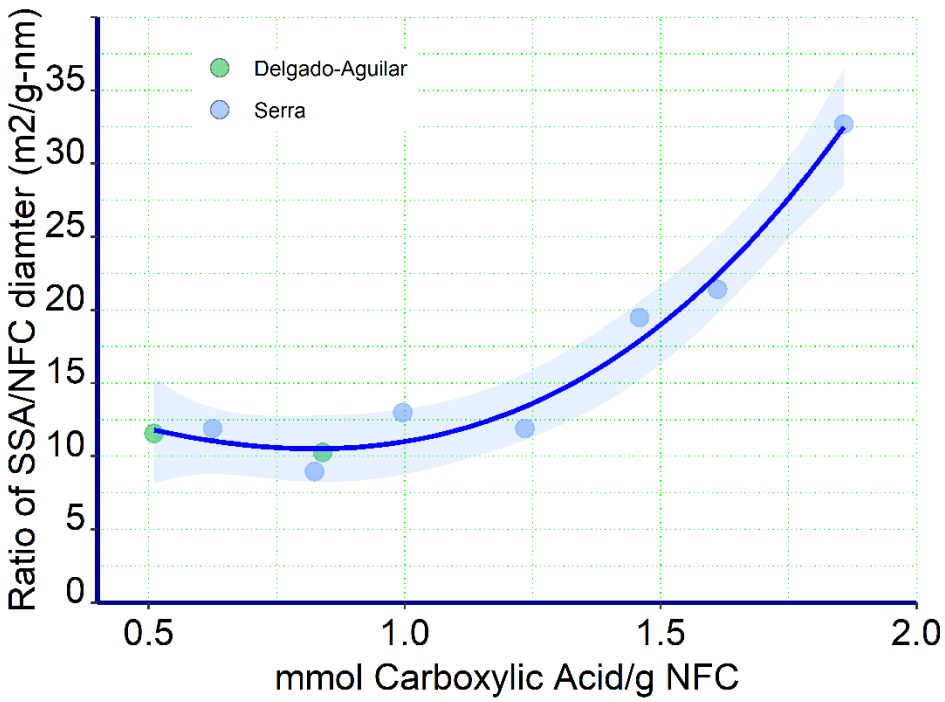

Figure 5.4.Normalized SSA to diameter at varying NFC surface charge for TEMPO-NFC.

Previous studies have found a strong correlation between the SSA normalized to NFC diameter and the surface charge of the TEMPO-NFC fibers[65,72]. Increasing carboxylic acid content is associated with increased fibrillation. The observation measured in this study is likely a result of the aspect ratio being driven by length and relatively unaffected by diameter. The length being longer for the lower charge nanofibers resulted in greater area for bonding which is in agreement with the improved strength measured in the reinforced paper with low charge nanofibers (NFC).

A plot of absorption of Congo red on the fibers shows reduced relative absorption by the high charge NFC versus the low charge NFC, see Figure 5.5

Table 5.3. Morphological characterization of the nanofibers (95% confidence interval shown for aspect ratio, length, and diameter).

				Langmuir				
Condition	Aspect Ratio	Length (nm)	Diameter (nm)	$[A]_{max}$, mg/g	K_L L/mol	r^2	SSA m^2/g	CI
Low Charge Fiber	80±9.0	237±19.5	3.2±0.27	94.8	0.0242	0.998	141.8	78
High Charge Fiber	60±11.1	195±30.1	3.6±0.41	64.5	0.0325	0.997	96.5	79

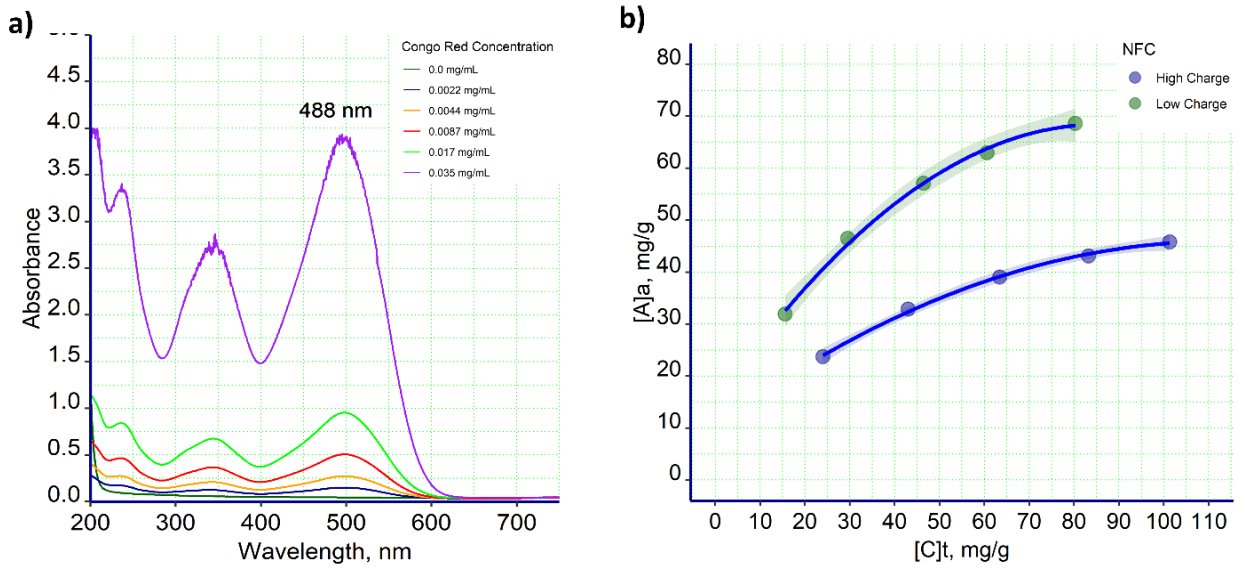

Figure 5.5.a) UV absorption calibration curves, b) Langmuir isotherm predicted equilibrium concentration,$[A]_a$, of the applied dye adsorbed on nanofiber (mg/g) for different dye concentrations (W/W fiber).

Scanning electron microscope images show that as you increase the NFC at low charge, the sheet begins to densify relative to the base sheet. The grammage of the hand sheets produced averaged 63.5 (±0.37) gsm. Different NFC levels and charges did not result in significant structural differences on the sheet surface , see Figure 5.6a-f. Scans of the edge show, however, that at the higher charge the sheet is less densified as shown in Figure 5.6g-h. The caliper of the lower charge nanofibrillated cellulose was 4.19 (±0.08) microns while the caliper of the high charge was 4.61 (±0.05) microns .The base sheet caliper measured 4.57 (±0.05) microns.

Fiber retention was highest with the lower charge nanofibrillated cellulose, 95.3%. The high charge fiber formed visible fiber flocs at the 10% reinforcement level observed in the fiber pad. As NFC addition and charge were increased, fiber retention was reduced to 92.2%. This is consistent with previous observations that the higher charge NFC at the higher addition rate may be saturating the surface and causing charge reversal consistent with polymeric flocculant theory[66].

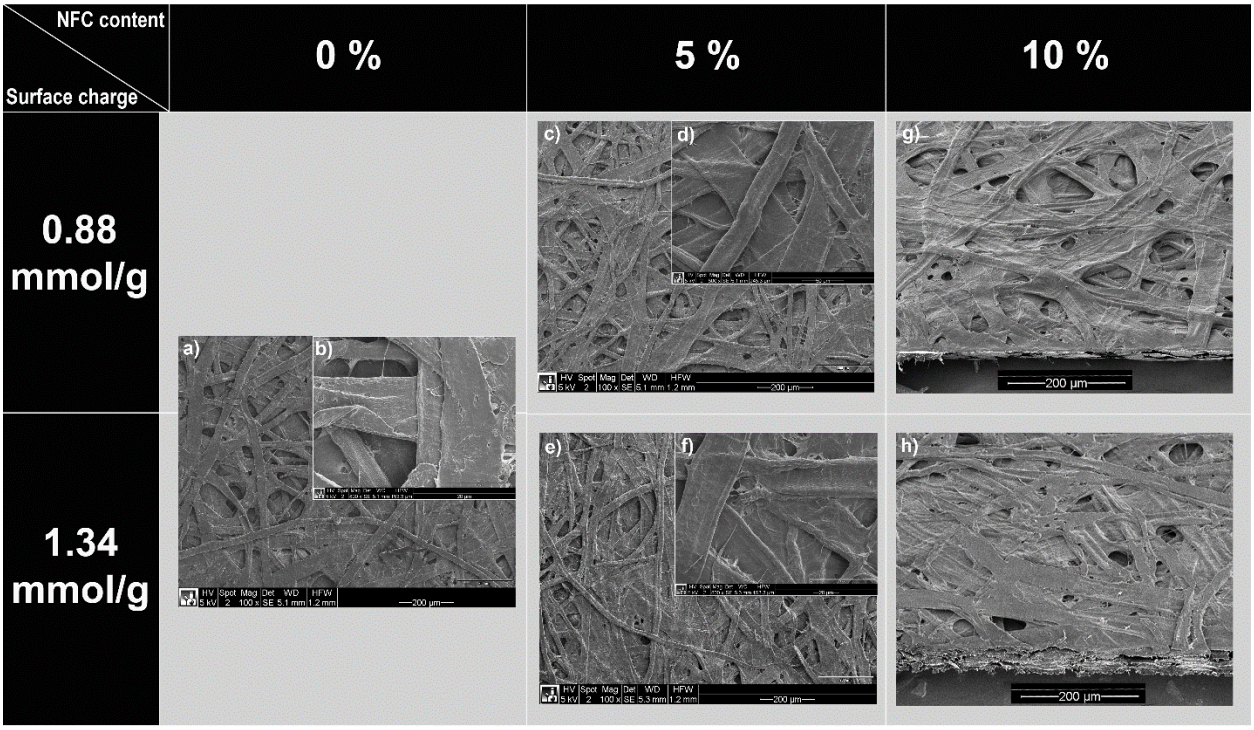

Figure 5.6. a-b) base sheet, c-d) 5% NFC addition at low charge, e-f) 5% NFC addition at high charge. Paper edge view g) 10% NFC reinforcement - low charge (4.19 ±0.08 microns), h) 10% NFC reinforcement at high charge (4.61 ±0.05 microns). See appendix for large scale images.

5.3.2 Structural Paper Characterization.

The anionic surface charge on the nanofibrillated cellulose provided electrostatic attraction with the cationic polyacrylamides (cPAM) to bind with the cellulose fibers. The maximum tensile strength and permeability occur when the surface charge is low and the NFC content is at 10% (W/W) shown in Figure 5.7a-b. At higher charge, increased NFC addition level produced fiber flocs resulting in reduced strength and permeability response. This may be due to the saturation of the fiber surface with high charge APS-NFC creating increased electrostatic repulsion between fibers. The APS-NFC behaves like a microparticle in combination with the bridging polymer which would normally reduce the flocculation of fibers at higher surface coverage[67]. The

polyelectrolyte may be too low in concentration to effectively screen the electrostatic interaction between fiber and the higher charge NFC inducing floc formation[47].

With bonding degree between fibers already high (the bleach softwood Kraft was refined in a PFI mill to the maximum tensile and tear development) the addition of NFC resulted in lower tear relative to the base sheet, see Table 5.4, which is consistent with a highly bonded sheet[68,69], see Table 5.4.

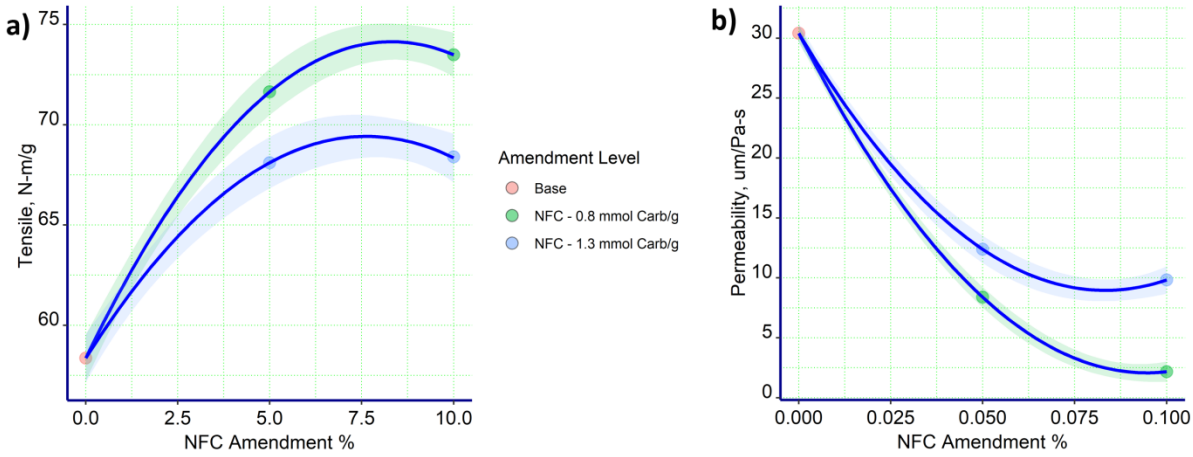

Figure 5.7. a) Influence of NFC surface charge and addition level on tensile strength. b) influence on sheet permeability.

The tensile (N-m/g) increased by 25.9% at 10% NFC reinforcement with low surface charge fiber relative to the base paper. Young's modulus increased by 18.6%. The greatest increase in the modulus was at the highest charge and lowest reinforcement level. The elongation curve for the high charge and high addition rate were almost identical to the low addition rate. It may be attributed to the increased flocculation that was observed with the high charge. There was no measured decrease in elongation at break indicating that the flexibility of the base sheet persists and that the NFC is improving the load carrying capacity of the fiber, as shown in the load-elongation curve Figure 5.8.

Table 5.4. Physical test summary data of nanocellulose reinforced paper (mean ±SD)..

Condition	Tensile (N-m/g)	TEA (J/g)	Tear (mN-m²/g)	Modulus (GPa)	Strain (%)	Permeability (µm/Pa-s)
BASE	58.4 ±1.2	0.84 ±0.07	18.3 ±1.2	14.0 ±2.5	3.54 ±0.03	29.9 ±4.5
NFC-5-LC	71.6 ±1.8	1.21 ±0.07	16.3 ±1.1	14.9 ±2.2	3.30 ±0.02	8.4 ±1.5
NFC-10-LC	73.5 ±2.8	1.08 ±0.37	14.9 ±1.4	16.6 ±2.3	3.44 ±0.06	2.2 ± 0.6
NFC-5-HC	68.5 ±3.1	0.92 ±0.31	14.8 ±1.4	16.0 ±1.3	4.05 ±0.05	12.2 ±1.9
NFC-10-HC	67.4 ±3.4	1.02 ±0.18	16.1 ±1.5	15.3 ±2.0	2.85 ±0.03	9.8 ±1.7

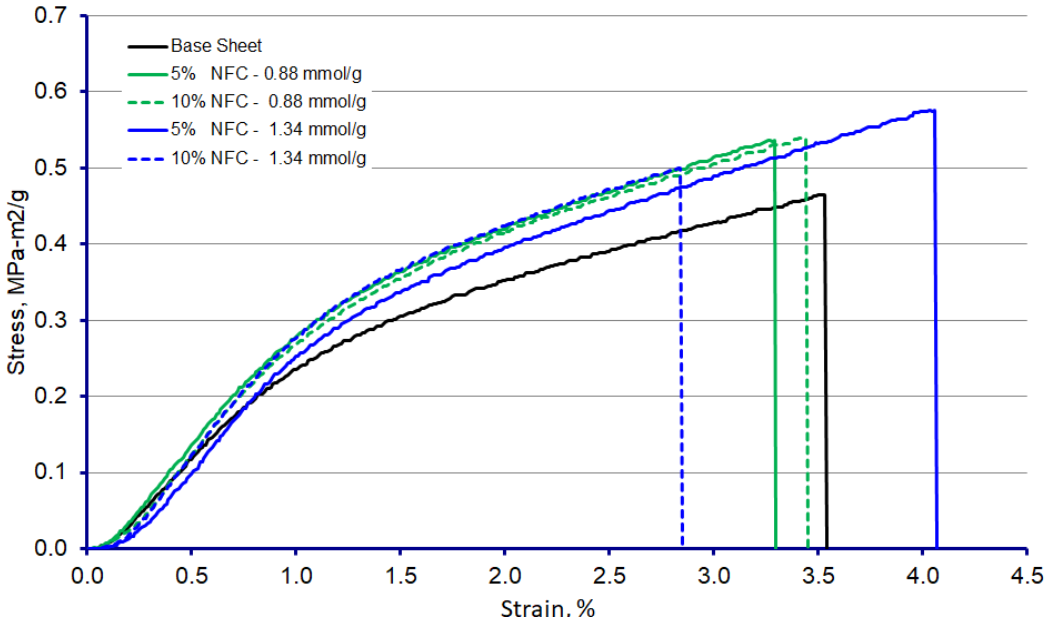

Figure 5.8. Specific stress versus strain. Gauge length set at 100mm, sample width of 15mm.

Table 5.5. Publications applying TEMPO-NFC as reinforcement in paper compared to APS-NFC. Retention aids listed are cationic starch (CS) and cationic polyacrylamide (CPAM).

NFC Type	Retention Aid	Addition Level	Charge (mmol/g)	Tensile (N-m/g)	Permeability (µm/Pa-s)
Table 3 Summary	CPAM	5-10%	0.88-1.34	67-73.5	2.2-12.2
Gonzalez(2012)[70]	CS	3-9%	-	31-51.3	-
Alcalá(2013)[71]	none	3-12%	0.40	-	-
Delgado-Aguilar (2015)[72]	CS	2.2-3%	0.51-0.84	34-40.3	-
Balea(2016)[73]	CPAM	3-5%	0.59-0.75	44-62.6	1.04-3.24
Balea(2017)[74]	CPAM	0.5-3%	0.17-1.18	44-47.9	-
Espinosa(2017)[12]	none	1-5	0.36	-	-
Balea (2019)[75]	CPAM	1-3%	0.25-1.04	-	0.61-8.3

Lower surface charge at higher addition rates resulted in a significant reduction in permeability as shown in Figure 5.7b. This is consistent with published findings showing that as

charge is reduced and addition rate increased, permeability for TEMPO-NFC reinforced paper is similarly reduced. Increasing the surface charge of nanofibers was observed to lower permeability but not to the extent that NFC of lower charge achieved.

5.3.3 Principle component analysis

A principal component analysis was performed on the physical response data. The first principal component was attributed to the tensile, tensile energy absorption and breaking length of the fibers which accounted for 67% of the total variance in the data. The percentage of NFC reinforcement influenced these response variables with surface charge to a lesser extent. An analysis of variance (ANOVA) on each individual response confirmed that tensile, tear and stretch were significantly influenced by surface charge. NFC Surface charge was not significant, at the 0.95 confidence level, for tensile energy absorption and breaking length. Reinforcement was significant at the 0.95 confidence level for tensile, stretch, breaking length and tear. There was strong interaction between surface charge and NFC amendment level for all responses

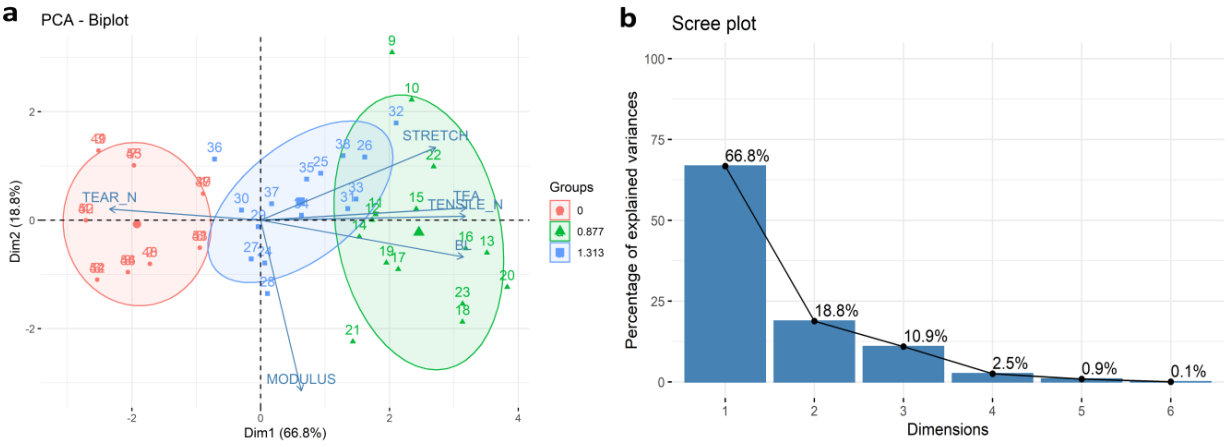

Figure 5.9. Principal component analysis of a) mechanical properties at varying NFC charge, b) scree plot of principal component for mechanical properties.

The second principal component accounted for 19% of the variance in the data due to elastic modulus and stretch of the fibers. These response variables were primarily impacted by the surface charge of the fibers. The NFC amendment level (%NFC) was also statistically significant for stretch but not for the elastic modulus. The third principal component is attributed to the variance in the tear data.

5.4 Conclusions

APS-oxidized nanofibers were produced from bleached northern softwood Kraft fibers with surface charge 0.88 and 1.34 mmol/g carboxylic acid and aspect ratios of 80 and 60 respectively. The tuned NFC fibers were added to softwood pulp as a reinforcement at 5 and 10% by weight. The addition of a high aspect ratio NFC at both amendment levels produced a composite network of cellulose fibers with superior barrier and strength properties. At 10% addition permeability was reduced by 93% to 2.2 μm/Pa-s and tensile development increased by 25.9% to 73.5 N-m/g.

Increasing the surface charge of nanofibrillated cellulose resulted in the formation of large disperse flocs which may be a result of electrostatic repulsion caused by higher fiber surface saturation consistent with polymeric flocculation theory. The lower retention at high NFC addition and higher surface charge suggests that tuning the polyelectrolyte and cPAM addition level is needed to mitigate the floc formation observed with higher surface charge NFC and addition rates. The elastic modulus for the higher surface charge NFC was the only response that was higher than the low aspect low charge fibers. If a stiffer material is required, we can utilize an NFC fiber with a higher surface charge. A low-charge fiber can be engineered to design a material with improved flexibility and lower permeability. These results demonstrate that applying a response surface method to tune the morphology and surface chemistry of APS-NFC fibers achieves a comparable

physical response as TEMPO-produced fibers. Hence APS-NFC could replace expensive and unsustainable chemicals for improving the sheet properties of paper and paperboard.

References

[1] Hubbe, M. A., Prospects for maintaining strength of paper and paperboard products while using less forest resources: A Review. *BioResources*, **2013**, 9(1). DOI: 10.15376/biores.9.1.1634-1763

[2] Carr, D., Tokarz, M., Silica nanoparticles build bridge to better retention, sheet formation. *Pulp Pap-Canada*, **2006**, 80(2), 34.

[3] Swerin, A., Glad-Nordmark, G., Ödberg, L., Adsorption and flocculation in suspensions by two cationic polymers : Simultaneous and sequential addition. *J. Pulp Paper Sci*., **1997**, 23(8), J389-J393.

[4] Ahola, S., Myllytie, P., Österberg, M., Teerinen, T., Laine, J., Effect of polymer adsorption on cellulose nanofibril water binding capacity and aggregation. *Bioresources*, **2008**, 3(4), 1315-1328.

[5] Korhonen, M., Laine, J., Flocculation and retention of fillers with nanocelluloses. *Nordic Pulp & Paper Research Journal*, **2014**, 29(1), 119–128. DOI:10.3183/npprj-2014-29-01-p119-128

[6] Lenze, C.J., Peksa, C.A., Sun, W., Intact and broken cellulose nanocrystals as model nanoparticles to promote dewatering and fine-particle retention during papermaking. *Cellulose* **2016**, 23, 3951–3962 . DOI: 10.1007/s10570-016-1077-9

[7] Charani, P.R., Moradian, M.H., Utilization of Cellulose Nanofibers and cationic polymers to improve breaking length of paper. *Cell. Chem. Tech*., **2019**, 53(7–8), 767–774. DOI: 10.35812/cellulosechemtechnol.2019.53.75

[8] Cha, R., Wang, C., Cheng, S., He, Z., Jiang, X., Using carboxylated nanocrystalline cellulose as an additive in cellulosic paper and poly (vinyl alcohol) fiber paper, *Carbohyd. Polym*., **2014**, 110, 298-301, DOI: 10.1016/j.carbpol.2014.04.003.

[9] Campano, C., Merayo, N., Balea,A., Tarrés, Q., Delgado-Aguilar, M., Mutjé,P., Negro, C., Blanco, Á., Mechanical and Chemical Dispersion of Nanocelluloses to Improve Their Reinforcing Effect on Recycled Paper. *Cellulose*, **2018**, 25, no. 1, 269-80. DOI: 10.1007/s10570-017-1552-y

[10] Xu, Q., Li, W., Cheng, Z., Yang, G., Qin, M.. TEMPO/NaBr/NaClO-Mediated Surface Oxidation of Nanocrystalline Cellulose and Its Microparticulate Retention System with Cationic Polyacrylamide. *Bioresources*, **2013**, 9(1), 994-1006. DOI: 10.15376/biores.9.1.994-1006

[11] Merayo, N., Balea, A., de la Fuente, E., Blanco, Á., Negro, C., Interactions between cellulose nanofibers and retention systems in flocculation of recycled fibers. *Cellulose*, **2016**, 24(2), 677–692. DOI:10.1007/s10570-016-1138-0

[12] Espinosa, E., Domínguez-Robles, J., Sánchez, R., Tarrés, Q., Rodríguez, A., The effect of pre-treatment on the production of lignocellulosic nanofibers and their application as a reinforcing agent in paper. *Cellulose*, **2017**, 24(6), 2605–2618. DOI:10.1007/s10570-017-1281-2

[13] Taipale, T., Österberg, M., Nykänen, A., Ruokolainen, J.,Laine, J., Effect of microfibrillated cellulose and fines on the drainage of kraft pulp suspension and paper strength. *Cellulose*, **2010**, 17(5), 1005–1020. DOI:/10.1007/s10570-010-9431-9

[14] Miyawaki, S., Katsukawa, S., Abe, H., Iijima, Y., Isogai, A., Additive for papermaking and paper containing the same, **2009**, WO 2009122982 (A1).

[15] Brodin, F. W., Gregersen, Ø. W., Syverud, K., Cellulose nanofibrils: Challenges and possibilities as a paper additive or coating material – a review. *Nordic Pulp & Paper Research Journal*, **2014**, 29(1), 156–166. DOI:10.3183/npprj-2014-29-01-p156-166

[16] Hu, F., Zeng, J., Cheng, Z., Wang, X., Wang, B., Zeng, Z., Chen, K., Cellulose nanofibrils (cnfs) produced by different mechanical methods to improve mechanical properties of recycled paper. *Carbohydrate Polymers*, **2021**, 254, 117474. DOI: 10.1016/j.carbpol.2020.117474

[17] Celzard, A., Fierro, V., Kerekes, R., Flocculation of cellulose fibres: New comparison of crowding factor with percolation and effective-medium theories. *Cellulose*, **2009**, 16(6), 983–987. DOI: 10.1007/s10570-009-9314-0

[18] Sanchez-Salvador, J. L., Balea, A., Monte, M. C., Negro, C., Miller, M., Olson, J., Blanco, A., Comparison of mechanical and chemical nanocellulose as additives to reinforce recycled cardboard. *Scientific Reports*, **2020**, 10(1). DOI:10.1038/s41598-020-60507-3

[19] Haunreiter, K., Dichiara, A., Gustafson, R., Nanocellulose by ammonium persulfate oxidation – an alternative to TEMPO-mediated oxidation., *ACS Sustainable Chemistry & Engineering*, **2022**.

[20] Pääkkö, M, Ankerfors, M, Kosonen, H, Nykänen, A, Ahola, S, Österberg, M, Ruokolainen, J, Laine, J, Larsson, P. T, Ikkala, O, Lindström, T., Enzymatic Hydrolysis Combined with Mechanical Shearing and High-Pressure Homogenization for Nanoscale Cellulose Fibrils and Strong Gels. *Biomacromolecules*, **2007**, 8, 6 1934-941. DOI: 10.1021/bm061215p

[21] Jiang, H., Wu, Y., Han, B., & Zhang, Y., Effect of oxidation time on the properties of cellulose nanocrystals from hybrid poplar residues using the ammonium persulfate. *Carbohyd. Polym.*, **2017**, 174, 291-298. DOI: 10.1016/j.carbpol.2017.06.080

[22] Gicquel, E., Bras, J., Rey, C., Putaux, J.-L., Pignon, F., Jean, B., & Martin, C., Impact of sonication on the rheological and colloidal properties of highly concentrated cellulose nanocrystal suspensions. *Cellulose*, **2019**, 26(13–14), 7619–7634. DOI: 10.1007/s10570-019-02622-7

[23] Chen, W., Yu, H., Liu, Y., Chen, P., Zhang, M., & Hai, Y., Individualization of cellulose nanofibers from wood using high-intensity ultrasonication combined with chemical pretreatments. *Carbohyd. Polym.,* **2011**, 83(4), 1804–1811. DOI: 10.1016/j.carbpol.2010.10.040

[24] Canadian Standards Association (CSA), Cellulosic nanomaterials – Test methods for characterization (CSA Z5100-14), Report, 2017.

[25] Nečas, D., Klapetek, P., Gwyddion: an open-source software for SPM data analysis, *Cent. Eur. J. Phys*., **2021**, 10(1) 181-188, DOI: 10.2478/s11534-011-0096-2

[26] Schneider, C. A.; Rasband, W. S., Eliceiri, K. W., NIH Image to ImageJ: 25 years of image analysis, *Nat. Methods*, **2012**, 9(7): 671-675, DOI: 10.1038/nmeth.2089

[27] Yu, H., Zhang, D., Lu, F., & Yao, J., New Approach for Single-Step Extraction of Carboxylated Cellulose Nanocrystals for Their Use As Adsorbents and Flocculants. *ACS Sustain. Chem. Eng*., **2016**, 4(5), 2632-2643. doi:10.1021/acssuschemeng.6b00126

[28] Araki, J., Wada, M., & Kuga, S., Steric Stabilization of a Cellulose Microcrystal Suspension by Poly(ethylene glycol) Grafting. *Langmuir*, **2001**, 17(1), 21-27. http://dx.doi.org/10.1021/la001070m

[29] Arola, S., Tammelin, T., Setälä, H., Tullila, A., & Linder, M. B., Immobilization–Stabilization of Proteins on Nanofibrillated Cellulose Deriva-tives and Their Bioactive Film Formation. *Biomacromolecules*, **2012**, 13(3), 594-603. http://dx.doi.org/10.1021/bm201676q

[30] Mascheroni, E., Rampazzo, R., Ortenzi, M. A., Piva, G., Bonetti, S., & Piergiovanni, L., Comparison of cellulose nanocrystals obtained by sulfuric acid hydrolysis and ammonium persulfate, to be used as coating on flexible food-packaging materials. *Cellulose*, **2016**, 23(1), 779-793. http://dx.doi.org/10.1007/s10570-015-0853-2

[31] Woodcock, S., Henrissat, B., Sugiyama, J., Docking of congo red to the surface of crystalline cellulose using molecular mechanics. *Biopolymers*, **1995**, 36(2), 201–210. DOI:10.1002/bip.360360208

[32] Ougiya, H., Hioki, N., Watanabe, K., Moringa, Y., Yoshinga, F., Samejima, M., Relationship between the physical properties and surface area of cellulose derived from adsorbates of various molecular sizes. Bioscience, *Biotechnology, and Biochemistry*, **1998**, 62(10), 1880–1884. DOI: 10.1271/bbb.62.1880

[33] Inglesby, M.K., Zeronian, S.H., Direct Dyes as Molecular Sensors to Characterize Cellulose Substrates. *Cellulose* (London) 9, no. 1 (**2002**): 19-29.

[34] Inglesby, M.K., Zeronian, S.H., Direct Dyes as Molecular Sensors to Characterize Cellulose Substrates. *Cellulose* (London) 9, no. 1 (**2002**): 19-29.

[35] Kim, K.Y., Chung, W.Y, Lim, D.Y., A study on fabrication of cellulose nanofibers in water using a microfluidizer. Technical Proceedings of the 2011 NSTI Nanotechnology Conference and Expo, *NSTI-Nanotech*, **2011**. 1. 66-69.

[36] Spence, K. L., Venditti, R. A., Rojas, O. J., Habibi, Y., Pawlak, J. J., A comparative study of energy consumption and physical properties of microfibrillated cellulose produced by different processing methods. *Cellulose*, **2011**, 18(4), 1097–1111. DOI: 10.1007/s10570-011-9533-z

[37] Serra-Parareda, F., Aguado, R., Tarrés, Q., Mutjé, P., Delgado-Aguilar, M., Potentiometric back titration as a robust and simple method for specific surface area estimation of lignocellulosic fibers. *Cellulose*, **2021**, 28(17), 10815–10825. DOI: 10.1007/s10570-021-04250-6

[38] Yoshida, H., Kataoka, T., Maekawa, M., Nango, M., Surface diffusion of direct dyes in porous cellulose membranes. *The Chemical Engineering Journal*, **1989**, 41(1). DOI: 10.1016/s0300-9467(98)80009-9

[39] Shaheed, N., Javanshir, S., Esmkhani, M., Dekamin, M. G., Naimi-Jamal, M. R., Synthesis of nanocellulose Aerogels and Cu-BTC/nanocellulose aerogel composites for adsorption of organic dyes and heavy metal ions. *Scientific Reports*, **2021**, 11(1). DOI: 10.1038/s41598-021-97861-9

[40] Inglesby, M. K., Zeronian, S. H., The accessibility of cellulose as determined by Dye adsorption. *Cellulose*, **1996**, 3(1), 165–181. DOI: 10.1007/bf02228799

[41] Ferrer, A., Filpponen, I., Rodríguez, A., Laine, J.; Rojas, O. J., Valorization of residual empty palm fruit bunch fibers (EPFBF) by microfluidization: Production of nanofibrillated cellulose and EPFBF nanopaper. *Bioresource Technology*, **2012**, 125, 249–255. DOI: 10.1016/j.biortech.2012.08.108

[42] Goodrich, J. D.,Winter, W. T., A-chitin nanocrystals prepared from shrimp shells and their specific surface area measurement. *Biomacromolecules*, **2006**, 8(1), 252–257. https://doi.org/10.1021/bm0603589

[43] Liu, Y., Is the free energy change of adsorption correctly calculated? *Journal of Chemical & Engineering Data*, **2009**, 54(7), 1981–1985. DOI: 10.1021/je800661q

[44] Hsieh, C.-T., Teng, H., Langmuir and Dubinin-Radushkevich analyses on equilibrium adsorption of activated carbon fabrics in aqueous solutions. Journal of Chemical Technology & *Biotechnology*, **2000**, 75(11), 1066–1072. DOI: 10.1002/1097-4660(200011)75:11<1066::aid-jctb321>3.0.co;2-z

[45] Ougiya, H., Hioki, N., Watanabe, K., Moringa, Y., Yoshinaga, F., Samejima, M.,. Relationship between the physical properties and surface area of cellulose derived from adsorbates of various molecular sizes. *Bioscience, Biotechnology, and Biochemistry*, **1998**, 62(10), 1880–1884. https://doi.org/10.1271/bbb.62.1880

[46] TAPPI Method T248 sp-15, Laboratory beating of pulp (PFI mill method), Technical Association of the Pulp and Paper Industry. T.A.P.P.I. standards: *Testing methods, recommended practices, specifications of the Technical Association of the Pulp and Paper Industry*. **2015**, New York: Technical Association of the Pulp and Paper Industry.

[47] Anderson, T. H., Donaldson, S. H., Zeng, H., Israelachvili, J. N., Direct measurement of double-layer, van der waals, and polymer depletion attraction forces between supported cationic bilayers. *Langmuir*, **2010**, 26(18), 14458–14465. DOI:10.1021/la1020687

[48] Wågberg, L., Björklund, M., Åsell, I., Swerin, A., On the mechanism of flocculation by microparticle retention-aid systems. *Tappi Journal*. **1996**, 79. 157-164.

[49] TAPPI Method T205 sp-95., Forming handsheets for physical tests of pulp., T.A.P.P.I. standards: *Testing methods, recommended practices, specifications of the Technical Association*

of the Pulp and Paper Industry, **1995**, New York: Technical Association of the Pulp and Paper Industry.

[50] TAPPI method T261 cm-10, Fines fraction by weight of paper stock by wet Screening, Technical Association of the Pulp and Paper Industry. T.A.P.P.I. standards: *Testing methods, recommended practices, specifications of the Technical Association of the Pulp and Paper Industry*, **2010**, New York: Technical Association of the Pulp and Paper Industry.

[51] Britt, K.W. Unbehend, J.E. (1976) : New method of monitoring retention, Tappi, 59(2), 67-70

[52] Britt, K. W., & KW, B. (1973). Retention of additives during sheet formation. TAPPI 1973; VOL. 56; NO 3; PP. 83-86

[54] TAPPI Method T261 cm-10, Fines fraction by weight of paper stock by wet Screening, Technical Association of the Pulp and Paper Industry. T.A.P.P.I. standards: *Testing methods, recommended practices, specifications of the Technical Association of the Pulp and Paper Industry*, **2010**, New York: Technical Association of the Pulp and Paper Industry.

[55] TAPPI Method T402 sp-13., Standard Conditioning and Testing Atmosphere for Paper, Board, Pulp Handsheets and Related Products. Technical Association of the Pulp and Paper Industry. T.A.P.P.I. standards: *Testing methods, recommended practices, specifications of the Technical Association of the Pulp and Paper Industry*, **2013**, New York: Technical Association of the Pulp and Paper Industry.

[56] TAPPI Method T562 om-10, CIE whiteness and tint of paper and paperboard (45/0 geometry, C/2 illuminant/observer), Technical Association of the Pulp and Paper Industry, T.A.P.P.I. standards: *Testing methods, recommended practices, specifications of the Technical Association of the Pulp and Paper Industry*, **2010**, New York: Technical Association of the Pulp and Paper Industry.

[57] TAPPI Method T460 om-96, "Air resistance of paper (Gurley method), Technical Association of the Pulp and Paper Industry. T.A.P.P.I. standards: *Testing methods, recommended practices, specifications of the Technical Association of the Pulp and Paper Industry*, **1996**, New York: Technical Association of the Pulp and Paper Industry.

[58] TAPPI Method T494 om-13, Tensile properties of paper and paperboard, Technical Association of the Pulp and Paper Industry, T.A.P.P.I. standards: *Testing methods, recommended practices, specifications of the Technical Association of the Pulp and Paper Industry*, **2013**, New York: Technical Association of the Pulp and Paper Industry.

[59] TAPPI Method T414 om-12, Internal tearing resistance of paper (Elmendorf-type method), Technical Association of the Pulp and Paper Industry. , T.A.P.P.I. standards: *Testing methods, recommended practices, specifications of the Technical Association of the Pulp and Paper Industry*, **2014**, New York: Technical Association of the Pulp and Paper Industry.

[60] Oksanen, J., Blanchet, F. G., Friendly, M., Kindt, R., Legendre, P., McGlinn, D., Minchin, P.R., O'Hara, R. B., Simpson, G. L., Solymos, P., Stevens, M. H. H., Szoecs, E., Wagner, H.,

vegan: *Community Ecology Package*, **2020**,. R package version 2.5-7. https://CRAN.R-project.org/package=vegan

[61] Kassambara, A., Mundt, F., factoextra: *Extract and Visualize the Results of Multivariate Data Analyses*, **2020**, R package version 1.0.7. https://CRAN.R-project.org/package=factoextra

[62] H. Wickham. ggplot2: *Elegant Graphics for Data Analysis*, **2016**, Springer-Verlag New York.

[63] Harpreet, S.B., *Average Stress vs. Strain plot*, **2021**, (https://www.mathworks.com/matlabcentral/fileexchange/69590-average-stress-vs-strain-plot), MATLAB Central File Exchange. Retrieved April 10, 2021.

[64] Zhong, R., Wille, K., Equal Arc Segment Method for Averaging Data Plots Exemplified for Averaging Stress versus Strain Curves of Pervious Concrete. *J. Mater. Civ. Eng.*, **2016**, 28, no. 1 4015071. http//dx.doi.org/10.1061/(asce)mt.1943-5533.0001345

[65] Serra, A., González, I., Oliver-Ortega, H., Tarrès, Q., Delgado-Aguilar, M., Mutjé, P.,. Reducing the amount of catalyst in tempo-oxidized cellulose nanofibers: Effect on properties and cost. *Polymers*, **2017**, 9(11), 557. DOI:10.3390/polym9110557

[66] Swerin, A., Ödberg, L., Wågberg, L., An extended model for the estimation of flocculation efficiency factors in multicomponent flocculant systems. *Colloids and Surfaces A: Physicochemical and Engineering Aspects*, **1996**, 113(1-2), 25–38. DOI: 10.1016/0927-7757(95)03506-0

[67] Korhonen, M., Laine, J., Flocculation and retention of fillers with nanocelluloses. *Nordic Pulp & Paper Research Journal*, **2014**, 29(1), 119–128. DOI: 10.3183/npprj-2014-29-01-p119-128

[68] Petroudy, S. R., Sheikhi, P., Ghobadifar, P., Sugarcane bagasse paper reinforced by cellulose nanofiber (CNF) and bleached softwood Kraft (BSWK) pulp. *Journal of Polymers and the Environment*, 2016, 25(2), 203–213. DOI:10.1007/s10924-016-0800-9

[69] Cowan, W., Explaining handsheet tensile and tear in terms of fiber-quality numbers. *Tappi Press*, **1995**, 78, 101–110 .

[70] González, I., Boufi, S., Pèlach, M. A., Alcalà, M., Vilaseca, F., Mutjé, P., Nanofibrillated cellulose as paper additive in eucalyptus pulps. *BioResources*, **2012**, 7(4). DOI:10.15376/biores.7.4.5167-5180

[71] Alcalá, M., González, I., Boufi, S., Vilaseca, F., Mutjé, P., All-cellulose composites from unbleached hardwood kraft pulp reinforced with nanofibrillated cellulose. *Cellulose*, **2013**, 20(6), 2909–2921. DOI:10.1007/s10570-013-0085-2

[72] Delgado-Aguilar, M., González Tovar, I., Tarrés, Q., Alcalá, M., Pèlach, M. À., Mutjé, P. Approaching a low-cost production of cellulose nanofibers for papermaking applications. *BioResources*, **2015**, 10(3). DOI:10.15376/biores.10.3.5345-5355

[73] Balea, A., Blanco, Á., Monte, M. C., Merayo, N., Negro, C., Effect of bleached eucalyptus and pine cellulose nanofibers on the physico-mechanical properties of Cartonboard. *BioResources*, **2016**, 11(4). DOI:10.15376/biores.11.4.8123-8138

[74] Balea, A., Merayo, N., De La Fuente, E., Negro, C., Blanco, Á.,Assessing the influence of refining, bleaching and tempo-mediated oxidation on the production of more sustainable cellulose nanofibers and their application as paper additives. *Industrial Crops and Products*, **2017**, 97, 374–387. DOI:10.1016/j.indcrop.2016.12.050

[75] Balea, A., Sanchez-Salvador, J. L., Monte, M. C., Merayo, N., Negro, C., Blanco, A., In situ production and application of cellulose nanofibers to improve recycled paper production. *Molecules*, **2019**, 24(9), 1800. DOI:10.3390/molecules24091800

Chapter 6. - CONCLUSIONS – FUTURE RECOMMENDATIONS

6.1 Conclusions

This work describes the application of ammonium persulfate in oxidation reactions of both lignin free and lignin containing agricultural residuals, the bine remaining after harvest of hops, to produce nanofibrillated cellulose. The results demonstrate that chemical and morphological characteristics of nanocellulose can be engineered through careful control of temperature, time, and applied ammonium persulfate. Using response surface methodology, the surface chemistry was impacted by all three treatment conditions. Surface charge developed ranged from 0.64 mmol/g to 1.44 mmol/g. The length of the fibers produced was determined by increasing time and temperature. Diameter dropped rapidly indicating the rapid penetration of reactants into the fibers and was influenced only by temperature. The crystallinity of the fibers was governed by temperature only while crystallite size was influenced by applied ammonium persulfate and time.

Kinetics of the reaction showed pseudo second order reaction kinetics. Activation of the ammonium persulfate was rapid, reaching an asymptotic limit after 45 minutes. Reaction rate was also strongly influenced by the consistency or concentration of applied ammonium persulfate. Increasing consistency resulted in increasing yields but a decrease in surface chemistry development.

Nanocellulose was produced from lignin containing biomass with surface charge ranging from 0.4 mmol/g to 1.1 mmol/g. Unbleached northern softwood developed surface charge at a much slower rate than for the bleached softwood and at 50% lower charge. Residual biomass, hop bine, was shown to develop surface charge at the same rate as the unbleached wood, however, the

levels of charge developed were only about 10% lower than for bleached wood. As the reaction progressed, the chromophores were slowly bleached as well.

It was demonstrated that the ammonium persulfate oxidized fibers required greater mechanical treatment when compared to TEMPO oxidized fibers. Crystallinity also increased with increasing passes through a microfluidizer, however, yield gains were substantial.

Using ammonium persulfate oxidized nanofibers as a reinforcement in paper resulted in significant improvements in tensile correlating with the surface charge of the fiber. As surface charge increased, tensile development was lower while Young's modulus increased. The nanofibers improved the load carrying capacity of the paper. This correlated well with the higher surface area of the low charge fibers which would promote greater relative bonded area. The permeability of the sheets was reduced by 94% compared to a nanofiber free base sheet. Utilizing a retention system, retention of nanofibers in the sheet was 95%.

Although the hop bine was shown to have a low bulk density relative to other fiber sources, the available biomass annual was not insignificant as a feed stock for engineered fiber production. The issue with hop bine is the short harvest window and low bulk density, however, the work in Chapter 4 demonstrated that nanofibers can be engineered using the model without additional pretreatment steps.

A life cycle assessment examining the impact of removing this biomass shows that the greatest negative impact is the loss of carbon soil sequestration and increased demand for inorganic fertilizer. The spent liquor from oxidation of hop bine with ammonium persulfate may resolve the need for additional inorganic fertilizer and may be a more effective means of returning carbon to the soil. Compared to other life cycle assessment of residual biomass such as wheat straw, the findings are consistent. This preliminary life cycle is positioned to be an inventory for a life cycle

analysis that evaluates the production of NFC from hop bine residuals and return of the spent APS liquor back to the field.

This work provides the framework for building an optimized "green" process to oxidize unbleached woody and non-wood residual biomass into designer nanofibers. The novel methods described fill the gaps in current capability to turn materials now considered waste into value-added co-products. As demonstrated, the performance of the nanofibers produced matches or exceeds current production methods such as TEMPO.

6.2 Future Work

There are three areas of investigation that are worthy of continued work using the prior work as a basis. With the establishment of a response surface model, the first step should be to begin optimizing the process to maximize the yield of nanofibers. There is additional experimental work towards expanding the response surface experimental boundary that would include biomass pretreatment such as with formic acid in order to reduce the demand for APS at a specific surface charge and oxidation experiments using varying concentrations of hydrochloric acid to determine at which point nanofibrillated cellulose becomes crystalline nanofibrillated cellulose and through extension develop a response surface focused on tuning CNC fibers. The second area would be in investigating the feasibility of returning the spent APS liquor back to the soil as an amendment. And lastly a combined life cycle assessment and technoeconomic study of the scaled APS-NFC process compared against the TEMPO-NFC and the super mass colloider-NFC processes. In summary there are four distinct areas suggested for future investigation;

1) Process Optimization of NFC
2) Fiber Pretreatment and extension of RSM
3) Spent APS liquor as a soil amendment

4) LCA/Techno-economic study Scale up

6.2.1 Process Optimization

A low ammonium persulfate concentration (low consistency) was selected to eliminate the interaction of concentration gradient on the treatment conditions selected. The resulting yield was quite low but sufficient to produce nanofibers for analysis. Subsequent initial optimization work found that the energy applied during ultrasonic mechanical treatment was too low for APS-NFC whereas it was sufficient for TEMPO-NFC. Yields achieved ranged from 4-10% with length and diameter unaffected.

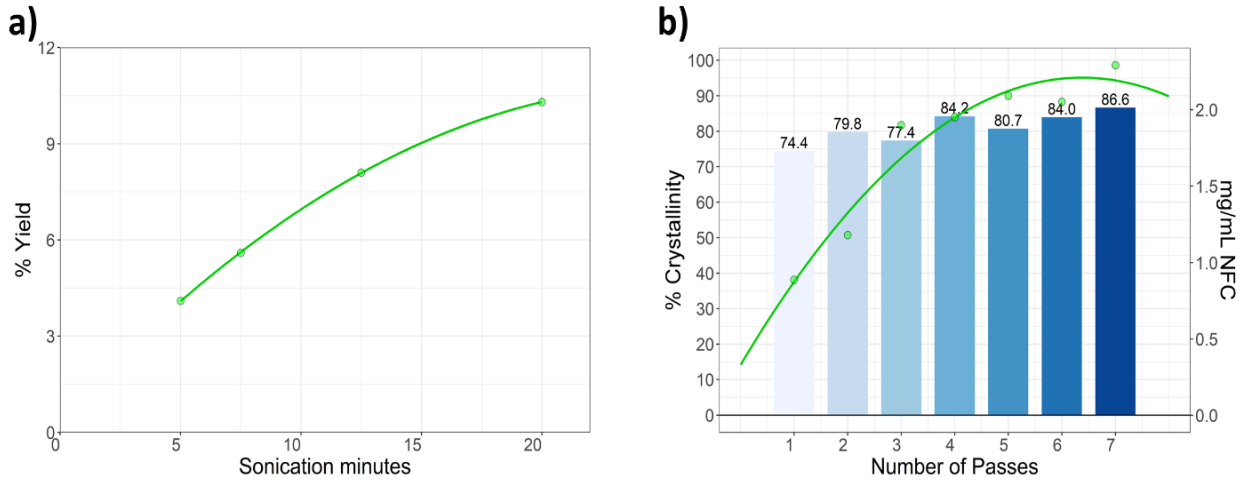

Figure 6.1. a)Applied sonication energy vs yield of nanocellulose., b) concentration of nanofibers in supernatant and change in crystallinity with passes through the microfluidizer.

Ammonium persulfate oxidation of lignocellulosic biomass to nanofibrillated cellulose at higher concentration coupled with creasing the energy in a stepwise fashion achieved yields of up to 20%. This is likely the upper maximum yield achievable at the concentration used in this study. Work raising the concentration and utilizing the microfluidizer demonstrated that the crystallinity changed as the concentration in the supernatant increased with each pass up to an asymptotic limit similar to what was achieved after sonication shown in Figure 6.1.

Films produced from NFC following this mechanical treatment and reinforced with 5-10% PEOX (Poly 2-ethyl-2-oxazoline), a 200,000 molecular weight biocompatible polymer supplied by Fisher Scientific, were less brittle than NFC films without reinforcement and transparency was unaffected, see Figure 6.2. This represents an additional method to the common PVA reinforcment with potential for assessing the strength properties of the nanofibers formed[1].

Figure 6.2. Film produced from 95% nanofibers and 5% PEOX, printed with a laser printer.

6.2.2 Soil Amendment

Sulfur, as sulphate ion, is an important nutrient in the growth of plants and has been identified a key component in plant metabolism[2,3]. Sulfur containing metabolites protect the plant from pathogens and assist in mitigating abiotic and biotic stress. Glutathion helps to detoxify

heavy metals through conjugation with sulfhydryl groups for example. Optimization of the amount of sulfur uptake is performed by sulfate transporters binding proteins, SULTR family[4]. The expression of these transporters has been found to follow colonization by mycorrhizal fungi in symbiosis with the plant.

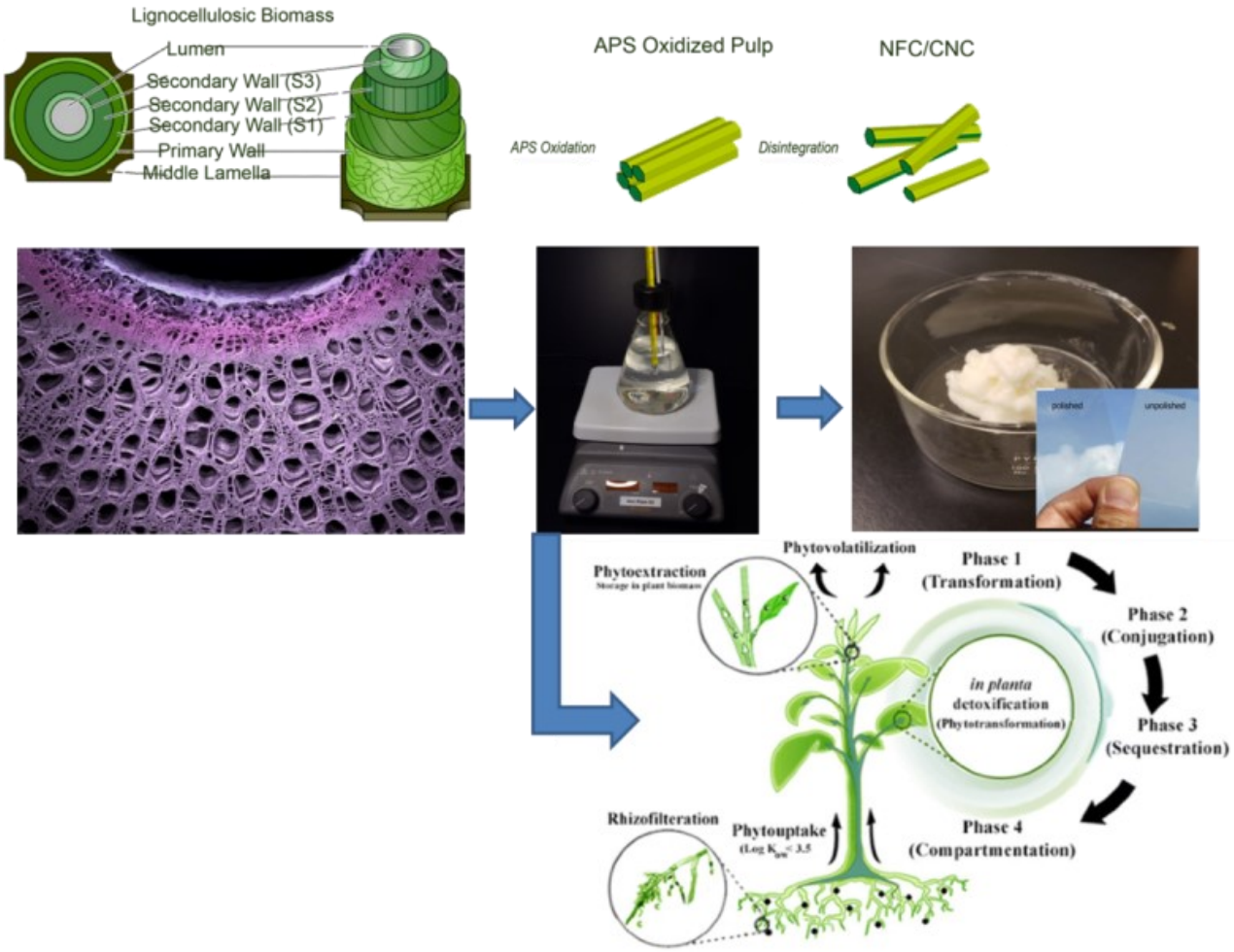

Figure 6.3.. Ammonium persulfate oxidation of lignocellulosic biomass to nanofibrillated cellulose coupled with phytoremediation of spent liquor[5,6,7].

Production of 1 metric ton of nanofibrillated cellulose requires remediating 460 kg of spent ammonium persulfate adds129 kg of sulfur and 56.7 kg of nitrogen and may introduce increased H ion to the soil[8]. It would require 3.8 hectares based on study conditions[9]. Colonizing plants with combinations of fungal endophytes could increase the uptake of sulfur, reduce biotic and

abiotic stress thus reducing or eliminating the environmental impact of the chemical process. The result – a holistic "green" oxidation process, see Figure 6.3.

6.2.3 Techno-economic Study

The present work was compared to other published cost data, normalized for Washington state power prices. Chemical cost numbers were adjusted for bulk spot prices at current market price Summer 2021. The relativized cost for ammonium persulfate in this work was consistent with work published by Filipova but at an improved efficiency when compared to the surface charge developed. Compared to TEMPO produced nanofibers at the same surface charge, this work was 1/20th the "beaker" cost, see Table **6.1**.

Table 6.1. APS versus TEMPO laboratory cost of production

Treatment	**$/kg CNF**	**Relativized $/kg CNF**	**mmol Carb/g**
TEMPO (Filipova 2020)	$7.20	$16.81	0.149
APS (Filipova 2020)	$6.91	$6.78	0.133
TEMPO (Serra 2017)	$9.02	$105.19	0.271
TEMPO (Delgado 2015)	$205.73	$104.73	0.840
APS (Haunreiter 2020)		$5.43	0.881

A comparison of ammonium persulfate cost to TEMPO cost may be made in this analysis, but it does not provide a realistic assessment of scaled production using ammonium persulfate. A techno-economic analysis should use the median existing production rates for nanocellulose; annual production of 49K Kg/year, as the basis for the mass and energy balance and economic assessment of producing nanofibrillated cellulose using ammonium persulfate. A simplified proposed process overview divides it into four distinct system blocks; A100 Oxidation Process, A200 – Ultrafiltration Process, A300 – Mechanical Treatment, and A400 – Concentration. A simplified process diagram for process A100 as an example is shown in Figure 6.4. The reactor will likely require some type of helical agitation and a non-contact heating process, jacketed or

othewise. A potential problem analysis will need to be conducted once a process design has been determined. Example mass and energy balance for A100 is provided in Table 6.2.

Table 6.2. Mass and Energy balance for a 4 unit oxidation process, A100.

Heat Balance		
Specific Heat Pulp	1.50	kJ/kg
Specific Heat Water	4.19	kJ/kg
Steam Pressure	5.00	bar
Steam Enthalpy	2085.00	kJ/kg
Ramp 1		
Delta T	50.00	C
Bring up Time	15.00	min
Initial Heat Demand	287.19	kJ/s
Steam flow	8.265	kg/min
Total Steam	123.969	kg
Cook Phase		
Delta T	5.00	C
Bring up Time	360.00	min
Initial Heat Demand	1.20	kJ/s
Steam flow	0.034	kg/min
Total Steam	12.397	kg/min
Condensate		
Temperature	70.00	C
Enthalpy Cond at P	640.12	kJ/kg
Enthalpy Cond at Atm	417.51	kJ/kg
Heat of Vaporization	2257.920	kJ/kg
% Flash Steam	9.86%	kg/min
Condensate Flow	122.921	kg/min
Target Production	150	kg/day
Number of batches/day/tank	4	
Number of tanks	3.19	

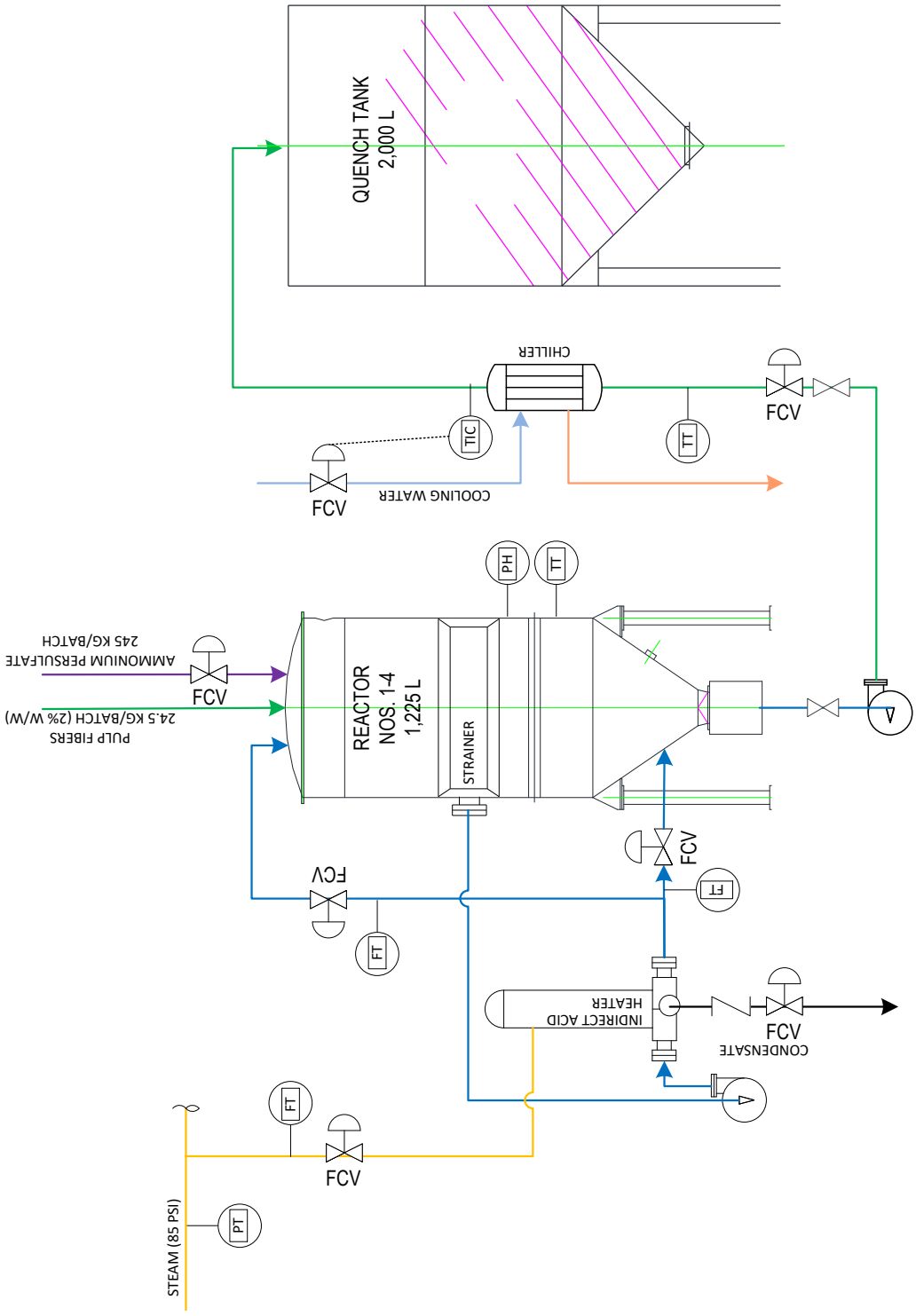

Figure 6.4 Reaction Process (A100) showing reactor and quench tank. Reactor is shown without agitator.

References

[1] Forti, E. S., El Awad Azrak, S. M., Ng, X. Y., Cho, W., Schueneman, G. T., Moon, R. J., Fox, D. M., Youngblood, J. P., Mechanical enhancement of cellulose nanofibril (CNF) films through the addition of water-soluble polymers. *Cellulose,* **2021**,. DOI:10.1007/s10570-021-03937-0

[2] Davidian,J-C., Kopriva,S, Regulation of Sulfate Uptake and Assimilation—the Same or Not the Same?, *Molecular Plant*, **2010**, Volume 3, Issue 2, Pages 314-325, DOI: 10.1093/mp/ssq001.

[3] Takahashi, H., Sulfate transport systems in plants: Functional diversity and molecular mechanisms underlying regulatory coordination. *Journal of Experimental Botany*, **2019**, 70(16), 4075-4087. DOI: 10.1093/jxb/erz132

[4] Przybyla-Toscano, J., Roland, M., Gaymard, F., Couturier, J., Rouhier, N., Roles and maturation of iron-sulfur proteins in plastids. *Journal of biological inorganic chemistry*, **201**8, 23(4), 545–566. DOI: 10.1007/s00775-018-1532-1

[5] Rytioja, J., Hildén, K., Yuzon, J., Hatakka, A., de Vries, R. P., Mäkelä, M. R., Plant-polysaccharide-degrading enzymes from basidiomycetes. *Microbiology and Molecular Biology Reviews*, **2014**, 78(4), 614–649. DOI: 10.1128/mmbr.00035-14.

[6] Daicho, K., Saito, T., Fujisawa, S., Isogai, A., The crystallinity of nanocellulose: Dispersion-induced disordering of the grain boundary in biologically structured cellulose. *ACS Applied Nano Materials*, **2018**, 1(10), 5774–5785. DOI: 10.1021/acsanm.8b01438

[7] Ijaz, A., Imran, A., Anwar ul Haq, M., Khan, Q. M., Afzal, M., Phytoremediation: Recent advances in plant-endophytic synergistic interactions. *Plant and Soil*, **2015**, 405(1-2), 179–195. DOI: 10.1007/s11104-015-2606-2

[8] Haunreiter, K. J., Dichiara, A., Gustafson, R., Structural and chemical characterization of hop bine fibers and their applications in the paper industry. *Industrial Crops and Products*, **2021**, 174, 114217. DOI: 10.1016/j.indcrop.2021.114217

[9] Sweeney, D. W.,Moyer, J. L., Sulfur source and placement for newly established endophyte-free tall fescue1. *Communications in Soil Science and Plant Analysis*, **2001**, 32(7-8), 1149–1162. https://doi.org/10.1081/css-100104106

APPENDIX

A. SUPPLEMENTARY – CHAPTER 2

This section contains the raw data used in modeling, definitions, inputs, maps utilized, and model output data for the life cycle assessment.

Impact Categories provided by Roy Farms.

Impact Category	Unit	Hop Flower (kg)
global warming	kg CO2 eq	4.60E+00
eutrophication	Kg N eq	5.50E-02
water use	liter	2.70E+03
land use	m2 year	5.60E+00
ozone depletion	kg CFC-11 eq	2.10E-07
smog	kg 03 eq	2.20E-01
acidification	kg SO2 eq	2.10E-02
human health	CTUh	6.90E-07
respiratory effect	kg PM2.5 eq	1.80E-03
Eco toxicity	CTUe	1.40E+01
fossil fuel	MJ surplus	5.40E+00

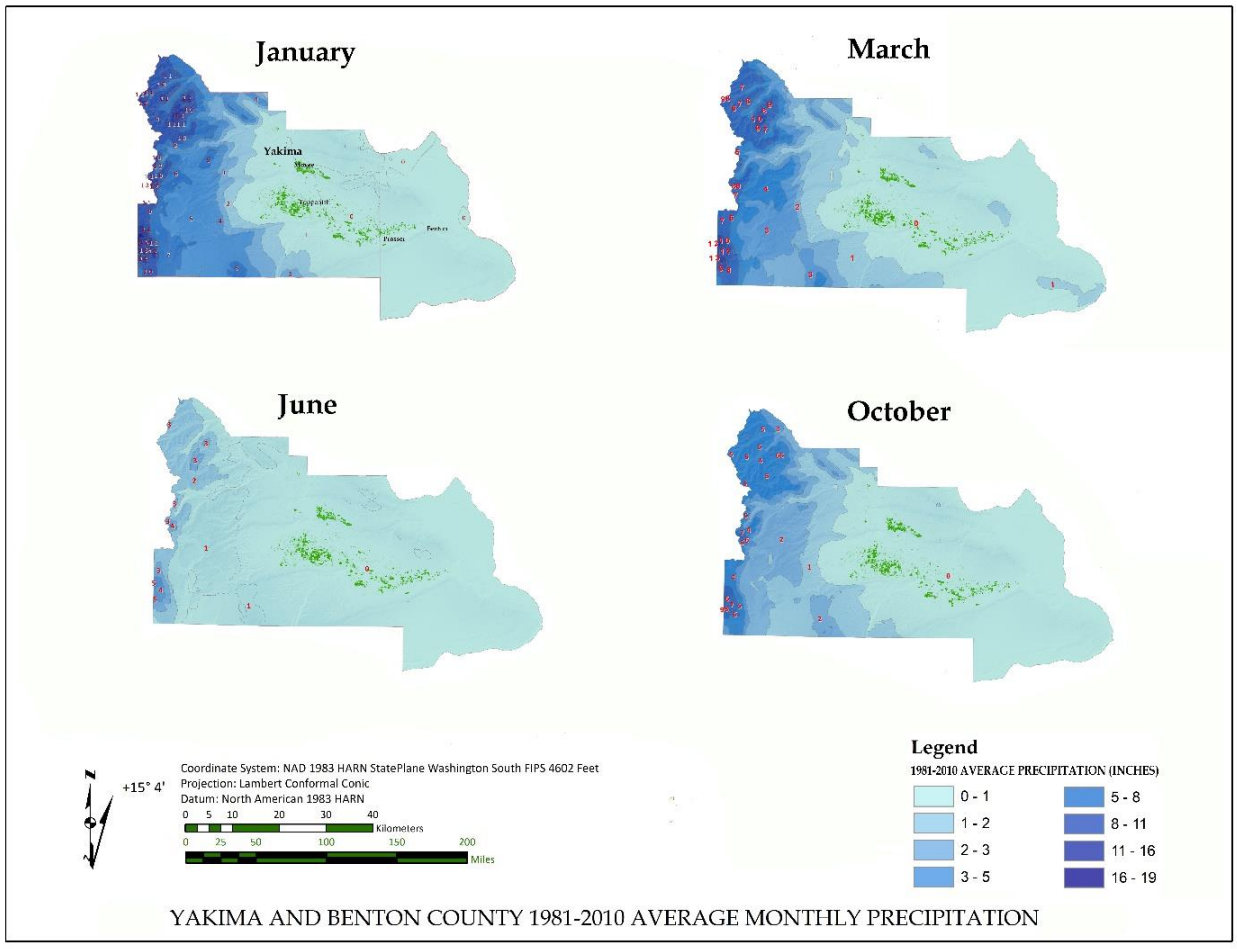

Figure A.1.. ArcGis Annual rain fall for Yakima and Benton County

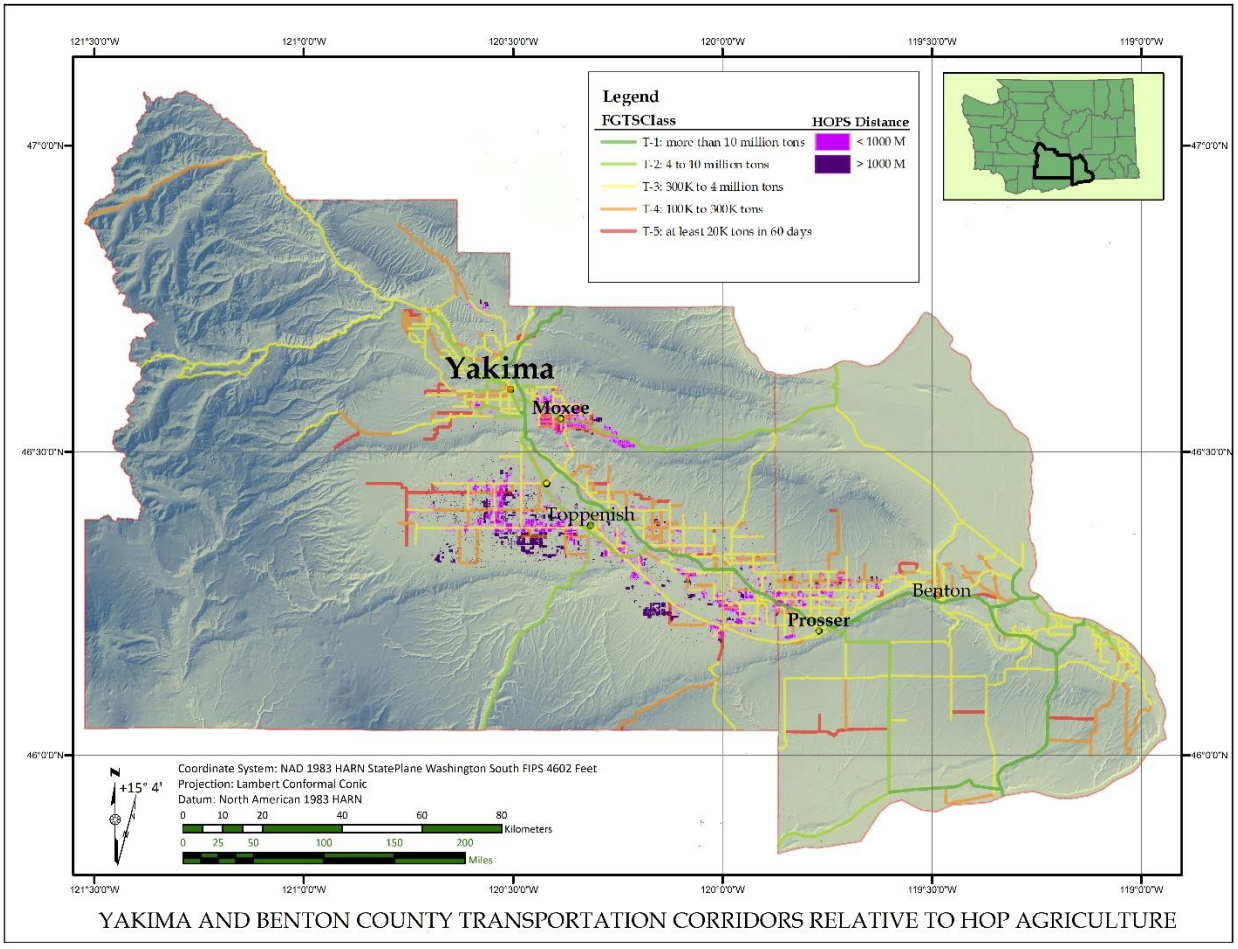

Figure A.2. Distances from Hop Farms to nearest transportation corridor

Table A.1. DNDC model output varying hop bine separation

Hop Bine Co-Product	100% Bine				90% Bine			
	4.28%	2.19%	93.52%		4.28%	2.19%	93.52%	
Soil Nitrogen Balance (kg N/ha/yr)	**Loamy Sand**	**Sandy Loam**	**Silt Loam**	**Totals**	**Loamy Sand**	**Sandy Loam**	**Silt Loam**	**Totals**
Manure N Input	-83.8	-83.8	-83.8	-83.8	-87.1	-87.1	-87.1	-87.1
Crop stub N input	-4.9	-4.8	-4.8	-4.8	-4.7	-4.8	-4.8	-4.8
Crop root N input	-13.0	-13.1	-13.1	-13.1	-12.9	-13.0	-13.0	-13.0
Weeds N input	0.0	0.0	0.0	0.0	0.0	0.0	0.0	0.0
Atm N deposit	-96.2	-96.2	-96.2	-96.2	-96.2	-96.2	-96.2	-96.2
Fertilizer N input	-119.6	-119.6	-119.6	-119.6	-116.4	-116.4	-116.4	-116.4
N fixation	0.0	0.0	0.0	0.0	0.0	0.0	0.0	0.0
N leaching	113.4	113.2	108.6	108.9	110.8	110.6	106.0	106.3
N runoff	0.0	0.0	0.0	0.0	0.0	0.0	0.0	0.0
N uptake by crop	165.3	166.3	166.3	166.2	164.4	166.4	165.5	165.5
N uptake by weeds	0.0	0.0	0.0	0.0	0.0	0.0	0.0	0.0
NH3 volatilization	1.5	1.4	1.7	1.7	1.4	1.3	1.6	1.6
N2O flux	2.0	2.0	2.0	2.0	2.0	2.0	1.9	1.9
NO Flux	0.4	0.4	0.4	0.4	0.4	0.4	0.4	0.4
N2 flux	2.0	2.2	5.7	5.5	2.1	2.3	5.8	5.6
Change in soil N storage	-32.7	-32.0	-32.7	-32.7	-36.3	-35.5	-36.2	-36.2
Soil Carbon Balance (kg C/ha/yr)								
Manure N Input	-1467.0	-1467.0	-1467.0	-1466.9	-1595.0	-1595.0	-1595.0	-1594.8
Crop residue C input	-86.8	-84.3	-84.3	-84.4	-83.4	-83.9	-83.9	-83.9
Crop root C input	-648.8	-652.6	-652.7	-652.5	-645.3	-649.3	-649.7	-649.4
Weeds C input	0.0	0.0	0.0	0.0	0.0	0.0	0.0	0.0
Soil CO2 flux	1187.6	1277.5	1323.4	1316.5	1259.3	1352.3	1400.2	1393.0
DOC Leaching	0.0	0.0	0.0	0.0	0.0	0.0	0.0	0.0
CH4 Emission	0.0	0.0	0.0	0.0	0.0	0.0	0.0	0.0
Change in soil C storage	-1012.0	-926.4	-880.0	-886.6	-1064.4	-975.8	-928.5	-935.3

Hop Bine Co-Product	80% Bine				70% Bine			
	4.28%	2.19%	93.52%		4.28%	2.19%	93.52%	
Soil Nitrogen Balance (kg N/ha/yr)	**Loamy Sand**	**Sandy Loam**	**Silt Loam**	**Totals**	**Loamy Sand**	**Sandy Loam**	**Silt Loam**	**Totals**
Manure N Input	-90.3	-90.3	-90.3	-90.3	-93.5	-93.5	-93.5	-93.5
Crop stub N input	-4.7	-4.7	-4.7	-4.7	-4.7	-4.7	-4.7	-4.7
Crop root N input	-12.8	-12.9	-12.9	-12.9	-12.7	-12.8	-12.9	-12.9
Weeds N input	0.0	0.0	0.0	0.0	0.0	0.0	0.0	0.0
Atm N deposit	-96.2	-96.2	-96.2	-96.2	-96.2	-96.2	-96.2	-96.2
Fertilizer N input	-113.1	-113.1	-113.1	-113.1	-109.9	-109.9	-109.9	-109.9
N fixation	0.0	0.0	0.0	0.0	0.0	0.0	0.0	0.0
N leaching	108.3	108.2	103.6	103.9	105.9	106.0	101.3	101.6
N runoff	0.0	0.0	0.0	0.0	0.0	0.0	0.0	0.0
N uptake by crop	163.5	164.5	164.7	164.6	161.9	163.5	163.8	163.7
N uptake by weeds	0.0	0.0	0.0	0.0	0.0	0.0	0.0	0.0
NH3 volatilization	1.4	1.2	1.5	1.5	1.3	1.2	1.4	1.4
N2O flux	1.9	1.9	1.8	1.8	2.4	1.8	1.7	1.7
NO Flux	0.4	0.4	0.4	0.4	0.4	0.4	0.4	0.4
N2 flux	2.1	2.3	5.9	5.7	2.2	2.3	5.9	5.7
Change in soil N storage	-39.7	-38.8	-39.4	-39.4	-43.0	-42.1	-42.6	-42.6
Soil Carbon Balance (kg C/ha/yr)								
Manure N Input	-1723.0	-1723.0	-1723.0	-1722.8	-1850.0	-1850.0	-1850.0	-1849.8
Crop residue C input	-82.9	-83.4	-83.5	-83.5	-82.1	-82.9	-83.1	-83.0
Crop root C input	-641.6	-645.7	-646.4	-646.1	-635.5	-641.7	-642.8	-642.4
Weeds C input	0.0	0.0	0.0	0.0	0.0	0.0	0.0	0.0
Soil CO2 flux	1330.6	1427.0	1475.7	1468.3	1409.9	1501.1	1551.3	1544.0
DOC Leaching	0.0	0.0	0.0	0.0	0.0	0.0	0.0	0.0
CH4 Emission	0.0	0.0	0.0	0.0	0.0	0.0	0.0	0.0
Change in soil C storage	-1116.9	-1025.1	-977.2	-984.1	-1166.7	-1073.4	-1024.7	-1031.7

Hop Bine Co-Product	60% Bine				50% Bine			
	4.28%	2.19%	93.52%		4.28%	2.19%	93.52%	
Soil Nitrogen Balance (kg N/ha/yr)	**Loamy Sand**	**Sandy Loam**	**Silt Loam**	**Totals**	**Loamy Sand**	**Sandy Loam**	**Silt Loam**	**Totals**
Manure N Input	-96.8	-96.8	-97.0	-97.0	-100.1	-100.1	-100.1	-100.1
Crop stub N input	-4.6	-4.7	-4.7	-4.7	-4.6	-4.7	-4.7	-4.7
Crop root N input	-12.6	-12.8	-12.8	-12.8	-12.5	-12.7	-12.7	-12.7
Weeds N input	0.0	0.0	0.0	0.0	0.0	0.0	0.0	0.0
Atm N deposit	-96.2	-96.2	-96.2	-96.2	-96.2	-96.2	-96.2	-96.2
Fertilizer N input	-106.7	-106.7	-106.7	-106.7	-103.4	-103.4	-103.4	-103.4
N fixation	0.0	0.0	0.0	0.0	0.0	0.0	0.0	0.0
N leaching	104.2	104.0	99.3	99.6	102.1	102.1	97.3	97.6
N runoff	0.0	0.0	0.0	0.0	0.0	0.0	0.0	0.0
N uptake by crop	161.2	162.5	162.8	162.7	159.7	161.4	161.9	161.8
N uptake by weeds	0.0	0.0	0.0	0.0	0.0	0.0	0.0	0.0
NH3 volatilization	1.2	1.1	1.4	1.4	1.1	1.0	1.3	1.3
N2O flux	1.7	1.7	1.7	1.7	2.1	1.6	1.6	1.6
NO Flux	0.3	0.4	0.4	0.4	0.3	0.3	0.4	0.4
N2 flux	2.0	2.2	5.8	5.6	2.0	2.1	5.7	5.5
Change in soil N storage	-46.3	-45.2	-45.8	-45.8	-49.4	-48.3	-48.9	-48.9
Soil Carbon Balance (kg C/ha/yr)								
Manure N Input	-1978.0	-1978.0	-1978.0	-1977.8	-2106.0	-2106.0	-2106.0	-2105.8
Crop residue C input	-817.0	-82.4	-82.6	-114.0	-81.0	-81.8	-82.1	-82.0
Crop root C input	-632.7	-637.7	-639.2	-638.8	-626.7	-633.5	-635.4	-634.9
Weeds C input	0.0	0.0	0.0	0.0	0.0	0.0	0.0	0.0
Soil CO2 flux	1472.6	1576.0	1626.9	1619.0	1543.8	1649.9	1702.9	1694.8
DOC Leaching	0.0	0.0	0.0	0.0	0.0	0.0	0.0	0.0
CH4 Emission	0.0	0.0	0.0	0.0	0.0	0.0	0.0	0.0
Change in soil C storage	-1219.8	-1122.1	-1072.9	-1080.2	-1269.8	-1171.4	-1120.6	-1128.0

Hop Bine Co-Product	40% Bine				30% Bine			
	4.28%	2.19%	93.52%		4.28%	2.19%	93.52%	
Soil Nitrogen Balance (kg N/ha/yr)	**Loamy Sand**	**Sandy Loam**	**Silt Loam**	**Totals**	**Loamy Sand**	**Sandy Loam**	**Silt Loam**	**Totals**
Manure N Input	-103.3	-103.3	-103.3	-103.3	-106.5	-106.5	-106.5	-106.5
Crop stub N input	-4.6	-4.6	-4.6	-4.6	-4.5	-4.6	-4.6	-4.6
Crop root N input	-12.4	-12.6	-12.6	-12.6	-12.3	-12.5	-12.5	-12.5
Weeds N input	0.0	0.0	0.0	0.0	0.0	0.0	0.0	0.0
Atm N deposit	-96.2	-96.2	-96.2	-96.2	-96.2	-96.2	-96.2	-96.2
Fertilizer N input	-100.2	-100.2	-100.2	-100.2	-97.0	-97.0	-97.0	-97.0
N fixation	0.0	0.0	0.0	0.0	0.0	0.0	0.0	0.0
N leaching	100.6	100.4	95.6	95.9	99.2	98.9	93.9	94.2
N runoff	0.0	0.0	0.0	0.0	0.0	0.0	0.0	0.0
N uptake by crop	158.4	160.2	160.8	160.7	157.0	159.0	159.7	159.6
N uptake by weeds	0.0	0.0	0.0	0.0	0.0	0.0	0.0	0.0
NH3 volatilization	10.1	1.0	1.2	1.6	1.0	0.9	1.1	1.1
N2O flux	2.0	1.6	1.5	1.5	1.9	1.5	1.5	1.5
NO Flux	0.3	0.3	0.3	0.3	0.3	0.3	0.3	0.3
N2 flux	1.8	2.0	5.6	5.4	1.7	1.9	5.5	5.3
Change in soil N storage	-52.5	-51.3	-51.8	-51.8	-55.5	-54.3	-54.9	-54.9
Soil Carbon Balance (kg C/ha/yr)								
Manure N Input	-2233.0	-2233.0	-2233.0	-2232.8	-2361.0	-2361.0	-2361.0	-2360.8
Crop residue C input	-80.3	-82.1	-81.6	-81.5	-79.6	-80.6	-81.0	-80.9
Crop root C input	-621.8	-628.9	-631.3	-630.8	-616.4	-624.0	-626.9	-626.3
Weeds C input	0.0	0.0	0.0	0.0	0.0	0.0	0.0	0.0
Soil CO2 flux	1614.6	1724.2	1778.3	1769.9	1686.2	1798.3	1854.3	1845.7
DOC Leaching	0.0	0.0	0.0	0.0	0.0	0.0	0.0	0.0
CH4 Emission	0.0	0.0	0.0	0.0	0.0	0.0	0.0	0.0
Change in soil C storage	-1320.5	-1218.9	-1167.6	-1175.2	-1370.8	-1267.3	-1214.6	-1222.3

Hop Bine Co-Product	20% Bine				0% Bine			
	4.28%	2.19%	93.52%		4.28%	2.19%	93.52%	
Soil Nitrogen Balance (kg N/ha/yr)	**Loamy Sand**	**Sandy Loam**	**Silt Loam**	**Totals**	**Loamy Sand**	**Sandy Loam**	**Silt Loam**	**Totals**
Manure N Input	-109.8	-109.8	-109.7	-109.7	-116.2	-116.2	-116.2	-116.2
Crop stub N input	-4.5	-4.5	-4.6	-4.6	-4.4	-4.4	-4.5	-4.5
Crop root N input	-12.2	-12.4	-12.4	-12.4	-11.9	-12.1	-12.2	-12.2
Weeds N input	0.0	0.0	0.0	0.0	0.0	0.0	0.0	0.0
Atm N deposit	-96.2	-96.2	-96.2	-96.2	-96.2	-96.2	-96.2	-96.2
Fertilizer N input	-93.7	-93.7	-93.7	-93.7	-87.3	-87.3	-87.3	-87.3
N fixation	0.0	0.0	0.0	0.0	0.0	0.0	0.0	0.0
N leaching	97.9	97.5	92.5	92.8	96.2	95.5	90.1	90.5
N runoff	0.0	0.0	0.0	0.0	0.0	0.0	0.0	0.0
N uptake by crop	155.5	157.4	158.3	158.1	151.5	153.9	155.2	155.0
N uptake by weeds	0.0	0.0	0.0	0.0	0.0	0.0	0.0	0.0
NH3 volatilization	1.0	0.9	1.1	1.1	0.9	0.8	0.9	0.9
N2O flux	1.7	1.4	1.4	1.4	1.5	1.3	1.3	1.3
NO Flux	0.3	0.3	0.3	0.3	0.3	0.3	0.3	0.3
N2 flux	1.5	1.8	5.4	5.2	1.2	1.5	5.1	4.9
Change in soil N storage	-58.5	-57.2	-57.7	-57.7	-64.5	-63.0	-63.4	-63.4
Soil Carbon Balance (kg C/ha/yr)								
Manure N Input	-2488.0	-2488.0	-2488.0	-2487.8	-2744.0	-2744.0	-2744.0	-2743.7
Crop residue C input	-78.8	-79.8	-80.3	-80.2	-76.9	-78.1	-78.8	-78.7
Crop root C input	-610.1	-618.0	-621.5	-620.9	-594.7	-604.2	-609.3	-608.5
Weeds C input	0.0	0.0	0.0	0.0	0.0	0.0	0.0	0.0
Soil CO2 flux	1756.7	1872.2	1929.5	1920.7	1896.8	2020.3	2080.4	2071.0
DOC Leaching	0.0	0.0	0.0	0.0	0.0	0.0	0.0	0.0
CH4 Emission	0.0	0.0	0.0	0.0	0.0	0.0	0.0	0.0
Change in soil C storage	-1420.3	-1313.7	-1260.4	-1268.3	-1518.8	-1406.0	-1351.7	-1359.9

B. SUPPLEMENTAL – CHAPTER 3

B.1. LIGNOCELLULOSIC BIOMASS MACERATION PROCEDURE

This method is for macerating wood fiber to isolate and preserve the wood fibers for subsequent analysis, either microscopic or fiber quality. The mild conditions result in minimal fiber damage.

B.1.1.1. Reagents

The maceration fluid is prepared by combining 1 part of a 30% solution of hydrogen peroxide, 4 parts of distilled water, and 5 parts of glacial acetic acid. Be sure to use a clean bottle and prepare this solution in the fume hood. Avoid contact with the solution, wear gloves if necessary. If you are dealing with a kiln dried sample – you may prepare a 1:1 solution of 30% Hydrogen peroxide and acetic acid

[1].

B.1.1.2. Procedure

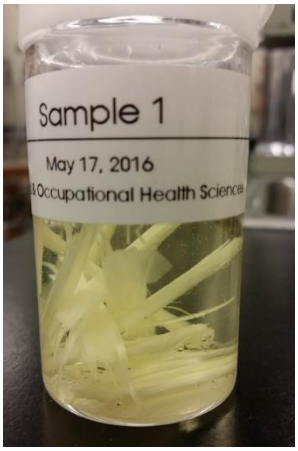

1. Place biomass pieces (about half the size of a match stick) into a solution of: 1:4:5 H_2O_2 (30%): DI water: glacial acetic acid.
2. Incubate at 56 °C for 3 days. L:W (Liquor to wood) ratio of 40:1. If maceration is complete, the fluid will be clear and the wood segments whitish to translucent. If the material is not as described, add fresh macerating solution and incubate for an additional 2-3 days.
3. Wash with three changes of DI water, several hours per change. Keep samples in water until needed for analysis.

4. Mild mechanical treatment will be required to separate the fiber bundles. A British disintegrator is recommended.

C. SUPPLEMENTAL – CHAPTER 4

C.1. PRELIMINARY INVESTIGATION

The method of steepest ascent was used to find the maximum path as a guide for future experiments[2,3]. The green boundary is the boundary of the experimental design as described in the central composite design matrix. This method was used to guide the experiments for reproducibility and repeatability testing.

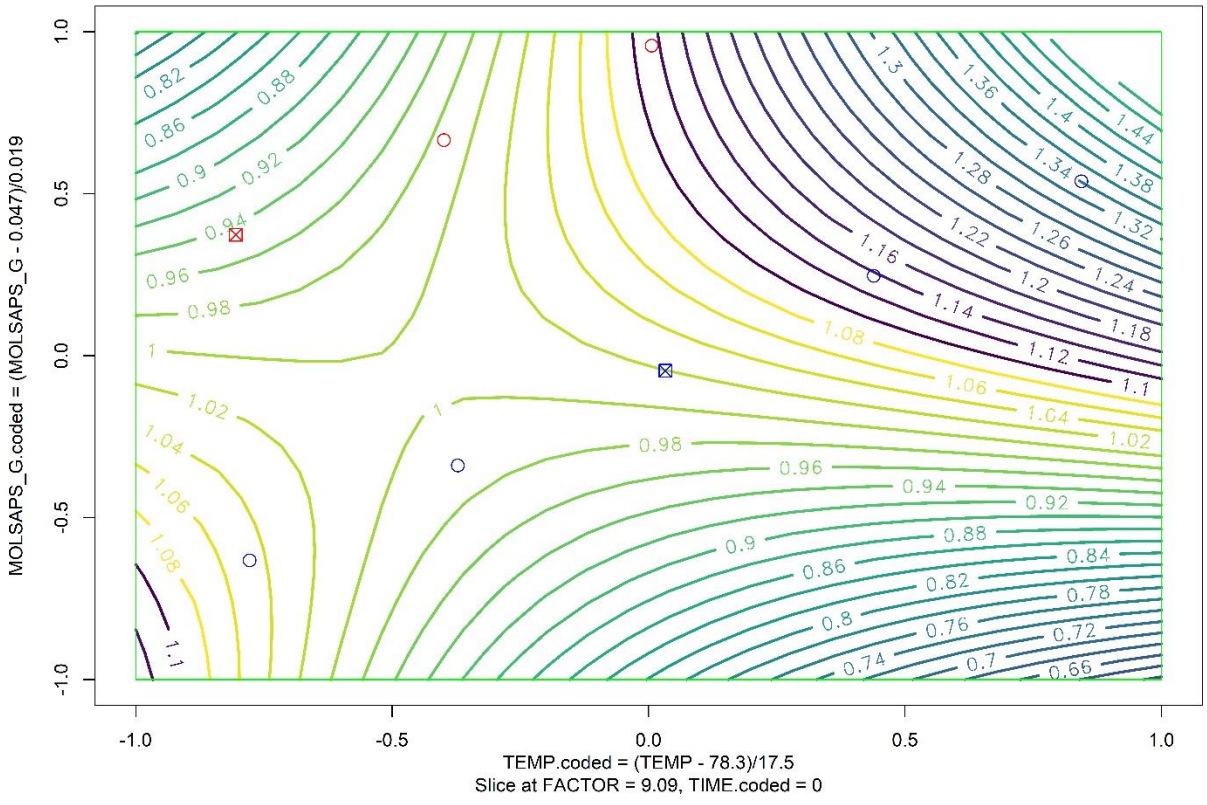

Figure A.3.. Surface plot of carboxylic acid charge indicating rising ridge points in blue.

The following tables are the output statistics of the response surface analysis for each response.

Table A.2. Second Order response surface fit for aspect ratio.

```
                            Estimate Std. Error t value  Pr(>|t|)
(Intercept)                 60.73769    6.49431  9.3524 0.0007279 ***
FACTOR                      -0.38572    0.32224 -1.1970 0.2974073
MOLSAPS_G.coded              8.67913    2.26278  3.8356 0.0185289 *
TEMP.coded                  -6.92357    2.02426 -3.4203 0.0267729 *
TIME.coded                  -2.13044    2.12330 -1.0034 0.3724607
MOLSAPS_G.coded:TEMP.coded -25.32351    5.11597 -4.9499 0.0077618 **
MOLSAPS_G.coded:TIME.coded  10.80916    5.11913  2.1115 0.1023146
TEMP.coded:TIME.coded       -0.14298    4.67844 -0.0306 0.9770833
MOLSAPS_G.coded^2            4.38421    7.20405  0.6086 0.5756712
TEMP.coded^2                 4.37019    5.41354  0.8073 0.4647767
TIME.coded^2                 6.06420    5.96238  1.0171 0.3666323
---
Signif. codes:  0 ‘***’ 0.001 ‘**’ 0.01 ‘*’ 0.05 ‘.’ 0.1 ‘ ’ 1

Multiple R-squared:  0.9391,     Adjusted R-squared:  0.7867
F-statistic: 6.165 on 10 and 4 DF,  p-value: 0.04724

Analysis of Variance Table


Response: mean.Y_VALUE
                                                Df Sum Sq Mean Sq F value  Pr(>F)
FACTOR                                           1  76.57  76.572  4.1026 0.11279
FO(MOLSAPS_G.coded, TEMP.coded, TIME.coded)      3 515.60 171.868  9.2083 0.02870
TWI(MOLSAPS_G.coded, TEMP.coded, TIME.coded)     3 537.49 179.164  9.5992 0.02673
PQ(MOLSAPS_G.coded, TEMP.coded, TIME.coded)      3  20.92   6.972  0.3736 0.77765
Residuals                                        4  74.66  18.664
Lack of fit                                      4  74.66  18.664
Pure error                                       0   0.00

Stationary point of response surface:
MOLSAPS_G.coded      TEMP.coded      TIME.coded
     -0.1286473       0.4242374       0.2953124

Stationary point in original units:
mean.MOLSAPS_G      mean.TEMP      mean.TIME
     0.0462557     87.4241544    422.0156011
```

Table A.3. Second order response surface analysis for crystallite size

```
                           Estimate Std. Error t value  Pr(>|t|)
(Intercept)                49.52675    1.96881 25.1556 4.004e-08 ***
FACTOR                      0.11740    0.12003  0.9781  0.360622
MOLSAPS_G.coded             4.21056    1.45661  2.8907  0.023294 *
TEMP.coded                  2.03580    0.97235  2.0937  0.074563 .
TIME.coded                 -0.83070    1.00390 -0.8275  0.435267
MOLSAPS_G.coded:TEMP.coded -3.44478    1.76903 -1.9473  0.092539 .
MOLSAPS_G.coded:TIME.coded  4.50953    1.76903  2.5492  0.038150 *
TEMP.coded:TIME.coded       1.04240    1.79230  0.5816  0.579077
MOLSAPS_G.coded^2          -2.21363    1.72447 -1.2837  0.240117
TEMP.coded^2               -7.32402    1.58196 -4.6297  0.002399 **
TIME.coded^2               -7.16893    1.87938 -3.8145  0.006589 **
---
Signif. codes:  0 ‘***’ 0.001 ‘**’ 0.01 ‘*’ 0.05 ‘.’ 0.1 ‘ ’ 1

Multiple R-squared:  0.9278,     Adjusted R-squared:  0.8248
F-statistic: 9.002 on 10 and 7 DF,  p-value: 0.00403

Analysis of Variance Table

Response: mean.CRYSTALLITE_ag
                                                Df  Sum Sq Mean Sq F value   Pr(>F)
FACTOR                                           1 112.560 112.560 41.0793 0.000364
FO(MOLSAPS_G.coded, TEMP.coded, TIME.coded)      3  27.202   9.067  3.3092 0.087076
TWI(MOLSAPS_G.coded, TEMP.coded, TIME.coded)     3  29.122   9.707  3.5428 0.076273
PQ(MOLSAPS_G.coded, TEMP.coded, TIME.coded)      3  77.771  25.924  9.4610 0.007374
Residuals                                        7  19.180   2.740
Lack of fit                                      5  18.452   3.690 10.1300 0.092279
Pure error                                       2   0.729   0.364

Stationary point of response surface:
MOLSAPS_G.coded      TEMP.coded      TIME.coded
     1.5057244      -0.1865068       0.4020817

Stationary point in original units:
mean.MOLSAPS_G      mean.TEMP      mean.TIME
    0.07730876    76.73613154   444.43715678
```

Table A.4. Second order response surface analysis of the crystallinity index.

```
                              Estimate  Std. Error t value Pr(>|t|)
(Intercept)                 2.1582e+00  8.8189e-01  2.4472  0.04429 *
FACTOR                     -1.3142e-03  1.9880e-03 -0.6611  0.52973
MOLSAPS_G.coded            -2.8398e+01  1.1588e+01 -2.4507  0.04406 *
TEMP.coded                 -9.1512e-03  1.4868e-02 -0.6155  0.55769
TIME.coded                 -1.3320e-03  9.2624e-04 -1.4381  0.19357
MOLSAPS_G.coded:TEMP.coded  1.6932e-01  8.8122e-02  1.9214  0.09613 .
MOLSAPS_G.coded:TIME.coded  1.7519e-02  7.3435e-03  2.3857  0.04848 *
TEMP.coded:TIME.coded       1.6771e-05  8.0778e-06  2.0762  0.07652 .
MOLSAPS_G.coded^2           7.7348e+01  7.9120e+01  0.9776  0.36084
TEMP.coded^2               -3.2938e-05  8.5558e-05 -0.3850  0.71168
TIME.coded^2               -1.2606e-06  7.0585e-07 -1.7860  0.11727
---
Signif. codes:  0 ‘***’ 0.001 ‘**’ 0.01 ‘*’ 0.05 ‘.’ 0.1 ‘ ’ 1

Multiple R-squared:  0.7817,     Adjusted R-squared:  0.4698
F-statistic: 2.506 on 10 and 7 DF,  p-value: 0.1177

Analysis of Variance Table

Response: mean.CRYST
                                                Df    Sum Sq   Mean Sq F value  Pr(>F)
FACTOR                                           1 0.0000092 0.0000092  0.0122 0.91503
FO(MOLSAPS_G.coded, TEMP.coded, TIME.coded)      3 0.0016570 0.0005523  0.7348 0.56361
TWI(MOLSAPS_G.coded, TEMP.coded, TIME.coded)     3 0.0102934 0.0034311  4.5645 0.04496
PQ(MOLSAPS_G.coded, TEMP.coded, TIME.coded)      3 0.0068811 0.0022937  3.0514 0.10137
Residuals                                        7 0.0052618 0.0007517
Lack of fit                                      5 0.0049171 0.0009834  5.7060 0.15582
Pure error                                       2 0.0003447 0.0001723

Stationary point of response surface:
MOLSAPS_G.coded      TEMP.coded      TIME.coded
     0.08785679     87.36261916      0.85131627

Stationary point in original units:
mean.MOLSAPS_G      mean.TEMP      mean.TIME
    0.08785679    87.36261916     0.85131627
```

Table A.5. Second order response surface analysis – carboxylic acid content.

```
                             Estimate Std. Error t value  Pr(>|t|)
(Intercept)                 0.8799364  0.0620992 14.1698 < 2.2e-16 ***
FACTOR                      0.0230327  0.0038858  5.9274 1.094e-07 ***
MOLSAPS_G.coded             0.1765158  0.0294003  6.0039 8.032e-08 ***
TEMP.coded                  0.1096341  0.0232816  4.7091 1.245e-05 ***
TIME.coded                  0.1332507  0.0271429  4.9092 5.886e-06 ***
MOLSAPS_G.coded:TEMP.coded  0.3342164  0.0614124  5.4422 7.548e-07 ***
MOLSAPS_G.coded:TIME.coded  0.1789297  0.0596386  3.0002  0.003751 **
TEMP.coded:TIME.coded      -0.1202667  0.0546388 -2.2011  0.031075 *
MOLSAPS_G.coded^2          -0.1023859  0.0667593 -1.5337  0.129686
TEMP.coded^2                0.0198190  0.0405057  0.4893  0.626189
TIME.coded^2               -0.2005394  0.0606063 -3.3089  0.001491 **
---
Signif. codes:  0 ‘***’ 0.001 ‘**’ 0.01 ‘*’ 0.05 ‘.’ 0.1 ‘ ’ 1

Multiple R-squared:  0.8702,     Adjusted R-squared:  0.8514
F-statistic: 46.27 on 10 and 69 DF,  p-value: < 2.2e-16

Analysis of Variance Table

Response: CARB
                                            Df Sum Sq Mean Sq  F value    Pr(>F)
FACTOR                                       1 3.3717  3.3717 347.5687 < 2.2e-16
FO(MOLSAPS_G.coded, TEMP.coded, TIME.coded)  3 0.5432  0.1811  18.6650 5.709e-09
TWI(MOLSAPS_G.coded, TEMP.coded, TIME.coded) 3 0.4281  0.1427  14.7112 1.668e-07
PQ(MOLSAPS_G.coded, TEMP.coded, TIME.coded)  3 0.1455  0.0485   4.9987  0.003397
Residuals                                   69 0.6694  0.0097
Lack of fit                                  4 0.4151  0.1038  26.5222 4.628e-13
Pure error                                  65 0.2543  0.0039

Stationary point of response surface:
MOLSAPS_G.coded      TEMP.coded      TIME.coded
    -0.01912722     -0.84954773      0.57844108

Stationary point in original units:
   MOLSAPS_G         TEMP         TIME
  0.04833658  65.13291472 481.47262785
```

C.2. ANALYTICAL METHODS

C.2.1. Conductometric Titration

The method used here converts the carboxylic acids on the cellulose to their hydrogen form with the addition of 0.1M Hydrochloric acid. This becomes the strong acid titrated to the first inflection point. The second inflection point is the weak carboxylic acid. The solution may be buffered to stabilize readings, however, the additional ionic concentration may overwhelm the conductivity reading and obscure the second inflection point if added in excess of 0.001M. The use of NaCl for buffering the solution also serves to level out the Donnan effect. This results in an unequal distribution of ionic species between the interior and exterior of the fiber[4]. The conductance of the solution is the product of all each ionic species in the solution and their equivalent conductance.

Table A.6. Equivalent Conductance (25 °C, in H2O, very high dilution)[5]

Cations	**[S*cm2/mol]**	**Anions**	**[S*cm2/mol]**
H+	349.8	OH-	198.6
Li+	38.7	Cl-	76.4
Na+	50.1	HCO3-	44.5
Formate[6] (HCOO−)	54.64		
Acetate CH3COO−	40.92		

Temperature influences the equivalent conductance in a different manner by increasing the motion of the ionic species in the solution. The increased mobilityof the ions result in a higher measured conductivity. Weak electrolytes, higher temperature raises the dissociation rate and the conductivity.

During the progress of the titration, the volume is continually changing. The conductivity reading must be adjusted to account for the dilution effect of the additional titrant volume.

Determination of carboxylic acid content and degree of oxidation in cellulose pulp[7,8,9,10,11,12]. An effective conductometric titration requires charged groups on the surface of the CNCs or NFCs to be fully protonated. For strong acids, aqueous suspensions are titrated directly by NaOH yielding a titration curve with a sharp transition at the equivalence point. Weak acids required the addition of a strong acid to the suspension in order to establish a measureable reduction in conductivity at the beginning of the titration. The weak acid content is determined from the extended plateau between the acidic and basic regions[13].

The initial descending branch of the curve represents neutralization of the hydrogen ions dissociated from the strong acid groups. Near the first equivalence point, the weaker carboxylic acid groups begin to dissociate and contribute to the measured conductance. The conductance in second branch changes little. This is due to the low level of hydrogen ions in equilibrium with the weak acid as the titration progresses. At the second equivalence point, conductance increases in proportion to the excess sodium hydroxide[4].

C.2.2.Carboxylic Acid Titration

C.2.2.1. Procedure

1. Weight out approximately 0.1g of oven dry pulp. Estimate this from your starting mass and final volume. [*Example: started with 2.5 g of OD fiber and final volume of 30 ml for approximately 8.3% consistency. Weigh out approximately 1.2 g of the wet biomass to obtain 0.1g of oven dry pulp.]*
2. Transfer fiber to a 40.0 ml distillation vial.
3. Add 10 ml of 0.01M HCl.
4. Measure out 190 ml of deionized water. Use this to fill the distillation vial.

5. Place in sonic bath with ice for 15 minutes. This exchanges the Na cations bound to the COOH group by H ions. The ice prevents the suspension from overheating and loss of volume. If a sonic bath is unavailable – allow to sit for at least 2 hours at room temperature.
6. Allow sonicated samples to warm up to room temperature for 2 hours.
7. Transfer contents to a 400 ml beaker using the remaining 190 ml of deionized water to rinse the scintillation vial. Final volume should be 200 ml.
8. Titrate with 0.01M NaOH in 0.25 ml increments, recording the conductivity. A plot of the data will show the presence of a strong acid (excess of HCl) and a weak acid that corresponds to carboxyl content. The titration can be stopped when a pH > 10.4 is reached or you reach the starting conductivity.
9. Using a Buchner funnel and filter paper, tare the filter paper, then filter the slurry to capture the fiber. Place in a 105 °C drying oven for 24 hours to calculate the actual mass, m, of oven dry pulp used.
10. The conductivity is proportional to the amount of electrolytic solution. Therefore it is essential that the measured conductivity be corrected for the volume of added NaOH at each titration point.

$$\text{Conductivity}_c = \text{Conductivity}_m * \frac{(V_i + V_0)}{V_i}$$

V_i is the initial suspension volume including any HCl or buffers added.

V_0 is the volume of NaOH added at each point.

11. Carboxyl Content

$$C = \frac{c * (V_2 - V_1)}{m}$$

C: is the mmol/g of carboxyl

V_1 and V_2 : is the amount of NaOH (ml) corresponding to the first and second inflection points.

c : is the mol/L of NaOH

m: is the oven dry mass of pulp (g)

C.2.3.Residual Ammonium persulfate Titration

Persulfate is determined by titration of a standardized potassium permanganate solution with a standardized ferrous ammonium sulfate solution, a back titration technique.

C.2.3.1. Reagents

In the preparation of reagents, use only chemicals of analytical grade and distilled water.

1.0 N Sulfuric Acid, H_2SO_4

0.5 N Ferrous Ammonium Sulfate, $Fe(NH_4)_2(SO_4)_2 \cdot 6H_2O$

C.2.3.2. Procedure

1. To a 250 mL Erlenmeyer flask, pipette 2-20 mL of persulfate solution (depending on the approximate solution concentration).
2. Add 50 mL of a 1 N H_2SO_4 solution.
3. Add exactly 40 mL of 0.5 N ferrous ammonium sulfate solution. Swirl constantly while adding the ferrous ammonium sulfate solution.
4. Let stand for one minute and titrate with 0.5 N $KMnO_4$ to a permanent pink endpoint

3. Calculations

$$\frac{g}{L}APS = \frac{(V_{mb} - V_t)N_{KMnO_4} * 114}{V_{sample}}$$

C.5.1. Oxalic Acid standardization of Titrant

Sodium hydroxide solutions pick up carbon dioxide from the air. This contamination can affect the strength of the base solution and can spoil the sharpness of the end point in the titration. The procedure below is designed to prepare and standardize carbonate-free NaOH:

$$2NaOH + H_2C_2O_4 - 2H_2O \rightarrow 2Na_2C_2O_4 + 4H_2O$$

C.5.1.1. Reagents

0.5N NaOH

0.01N NaOH

0.5N Oxalic Acid (31.5g/1000ml) MW: 126

0.01N Oxalic Acid (0.63g/1000ml)

C.5.1.2. Procedure

1. Weigh ~0.63 g of dried KHP (MW = 126 g/mol) into an Erlenmeyer flask and dissolve in 1000 mL of distilled water. Record the amount of mass used.
2. Add 4 drops of phenolphthalein indicator into the flask and titrate to the first permanent appearance of pink. Near the endpoint, add the NaOH dropwise to determine the total volume most accurately.

C.5.1.3. Calculation

Calculate Concentration of KHP:

$$(\quad)g\ KHP * \frac{1\ mol\ KHP}{204.23\ g} = (\quad)\ moles\ KHP$$

$$\frac{(\quad)\ moles\ KHP}{(\quad)L\ H_2O} = (\quad)M(\frac{mol}{L})\ KHP$$

Calculate Concentration of NaOH:

$$(\quad)\ moles\ KHP * \frac{1\ mol\ NaOH}{1\ mol\ KHP} = (\quad)\ moles\ NaOH$$

$$\frac{(\quad)\ moles\ NaOH}{(\quad)\ L\ NaOH} = (\quad)\ M(\frac{mol}{L})\ NaOH$$

C.3. AUTOMATION OF TITRATOR

Conductometric titrations can be both time consuming and a challenge to detect the inflection point. Small changes in titrant volume, 0.5 ml, can result in over shooting an inflection point. An automated system that could control titrant volumes down to 0.1 ml was necessary.

Several papers have been published by scientists automating pH meters using Arduino based circuit controls. The software was written using Arduino native code. Based on these papers, a circuit design was developed that incorporated aspects from these papers, Figure A.4. All papers utilized stand-alone probes. The objective of this was to take an existing conductivity meter and an existing digital balance, feed their outputs to the Arduino, and control titration volume based on the conductivity and balance readings. This would allow for better control of equilibrium being achieved before additional titrant is added.

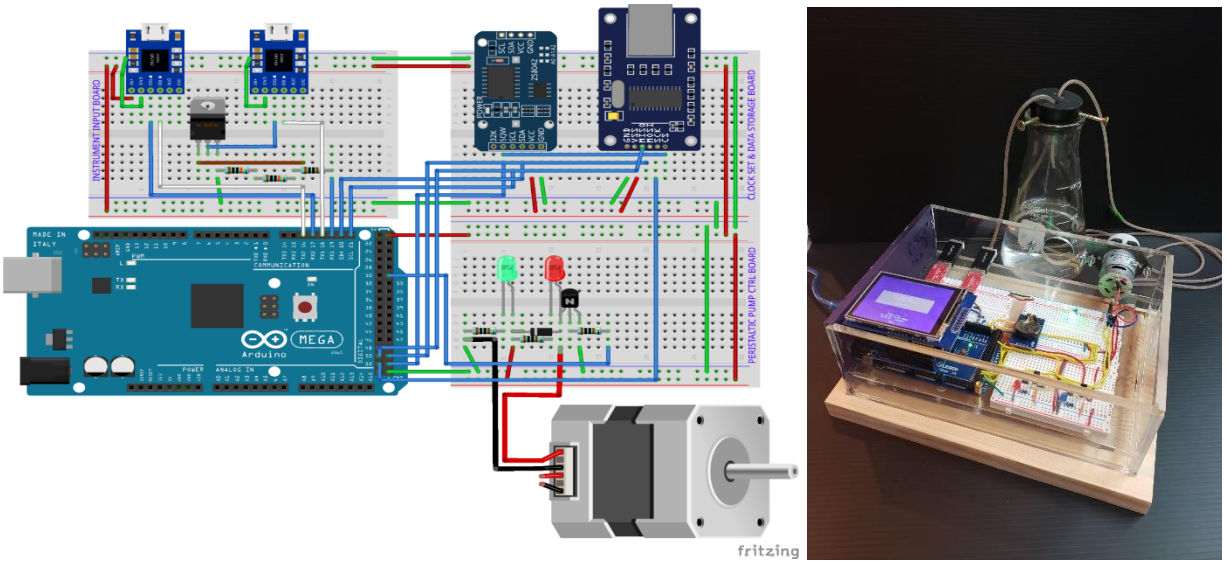

Figure A.4. – Circuit board diagram for Conductometric titration control

A 12V DC, 3W peristaltic pump was calibrated for a 2mm diameter tubing. It delivered 0.225 ml/sec. Which is then set in the code with an appropriate delay to allow the measurement to equilibrate.

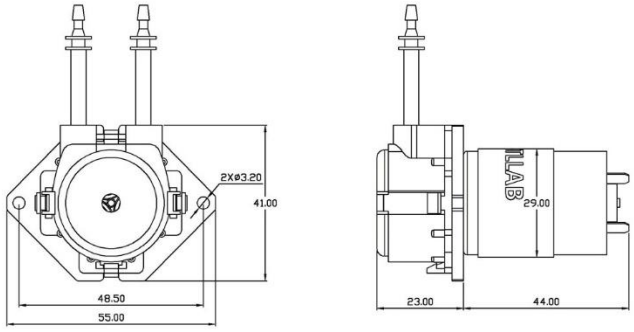

ID×OD	FLOWRATE
1.0×3.0 (mm)	2~17 mL/min
2.0×4.0 (mm)	5~40 mL/min
3.0×5.0 (mm)	19~100 mL/min

Figure A.5.. 12V dc peristaltic titrant delivery pump

An ELEGOO UNO R3 2.8 Inches TFT Touch Screen with SD Card was added as an interface to eventually control the pump and software as well as to allow easier data logging from the conductivity meter and digital balance.

C.6.1. Microfluidization

The Microfluidizer high shear fluid processor relies upon the forces of shear, impact, and occasionally cavitation. The Microfluidizer processor acts as a large pump that forces a formulation through a very small orifice (i.e. micro channels). The pressures can be as low as 3.4 MPa/500 psi and go as high as 275 MPa/40,000 psi.

Intensifier Pump: Inside the air motor, air pressure pushes a large piston which, in turn, pushes a smaller (product) plunger in the intensifier pump. The air pressure over the area of the large piston is greatly intensified when it is transferred to the reduced area of the smaller product plunger. The air motor and pump are separated by an isolator; therefore, the product cannot be contaminated from the air supply, nor can there be carry over of the product into the air motor.

Interaction Chamber: The product stream enters the interaction chamber and passes through geometrically fixed microchannels, causing it to accelerate to very high velocities. It is here that the product is acted upon by two primary forces, which bring about the desired results:

• Shear - deformation of the product stream; occurring from contact with channel walls at high velocity.

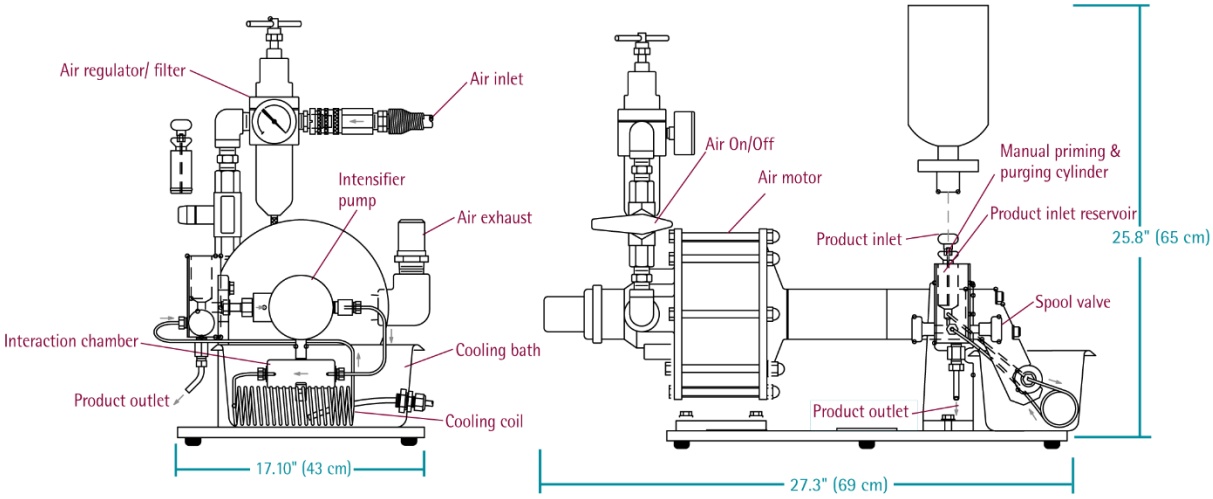

Figure A.6.. Schematic of microfluidizer

In addition, the pressure also raises the temperature of the sample. It is estimated that for every 1000 psi of pressure applied to water, the temperature will rise by 1.0ºC-1.7ºC. The residence time inside the chamber is 1-5 milliseconds.

The following SOP describes procedures that should be followed to avoid plugging and chamber damage on the lab microfluidizer.

C.6.1.1. Priming the Pump

1. Make sure the air supply valve is turned off prior to starting.
2. Place ice and water nn the bath to keep your sample cool.
3. Initially, start-up with DI water.
4. Load about 100 mL DI water into the feed chamber and push the piston into the chamber.
5. Turn on your air supply by turning the regulator handle counter clockwise. Adjust the air pressure, shown on your pressure gauge, to approximately 15-20 psi (3500-4700 psi process pressure). This is to allow the machine to stroke slowly during priming.

6. Operate the pump very slowly, applying manual pressure with the palm of your hand to the chamber piston assembly. The machine should now be primed.

7. Measure the flow rate of your system at 10,000 psig using water at 0-25°C as a standard reference fluid.
8. Set your air pressure to 43 psi (Air Pressure * 233 = Process Pressure)
9. Start the machine.
10. Measure the time it takes to fill a container of known volume.
11. Calculate flow rate in ml/min or other convenient units.

C.6.1.2. Sample Processing

Pulp slurry (0.1% consistency) may now be added to the chamber. Make sure that there are no large fiber bundles present.

1. Set the spool valve for multi pass or single pass operation. For single pass – ensure that you have a container positioned to collect your sample.
2. Operate pump until all of the sample has been processed through.
3. Clean the microfluidizer with 100 ml of deionized water – pump this through the unit after processing your sample.

C.7.1. AFM sample preparation method

Droplet-evaporation or adsorption methods are used for preparing AFM samples from liquid suspensions.

C.7.1.1. Materials

10 mm Muscovite Mica [$(KAl_2(OH)_2(AlSi_3O_{10})$]

12 mm steel disc

L-lysine

Nitrogen gas

C.7.1.2. Procedure

1. The mica disk must first be glued the steel disc. This accomplishes two things. First it protects the fragile mica substrate. Second it makes transferring the sample from a magnetic storage container to the AFM more easily.
2. Place the prepared disc in a magnetic closed sample container that will ensure the sample is protected from movement and dust.

   An atomically clean surface is required before the nanocellulose may be deposited onto the mica surface. The process requires using masking tape.
3. Place the masking tape over the mica, then pull rapidly to remove a layer. Repeat until a complete disk layer is removed.
4. Place the cleaved disk-mica slide into the container.
5. Add 100 ul of poly L-lysine to the surface. After 10 minutes, rinse the mica-slide with deionized water. Dry the treated mica-slide with nitrogen gas.
6. Nanocellulose solution should be produced to 0.1 mg/ml. Place 100 ul onto the substrate. environmental contamination.

D. SUPPLEMENTAL – CHAPTER 5

Plots of stress versus strain represent average of measurements for each level of hand sheets produced. The resulting curve displays the standard deviation in measurements of the block of measured hand sheets.

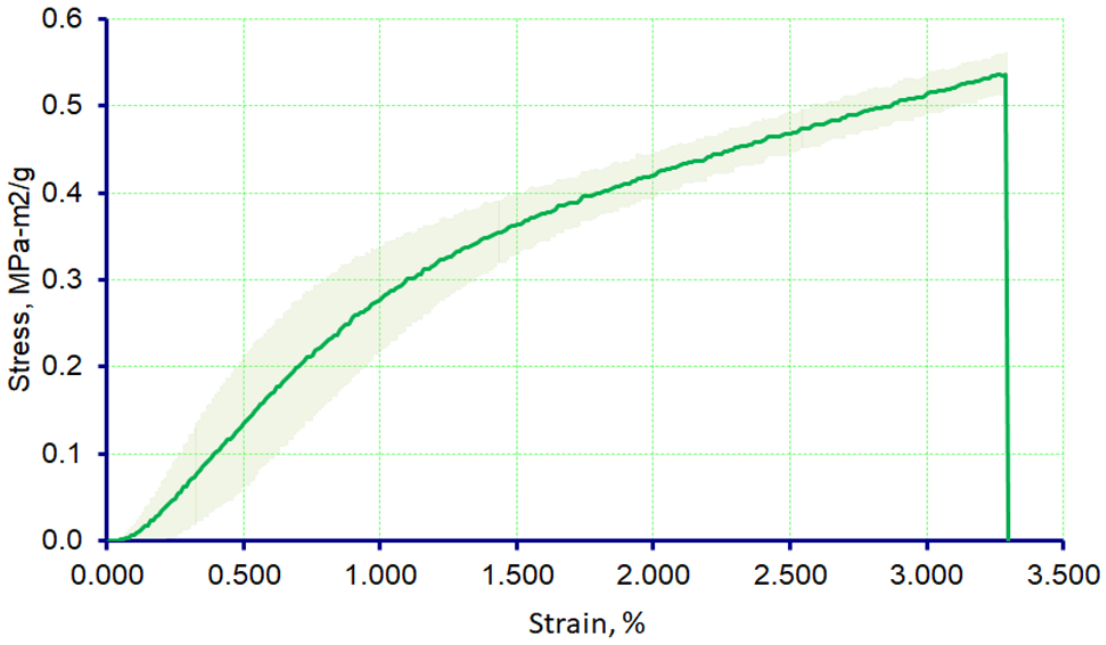

Figure A.7..Elongation curve with standard deviation of measurements for 5% NFC – low charge.

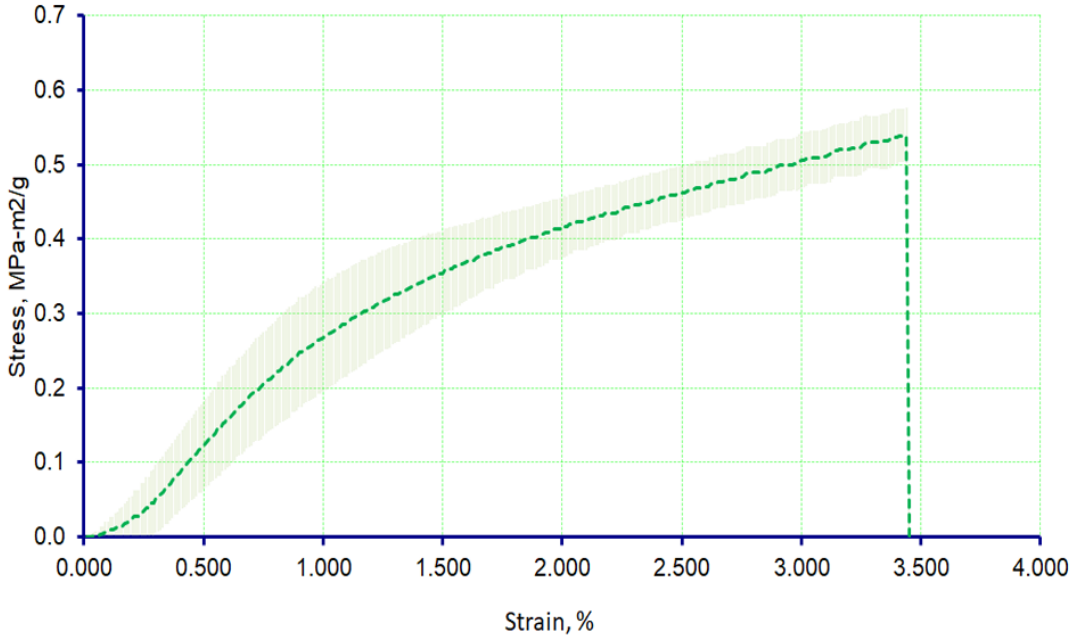

Figure A.8. Elongation curve with standard deviation of measurements for 10% NFC – low charge.

.

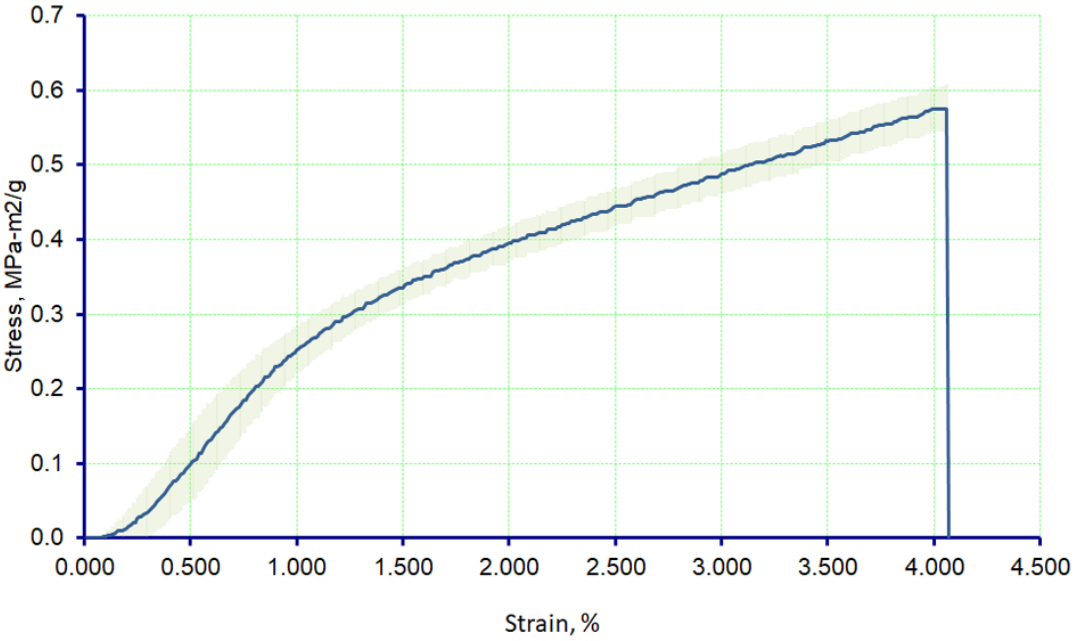

Figure A.9. Elongation curve with standard deviation of measurements for 5% NFC – high charge.

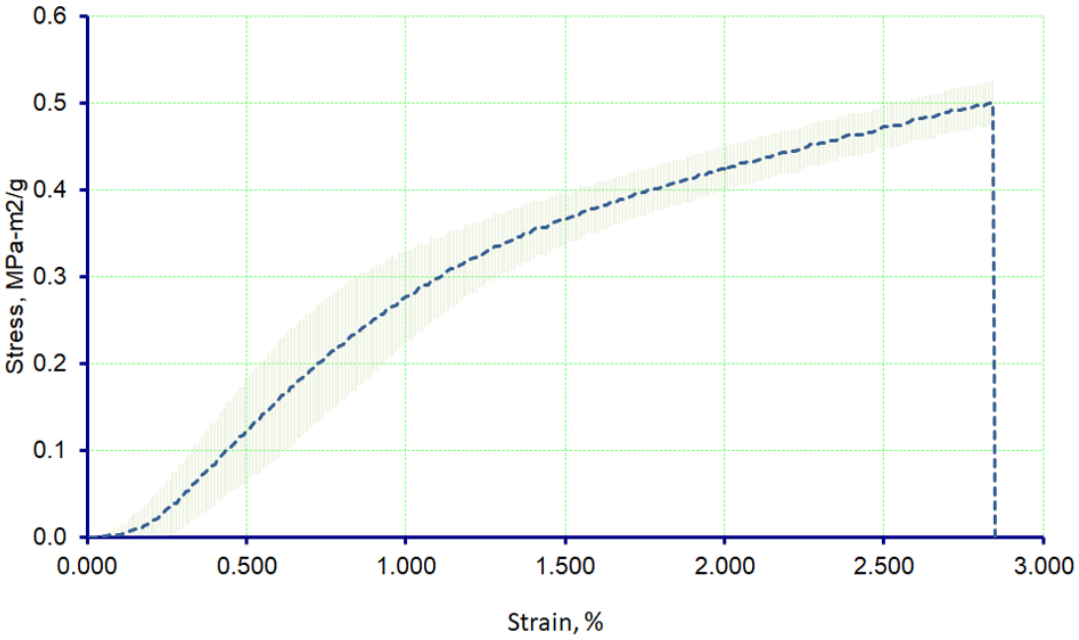

Figure A.10. Elongation curve with standard deviation of measurements for 10% NFC – high charge.

Permanova analysis of NFC amended hand sheets was conducted on measured response variables[14,15]. Permanova was applied to the non-parametric multivariate data[16]. The ordination of the data set was performed using the explanatory data. The data was first relativized by standardize method for each treatment response in order to adjust for differences in the spread of values. This was followed by Euclidean distance calculation for all three response variables. The permutational multivariate analysis of variance (PERMANOVA) tested the overall affect each explanatory variable had on these response variables[17]. The data does not contain zero values so a Euclidean distance for the dissimilarity measure is appropriate. Bray-Curtis dissimilarity may be sensitive to differences in the frequency of diameters.

A screeplot was produced to determine how many principal components should be kept. The plot indicates that the optimum number of clusters is 3. The method used was the silhouette

found in fviz_nbclust function. The dataset was then portioned into 3 clusters using the kmeans function.

Table A.7. L value analysis of variance and interactions.

```
adonis2(formula = PROJ_DATA.resp.color.rel$L ~ NFC_P + CARB + NFC_P:CARB,
data = PROJ_DATA.color.explan, method = "euc")
           Df SumOfSqs      R2         F Pr(>F)
NFC_P       1    0.738 0.00794    2.1876  0.145
CARB        1   59.031 0.63474  174.8787  0.001 ***
NFC_P:CARB  1    2.850 0.03065    8.4440  0.005 **
Residual   90   30.380 0.32667
Total      93   93.000 1.00000
---
Signif. codes:  0 '***' 0.001 '**' 0.01 '*' 0.05 '.' 0.1 ' ' 1
```

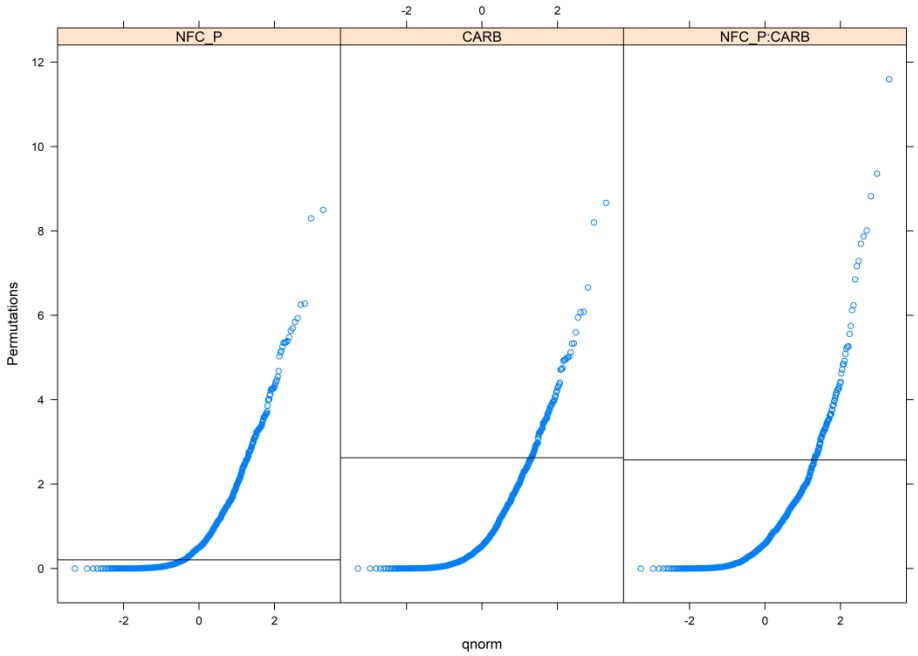

Table A.8. a Value analysis of variance and interactions

```
adonis2(formula = PROJ_DATA.resp.color.rel$a ~ NFC_P + CARB + NFC_P:CARB,
data = PROJ_DATA.color.explan, method = "euc")
           Df SumOfSqs      R2         F Pr(>F)
NFC_P       1    1.811 0.01947    4.4159  0.040 *
CARB        1   54.273 0.58358  132.3430  0.001 ***
NFC_P:CARB  1    0.008 0.00009    0.0206  0.882
Residual   90   36.908 0.39686
Total      93   93.000 1.00000
---
Signif. codes:  0 '***' 0.001 '**' 0.01 '*' 0.05 '.' 0.1 ' ' 1
```

Table A.9. b Value analysis of variance and interactions

```
adonis2(formula = PROJ_DATA.resp.color.rel$b ~ NFC_P + CARB + NFC_P:CARB,
data = PROJ_DATA.color.explan, method = "euc")
           Df SumOfSqs      R2        F Pr(>F)
NFC_P       1    0.909 0.00977   4.6160  0.030 *
CARB        1   74.265 0.79855 377.1280  0.001 ***
NFC_P:CARB  1    0.103 0.00111   0.5227  0.484
Residual   90   17.723 0.19057
Total      93   93.000 1.00000
---
Signif. codes:  0 ‘***’ 0.001 ‘**’ 0.01 ‘*’ 0.05 ‘.’ 0.1 ‘ ’ 1
```

Table A.10. R457 Value anlaysis of variance and interactions.

```
adonis2(formula = PROJ_DATA.resp.color.rel$R457 ~ NFC_P + CARB + NFC_P:CARB,
data = PROJ_DATA.color.explan, method = "euc")
           Df SumOfSqs      R2       F Pr(>F)
NFC_P       1    3.021 0.03248  4.8549  0.026 *
CARB        1   29.056 0.31243 46.6994  0.001 ***
NFC_P:CARB  1    4.925 0.05296  7.9161  0.006 **
Residual   90   55.998 0.60213
Total      93   93.000 1.00000
---
Signif. codes:  0 ‘***’ 0.001 ‘**’ 0.01 ‘*’ 0.05 ‘.’ 0.1 ‘ ’ 1
```

Principal Component Analysis – Color

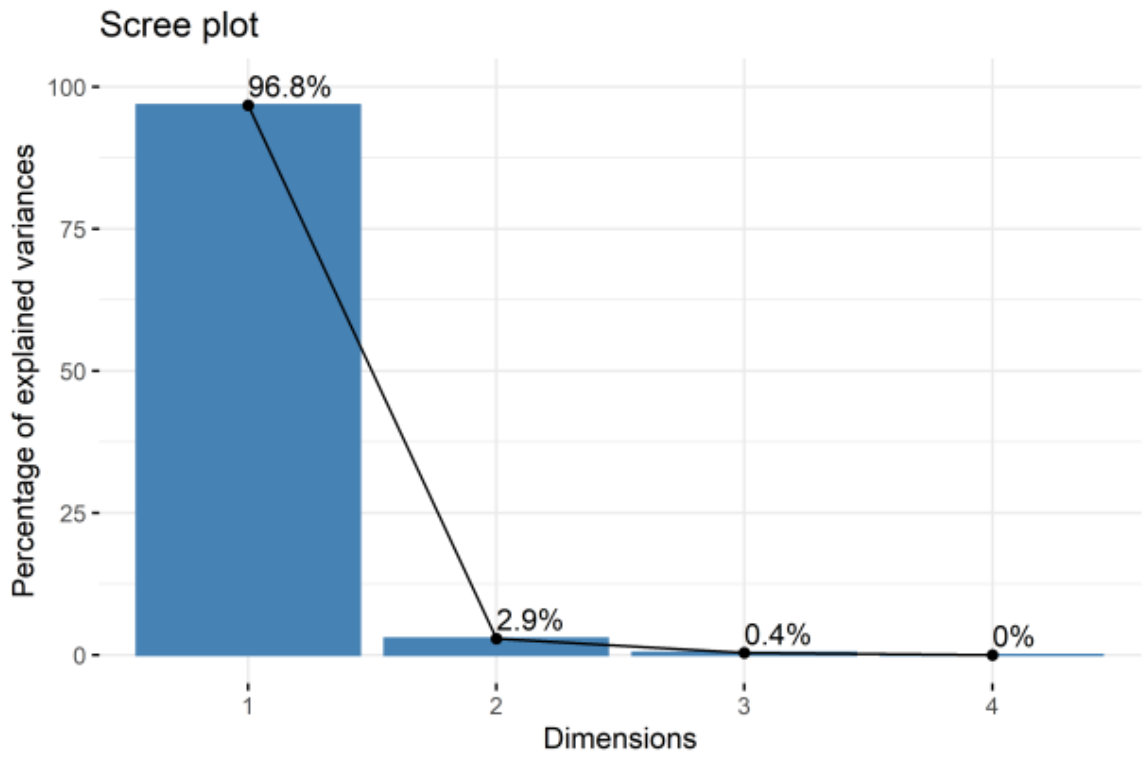

Figure A.11. Scree plot of principle components.

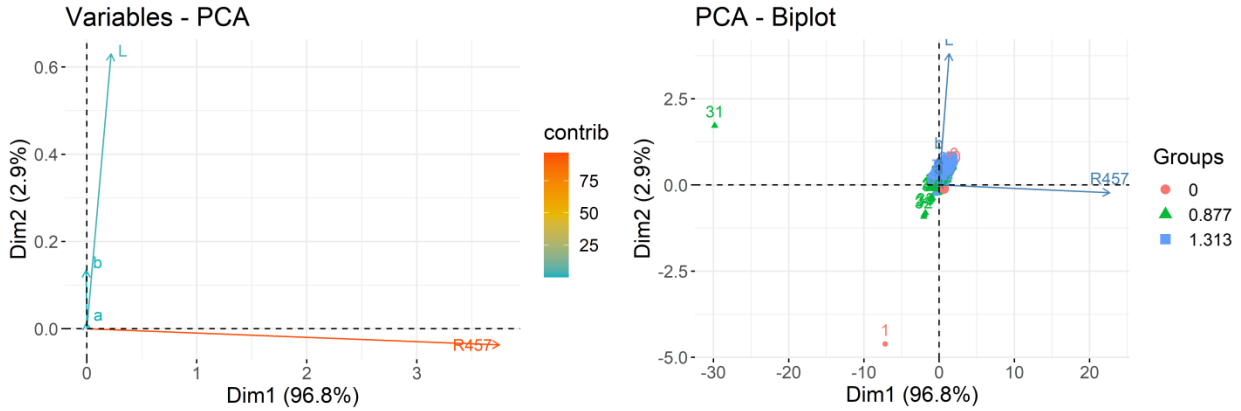

Figure A.12. Plot of first two principal components and vectors of the response variables for optical properties

Strength Data

Table A.11. Normalized Tensile (mN-m/g) analysis of variance and interactions

```
adonis2(formula = PROJ_DATA.resp.tensile.rel$TENSILE_N ~ NFC_P + CARB +
NFC_P:CARB, data = PROJ_DATA.tensile.explan, method = "euc")
           Df SumOfSqs      R2       F Pr(>F)
NFC_P       1   29.587 0.55825 360.238  0.001 ***
CARB        1    3.910 0.07377  47.601  0.001 ***
NFC_P:CARB  1   15.397 0.29050 187.460  0.001 ***
Residual   50    4.107 0.07748
Total      53   53.000 1.00000
---
Signif. codes:  0 ‘***’ 0.001 ‘**’ 0.01 ‘*’ 0.05 ‘.’ 0.1 ‘ ’ 1
```

Table A.12. Normalized Stretch (% - m2/g) analysis of variance and interactions

```
adonis2(formula = PROJ_DATA.resp.tensile.rel$STRETCH_N ~ NFC_P + CARB +
NFC_P:CARB, data = PROJ_DATA.tensile.explan, method = "euc")
           Df SumOfSqs      R2       F Pr(>F)
NFC_P       1    8.202 0.15475 10.6658  0.002 **
CARB        1    3.994 0.07535  5.1933  0.029 *
NFC_P:CARB  1    2.356 0.04445  3.0640  0.079 .
Residual   50   38.449 0.72545
Total      53   53.000 1.00000
---
Signif. codes:  0 ‘***’ 0.001 ‘**’ 0.01 ‘*’ 0.05 ‘.’ 0.1 ‘ ’ 1
```

Table A.13. TEA analysis of variance and interaction.

```
adonis2(formula = PROJ_DATA.resp.tensile.rel$TEA ~ NFC_P + CARB + NFC_P:CARB,
data = PROJ_DATA.tensile.explan, method = "euc")
           Df SumOfSqs      R2       F Pr(>F)
NFC_P       1   23.699 0.44716 79.4141  0.001 ***
CARB        1    0.515 0.00973  1.7272  0.176
```

```
NFC_P:CARB  1   13.864 0.26158 46.4556  0.001 ***
Residual   50   14.921 0.28154
Total      53   53.000 1.00000
---
Signif. codes:  0 ‘***’ 0.001 ‘**’ 0.01 ‘*’ 0.05 ‘.’ 0.1 ‘ ’ 1
```

Table A.14. Breaking Length, m, analysis of variance and interaction

```
adonis2(formula = PROJ_DATA.resp.tensile.rel$BL ~ NFC_P + CARB + NFC_P:CARB,
data = PROJ_DATA.tensile.explan, method = "euc")
           Df SumOfSqs      R2        F Pr(>F)
NFC_P       1   29.801 0.56228 198.2704  0.001 ***
CARB        1    0.033 0.00062   0.2181  0.616
NFC_P:CARB  1   15.651 0.29531 104.1327  0.001 ***
Residual   50    7.515 0.14180
Total      53   53.000 1.00000
---
Signif. codes:  0 ‘***’ 0.001 ‘**’ 0.01 ‘*’ 0.05 ‘.’ 0.1 ‘ ’ 1
```

Table A.15. Normalized Tear Strength (mN-m2/g) analysis of variance and interaction.

```
adonis2(formula = PROJ_DATA.resp.tensile.rel$TEAR_N ~ NFC_P + CARB +
NFC_P:CARB, data = PROJ_DATA.tensile.explan, method = "euc")
           Df SumOfSqs      R2       F Pr(>F)
NFC_P       1   26.481 0.49963 63.2804  0.001 ***
CARB        1    2.602 0.04910  6.2183  0.015 *
NFC_P:CARB  1    2.994 0.05649  7.1550  0.016 *
Residual   50   20.923 0.39478
Total      53   53.000 1.00000
---
Signif. codes:  0 ‘***’ 0.001 ‘**’ 0.01 ‘*’ 0.05 ‘.’ 0.1 ‘ ’ 1
```

Table A.16. Modulus analysis of variance and interaction

```
adonis2(formula = PROJ_DATA.resp.tensile.rel$MODULUS ~ NFC_P + CARB +
NFC_P:CARB, data = PROJ_DATA.tensile.explan, method = "euc")
           Df SumOfSqs      R2       F Pr(>F)
NFC_P       1    2.035 0.03840  2.4873  0.120
CARB        1    9.038 0.17052 11.0449  0.002 **
NFC_P:CARB  1    1.013 0.01912  1.2385  0.272
Residual   50   40.914 0.77195
Total      53   53.000 1.00000
---
Signif. codes:  0 ‘***’ 0.001 ‘**’ 0.01 ‘*’ 0.05 ‘.’ 0.1 ‘ ’ 1
```

Permeability & Retention Data

Table A.17. Permeability analysis of variance and interactions.

```
adonis2(formula = PROJ_DATA.resp.permeability.rel$PERM_N ~ NFC_P + CARB +
NFC_P:CARB, data = PROJ_DATA.permeability.explan, method = "euc")
            Df SumOfSqs      R2        F Pr(>F)
NFC_P        1  171.385 0.76854 1944.388  0.001 ***
CARB         1    2.077 0.00931   23.564  0.001 ***
```

```
NFC_P:CARB   1   30.147 0.13519  342.020  0.001 ***
Residual   220   19.392 0.08696
Total      223  223.000 1.00000
---
Signif. codes:  0 ‘***’ 0.001 ‘**’ 0.01 ‘*’ 0.05 ‘.’ 0.1 ‘ ’ 1
```

Table A.18. Retention analysis of variance and interactions.

```
adonis2(formula = PROJ_DATA.resp.retention.rel$RETAINED ~ NFC_P + CARB +
NFC_P:CARB, data = PROJ_DATA.retention.explan, method = "euc")
           Df SumOfSqs      R2      F Pr(>F)
NFC_P       1   2.9451 0.26774 4.0255  0.045 *
CARB        1   2.0950 0.19046 2.8636  0.107
NFC_P:CARB  1   0.1069 0.00972 0.1462  0.793
Residual    8   5.8529 0.53208
Total      11  11.0000 1.00000
---
Signif. codes:  0 ‘***’ 0.001 ‘**’ 0.01 ‘*’ 0.05 ‘.’ 0.1 ‘ ’ 1
```

Principal Component Analysis – Carboxylic Acid Content NFC

Table A.19. Analysis of the loadings for each principal component.

```
>           head(var$coord)
               Dim.1       Dim.2     Dim.3        Dim.4       Dim.5          Dim.6
TEA        0.8672537  0.34259954 0.3191833  0.005397572  0.09411544  0.0348319898
BL         0.9708377  0.03899571 0.1311872 -0.100768171  0.09179168 -0.0405570005
MODULUS    0.3869670 -0.80461192 0.3154325  0.288933877 -0.03683127 -0.0008449206
TENSILE_N  0.9249023  0.27487497 0.0481972 -0.084153603 -0.20267244 -0.0003182589
STRETCH_N -0.5359430  0.72336052 0.2858307  0.297815543 -0.01902411 -0.0155218786
TEAR_N    -0.7540158 -0.14565552 0.5538678 -0.290161864 -0.02754858 -0.0019476623

>           head(var$contrib)
              Dim.1     Dim.2      Dim.3       Dim.4      Dim.5        Dim.6
TEA       21.153259  8.466634 16.7183731  0.01064691 14.5597682 39.091318502
BL        26.508082  0.109691  2.8242065  3.71085135 13.8496666 52.997502732
MODULUS    4.211461 46.699278 16.3277558 30.50870211  2.2298014  0.023001467
TENSILE_N 24.058951  5.450140  0.3812039  2.58804745 67.5183946  0.003263509
STRETCH_N  8.078342 37.743906 13.4069932 32.41317121  0.5948965  7.762691312
TEAR_N    15.989905  1.530351 50.3414676 30.76858097  1.2474728  0.122222477
```

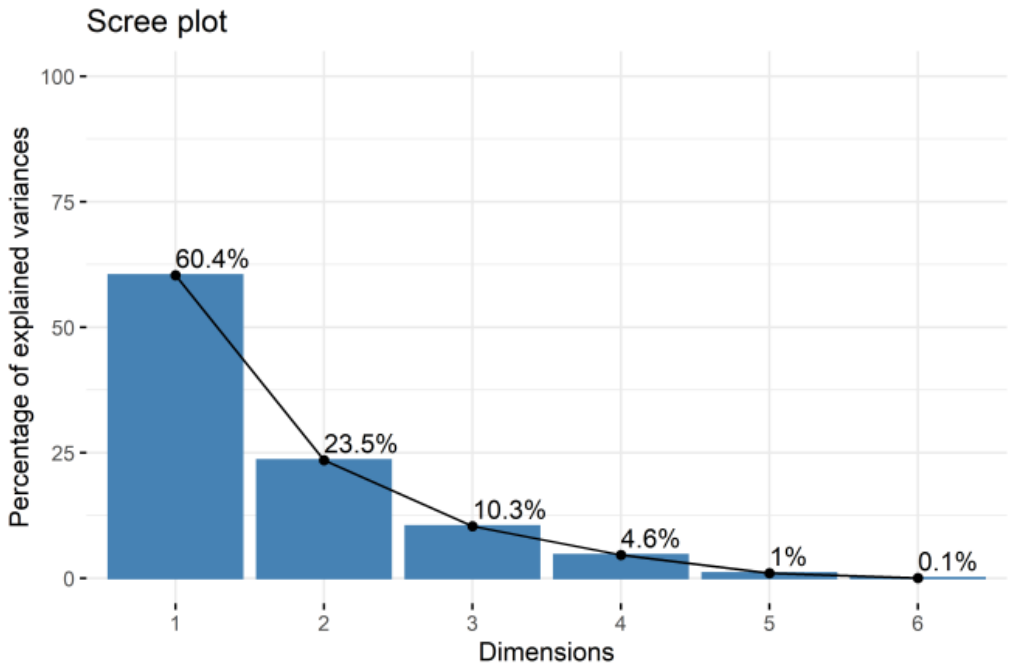

Figure A.13. Scree plot of the principal components associated with the mechanical response and carboxylic acid surface charge level of NFC.

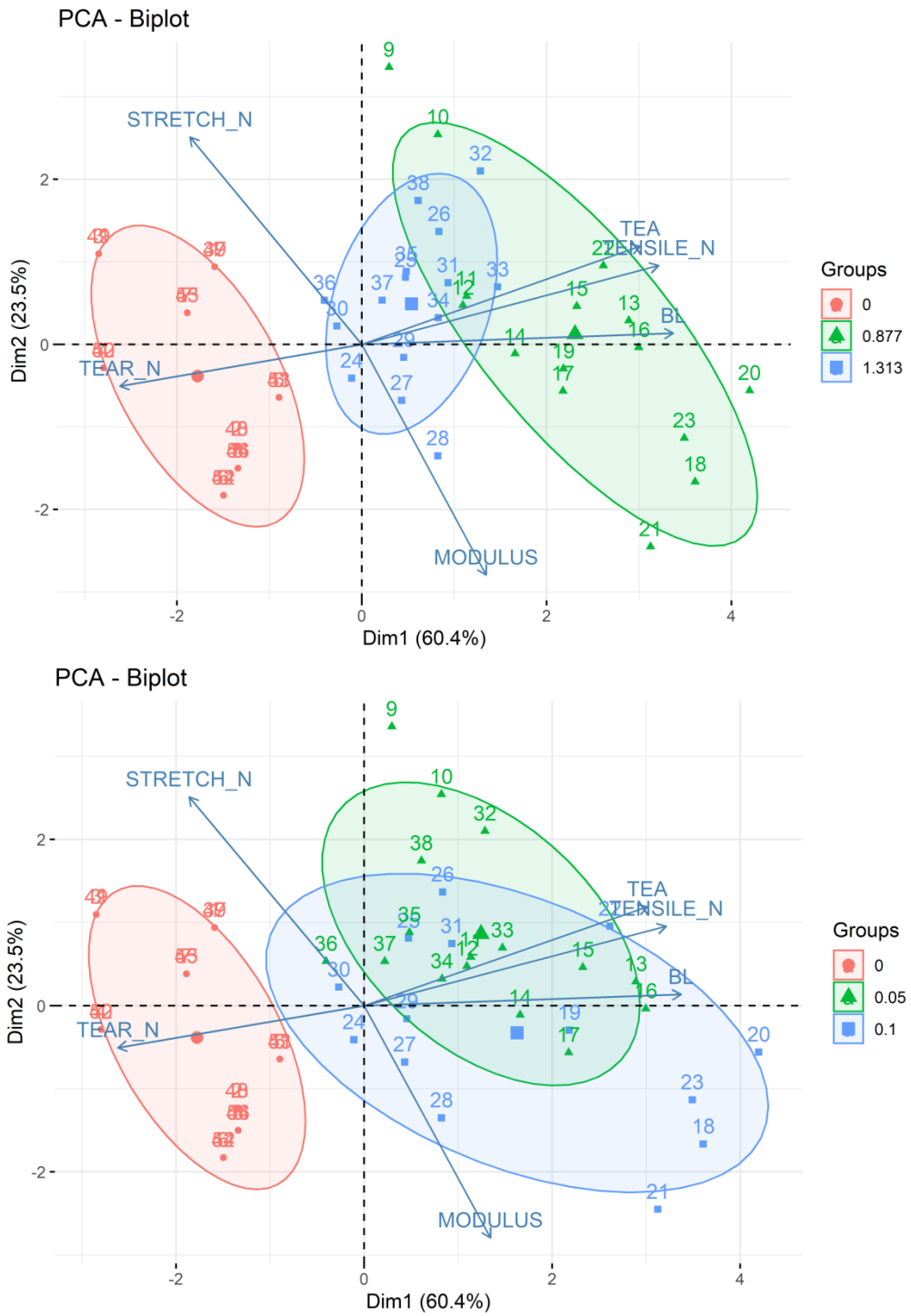

Figure A.14. Response variable vectors for charge (top) and percent addition (bottom) of NFC.

Table A.20. Analysis of variance for opacity response and treatment interaction.

```
adonis2(formula = PROJ_DATA.resp.opacity.rel$OPACITY ~ NFC_P + CARB +
NFC_P:CARB, data = PROJ_DATA.opacity.explan, method = "euc")
            Df SumOfSqs      R2        F Pr(>F)
NFC_P        1   54.827 0.50300 153.9197  0.001 ***
CARB         1   16.046 0.14721  45.0477  0.001 ***
NFC_P:CARB   1    0.370 0.00339   1.0375  0.320
Residual   106   37.758 0.34640
Total      109  109.000 1.00000
---
Signif. codes:  0 ‘***’ 0.001 ‘**’ 0.01 ‘*’ 0.05 ‘.’ 0.1 ‘ ’ 1
```

Table A.21. Analysis of variance for scatter measurement and evaluation of treatment interaction.

```
adonis2(formula = PROJ_DATA.resp.opacity.rel$SCATTER ~ NFC_P + CARB +
NFC_P:CARB, data = PROJ_DATA.opacity.explan, method = "euc")
            Df SumOfSqs      R2       F Pr(>F)
NFC_P        1   86.423 0.79287 3870.37  0.001 ***
CARB         1   13.670 0.12541  612.19  0.001 ***
NFC_P:CARB   1    6.541 0.06001  292.92  0.001 ***
Residual   106    2.367 0.02171
Total      109  109.000 1.00000
---
Signif. codes:  0 ‘***’ 0.001 ‘**’ 0.01 ‘*’ 0.05 ‘.’ 0.1 ‘ ’ 1
```

Principal Component Analysis - Opacity

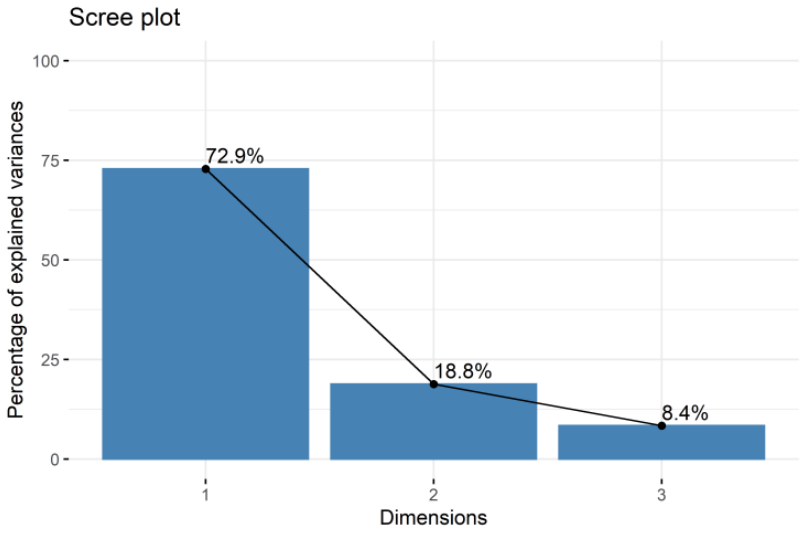

Figure A.15. Scree plot for optical response.

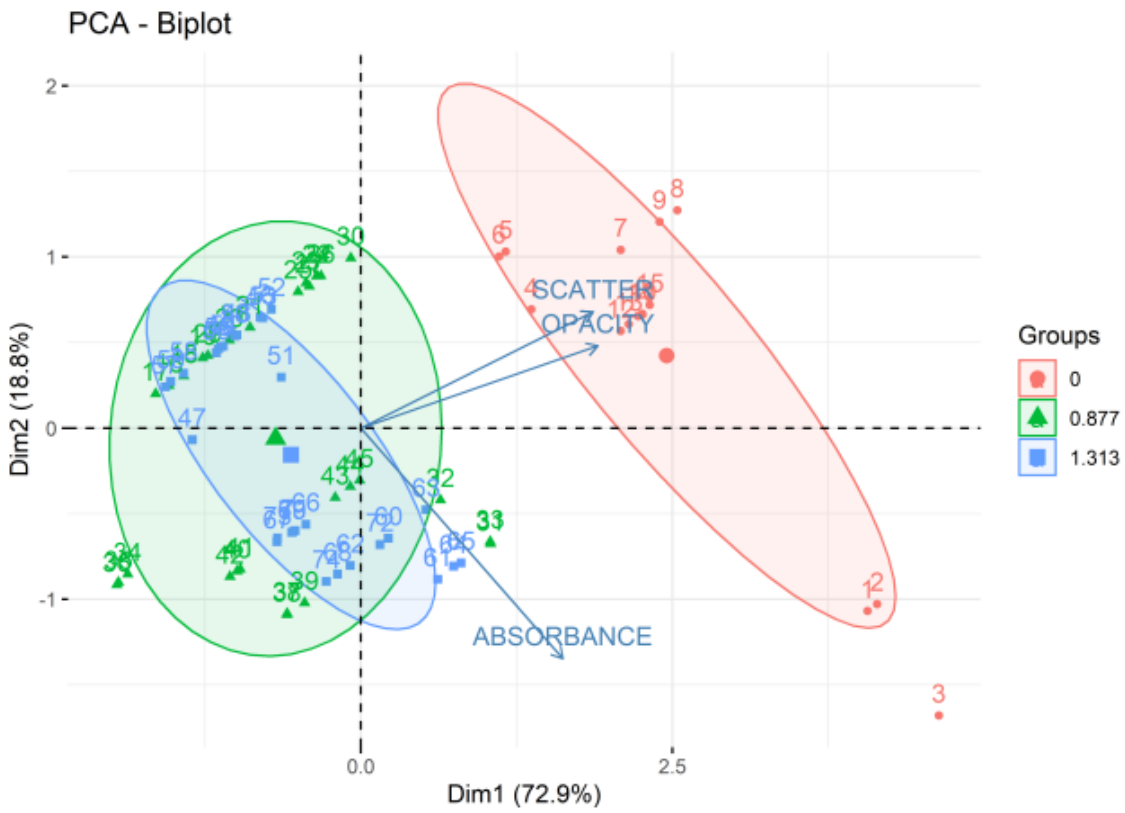

Figure A.16. Optical response variable vectors for surface charge of NFC.

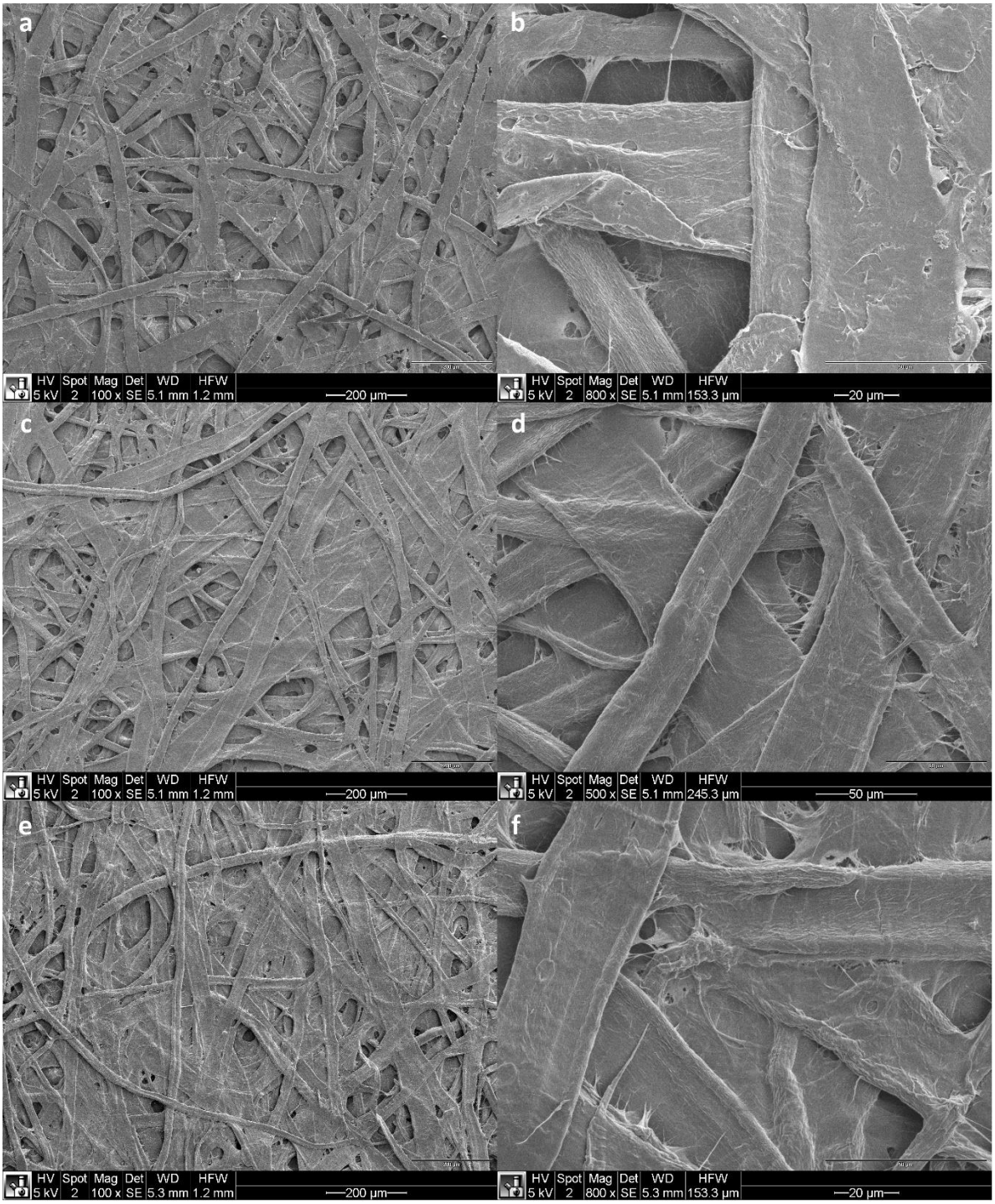

Figure A.17. a-b) base sheet, c-d) 5% NFC addition at low charge, e-f) 5% NFC addition at high

charge

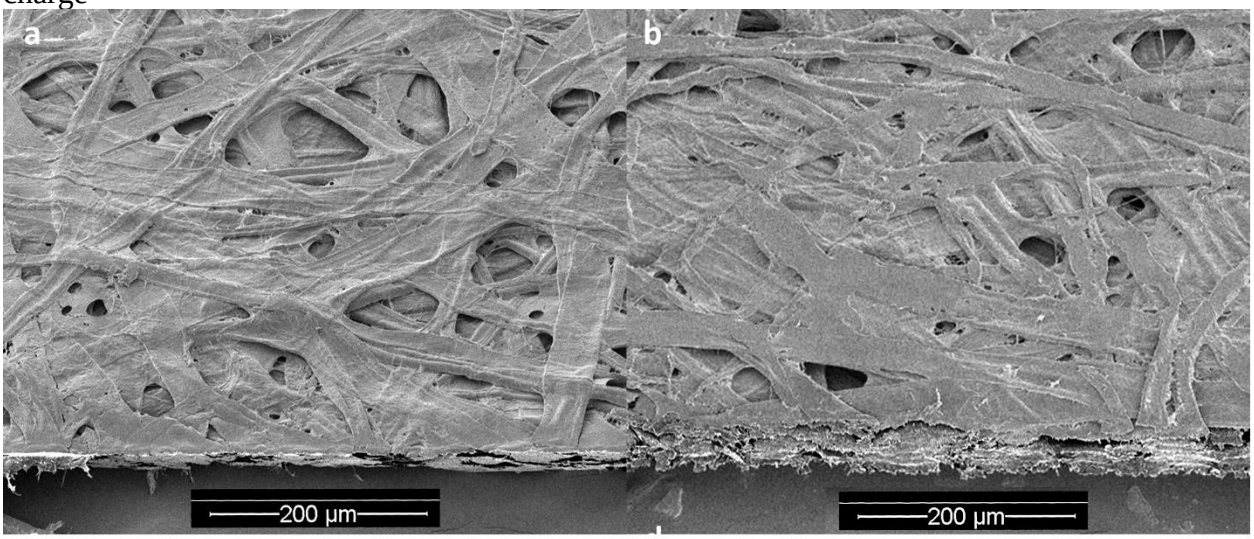

Figure A.18 Paper edge view a) 10% NFC reinforcement - low charge (4.19 ±0.08 microns), b) 10% NFC reinforcement at high charge (4.61 ±0.05 microns).

Figures A.6 and A.7 are larger versions of what is displayed in Chapter 5. The following images reveal details of the fibrillation between fibers in the low charge high addition rate papers.

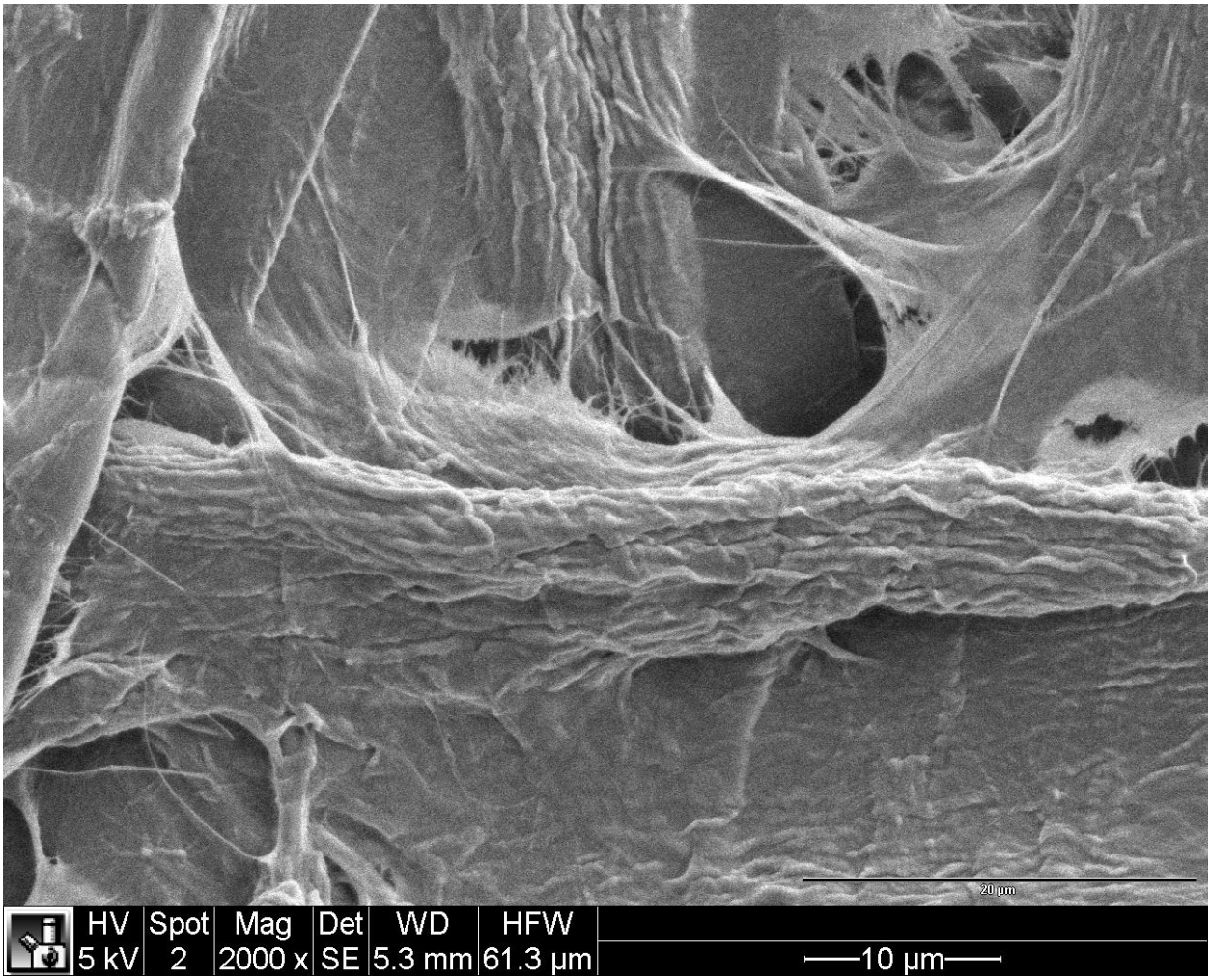

Figure A.19. Image of 5% NFC amendment, low charge with visible fibrils spanning paper fibers.

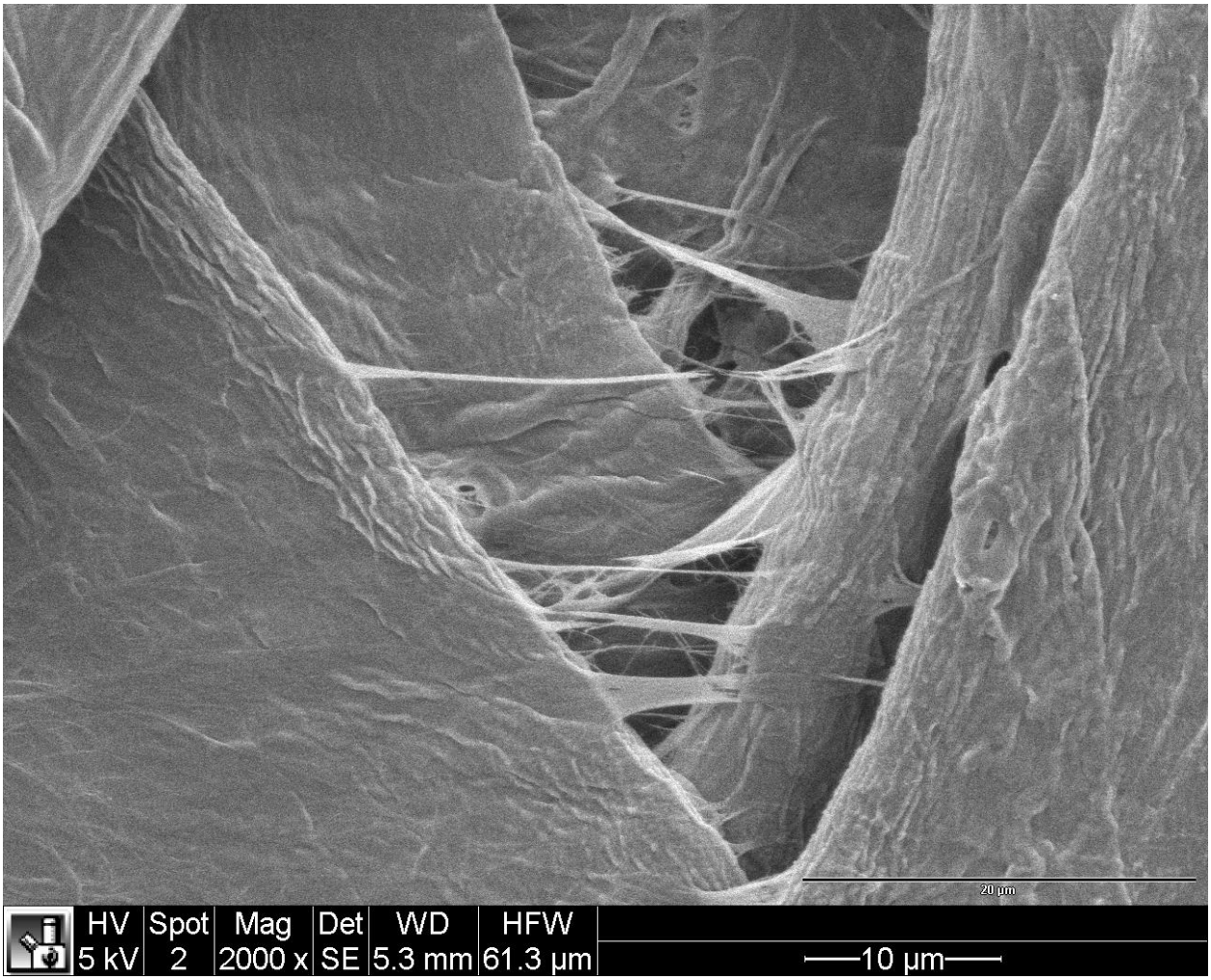

Figure A.20. Image shows fibrillation between fibers in the sheet for 5% NFC – low charge amendment.

The fibrils present in the figures A.7 through A.10 are too large to be considered nanofibrillated cellulose. The coating used to pre-treat the samples for SEM analysis is on the order of 2-3 nm in thickness which would obscure any detail in nanofibers. The smoothed edges and surface texture in the images would indicate that the surface may be covered by coated nanofibers. This can be seen in both Figure A.9 and A.10.

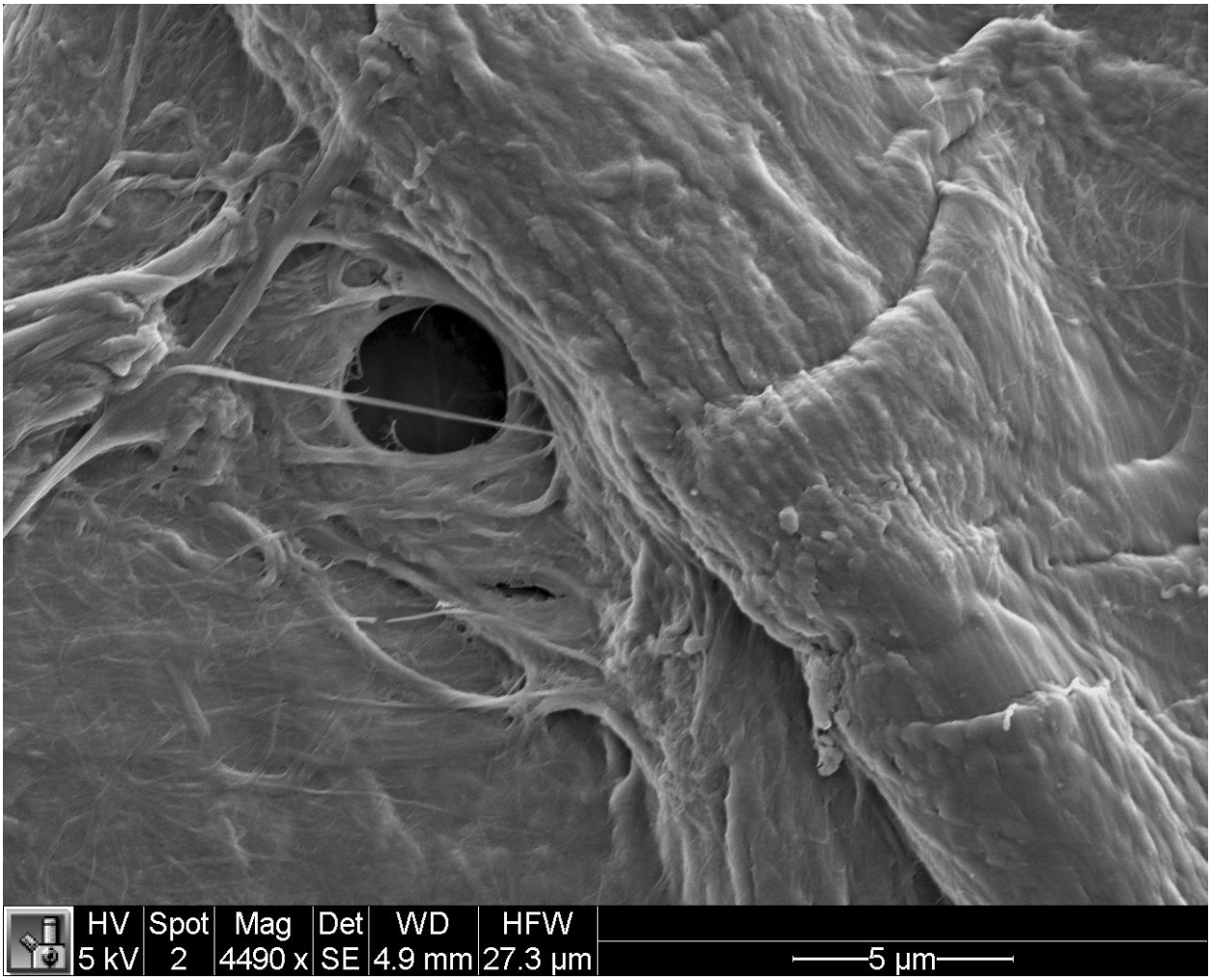

Figure A.21. Image showing fibril layers visible on the surface of the fibers.

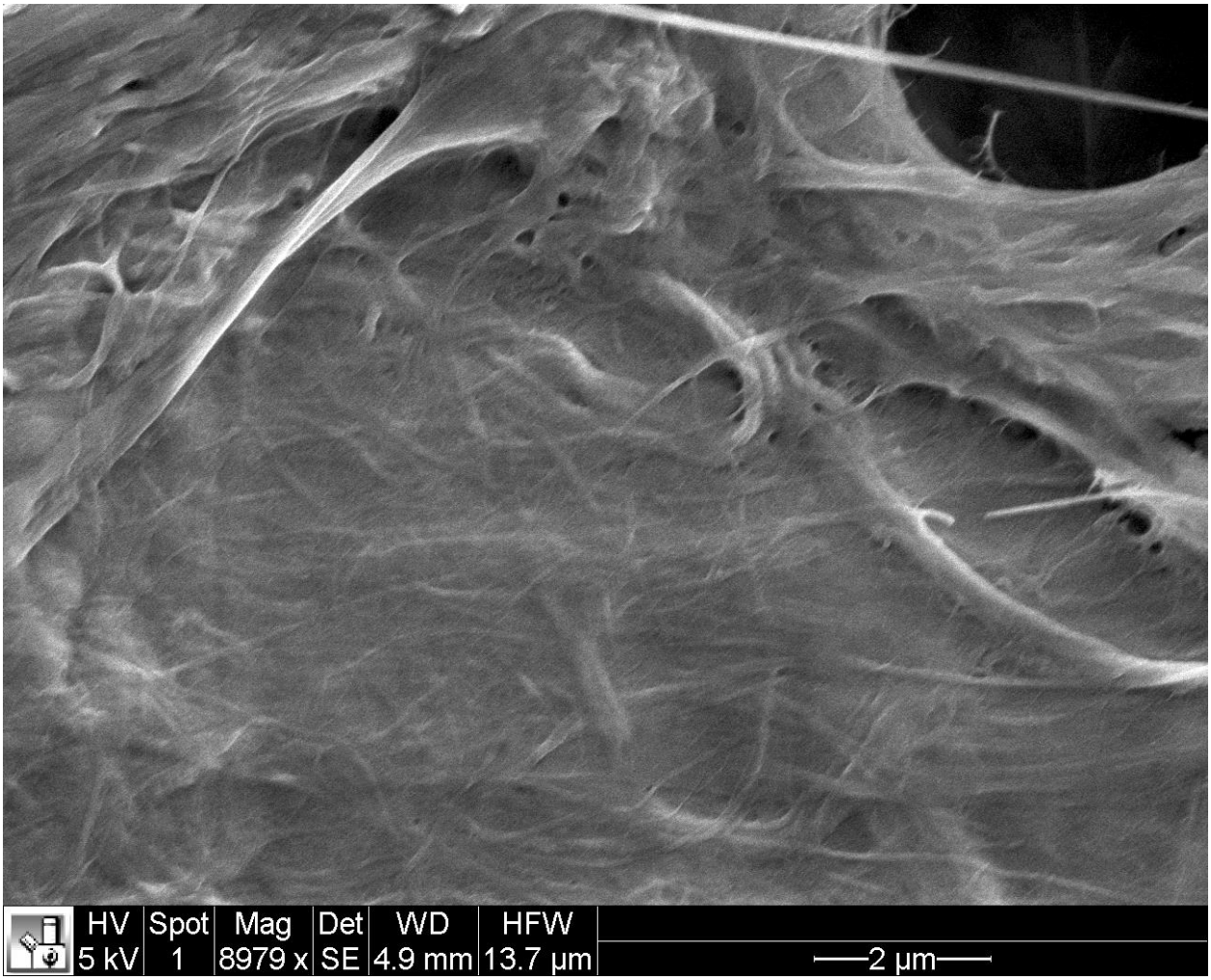

Figure A.22. Closeup of figure A.9 showing fibrills layering over the cellulose fibers.

References

[1] Ruzin, S. E., Maceration using Acetic Acid and Peroxide. *Plant Microtechnique and microscopy* (p. 132). **1999**, ISBN 0 19 508956 1, Oxford University Press.

[2] Lee, D. H., Kim, S. H., Byun, J. H., A method of steepest ascent for multiresponse surface optimization using a desirability function method. *Quality and Reliability Engineering International*, **2020**, 36(6), 1931–1948. DOI:10.1002/qre.2666

[3] Lenth R.V., Response-Surface Methods in R, Using rsm. *Journal of Statistical Software*, **2009**, **32**(7), 1–17.https://www.jstatsoft.org/v32/i07/.

[4] Katz, S., Beatson, R. P., Scallan, A. M. The determination of strong and weak acidic groups in sulfite pulp. *Svensk Paperstidning*, **1984**, 6, R48–R53.

[5] Mettler-Toledo International Inc. (2020, April 14). Guide to Conductivity Theory. Retrieved from https://www.mt.com/us/en/home/library/guides/process-analytics/conductivity-theory-guide.html

[6] Apelblat, A., Dissociation constants and limiting conductances of organic acids in water. *Journal of Molecular Liquids*, **2002**, 95(2), 99–145. DOI:10.1016/s0167-7322(01)00281-1

[7] Yu, H., Zhang, D., Lu, F., Yao, J., New Approach for Single-Step Extraction of Carboxylated Cellulose Nanocrystals for Their Use As Adsorbents and Flocculants. *ACS Sustainable Chemistry & Engineering*, **2016**, 4(5), 2632-2643. DOI:10.1021/acssuschemeng.6b00126

[8] Serra, A., González, I., Oliver-Ortega, H., Tarrès, Q., Delgado-Aguilar, M., Mutjé, P., Reducing the Amount of Catalyst in TEMPO-Oxidized Cellulose Nanofibers: Effect on Properties and Cost. *Polymers*, **2017**, 9(11), 557. DOI:10.3390/polym9110557

[9] Mascheroni, E., Rampazzo, R., Ortenzi, M. A., Piva, G., Bonetti, S., Piergiovanni, L., Comparison of cellulose nanocrystals obtained by sulfuric acid hydrolysis and ammonium persulfate, to be used as coating on flexible food-packaging materials. *Cellulose*, **2016**, 23(1), 779-793. DOI:10.1007/s10570-015-0853-2

[10] Jiang, H., Wu, Y., Han, B., Zhang, Y., Effect of oxidation time on the properties of cellulose nanocrystals from hybrid poplar residues using the ammonium persulfate. *Carbohydrate Polymers*, **2017**, 174, 291-298. DOI:10.1016/j.carbpol.2017.06.080

[11] Zhang, K., Sun, P., Liu, H., Shang, S., Song, J., Wang, D., Extraction and comparison of carboxylated cellulose nanocrystals from bleached sugarcane bagasse pulp using two different oxidation methods. *Carbohydrate Polymers*, **2016**, 138, 237-243. DOI:10.1016/j.carbpol.2015.11.038

[12] Delgado-Aguilar, M., González, I., Tarrés, Q., Pèlach, M. À, Alcalà, M., Mutjé, P., The key role of lignin in the production of low-cost lignocellulosic nanofibres for papermaking

applications. *Industrial Crops and Products*, **2016**, 86, 295-300. DOI:10.1016/j.indcrop.2016.04.010

[13] Foster, E. J., Moon, R. J., Agarwal, U. P., Bortner, M. J., Bras, J., Camarero-Espinosa, S., … Youngblood, J., Current characterization methods for cellulose nanomaterials. *Chemical Society Reviews*, **2018**, 47(8), 2609–2679. doi: 10.1039/c6cs00895j

[14] Oksanen, J., Guillaume Blanchet, F., Friendly, M., Kindt, R., Legendre, P., McGlinn, D., Minchin, P.R., O'Hara, R.B.., Simpson, G.L., Solymos, P., Stevens, M.H.H., Szoecs, E., Wagner,H., *vegan:Community Ecology Package. R package version 2.5-7*., **2020**, https://CRAN.R-project.org/package=vegan

[15] Anderson, M. J., Permutational multivariate analysis of variance (PERMANOVA). *Wiley StatsRef: Statistics Reference Online*, **2017**, 1–15. DOI:10.1002/9781118445112.stat07841

[16] Anderson, M. J. (2001). A new method for non-parametric multivariate analysis of variance. Austral Ecology, 26(1), 32–46. doi: 10.1111/j.1442-9993.2001.01070.pp.x

[17] Anderson, M. J. (2017). Permutational Multivariate Analysis of Variance (PERMANOVA). Wiley StatsRef: Statistics Reference Online, 1–15. doi: 10.1002/9781118445112.stat07841